UNIVERSITY OF SOUTHAMPTON

THE INTERACTION BETWEEN SPACE TETHER SYSTEMS AND THE ORBITAL SPACE DEBRIS ENVIRONMENT

by GAVIN LEE GITTINS (B.Sc)

THESIS SUBMITTED FOR THE DEGREE OF
DOCTOR OF PHILOSOPHY

FACULTY OF ENGINEERING AND APPLIED SCIENCE
SCHOOL OF ENGINEERING SCIENCES
AEROSPACE ENGINEERING

OCTOBER 2004

UNIVERSITY OF SOUTHAMPTON

ABSTRACT

FACULTY OF ENGINEERING AND APPLIED SCIENCE

SCHOOL OF ENGINEERING SCIENCES

AEROSPACE ENGINEERING

Doctor of Philosophy

THE INTERACTION BETWEEN SPACE TETHER SYSTEMS AND THE ORBITAL SPACE DEBRIS ENVIRONMENT

By Gavin Lee Gittins (B.Sc)

There have been a number of proposals for using tethers in space. One such proposal involves deploying an electrodynamic tether, at the end of a host spacecraft's mission, in order to reduce the spacecraft's post-mission orbital lifetime. However, a space tether is particularly vulnerable to the orbital debris environment. When fully deployed, a tether may have a very large cross-sectional area and, unlike most spacecraft, they are very susceptible to small debris impacts. It has been estimated that a debris fragment with a diameter smaller than half the tether diameter can cause a single strand tether system to fail. Therefore, a good understanding of the interactions between the space debris environment and a space tether is of vital importance.

The Tether Risk Assessment Program (TRAP) has been developed as an extremely flexible tool with state-of-the-art capabilities in tether collision and sever risk assessments. The integrated structure of the developed software enables a wide variety of analyses to be conducted and simulations of both historic and potential future fragmentation events to be performed. The model is also capable of modelling the historic, current and future background orbital debris environment. A highly novel aspect of the TRAP model is the implementation of the Probabilistic Continuum Dynamics (PCD) method, enabling the debris density to vary over the length of the tether system, providing a more realistic collision risk assessment. This method is an improvement over other traditional methods, which simply take an average debris density for the whole tether system. Another novel aspect is its capability to determine debris penetration depths, producing an accurate method of determining tether sever probabilities. This approach is much more advanced than current methods that simply use a lethality coefficient in order to determine a minimum fragment diameter capable of severing the tether. The TRAP model has undergone a vigourous validation programme to assess its accuracy. This has included simulating past tether missions and comparing with actual flight data. The validation exercise has greatly improved the confidence in the TRAP model for the prediction of realistic and accurate collision and sever risk assessments, for both single and double strand tether systems.

The validated TRAP model has been used for a number of case studies. The collision and sever probability risks associated with space tether systems arising from the orbital space debris environment have been extensively simulated. These simulations have considered both single and double strand tether systems, of various length and thickness, and should be of considerable interest to tether mission designers.

Contents

List of Figures

List of Tables

Acknowledgements

First and foremost the author wishes to thank Dr. Graham Swinerd for his supervision and encouragement throughout the course of the Ph.D programme without which none of this would have been possible.

A big thank you to Hugh Lewis and Neil Williams for their valuable comments and suggestions during the group meetings. Also a big thanks for their help and guidance throughout the Ph.D programme.

The author would like to acknowledge his friends and colleagues in the department who provided an enjoyable working environment.

Thank you to Roger Walker, Clare Martin and Hedley Stokes at QinetiQ for their valuable insights during the (quarterly) project meetings.

The author would also like to thank Adrian Tatnall and Richard Crowther for their suggestions in putting the final touches to the thesis.

Finally, a very big thank you to my parents for their constant support and encouragement.

Chapter 1

Introduction

Since the launch of Sputnik 1, in 1957, man has continued to launch satellites into Earth orbit. These launches, nearly 4,000 in total, have resulted in an over-populated environment, referred to as the orbital debris environment. The consequences of such a debris growth has resulted in an increased risk of satellites colliding with debris objects, causing significant damage or degradation. There exist two regions of near-Earth space that are most commonly used, Low Earth Orbit (LEO) and Geosynchronous Earth Orbit (GEO), and as a result it is these regions that contain the most orbital debris. Estimates of the current orbital debris density have suggested that the collision rate between large objects in LEO is about 1 collision every 10 to 20 years [1]. The collision rate in LEO already exceeds that in GEO by about two orders of magnitude, due to the LEO region being used much more. Assessing the threat posed to satellites from the space debris environment is not made any easier due to detector limitations, which prevent objects smaller than 10 cm in LEO, and 1 m in GEO, being tracked.

The number of objects in Earth orbit has continued to increase due to the presence of spacecraft and spent rocket bodies, solid rocket motor burns, nuclear reactor coolant leakages, surface material degradation, other mission-related objects, and on-orbit fragmentations. The latter has been the primary source of orbital debris in the past, the majority of which have been caused by explosions. Such fragmentation events can generate hundreds of large debris fragments, all of which contribute to the current debris density. It is believed that this debris density may already exceed a critical density in some regions of LEO, where random collisions will begin to occur and produce even

more debris fragments [1]. Once the rate of fragments being produced by random collisions begins to exceed the rate at which they are being removed, by atmospheric drag, the debris population will begin to grow exponentially, as fragments produced by these random collisions generate even more fragments. This process is referred to as collisional cascading, and it is the potential dominance of these uncontrollable random collisions over explosions as the main source of orbital debris that has prompted an increase into future orbital debris evolution studies.

The future trend of the orbital debris environment depends upon many different factors, such as the rate of future launch traffic, the rate of explosions/collisions, new space activities and the efforts made by operators to reduce and control the debris population growth. Such mitigation methods for reducing and controlling the debris growth is to de-orbit spacecraft and rocket bodies at the end of their mission lifetime. This can be achieved by performing a burn to either de-orbit the spacecraft or by placing the spacecraft into an orbit with a reduced orbital lifetime. However, due to the extra propellant required to perform such a manoeuvre this can be costly. This cost is exhibited by the need for increased propellant at launch or by a reduction in the payload's mission lifetime (due to the remaining propellant being used for performing de-orbit manoeuvres). However, a relatively new strategy for de-orbiting spacecraft has been proposed. This involves attaching a tether system to the spacecraft before launch, in order to de-orbit the spacecraft either by electrodynamic means or by momentum transfer.

Space tether systems have potential in offering a quick and elegant method for the de-orbiting of spacecraft. With the mass of a tether system being just 1 or 2 percent of the host spacecraft, an efficient de-orbiting device is possible, reducing a spacecraft's post-mission orbital lifetime, in LEO, from a few years to just a few weeks. Tethers may also be used for increasing an object's orbital altitude. One proposal is to deploy an electrodynamic tether from the International Space Station (ISS) to re-boost its orbit, removing the critical and constraining dependency of propellant supply from Earth. However, space tethers are particularly vulnerable to space debris impacts, with just one impact resulting in the possibility of mission failure. This, combined with their large cross-sectional areas, is a major concern regarding space tether systems. Hence, the interaction between a space tether system and the orbital debris environment must be well understood before such missions are carried out.

1.1 Objectives

With the large number of possible applications of space tethers, there is a growing need to develop a model that accurately predicts the collision and sever risks associated with a tether system arising from the orbital debris population. Most collision risk assessment models use a suitable 'binning' method, which allows the model to calculate the debris density within a given volume occupied by the 'target' spacecraft. However, since a space tether is typically many kilometres in length, the debris density may vary quite significantly over the length of the tether system. Hence, a suitable method is adopted to allow the debris density to vary along the length of the tether system, providing a more realistic, and accurate, collision risk assessment.

The objectives of the PhD are to:

- Review the current state-of-the-art knowledge of the space debris environment and the impact risks posed to orbiting spacecraft and tether systems.
- Develop a model that can predict the collision and sever probabilities associated with an orbiting space tether system arising from the orbital debris population.
- Assess and improve the model accuracy by a process of validation, involving comparisons with the literature and actual tether flight data.
- Apply the model to study the effects of the debris-induced failure rates of space tethers.

1.2 Model Overview

In fulfilling the PhD objectives, the Tether Risk Assessment Program (TRAP) has been developed at the University of Southampton, UK. The TRAP model is implemented in Visual C++ with a Microsoft Windows-OpenGL graphical user interface (GUI). Thus, a user friendly model has been developed, hiding the program's complex infrastructure, with a number of simple pop-up menus providing easy access to amend input variables. The integrated structure of the developed software enables a wide variety of analyses to be conducted, and simulations of both historic and potential future fragmentation events to be performed. The model is also capable of modelling the historic, current and

future background orbital debris environment. In combination, this allows the model to be applied to study the collision and sever risks associated with an orbiting space tether system, arising from such debris environments. The TRAP model has been rigorously developed and validated to ESA PSS-05 Software Engineering Standards [2].

The TRAP model consists of four main programs, Breakup, Tether, Analysis and Background. The Breakup Program uses the IDES breakup model [3] to simulate low or high intensity explosions, and catastrophic and non-catastrophic collisions. The Tether Program models the orbital dynamics of a rigid or non-rigid tether system. The tether is represented by a number of 'beads' that are connected by straight inelastic strands and can be used to model either single or double strand tether systems. The Analysis Program employs the method of Probabilistic Continuum Dynamics (PCD) to enable collision and sever risk assessments of the tether system when the debris cloud is encountered. Although the PCD method has been applied to study collision risk to satellites in the past [4], its application to space tethers here is novel. This method offers a distinct advantage over more traditional models by allowing the debris density to vary over the length of the tether system, providing a more realistic collision risk assessment. The determination of sever risk can be calculated using one of two methods. The first involves using a lethality coefficient which determines if the tether is severed by using the debris fragment diameter only. The second method, on the other hand, takes into account the relative velocity of the impact along with the object's mass. The calculation of the impact energy can then be used to determine if the tether was able to withstand the impact. Finally, the Background Program is able to model the historical, current and possible future orbital debris environments, providing collision and sever risks of tether systems exposed to such environments. In addition to the determination of collision and sever risks to a tether system, the TRAP model is also capable of modelling double strand tether systems. This allows comparisons to be made between single and double strand tether systems, providing a more detailed understanding of their relative merits.

1.3 Thesis Structure

The next chapter, Chapter 2, reviews the literature in order to describe our current knowledge and understanding of the orbital debris environment across the entire object size range. Firstly, the sources and sinks of the orbital space debris environment are

introduced and categorised. Then, the risks associated with such debris is discussed, paying particular attention to the formation of debris clouds. The discussion then looks at the future trends of the space debris environment if it were to develop unchecked, and mankind fails to take any mitigation action. This is often referred to as the 'business as usual' scenario. Appropriately, the discussion then looks at the various mitigation methods that can be implemented to help stabilise, or even reduce, the growth of orbital space debris. Finally, the prediction of the orbital space debris environment is presented showing the effects of suitable mitigation methods.

Chapter 3 introduces the space tether system concept while reviewing the literature. The different types of space tether systems are introduced along with a description of possible applications. The discussion then proceeds to past tether missions, outlining what has been learnt from such experiments. A number of future proposals are then introduced, before moving on to discuss how a space tether system could be used for performing de-orbit manoeuvres, as an aid to reducing the orbital space debris density. However, space tether systems are particularly vulnerable to space debris impacts. Hence, the chapter concludes by discussing a number of risk assessments that have been performed throughout the literature.

Chapter 4 outlines the equations of motion of an orbiting object and a space tether system that have been implemented into the TRAP model. The chapter begins by summarising the set of equations used to describe the ideal orbital motion of an object in Earth orbit. This then leads to the introduction of orbital perturbations, in particular J_2, J_3, and atmospheric drag, all of which are implemented into the TRAP model. The orbital motion of a tether system then follows. The dynamics of a general non-rigid tether system are introduced, before discussing some simplifications which lead to the rigid tether model. The massless tether model is then introduced which forms the basis for the 'bead' model that is implemented into the TRAP model. The method of validation is also discussed throughout the chapter in order to assess the accuracy of the implemented model.

Chapter 5 presents a full and comprehensive description of the TRAP model, developed during the course of the PhD programme. The four main sub-programmes are introduced, which are responsible for modelling - the fragmentation of an object due to an explosion or a collision; the dynamics of an orbital tether system; the collision and sever

risks associated with a debris cloud; and finally the collision and sever risks associated with the background debris population.

Chapter 6 applies the TRAP model to predict the collision and sever probabilities associated with an orbiting space tether system arising from the orbital debris environment. The predictions calculated cover a variety of past and future missions and considers both single and double strand tether systems. The chapter concludes by discussing a scenario closely resembling a specific reference case, which was discussed at the 21st Inter-Agency Debris Coordination Committee (IADC) meeting held in Bangalore, March 2003, providing some valuable insights into the benefits and risks of using tethers in space.

Chapter 7 provides a summary of the research undertaken, and the principal conclusions that have been reached, throughout the PhD programme. The points of discussion include the assessed accuracy of the TRAP model and its validity for making collision and sever predictions, and the implications of the debris-induced failure rate forecasts for space tether systems. Finally, recommendations for future research are summarised, including possible improvements to the TRAP model and suggestions for further simulations.

Chapter 2

The Space Debris Environment

Since the space age begun with the launch of Sputnik 1 in 1957, nominal space operations and on-orbit fragmentation events have resulted in a large number of man-made objects orbiting the Earth. Together with natural objects (meteoroids) they contribute to the space debris environment. As of 31st January 2002, 4,693 launches had resulted in 27,061 objects which have been tracked and catalogued by the United States Space Command (USSPACECOM) [5]. The corresponding catalogue of objects at this time had 8,993 entries, of which about 43% had resulted from one of the 170 fragmentation events up to May 2001. The USSPACECOM catalogue covers trackable objects larger than approximately 10 cm in LEO and objects larger than about 1 m in GEO. Figure 2.1 illustrates the USSPACECOM's radar and optical capabilities for tracking and cataloguing orbital debris. The smaller debris population, such as paint flakes and residue from rocket motor firings are also known to contribute to the debris environment. Current estimates suggest that the man-made debris environment, in most LEO regions is assumed to dominate the natural meteoroid contribution, with the exception of objects less than around 0.1 mm in size [5].

The current space debris population poses a collision threat, and hence a risk of damage to any orbiting objects exposed to the environment. The collision probability can be assessed by applying debris flux models for various sized objects and for specific target objects of interest. In general, the current risk from debris to a target object is not yet unacceptably high. However, for some operational spacecraft, and particularly manned missions, protective measures may be necessary to enable safe operations.

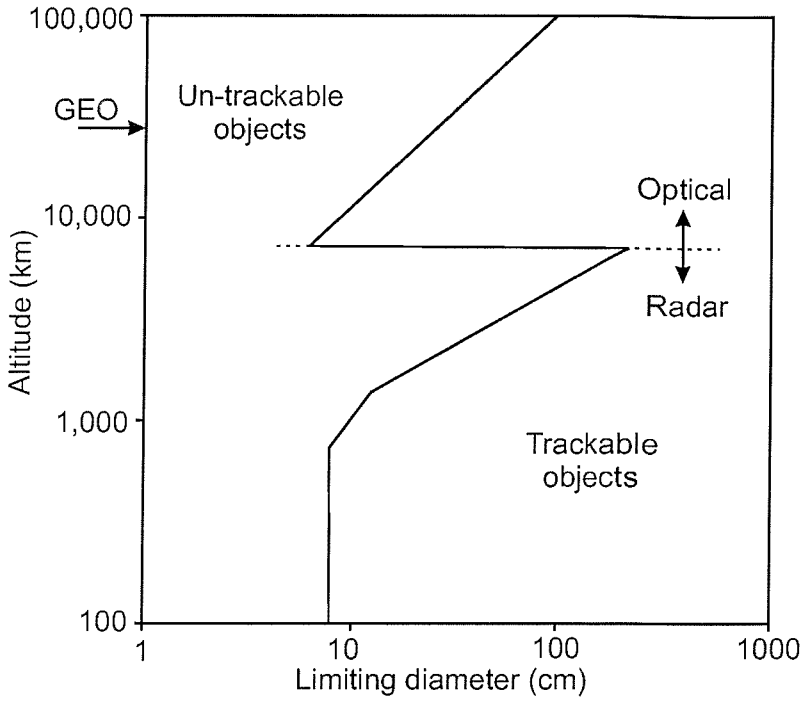

Figure 2.1: USSPACECOM's capabilities for tracking and cataloguing orbital debris [6]

If space flight operations continue as they have done in the past, then it is expected that these operational practices will lead to an onset of interactive collisions among the larger catalogued objects. Hence, fragments from such collisions, to date an insignificant source of debris, will grow and begin to dominate the environment. This could lead to a so called 'critical density' at some altitudes, resulting in a process of collisional cascading (i.e. fragments from collisions resulting in further collisions). However, before such a process begins, the debris population will grow and, due to the increasing number of objects, the collision risk to operational spacecraft will grow correspondingly.

To continue future safe operations in space, the uncontrolled growth of the space debris population must be avoided. A number of computer simulation models have been implemented to provide insights for different types of mitigation methods that limit and control the future growth of the space debris population. The outcome of such investigations suggest that mitigation methods stabilise and possibly reduce the number of future objects being released into the space environment. This can be achieved directly (e.g. by reducing mission related objects), or indirectly (e.g. by removing stored energy

from rocket bodies avoiding subsequent explosions). The implementation of such passive measures would help reduce the contribution to the debris environment arising from on-orbit fragmentation events - the dominant source in the past. Ultimately, only the removal of spacecraft and upper stages can suppress collisions as the dominant source of debris in the future. The ESA DELTA model has been used to show that this objective could be achieved by reducing the post-mission orbital lifetime of massive objects in LEO to 25 years [5]. This 25-year post-mission orbital lifetime has shown to significantly benefit the near-Earth space environment by reducing long-term collision risks. If lifetime reduction and de-orbiting of the spacecraft is not practical, then manoeuvring of the spacecraft to a disposal orbit (e.g. above LEO or GEO) is recommended.

2.1 The Current Situation

Since the launch of Sputnik 1 in 1957 the USSPACECOM has catalogued a total of 27,061 objects, as of 31st January 2002, that have been released into Earth orbit. The continuing increase in space activity and the various sources of debris have resulted in a continuous increase of the space debris population. This section discusses the current situation of the space debris environment and the mechanisms responsible for the creation and removal of orbital space debris.

Launch History

The USSPACECOM is responsible for collecting data on the space debris population using its Space Surveillance Network (SSN). The network consists of a number of optical and radar (mechanical and phased array) sensors responsible for detecting, tracking, cataloguing and identifying man-made objects orbiting the Earth. The USSPACECOM catalogue contains information on objects larger than approximately 10 cm in LEO, and larger than about 1 m in GEO. In October 2001, a total of 8,993 objects were recorded in the USSPACECOM catalogue resulting from 4,693 launches, approximately one third of the 27,061 objects that have been catalogued to date. The remaining two thirds of these objects have either re-entered the Earth's atmosphere, in a controlled manner (i.e. a de-orbit burn) or in an uncontrolled manner (i.e. natural decay), or have left near-Earth space (i.e. deep space missions). The current number of on-orbit

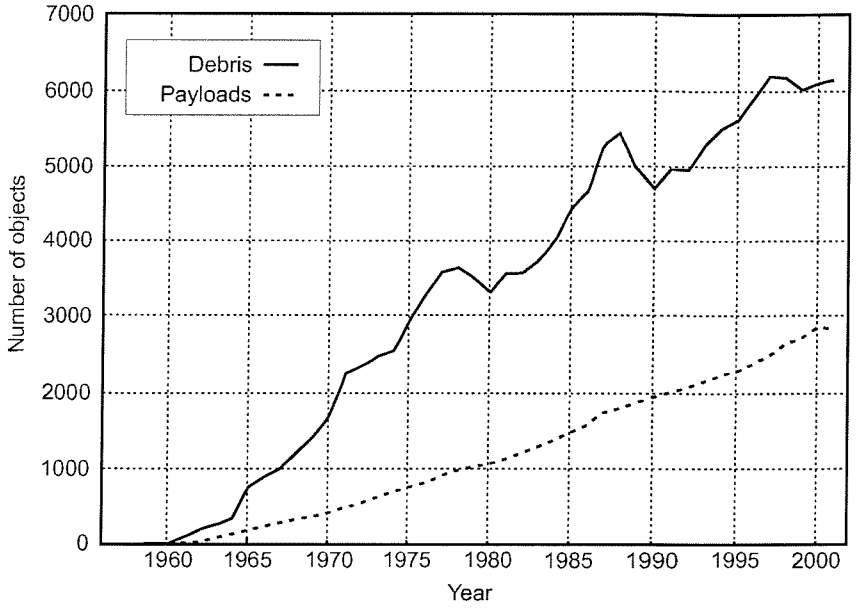

Figure 2.2: History of the on-orbit catalogue population [5]

catalogued objects versus time for debris and payloads is shown in Figure 2.2.

Of the current catalogue population only 6% can be assumed to be operational payloads. The remaining 94% of the catalogue can be broken down as non-operational payloads (24%), rocket bodies (17%), operational debris (10%) and payload and rocket debris (43%).

Historic Fragmentation Events

The primary contributor of orbital debris has been on-orbit fragmentation events. In total, 170 fragmentation events have been recorded up to 31st May 2001 [7]. The major causes of such fragmentation events are summarised in Table 2.1. The majority of fragmentation events have resulted from deliberate actions and propulsion related events. The cause of about one third of all fragmentation events, however, remains unknown.

One of the most severe fragmentation events to date occurred on the 13th November 1986, when the SPOT 1 Ariane third stage exploded violently into some 465 detectable fragments [8]. This explosion was believed to have occurred due to the mixing of residual

Cause	Events
Unknown	56
Aerodynamic	9
Deliberate Explosion	48
Propulsion Related	49
Electrical	7
Collision	1
Total	170

Table 2.1: Historical fragmentation events as of 31st May 2001 [5]

propellant.

The probability of collisions between catalogued objects is very low, but is becoming a greater threat as the number of orbiting objects continues to increase. To date there has been one validated case of such a collision. A French military research satellite, Cerise, was struck and partially disabled on the 24th July 1996 by an Ariane booster fragment [9, 10].

Non-Fragmentation Debris Sources

Non-fragmentation debris includes such objects as solid rocket motor particulates and slag, sodium potassium (NaK) reactor coolant liquid droplets, paint flakes and clusters of dipoles which formed after the 'Westford Needles' experiment in 1963 [11]. The knowledge of such debris, mainly in the sub-millimetre size range, is achieved by in-situ impact measurements, by on-orbit detectors, and from post-flight analysis of returned surfaces. NASA's Long Duration Exposure Facility (LDEF), for example, was covered by more than 30,000 craters visible to the naked eye. Approximately 5,000 of these had a diameter larger than 0.5 mm. The largest was 5 mm in diameter and was probably caused by a particle 1 mm in diameter [12]. As for ESA's European Retrievable Carrier (EURECA) the largest impact crater diameter was 6.4 mm [13]. However, the returned solar array of the Hubble Space Telescope (HST) gave data for the highest orbital altitude. An interesting finding was that the impact flux for the HST was considerably higher (by a factor of 2 to 8) than for EURECA for crater pit sizes larger than 200 to 300 μm [9]. The cases described above give some indication of the sub-millimetre debris population below 600 km altitude. Unfortunately, very little information is known about this debris population above this altitude, especially in the regions of high spatial

density (altitudes of about 800 to 1,000 km) as well as GEO. The launch of GORID (Geostationary ORbit Impact Detector) in 1996 was aimed at rectifying the situation in GEO, and although some initial results have been published by Drolshagen et al [14], investigations are continuing.

Atmospheric Drag

The orbital decay effects arising from atmospheric drag only affects objects orbiting in LEO below an altitude of about 1,000 km. The process is very slow and can take several months to several years before an object re-enters the Earth's atmosphere and burns up. For any objects orbiting above this altitude, the effects of atmospheric drag are considerably less effective. It can take hundreds or even thousands of years for orbits to decay to re-entry altitudes. An unfortunate attribute of atmospheric drag is the threat arising from an object as its orbital path decays and passes through lower orbital regions, resulting in interaction with other orbiting objects.

2.1.1 The Orbital Debris Environment

Orbital space debris generally refers to material that is left in orbit as a result of space activity, and is no longer serving any useful function. Studies have suggested that there is approximately 2,000,000 kg of orbital debris mass below an altitude of 2,000 km [6]. The mean number of objects in the LEO, MEO and GEO regions, according to the ESA MASTER-99 model [15, 16, 17], are highlighted in Table 2.2.

Figure 2.3 shows the spatial distribution of the catalogued population as of 21st August 1997 [9]. It clearly shows three pronounced peaks in LEO, MEO and GEO. The first of these peaks mostly relates to objects in near-circular orbits in the densely populated altitude region of around 1,000 km. In the MEO region, peak concentrations occur

Debris size	Objects in LEO	Objects in MEO	Objects in GEO
> 0.1 mm	1.03×10^{10}	1.6×10^{11}	2.5×10^{10}
> 1 mm	3.8×10^{7}	1.6×10^{8}	2.1×10^{7}
> 1 cm	121,289	173,244	20,703
> 10 cm	13,207	2,191	564

Table 2.2: Space debris population breakdown with size according to the ESA MASTER 99 model [5]

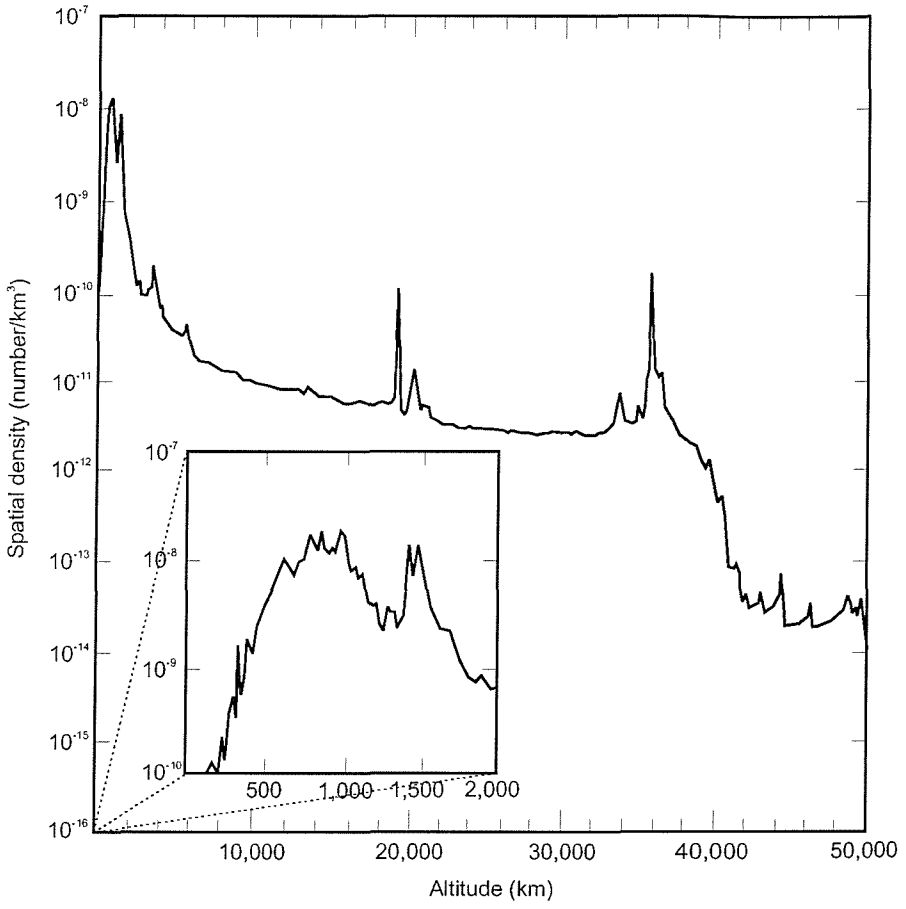

Figure 2.3: Spatial density distribution of catalogued objects as of 21st August 1997 **[9]**

around an altitude of 20,000 km relating to the 12 hour orbits (e.g. Molniya, GPS) and the GTO transfer orbits of 10.5 hours. The final peak around an altitude of 36,000 km is caused by the 24 hour orbit periods (e.g. near-GEO missions).

For the smaller debris population, space debris models have been developed to provide a mathematical description of the objects in Earth orbit. Figure 2.4 shows the spatial density for various size objects as predicted by the DAMAGE (Debris Analysis and Monitoring Architecture for the Geosynchronous Environment) model **[18, 19]** as of 1st May 2001. Note that the peaks for the objects greater than 10 cm, and 1 m, closely correspond to the catalogued spatial density values shown in Figure 2.3.

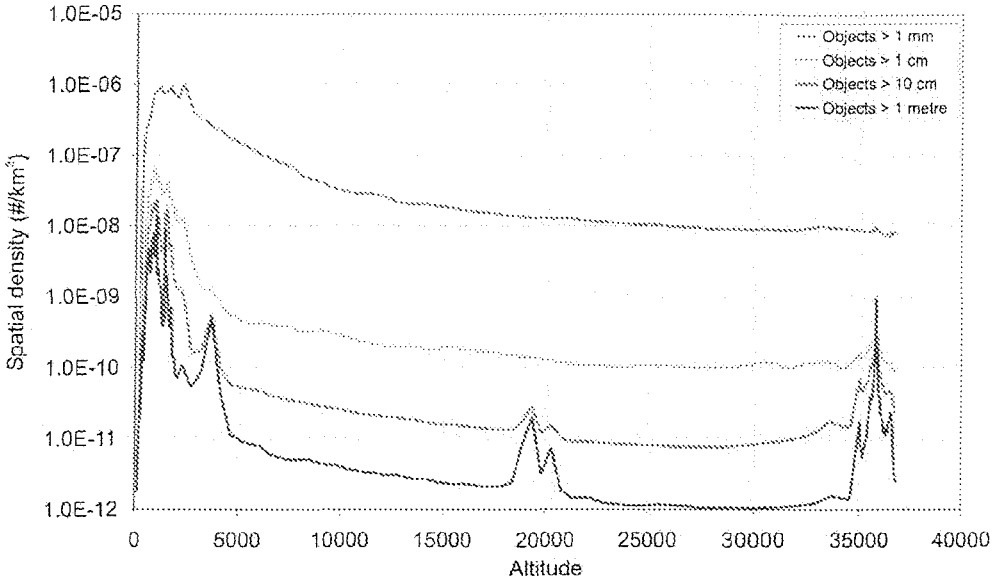

Figure 2.4: Spatial density distribution of predicted objects as of 1st May 2001 as predicted by the DAMAGE model

2.1.2 The Meteoroid Environment

The meteoroid environment encompasses particles of natural origin only, and nearly all of these meteoroids originate from either comets or asteroids in orbits around the Sun. There are two main meteoroid populations - stream and sporadic. The stream meteoroids are remnants of decaying comets, which retain their parent body orbit and create periods of high flux. The sporadic meteoroids, which randomly occur with no apparent pattern, are remnants of meteoroid streams that have dispersed throughout the solar system over many years as a result of gravitational perturbations. It has been estimated that approximately 200 kg of meteoroid mass is always moving through a volume within 2,000 km of the Earth [**6**]. They travel at exceptionally high speeds and have an average velocity, relative to an orbiting spacecraft of 20 km/s, although this can be as high as 70 km/s.

The meteoroid environment is defined as the average total meteoroid environment. This is composed of the average sporadic meteoroids and the yearly average of stream meteoroids. Figure 2.5 shows the relationship for the representative meteoroid and orbital debris environments for the Small Expendable Deployer System (SEDS-2) mission, which flew in March 1994 [**20**]. The graph clearly shows that the meteoroid environment

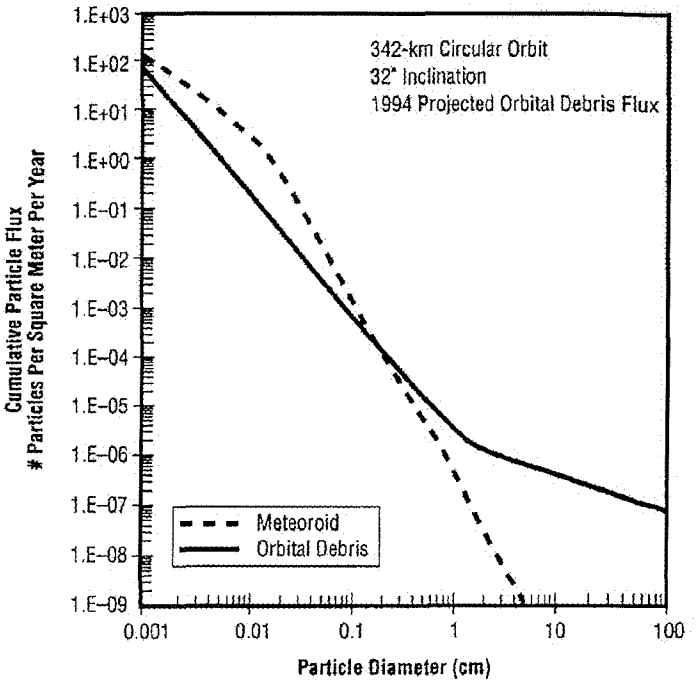

Figure 2.5: Cumulative particle flux as a function of particle diameter [**20**]

consists of higher particle flux levels for particles less than 0.1 cm, with orbital debris contributing higher particle flux levels for particles larger than 0.1 cm. A spacecraft encountering such meteoroid fluxes will mainly be subjected to surface degradation and should not suffer any serious consequences, such as mission failure. However, with the introduction of a space tether system into such an environment, the meteoroid population may cause substantial damage and even mission failure to single strand tether systems.

2.2 Risk Analysis

The probability of a collision with orbital debris depends on altitude, inclination, size and the length of time in orbit of a target object. For example, altitudes from 800 to 1,000 km contain an average population of 100 catalogued objects per 10 km altitude bands [**21**]. It has been estimated that a spacecraft in LEO is 100 times more likely to experience a collision than those in semi-synchronous and geosynchronous orbits [**22**].

The following sections consider the consequences of a debris fragment impacting an operational spacecraft in the LEO and GEO debris environments. The formation of, and potential risks associated with debris clouds are also considered.

2.2.1 Debris Classification

Although orbital debris have a number of different sources, sizes, and compositions, LEO objects may be classified using the following definitions:

- **Degrading** - objects with a diameter of less than 1 mm. The number of degrading debris objects in orbit has been estimated to be in its trillions, and information about this population has been gathered by examining the damage caused to returned surfaces. These in-situ measurement techniques have shown that damage from such collisions are reduced to component damage, craters, spallations, and degradation of spacecraft surfaces.

- **Damaging** - objects with a diameter between 1 mm and 10 cm. The number of damaging debris objects in orbit has been estimated to be of the order of tens of millions. Collisions with such debris can cause serious damage to a spacecraft, and the possibility of mission failure. It also results in the creation of a significant amount of small debris, increasing the local degrading debris population. The risk associated with this debris population is increased further by the fact that current technology is unable to adequately track, and hence catalogue such debris.

- **Catalogued** - objects with a diameter greater than 10 cm. The probability of collision with a catalogued debris object is very low because most of this population is monitored and catalogued by the USSPACECOM. However, such an impact would be catastrophic, with something of the order of 10^6 fragments 1 mm or larger being created.

The three debris populations introduced above can be found in all orbital regions. Frequently used regions, that offer benefits to spacecraft designers such as providing high-resolution images or retaining a constant longitude over the Earth, suffer from high debris density levels. The most densely populated regions are in LEO in the altitude range bands 800 to 1,000 km and 1,400 to 1,500 km.

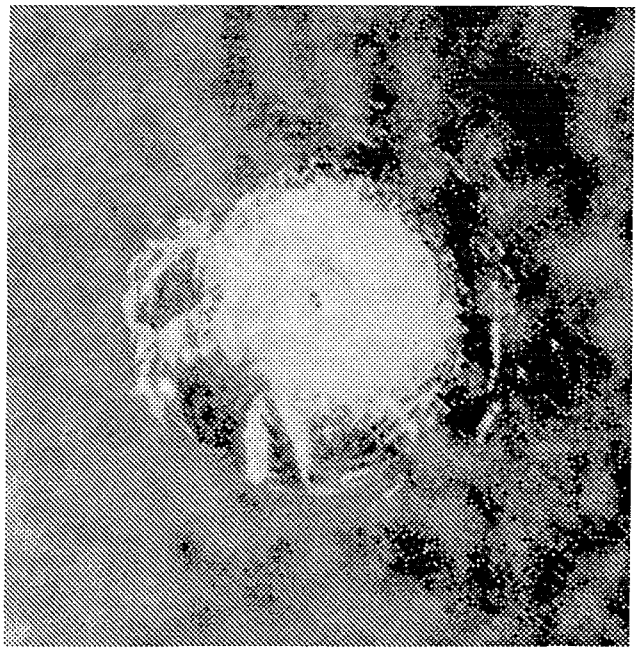

Figure 2.6: The damage sustained to a Space Shuttle window from a fleck of paint [**24**]

The average relative velocity of an impact in LEO is approximately 10 km/s, where even the smallest of objects can contain an amount of kinetic energy and momentum sufficient to damage a spacecraft. Figure 2.6, for example, shows a 4 mm diameter crater on the Space Shuttle window after a 0.2 mm diameter fleck of paint impacted with a relative velocity of about 3 to 6 km/s [**23**].

For GEO altitudes the average relative velocity of an impact is considerably lower than that of LEO, typically around 200 to 300 m/s in the GEO ring because of objects occupying similar orbits. However, relative velocities can be as high as 2 km/s, due to objects in highly eccentric (transfer) orbits crossing the GEO arc, and as such any collisions would still cause considerable damage to spacecraft. For example, a 1 cm fragment in GEO will have roughly the same damage potential as a 1 mm fragment in LEO. This can be shown mathematically using the kinetic energy equation, given by $\frac{1}{2}mv^2$, where m is the mass (kg) and v is the velocity (m/s). Hence, a 1 cm fragment in GEO with a mass of about 1.14×10^{-3} kg and a relative velocity of about 300 m/s will have a damage potential of about 51.3 Joules. While a 1 mm fragment in LEO with a mass of about 2.1×10^{-6} kg and a relative velocity of around 7 km/s will have a damage potential of 51.45 Joules. However, at GEO altitudes only objects 1 m or larger may be

tracked, making it impossible to detect and avoid some large debris objects. This could result in a catastrophic collision resulting in the possibility of mission failure.

2.2.2 Debris Clouds

A debris cloud is a large concentration of debris fragments in a well-defined region of space. They are formed when a space system fragments, caused either by an explosion or a collision. A debris cloud consists of three phases of evolution and continues to evolve from its formation. The first evolution phase occurs immediately after the original space system fragments, when the cloud is compact, dense and roughly spherical in shape, assuming that the fragments are ejected more or less isotropically - see phase 1 of Figure 2.7. The cloud will then quickly elongate along the space system's original orbital path because of the different velocities of the ejected fragments. Eventually the leading edge of the debris cloud will catch up with the trailing edge, hence encircling the Earth. It takes hours to days for an ensemble of fragments to reach this phase - see phase 2 of Figure 2.7. As the cloud continues to evolve it will wrap around on itself, taking the form of a spiral which is pinched at two locations. Two kinds of 'pinch' phenomena occur:

- **The pinch point** occurs at the original fragmentation point since all the debris will return through this point. Over time, the effects of orbital perturbations will tend to disperse the pinch point.
- **The pinch line** occurs along a radius in the original space system's orbital plane 180° from the pinch point, because all the debris must pass through the orbital plane along this line.

The effects arising from orbital perturbations greatly effect the evolution of the debris cloud. The zonal harmonic J_2, which represents the polar flattening of the Earth (also known as the equatorial bulge), for example, causes the right ascension of the ascending node to precess and the argument of perigee to recess in a secular fashion. The rate of change of Ω and ω will depend on the semi-major axis, inclination and the eccentricity of a fragment's orbit. Hence, the slight differences in the orbital elements of each fragment will result in different rates of changes in Ω and ω. This causes the values of Ω and ω of the clouds fragments to spread out over time, thus having a smearing effect on

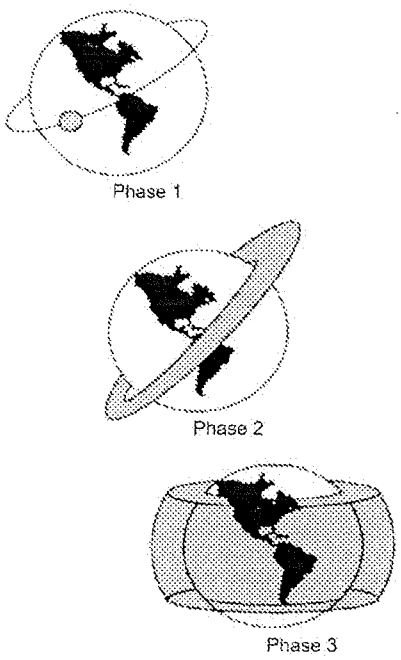

Figure 2.7: The evolution of a debris cloud **[22]**

the pinch locations. The continuing spread of the argument of perigee has the effect of transforming the pinched spiral into a torus. Meanwhile, the dispersion of the nodal positions causes the cloud to evolve into a band which encircles the Earth **[25]**. This last phase will be reached months to years after the initial fragmentation event - see phase 3 of Figure 2.7. Each evolution phase of a debris cloud will pose a different threat to an orbiting space system. These are outlined below.

- **A short-term** threat exists immediately after the original fragmentation event where the debris is very localised. An orbiting space system passing through the cloud, while it is still compact, will experience a very high debris density posing a significant threat to the space system's functionality.
- **An intermediate** threat exists when the cloud has evolved and wrapped around itself forming a torus. An orbiting space system encountering the cloud will experience a reduced debris density level.
- **A long-term** threat (of small magnitude) exists when the debris cloud has completely dispersed around the Earth and has become part of the background debris

environment.

A brief discussion will now focus on some case studies involving debris clouds that have been performed in the past demonstrating the three evolutionary phases of debris clouds.

Case Studies

Two case studies were performed by Swinerd et al [**26**] involving debris clouds. The first scenario described a constellation that was similar to that of the Iridium system, containing around 70 satellites in near-polar orbits at an altitude of around 800 km. The second was a Globalstar-like configuration consisting of 56 satellites at an altitude of around 1,400 km, distributed in orbit planes inclined at 52°. The case studies examined the collision risks associated with the two systems after one of the system satellites fragmented. The collision hazard assessment was completed using the Space Debris Simulation (SDS) suite [**4**]. The study showed that no major encounters occurred after about 20 days, for the worst case. However, with a simulation run period of just 30 days it was not possible to deduce that a further significant collision occurred at a later stage. However, given the fact that the cloud density had dropped below the background level (for debris $>$ 1 mm), it was thought unlikely.

Figure 2.8 shows the density of the simulated debris cloud and clearly shows the debris density reducing with time. This coincides with the three evolutionary stages of a debris

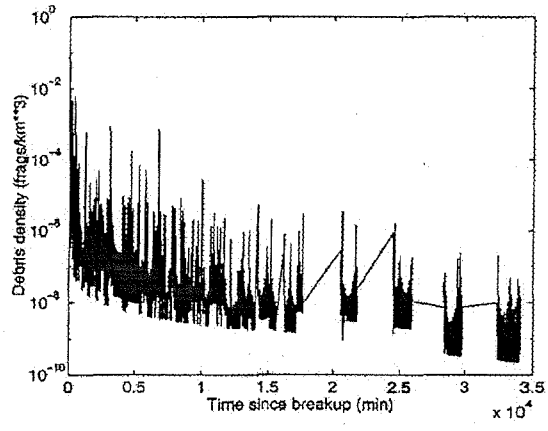

Figure 2.8: Density of simulated debris cloud [**26**]

cloud with a short-term hazard existing at the point of fragmentation and the long-term threat existing at the end of the simulation where the cloud density has dropped below that of the background density for that particular altitude.

2.3 The Future Situation

The future trend of the space debris environment will depend on whether the creation or removal of orbital debris dominates. In the past, the creation of orbital debris has dominated. Before we are able to determine the most effective mitigation measures to help in solving the space debris problem, it is essential to quantify the problem not only in terms of the current debris environment, but also in terms of its future growth. If the orbital debris population continues to grow, as it has done, then a critical level will be reached resulting in a number of random collisions, each producing even more fragments. When the rate of random collisions begins to exceed the removal rate, caused by natural decay, then the orbital debris population will begin to grow exponentially, as collision fragments themselves cause more collisions. This process is referred to as collision cascading [**1**] or as a chain reaction [**27**]. It is because of this potential dominance of uncontrollable random collisions that the need to establish guidelines on limiting orbital debris [**28**] and international debris mitigation practices [**29**] is paramount.

The following section discusses the space debris problem over the next century if mankind neglects to take any action on the problem. This type of scenario is usually referred to as 'business as usual', when no mitigation methods are implemented and the recent space traffic increase continues into the long-term future. A full breakdown is given in the next subsection of the debris source population for the 'business as usual' scenario as predicted by the ESA DELTA (Debris Environment Long Term Analysis) model [**30**] for both the LEO and GEO environments.

2.3.1 Business as Usual

If there were no debris mitigation measures implemented for future space activities then a continued growth of the large debris population will be expected over the next century. This is illustrated in Figure 2.9. The causes of such a growth would be attributed to the

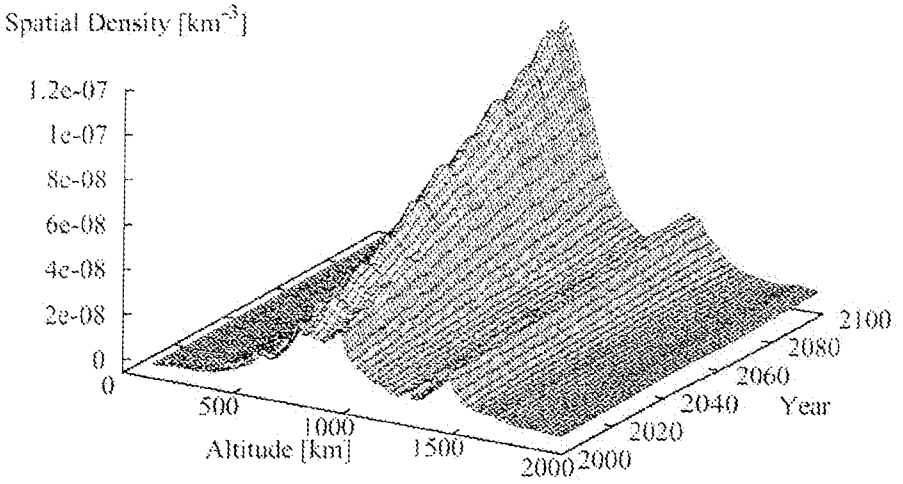

Figure 2.9: The spatial density evolution over altitude for LEO objects > 10 cm in size [5]

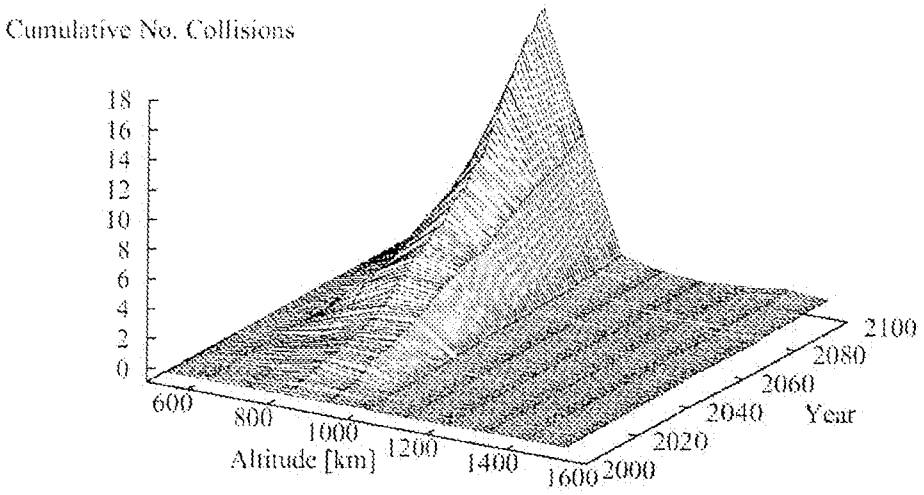

Figure 2.10: The cumulative number of collisions in LEO over altitude as predicted by the ESA DELTA model [5]

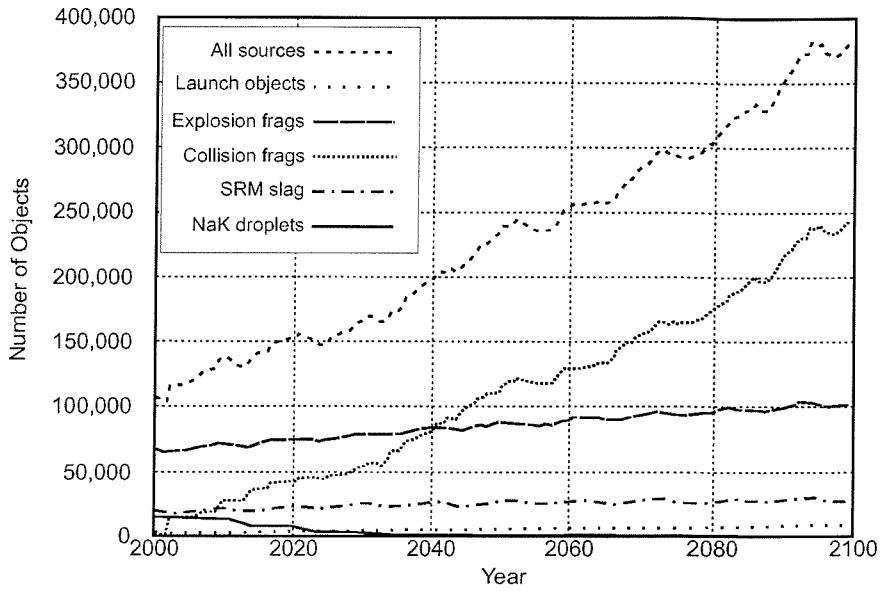

Figure 2.11: The evolution of the number of objects in LEO > 1 cm in size [**5**]

accumulation of launch and mission related objects and fragments produced from on-orbit fragmentation events. Unfortunately, such an increase would be sufficient to result in a growing number of collisions between these large objects in the LEO environment over the next century. These collisions would be most common in the highly-utilised 800 to 1,000 km altitude band, at near-polar inclinations - see Figure 2.10. The increase in collision activity over the next century would generate enough fragments to overwhelm all other debris sources in LEO. As a consequence, the population of the smaller debris objects would experience long-term exponential growth - see Figure 2.11.

Although no collisions were predicted by DELTA in the GEO region over the next century, the absence of any natural removal mechanism for debris objects can only result in an increase in population over time. Hence, if the increase in population goes unchecked over the centuries, then the onset of collision activity in GEO is to be expected.

The long-term evolution of the orbital debris environment is very sensitive to variations in the future traffic (launches and explosions), the introduction of new satellite constellation systems and nano-satellite swarms, and alterations to various aspects of satellite breakup models [**31**]. For example, if the future traffic rates increased by a factor of

two or more, then (without mitigation) the lethal centimetre sized debris population in LEO may increase by an order of magnitude or more over the next century.

The relationships used to model an on-orbit fragmentation event have been found to play a crucial part in the outcome of results produced by long-term debris environment models. These differ from one another, dependent upon the breakup model used. For example, the combination of different number, area-to-mass, and additional velocity distributions over fragment size can have a profound effect on the projected debris population over the next century. This was observed when the NASA 1998 breakup model [**32**] was used to generate fragments from explosions and collisions in the DELTA long-term projections. The results of the NASA breakup model produced many more collision fragments, and many more small explosion fragments compared to the older breakup models employed by DELTA. This led to significantly higher future population levels for the 'business as usual' scenario [**5**].

2.4 Mitigation Guidelines

In recent years there has been an increased awareness of the threats posed by the space debris environment. This realisation has resulted in the development of a number of mitigation guidelines [**28, 29**]. The aim of these mitigation guidelines is to help stabilise, or even reduce, the growth of orbital space debris. The most common categories of debris mitigation include:

- the prevention of on-orbit explosions and operational debris release,
- the reduction of particulates ejected from solid rocket motor firings, and
- the post-mission disposal of space systems.

The evaluation of such debris mitigation measures are associated with three major criteria:

- **Benefit** - The future collision rate must be stabilised, hence avoiding collision cascading and future exponential growth of the debris population. The population growth in operationally popular regions must also be brought under control by achieving stabilised or reduced levels of debris.

- **Risk** - The collision risk should be minimised over the long-term by keeping population levels as low as possible for all altitudes.
- **Cost** - The cost of mitigation measures should be kept to a minimum for all future space missions. This should also include the additional propellant requirements for post-mission disposal options.

The benefits of mitigation measures to the debris environment are clearly of primary concern, but at what risk and cost? Risk and cost are very important, but competing criteria. For example, a relatively low collision risk in the future will cost relatively more to achieve, and vice versa. Thus, a balance between them is essential to obtain an optimum, and to encourage commercial operators to implement such measures.

The consequences of performing mitigation measures such as passivation and post-mission disposal manoeuvres are considered in the following sections. Particular attention is paid to post-mission disposal manoeuvres, such as de-orbiting, directly or indirectly (placing the space system into a reduced orbital lifetime), and re-orbiting.

2.4.1 Passivation

The implementation of passivation would greatly reduce the amount of on-orbit explosions, which has been the dominant contributor of orbital debris in the past. Passivation procedures may include:

- burning or venting any residual propellants,
- venting all pressurised systems, and
- discharging batteries.

It is recommended by all space agencies to perform these mitigation measures, preventing further on-orbit explosions.

2.4.2 De-orbiting

The orbital lifetime for an object in LEO can be many thousands of years. Hence, to avoid the accumulation of large objects in LEO, a post-mission de-orbiting manoeuvre should be performed, either removing the spacecraft from orbit or placing it into

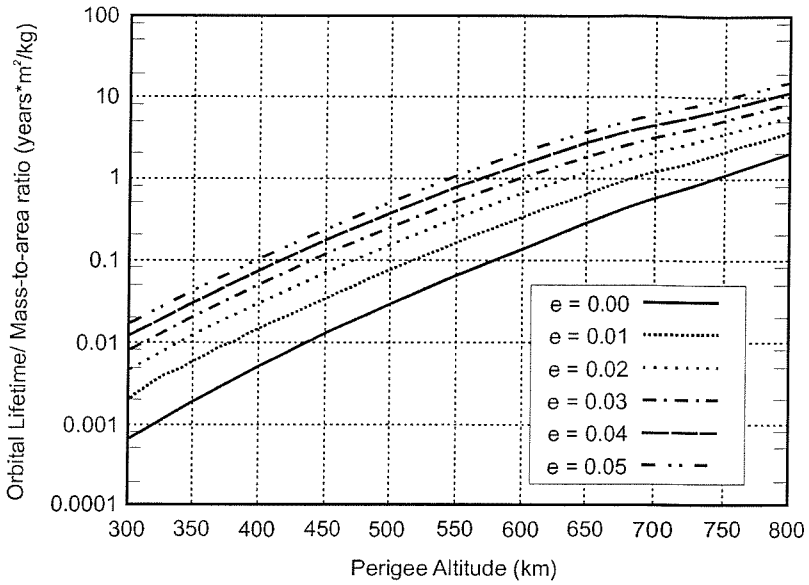

Figure 2.12: Orbital lifetime of LEO objects **[5]**

a reduced orbital lifetime. The ideal, and preferred method (as far as debris reduction is concerned), would be to perform a post-mission de-orbit manoeuvre completely removing the object from orbit. However, this can require a large amount of propellant, resulting in a shorter mission lifetime, and is not always feasible. Therefore, placing the spacecraft into an orbit with a reduced post-mission orbital lifetime is the next best solution and one that could significantly help in freeing-up the already over-populated debris environment.

Figure 2.12 illustrates the orbital lifetimes of near-circular LEO orbits (a constant medium solar activity defined by $F_{10.7} = 125 \times 10^{-22}$ W/m^2/Hz is assumed) **[5]**. For ESA's European Remote Sensing satellites, ERS-1 and ERS-2, that have near-circular orbits at altitudes of about 780 km, and mass-to-area ratios of about 75 kg/m^2, a post-mission orbital lifetime of about 100 years or more is to be expected. An analysis of the French SPOT-1 satellite, which operates at a similar orbit as ESA's ERS satellites, was shown to have a considerably shorter post-mission orbital lifetime of just 5 years when a number of apogee burns were performed to reduce its perigee altitude to 300 km.

A study by Walker et al **[5]** was performed to compare the de-orbiting capabilities of chemical and electrical propulsion systems in near-circular LEO orbits. The study also considers two different mass-to-area ratios of 20 kg/m^2 and 200 kg/m^2. The results

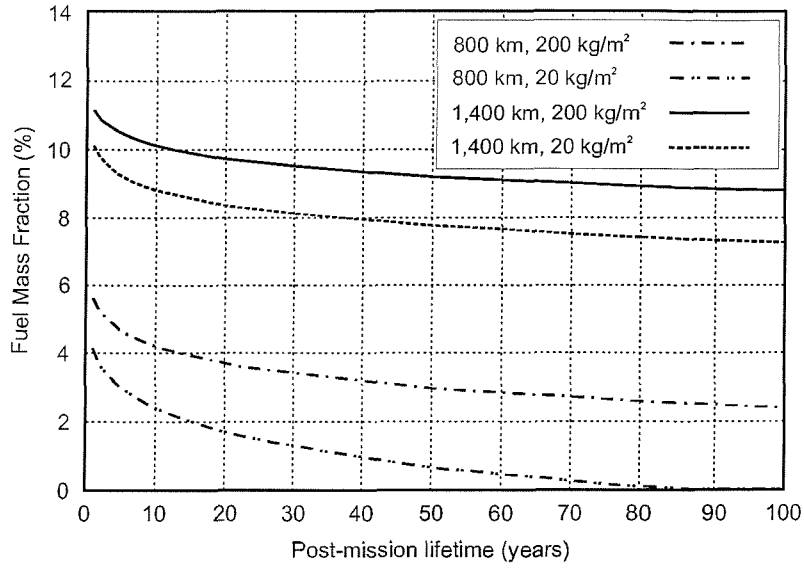

Figure 2.13: Fuel mass fraction versus post-mission lifetime for chemical propulsion [5]

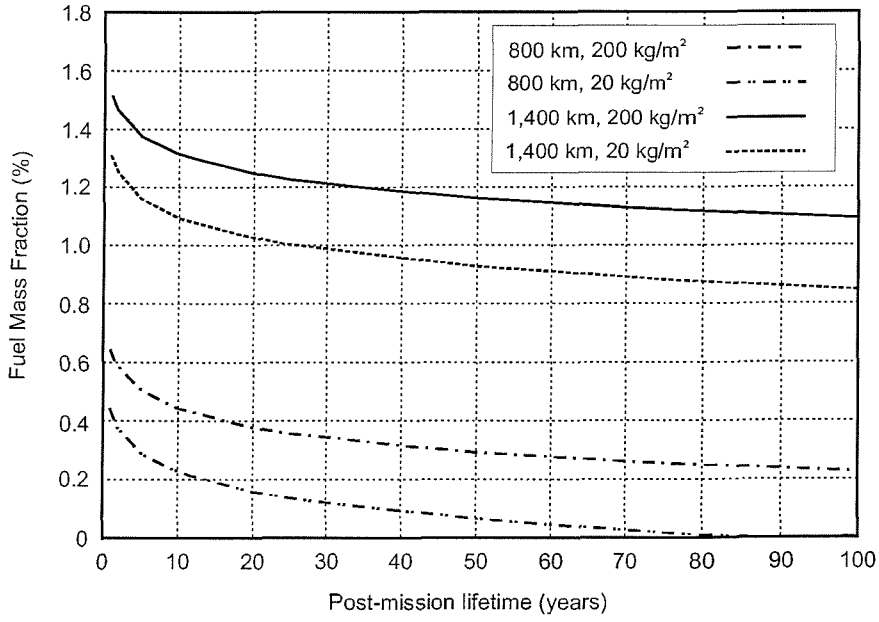

Figure 2.14: Fuel mass fraction versus post-mission lifetime for electrical propulsion [5]

indicated that electrical propulsion systems consumed nearly an order of magnitude less fuel (in terms of mass) than chemical propulsion systems to place the space system into the required post-mission orbital lifetime orbit - see Figures 2.13 and 2.14. This is particularly significant for altitudes around 1,400 km where the chemical fuel mass fraction is on the order of 8 to 11% of the host spacecraft. However, an electric propulsion system requires a more massive electrical power system which will have to be traded against fuel mass savings. Therefore, the net fuel mass savings plus any extra costs to achieve a reliable reduced post-mission orbital lifetime will be one of the main determining factors for choosing electric propulsion over chemical propulsion.

An interesting attribute from Figures 2.13 and 2.14 is the exponential characteristic for post-mission orbital lifetimes of less than 25 years. However, a reduction of post-mission orbital lifetime from 100 to 25 years requires just a low gradient linear increase in fuel mass fraction. Hence, a post-mission orbital lifetime of 25 years is recommended to prevent disproportionate increases in the fuel requirements.

2.4.3 Re-orbiting

Performing an orbital manoeuvre to reduce the post-mission orbital lifetime for a space system operating at an altitude of 1,400 km can be quite costly. Hence, the re-orbiting of such systems into a higher disposal orbit, around 2,000 km, was studied by Walker et al **[5]** - see Figure 2.15. They concluded, at the time of writing, that the collision activity of such re-orbiting procedures would be negligible over the next century. However, due to the lack of any natural removal mechanisms at these higher disposal orbits, these objects would remain long-term collision hazards for many centuries to come, allowing the region to reach a state of collisional instability easily, through overuse or by poor passivation. It is advised therefore to perform this manoeuvre only in exceptional circumstances, when placing a space system into an orbit with a reduced post-mission orbital lifetime is not feasible. However, re-orbiting is the only manoeuvre possible in GEO, at present. The DELTA model has shown that such re-orbiting mitigation measures can help to stabilise the potential collision risk in GEO, with no collisions being recorded by the DELTA model in the GEO ring over the next century **[5]**.

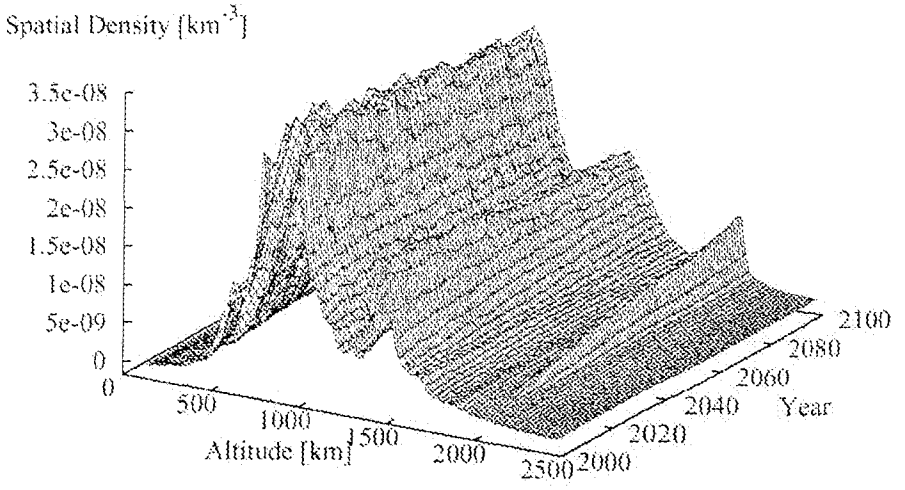

Figure 2.15: The spatial density evolution over altitude of objects > 10 cm in LEO for the LEO re-orbiting scenario [5]

2.5 Forecasting and Protection

With the increased awareness of the threat posed by orbital debris, spacecraft designers and mission operators are learning that mission lifetime collision risks are already moderate in some regions of LEO. Hence, for future mission success these risks must be properly assessed. If the mission collision risks are unacceptably high, then they must be effectively mitigated through changes to the mission (e.g. orbit selection) or spacecraft shielding.

The following sections consider the collision risks associated with spacecraft over the next century in LEO and GEO. The discussion also considers the various methods of protection that could be implemented to aid with reducing such risks.

2.5.1 Long-Term Forecasting

Two scenarios were considered by Walker et al [5] using the DELTA model to consider the effect of various mitigation measures on the future impact flux of LEO objects over the next century. The first was a low altitude manned mission at 450 km, with an inclination of 51.5°. The second was a remote sensing type mission in a sun-synchronous orbit inclined at 98.5° with an altitude of 800 km. It was found for the 'business as

usual' remote sensing mission, that the impact flux arising from the centimetre sized objects, was initially dominated by explosion fragments and NaK droplets. However, with relatively high decay rates these were quickly overtaken by the rapidly growing collision fragment source. For objects greater than 10 cm in size the impact flux to the remote sensing mission is initially dominated by explosion fragments and launch related objects. However, by the end of the century, large collision fragments may begin to dominate. Therefore, it was concluded that post-mission disposal is the most effective mitigation measure for such remote sensing mission scenarios, because it stabilises the risk from launch related objects and the rate of collisions.

For the manned mission, it was found that the impact flux arising from the centimetre sized objects was dominated by SRM slag particles and explosion fragments throughout the simulation. However, at the end of the simulation, fragments produced from collisions had grown to a similar level. For objects greater than 10 cm in size the impact flux is dominated by launch related objects and fragments produced from explosions decaying through the 450 km altitude band. Therefore, the most effective mitigation methods, for a low altitude man mission, would be passivation, SRM slag prevention and post-mission disposal to aid in reducing the smaller collision fragment population - see Figure 2.16. An unavoidable side effect of post-mission disposal of LEO objects, by lowering perigee altitude to ensure decay within a limited lifetime, is the increase of impact flux from larger objects along the lifetime limitation timescale (e.g. 25 years), which then stabilises at a higher level. It was found that longer post-mission orbital lifetimes produced higher stabilised flux levels - see Figure 2.17. The stabilised impact flux for the 25-year disposal de-orbit only slightly exceeds the 'business as usual' case scenario over the next half a century. Thereafter, the relative risk is lower. Any increase in the population due to de-orbit manoeuvres will not present an increase in collision risk since these large objects can be tracked and easily avoided by implementing the usual collision avoidance manoeuvres for manned missions. Hence, a 25-year post-mission orbital lifetime was found to provide a good compromise, for higher altitude missions, between:

- a 100-year post-mission orbital lifetime, of higher station manoeuvre cost and lower de-orbit cost, and
- a 10-year post-mission orbital lifetime, of lower station manoeuvre cost and higher

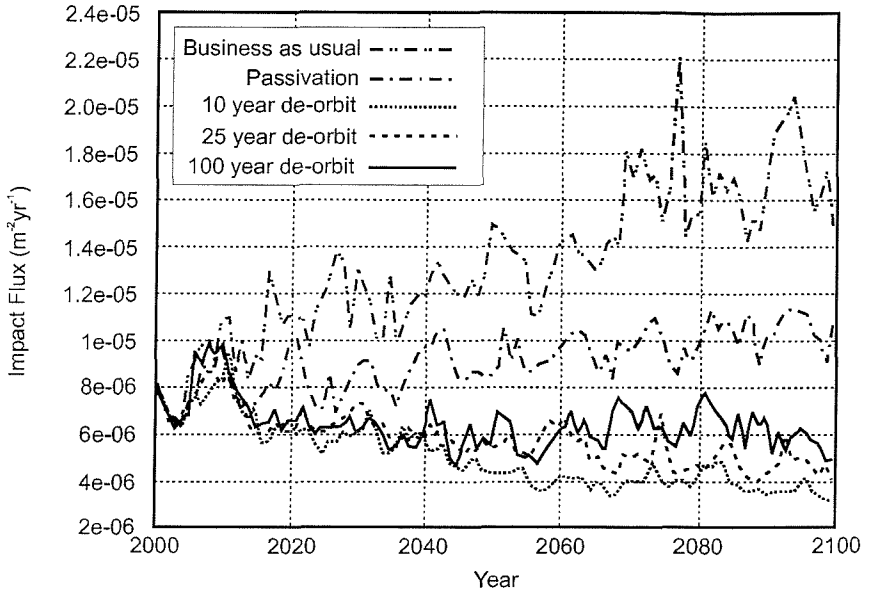

Figure 2.16: Total impact flux to a manned mission orbit for objects > 1 cm in size using various mitigation methods [**5**]

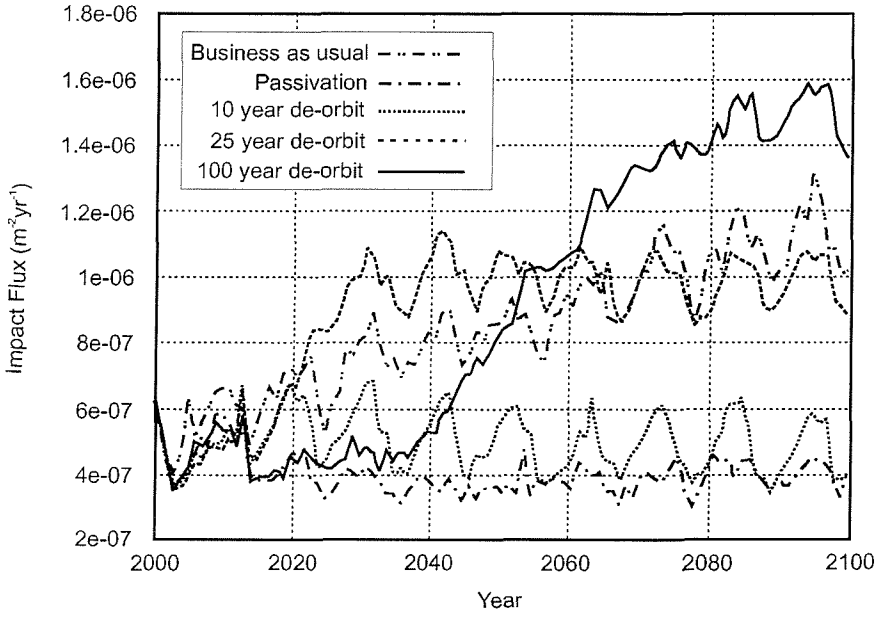

Figure 2.17: Total impact flux to a manned mission orbit for objects > 10 cm in size using various mitigation methods [**5**]

de-orbit cost.

For GEO missions, it was predicted that the impact flux concerning the centimetre sized objects, such as slag particles from solid motor firings, would dominate. Hence, introducing SRM slag prevention as a mitigation measure would help to contain the flux levels. For objects greater than 10 cm in size, the launch related objects are predicted to dominate. Hence, removal of space systems from the GEO region via re-orbiting to higher altitudes, combined with passivation, would be the most effective mitigation measure to control the growth in debris flux levels.

2.5.2 Spacecraft Protection

Protection of a spacecraft can be achieved using either passive or active protection. Passive protection strategies physically protect the spacecraft during a debris encounter by the use of shields. Current methods involve shielding the entire spacecraft or vital spacecraft components which if damaged may result in mission failure. Shields vary in design from the simple Whipple bumper, located at the front of the spacecraft wall, to complex layers of metal and ceramic/polymer fabrics that are designed to absorb the energy of particles resulting from the initial impact. A space station, for example, may use a stand off aluminium shield approximately 0.16 cm thick, with 30 layers of Mylar thermal insulation covering the structural wall. Such designs have been shown to protect against a collision of debris particles up to 0.5 cm in size **[33]**, although this will also depend on the impact energy.

Active protection involves the spacecraft performing a burn to physically avoid a debris encounter. However, collision avoidance is not an easy procedure and involves the following requirements:

1. debris detection,
2. debris orbit determination,
3. spacecraft preparation for manoeuvre,
4. manoeuvre execution, and
5. returning spacecraft to normal operations.

Identifying a debris fragment that will actually threaten the spacecraft in question whilst allowing time to perform an avoidance manoeuvre is a very difficult task. One method is passive sensing using optical or infrared sensors. For example, a visible light sensor with a 0.1 m^2 aperture will be able to detect a 1 cm object illuminated by the Sun 100 km away (depending upon albedo) . For objects hidden by the Earth's shadow, an infrared sensor with a 0.5 m^2 aperture would provide adequate detection at a range of 100 km. Another method involves the use of a space-based system for tracking objects and relaying their position and velocity to other satellites. The advantage of using this method over on-board sensors is the ability to provide an early warning [**33**].

For the US Space Shuttle Orbiter, an alert box measuring 5 km $\times$ 25 km $\times$ 5 km (radial $\times$ along-track $\times$ out-of-plane) is centred on the Space Shuttle position. A debris object predicted to pass within this alert box initiates increased sensor tracking and improved orbit determination. If an improved fly-by prediction indicates that the object will pass through a manoeuvre box measuring 2 km $\times$ 5 km $\times$ 2 km, an avoidance manoeuvre is performed.

The probability of a collision between an object greater than 10 cm and the Space Shuttle (in the case of no avoidance procedure) is of the order of 1 in 200,000 for a 10 day mission duration [**5**]. For objects that can not be tracked (i.e. less than 10 cm) the probability is of the order of 1 in 2,000. The impact velocity for objects greater than 1 cm and the Space Shuttle is typically of the order of 9 km/s. Between the STS-26 and STS-85 missions, a total of six collision avoidance manoeuvres were performed.

2.6 Discussion

Before discussing the implications of introducing a space tether system into Earth orbit, it is worth highlighting the important findings from this chapter. The first point to note is that collision risks associated with orbital debris in LEO is now considered to exceed the collision risks from the meteoroid population, with the exception of smaller objects less than around 0.1 mm in size. However, the opposite is probably true for GEO [**34, 35**]. The spatial density in LEO is altitude and inclination dependent with peak densities occurring at altitudes of 800 to 1,000 km and 1,400 to 1,500 km and at near-polar inclinations. These are popular operational orbits, and this trend will continue

into the foreseeable future. As such the impact risk in such orbits will continue to increase. However, with the implementation of appropriate mitigation measures, such as post-mission de-orbiting, the growth of orbital debris may be controlled.

There exists a certain amount of uncertainty in the long-term evolution of the orbital debris environment, although it is possible to predict collision fluxes with specific satellites over a range of scenarios using debris models such as SDS, DAMAGE and DELTA. Although these models can give estimates of the collision flux a satellite may experience during its mission, the probability of mission failure is still uncertain.

In recent years, a number of proposals regarding space tether systems have been considered. However, the introduction of such a device into the space debris environment comes with a new set of problems. Unlike a typical satellite, a space tether system may be many kilometres in length, resulting in a very large cross-sectional area. A space tether system would also lack vital shielding material, making it susceptible to the small debris population, where just one impact may result in mission failure. Hence, a good understanding of the interaction between a space tether system and the space debris environment is of exceptional importance.

Chapter 3

Space Tether Systems

The concept of using tethers in space was first proposed by Konstantin Tsiolkovsky after seeing the Eiffel Tower in 1895 [**36**]. He imagined a space tower extending from the Earth's surface to a geosynchronous orbit. Tsiolkovsky envisaged a 'celestial castle' orbiting at 35,800 km at the end of a spindle shaped cable with an elevator riding up the cable to the 'castle'. Almost 100 years later, Arthur C. Clarke [**37**] gave the concept of Tsiolkovsky's space elevator greater public awareness.

A 'spin-off' use of Tsiolkovsky's tower would be the ability to launch objects into orbit without the use of a rocket. With the elevator attaining orbital velocity as it rode up the cable, an object released at the top of the tower would also have the orbital velocity required to sustain a geosynchronous orbit [**38**]. However, constructing such a tower proved to be an impossible task, since it was determined that the material required to build such a tower would be twice the strength of any existing material including graphite, quartz and diamond [**38**]. Hence, Tsiolkovsky's space tower will remain in the realm of science fiction until new materials can be developed.

Although Tsiolkovsky's idea is somewhat impractical, the use of tethers in space offers a variety of practical applications. In recent years a number of proposals regarding the use of tethers in space have been put forward. Such proposals have included using such devices for boosting the International Space Station's orbit, removing the need for the expensive procedure of delivering the necessary propellant supply. More advanced proposals of using space tether systems for Jovian exploration are also being considered. Another concept is the use of space tethers to help relieve the space debris problem. The

idea is to attach an electrodynamic space tether system to a satellite which would be deployed after the mission has been completed. The interactions between the current-induced magnetic field of the tether and the Earth's magnetic field causes a Lorentz force, which opposes the motion of the tether. This would result in the satellite having a reduced orbital lifetime, freeing up the space it once occupied. It has been predicted that a tether system weighing just 1 to 2% of the host spacecraft may de-orbit an Iridium-type satellite, from an 850 km altitude, 50° inclined orbit, within about 3 months. Without the electrodynamic tether system, such a satellite may be in orbit for hundreds of years before atmospheric drag finally reduces the satellite's orbit height enough to cause re-entry and subsequent burn-up.

The introduction of electrodynamic tether systems to help resolve the space debris problem sounds like the ideal solution. However, space tethers are very susceptible to debris impacts. A single strand tether system introduced into the space debris environment, for example, has been predicted to have a lifetime of just a few days. This prediction was justified during the Small Expendable Deployer System (SEDS-2) mission when the tether was severed, allegedly by a micro-meteoroid, 3.7 days after deployment. A number of tether system designs have since been proposed, such as double strand and multi-strand tether systems, increasing a tether systems overall survivability in the space debris environment.

3.1 Tether Basics

A simple space tether system consists of a long cable that is used to couple two satellites to one another allowing the transfer of energy and momentum from one to the other. The tether is usually composed of thin strands of high strength fibres such as Spectra or Kevlar.

The following sections discuss two types of tether designs, mechanical and electrodynamic, with particular attention being paid to momentum transfer by mechanical tether systems, and propulsion and drag by electrodynamic tether systems.

3.1.1 Mechanical Tether Systems

A mechanical tether system consists of a long cable that is used to couple two objects together. The tether is deployed by pushing one of the objects up or down from the other. Once the two objects are separated by a sufficient distance, the gravitational force difference at the two locations will cause the objects to be 'pulled' apart. This is referred to as the 'gravity gradient force'. The tether can then be released at a controlled rate, pulled by the tension caused by the gravity gradient force. Once deployed the tether will have an equilibrium orientation that is aligned vertically if no other forces are acting on the tether. A mechanical tether system offers the possibility of multi-point atmospheric research and momentum transfers.

Momentum Transfers

A momentum exchange tether system allows momentum and energy to be transferred from one object to the other. An analysis performed by Lee-Bapty **[39]** demonstrated that the separation distance between two objects, half an orbit after tether release, is about seven times the initial length of the tether. This analysis is outlined below.

Consider two satellites, of equal masses, in a circular Keplerian orbit, connected by a tether. The two objects are then forced to orbit with an angular velocity equal to that of the tether system's centre of mass. This is given by

$$n = \sqrt{\frac{\mu}{R_0^3}}, \tag{3.1}$$

where R_0 is the position of the centre of mass and μ is Earth's gravitational constant. Therefore, the upper mass has an orbital velocity, V_u, which is higher than its local circular orbit speed, given by

$$V_u = n(R_0 + r_u) = nR_u, \tag{3.2}$$

where r_u is the distance from the tether system's centre of mass to the upper mass. Similarly, the lower mass would have a velocity, V_l, which is lower than its local circular orbit speed, given by

$$V_l = n(R_0 - r_l) = nR_l, \tag{3.3}$$

where r_l is the distance from the tether system's centre of mass to the lower mass. Note that $r_u + r_l = L$, where L is the total length of the tether. Hence, disconnecting the

tether would cause the two end-masses to become 'free-flyers' and would release them into new elliptical orbits. The upper mass, with its higher than local orbital velocity, at the disconnection point, would be at the perigee of its new orbit, while the lower mass would be at the apogee of its new orbit. The upper mass perigee position and velocity would be given by

$$R_{up} = R_u, \tag{3.4}$$

and

$$V_{up} \equiv V_u = \sqrt{\frac{\mu}{R_0^3}} R_u. \tag{3.5}$$

Similarly, the lower mass apogee position and velocity would be given by

$$R_{la} = R_l, \tag{3.6}$$

and

$$V_{la} \equiv V_l = \sqrt{\frac{\mu}{R_0^3}} R_l. \tag{3.7}$$

To obtain the apogee position of the upper mass, R_{ua}, and the perigee position of the lower mass, R_{lp}, we use the energy equation

$$\begin{aligned} V^2 &= \mu \left(\frac{2}{R} - \frac{1}{a} \right) \\ &= \frac{\mu}{aR} \left(2a - R \right), \end{aligned} \tag{3.8}$$

where $a = (R_p + R_a)/2$ is the semi-major axis. Thus at perigee we have

$$V_p^2 = \frac{2\mu R_a}{R_p(R_p + R_a)}, \tag{3.9}$$

or conversely

$$R_a = \left[\left(\frac{2\mu}{R_p V_p^2} \right) - 1 \right]^{-1} R_p. \tag{3.10}$$

Similarly, at apogee we have

$$V_a^2 = \frac{2\mu R_p}{R_a(R_p + R_a)}, \tag{3.11}$$

and

$$R_p = \left[\left(\frac{2\mu}{R_a V_a^2} \right) - 1 \right]^{-1} R_a. \tag{3.12}$$

Therefore, substituting for R_p and V_p from Equations (3.4) and (3.5) into (3.10) for the

upper mass we get

$$\begin{aligned} R_{ua} &= \left[2\left(\frac{R_0}{R_u}\right)^3 - 1\right]^{-1} R_u \\ &= \left[2\left(1 - \frac{r_u}{R_u}\right)^3 - 1\right]^{-1} R_u \\ &= R_0 + 7r_u + \mathrm{O}\left(\frac{L}{R}\right)^2, \end{aligned} \tag{3.13}$$

since $R_u = R_0 + r_u$. Similarly, substituting for R_a and V_a from Equations (3.6) and (3.7) into (3.12) for the lower mass we get

$$\begin{aligned} R_{lp} &= \left[2\left(\frac{R_0}{R_l}\right)^3 - 1\right]^{-1} R_l \\ &= \left[2\left(1 + \frac{r_l}{R_l}\right)^3 - 1\right]^{-1} R_l \\ &= R_0 - 7r_l + \mathrm{O}\left(\frac{L}{R}\right)^2, \end{aligned} \tag{3.14}$$

since $R_l = R_0 - r_l$. Hence, the distance between the apogee of the upper mass and the perigee of the lower mass is

$$\begin{aligned} R_{ua} - R_{lp} &= 7(r_u + r_l) + \mathrm{O}\left(\frac{L}{R}\right)^2 \\ &= 7L + \mathrm{O}\left(\frac{L}{R}\right)^2. \end{aligned} \tag{3.15}$$

Hence, the separation distance between the two end-masses half an orbit after disconnection is approximately seven times the length of the tether. Equations (3.13) and (3.14) also show that objects released from a hanging tether will have an apogee or perigee approximately seven times its initial height above or below the tether system's centre of mass, respectively. This distance can be significantly increased by introducing a swinging tether for additional boost.

A momentum exchange tether system could significantly reduce the launch cost by allowing the transfer of energy and momentum between an upper stage and its payload. While the payload gets an additional boost into a higher orbit, the upper stage will be placed into a lower orbit, resulting in a quicker re-entry and subsequent burn-up.

3.1.2 Electrodynamic Tether Systems

An electrodynamic tether system consists of a long conducting wire that is extended from a spacecraft. The tether system will then interact with the Earth's magnetic field

lines during its orbit. This motion of a conductor across the magnetic field induces a current along the length of the tether. The associated voltage can be up to several hundred volts per kilometre. Electrodynamic tether systems can be used for reducing or increasing the altitude of an object's orbit.

Drag System

In an electrodynamic drag system, the tether can be used to reduce the spacecraft's orbital altitude. This is achieved by collecting electrons from the ionospheric plasma at one end of the tether and expelling them back into the plasma at the other end of the tether. This allows the voltage to drive a current along the length of the tether. The current will produce a magnetic field which, in turn, will interact with the Earth's magnetic field causing a Lorentz force. This opposes the motion of the tether (and whatever is attached to it) so reducing the orbit height. Essentially, the tether converts orbital energy of the host spacecraft into electrical power, which is dissipated as ohmic heating in the tether. Figure 3.1 illustrates an electrodynamic drag system.

An electrodynamic tether drag system could provide an excellent resource to aid in the reduction of orbital debris, while providing potential cost savings. For example, attaching a tether and deployer system onto future satellites will remove the need to preserve on-board fuel for de-orbit manoeuvres at the end of its operational lifetime. This will result in longer mission lifetimes and lower operational costs.

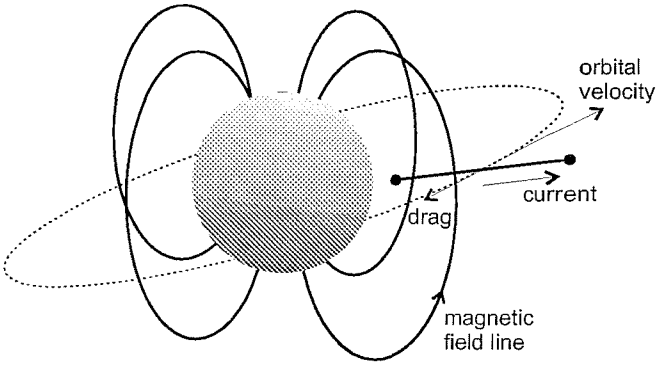

Figure 3.1: Electrodynamic drag system [**40**]

Propulsion System

In an electrodynamic propulsion system, the tether can be used to increase the altitude of the spacecraft's orbit. This is achieved by introducing a power supply to the tether system. The power supply is then used to drive the current in the opposite direction to which it would normally flow, hence 'pushing' against the Earth's magnetic field, raising the orbit of the tether system. The major advantage of propulsion tether systems over conventional space propulsion systems is that they require no extra propellant. This however must be traded against the cost and mass of the required power system. For example, a high voltage power supply (HVPS), producing 10 kW of electrical power to a 10 km long tether, would have an estimated mass of about 80 kg [41]. Figure 3.2 illustrates an electrodynamic propulsion system.

Provided that the cost and mass of the HVPS can be minimised, an electrodynamic propulsion system could significantly reduce launch costs, by reducing the amount of propellant required to deliver a payload to orbit. For example, a payload could be launched into LEO, where it would then deploy the tether system, producing electrodynamic propulsion, to deliver it to its final destination. This form of propulsion would also reduce the launch mass of the payload, reducing launch costs even further.

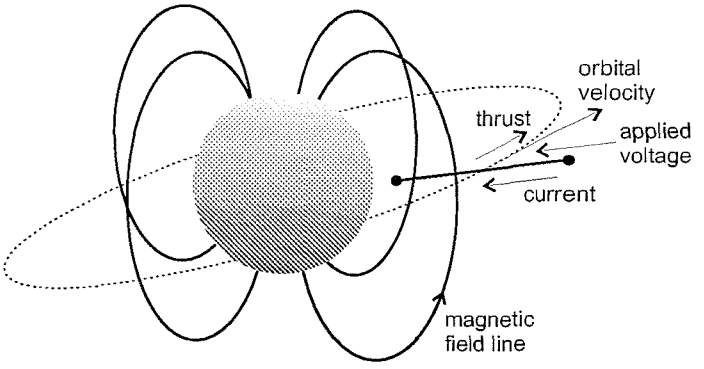

Figure 3.2: Electrodynamic propulsion system [40]

3.2 Tether Missions

The first use of tethers in space occurred during the Gemini XI and XII missions in 1966. Gemini XI was attached to an Agena rocket by a 30 m tether. Its thrusters were then fired perpendicular to the line of the tether, creating a cartwheel motion of the two spacecraft and producing a small amount of artificial gravity (0.00015 g). The Gemini XII mission made use of a tether to assess the feasibility of using a gravity gradient force to stabilise a manned spacecraft in a similar way to a dumb-bell type satellite [**39**].

It was not until 1974 when Giuseppe Colombo and Mario Grossi first proposed the Skyhook project that the use of extremely long tethers (hundreds of kilometres long) were seriously considered [**42**]. The proposal was for the Space Shuttle to deploy a satellite attached to a 100 km long tether. The Space Shuttle would be in orbit at an altitude of around 200 km with the satellite deployed vertically below. This would provide a platform for experiments to investigate the atmosphere, magnetosphere and gravity field at a height of 100 km, a region only attained by other means for limited periods.

The following section considers past tether missions, paying particular attention to those missions that have proved vital for laying down the foundations for future missions. Some future proposals for using tethers in space will also be discussed.

3.2.1 Past Missions

There have been a number of tether missions to date, and these are summarised in Table 3.1. As part of these missions, important milestones for tether research were achieved. In particular, the Tethered Satellite System, the Small Expendable Deployer System, the Plasma Motor Generator and the Tether Physics Survivability Spacecraft were very important missions in demonstrating a space tether system's ability to function in the harsh space environment.

The Tethered Satellite System

The Tethered Satellite System (TSS) [44] was first proposed to NASA and the Italian Space Agency (ASI) in 1974 by Giuseppe Colombo and Mario Grossi. Two missions,

Name	Date	Orbit	Length	Comments
Gemini XI	1966	LEO	30 m	spin stable, 0.15 rpm
Gemini XII	1966	LEO	30 m	local vertical, stable spin
H-9M-69	1980	sub-orbital	500 m	partial deployment
S-520-2	1981	sub-orbital	500 m	partial deployment
Charge-1	1983	sub-orbital	500 m	full deployment
Charge-2	1984	sub-orbital	500 m	full deployment
ECHO-7	1988	sub-orbital	?	magnetic field aligned
Oedipus-A	1989	sub-orbital	958 m	spin stable, 0.7 rpm
Oedipus-2B	1992	sub-orbital	500 m	full deployment
TSS-1	1992	LEO	< 1 km	electrodynamic, partially deployed, retrieved
SEDS-1	1993	LEO	20 km	downward deployment, swing and cut
PMG	1993	LEO	500 m	electrodynamic, upward deployment
SEDS-2	1994	LEO	20 km	local vertical stable, downward deployment
Oedipus-C	1995	sub-orbital	1 km	spin stable, 0.7 rpm
TSS-1R	1996	LEO	19.6 km	electrodynamic, severed
TiPS	1996	LEO	4 km	long life tether on orbit
ATEx	1999	LEO	< 1 km	partial deployment

Table 3.1: Past tether missions [**43**]

TSS-1 and TSS-2 were planned, the second of which closely resembled that first envisaged by Colombo and Grossi. However, due to a malfunction in the deployer mechanism of TSS-1, the second mission was cancelled and replaced with a re-flight of the first, TSS-1R. The purpose of the TSS missions was to provide a method of deploying a satellite on a long, gravity gradient stabilised tether from the Space Shuttle, providing a research facility for investigations in space physics and plasma electrodynamics. Figure 3.3 illustrates the TSS-1 satellite and tether attached to a 12 m boom extending from the Space Shuttle Orbiter.

TSS-1 was launched on July 31st, 1992 on STS-46, into a nominal orbit of 297 km altitude. Due to a malfunction in the tether deployer mechanism, however, the satellite was only deployed 268 m away from the Shuttle instead of the allotted 20 km. Despite this setback, over 20 hours of stable deployment in the near vicinity of the Space Shuttle Orbiter was achieved, the operational mode of greatest concern prior to the mission. The TSS-1 results conclusively showed that the basic concept of long gravity gradient stabilised tethers was sound, and settled several short deployment dynamics issues. They also reduced safety concerns and clearly demonstrated the feasibility of deploying

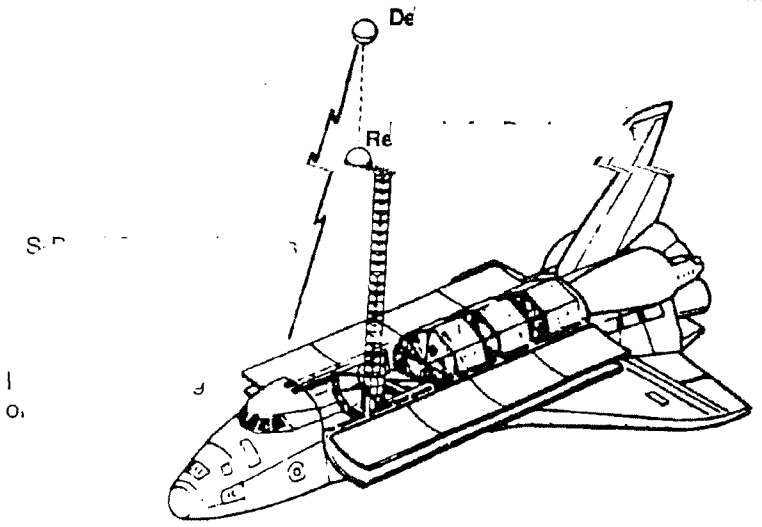

Figure 3.3: TSS satellite and tether attached to 12 m extendible boom [45]

the satellite to long distances [45].

TSS-1R, a re-flight of the first, was launched on February 22nd, 1996 on STS-75. However, after about 19.5 km of deployment the tether broke due to overheating of a weak spot in the tether's insulation. The satellite was intended to have been deployed 20 km above the Space Shuttle on a conducting tether where it would have remained for more than 20 hours to perform scientific experiments. This was to be followed by a second stop for an additional seven to nine hours of experimentation at a deployed distance of 2.5 km. However, during the deployment phase, which lasted more than five hours, significant science experimental activities had already been accomplished. Such activities included the measurement of the electromotive force (emf) generated by the motion of the tether through the Earth's magnetic field, satellite potential, tether current, charged particle distributions, and electric and magnetic fields [45]. The mission also demonstrated, inadvertently, the orbit raising capabilities of a tether when disconnected.

The Small Expendable Deployer System

The Small Expendable Deployer System (SEDS) [46] begun as a Small Business Innovative Research contract awarded to Joe Carroll by NASA. Two missions, SEDS-1 and

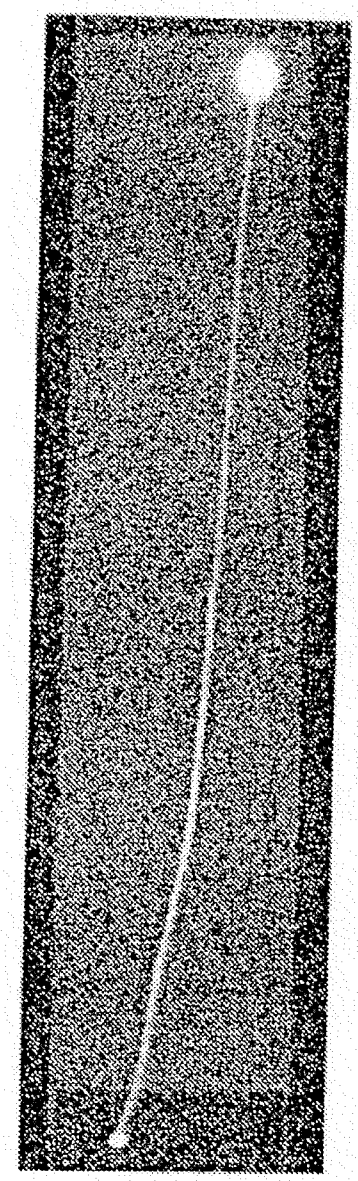

Figure 3.4: SEDS-2 tether in orbit with Delta II second stage at the top and end-mass at the bottom [47]

SEDS-2, were planned to fly as secondary payloads on board a Delta II launch vehicle. The purpose of the missions was to demonstrate the capabilities of de-orbiting a 25 kg payload from LEO (SEDS-1) using momentum transfer, and to study the use of a closed-loop control law to deploy a tethered payload along the local vertical (SEDS-2).

SEDS-1 was launched on March 29th, 1993, into a 195 × 705 km elliptical orbit, inclined at 34°. The mission was a complete success and demonstrated that SEDS hardware could be used to deploy a payload at the end of a 20 km long non-conducting tether. The re-entry prediction, after tether disconnection, was so accurate that a pre-positioned observer was able to videotape the payload re-entry and subsequent burn-up [47].

Following the success of SEDS-1, SEDS-2 was launched on March 9th, 1994, into a circular orbit at an altitude of 350 km. The mission successfully demonstrated that using a closed-loop control law, the tether could be deployed in a controlled manner reducing the libration along the local vertical. Afterwards, the tether was left attached to the Delta II second stage to study long term tether stability and micro-meteoroid impact risks. Unfortunately, the tether was severed, allegedly by a micro-meteoroid, 3.7 days after deployment which resulted in the payload re-entering within hours (due to increased area to mass ratio and momentum transfer). Approximately 7.2 km of tether remained attached to the Delta II second stage, and this survived with no apparent further breaks until re-entry on May 7th, 1994 [45]. SEDS-2, shown in Figure 3.4 before the sever event, was an easy naked eye object when viewed from the ground.

The Plasma Motor Generator

The Plasma Motor Generator (PMG) [48] experiment was designed to test the feasibility of using a hollow cathode assembly (HCA) to provide a low impedance bipolar electrical current between a spacecraft and the ionosphere [45]. The purpose of the mission was to demonstrate that such a configuration could function as either an orbit-boosting motor or as a generator converting orbital energy into electricity - see Figure 3.5.

PMG was launched on June 26th, 1993, as a secondary payload on a Delta II launch vehicle into an elliptical orbit of altitude 193 × 869 km, inclined at 25.7°. The PMG experiment duration, in terms of plasma contactor operation and consequential active environment interaction, lasted for about seven hours, until the batteries died. The experiment showed that a current can be fully reversible, operating either as a generator

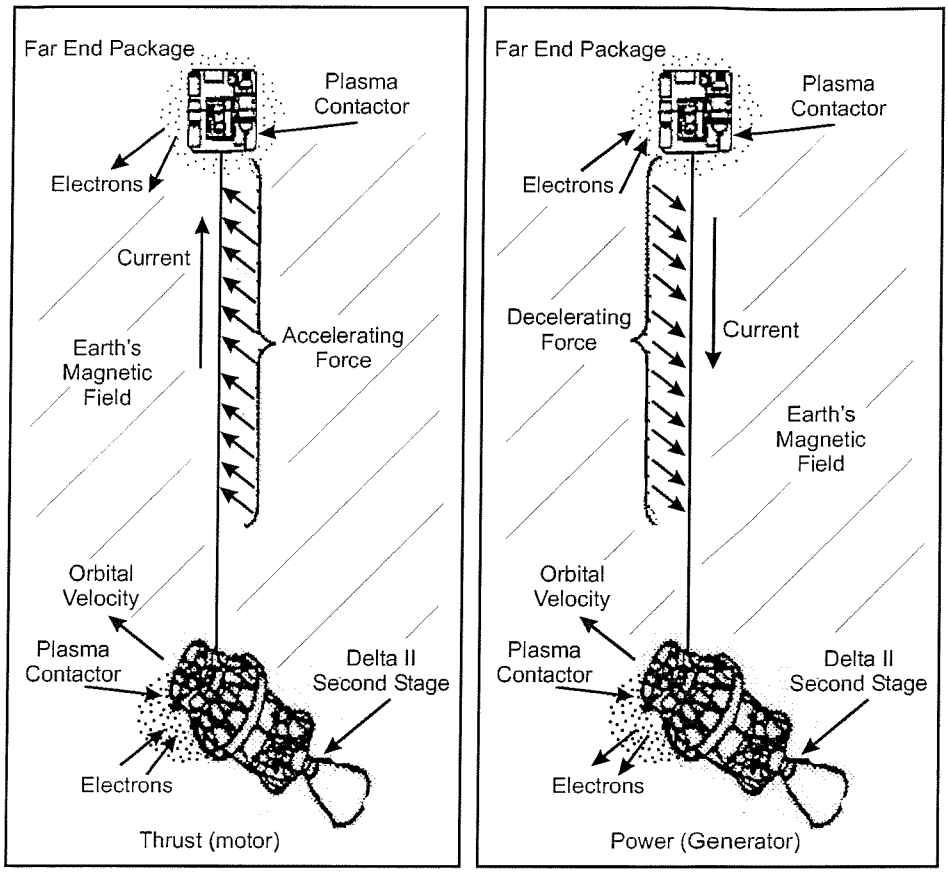

Figure 3.5: PMG system configuration **[45]**

system with electron current flow down the tether or as a motor with electron current driven up the tether.

The Tether Physics and Survivability Spacecraft

The Tether Physics and Survivability Spacecraft (TiPS) **[49, 50]** was designed to study the long term dynamics and survivability issues of tethered satellite systems. The experiment was a free flying satellite consisting of two end-bodies connected by a 4 km non-conducting tether - see Figure 3.6. The purpose of the mission was to study long term orbit and attitude dynamics and tether survivability issues.

TiPS was launched on June 20th, 1996, into a near-circular orbit at an altitude of 1,022 km, inclined at 63.4°. TiPS has provided a great deal of confidence in our ability to model tether dynamics. The experiment has also shown that tethers can be designed

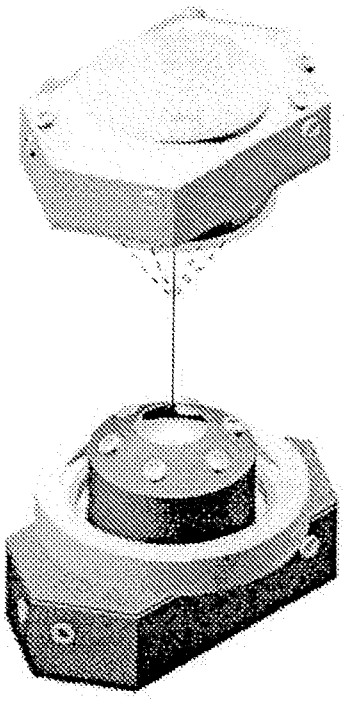

Figure 3.6: TiPS experiment in deployed configuration [**50**]

to survive the harsh space environment for long periods of time.

3.2.2 Future Proposals

Space tether systems have a strong potential for providing significant reductions in the cost of propulsion for a number of important applications, including spacecraft deployment, post-mission disposal, and satellite orbital maintenance. Such future proposals include the planned Propulsive Small Expendable Deployer System experiment. This will make use of the flight proven SEDS deployer system to deploy a 5 km bare copper tether, with an additional 10 km of Spectra, from a Delta II second stage. Hence, the interaction between the bare wire portion of the tether and the Earth's magnetic field will result in a drag force, thus, de-orbiting the Delta II second stage. This experiment is a precursor to utilisation of the technology on the International Space Station for re-boost and the electrodynamic tether upper stage demonstration mission, capable of orbit raising, lowering, and inclination changes. In addition, some consideration will be given to using this type of propulsion for future missions to Jupiter.

Propulsive Small Expendable Deployer System

NASA's Propulsive Small Expendable Deployer System (ProSEDS) has been planned for launch in 2004. The experiment will demonstrate the de-orbit capabilities of an electrodynamic tether system.

ProSEDS will be deployed from a Delta II second stage using a 5 km long, ultra-thin bare-wire tether connected to a 10 km long non-conducting tether composed of Spectra. The interaction of the bare-wire tether with the Earth's ionosphere will produce a drag effect, lowering the altitude of the Delta II second stage. During normal deployment a Delta II second stage will slowly be pulled back from 400 km altitude to Earth by atmospheric drag. This process will take on average around 120 days, when it eventually re-enters the atmosphere and burns up. ProSEDS is expected to de-orbit the Delta II second stage in about two weeks.

International Space Station Re-boost

The value of an electrodynamic tether re-boost system for the International Space Station (ISS) lies in its ability to couple power generation with thrust. Hence, attaching an electrodynamic tether re-boost system to the ISS does away with the most critical and constraining dependency on Earth - propellant supply. The station can supply its own power but not its own propellant. Add a tether and some additional storage capacity for supplies, and a self sufficient ISS is born.

For an electrodynamic tether re-boost system capable of delivering 0.5 to 0.8 N of thrust to the ISS at a cost of 5 to 10 kW of electrical power, a 10 km long aluminium tether with a width of about 0.6 to 10 mm will be required [**51**]. This would counteract the effects of atmospheric drag and greatly reduce the cost of launching the required propellants into orbit.

Re-useable Upper Stage Propulsion

An electrodynamic tether system can allow for cheaper launch costs by introducing a fully re-usable system in LEO. Such a system will require no propellant and little re-supply and will behave as an upper stage, delivering the payload to its final destination. This can be achieved by launching the payload into LEO, where it will rendezvous with

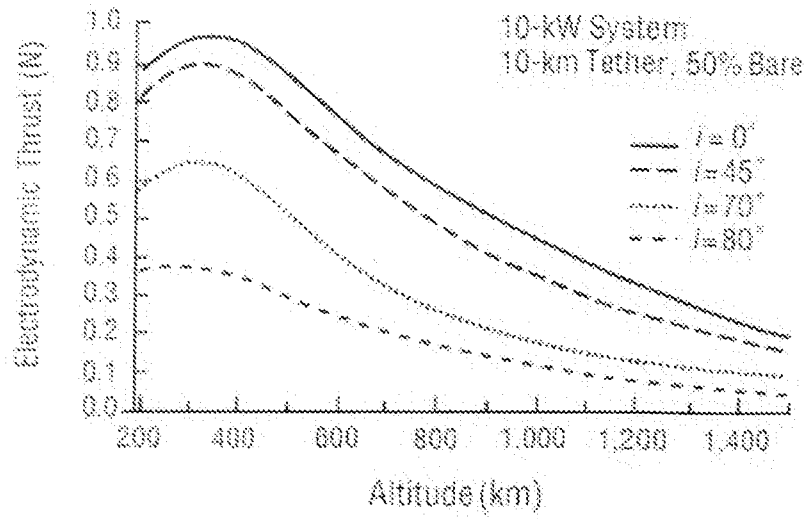

Figure 3.7: Electrodynamic propulsion system performance [**51**]

the tether system. It is then delivered to its new location before the tether system de-orbits to wait for the next payload arrival. Such a system could perform several orbital manoeuvring missions without re-supply, making it a low cost space asset. The performance of an electrodynamic propulsion system varies with orbital altitude and inclination. Figure 3.7 illustrates the performance of a 10 kW, 10 km tether system over altitude at various inclinations. The high voltage power supply required to deliver the 10 kW of electrical power is estimated to have a mass of about 80 kg [**41**]. Although this mass is quite high, the fact that the tether system is fully re-usable, and can deliver a number of payloads to their final destinations, results in a very cost effective payload delivery system.

Jovian Exploration

Following the success of the Galileo Jupiter-orbiter probe, there has been considerable interest in follow-on missions to Jupiter. For Galileo and all past deep space missions, radioisotope thermoelectric generators (RTG's) were used for generating electrical power. However, the risk of releasing plutonium into the terrestrial environment may rule out RTG's on future missions. The possibility of using solar arrays for electrical power generation has been considered. However, it is expected that due to high levels of radiation in the Jovian system solar arrays will rapidly degrade as a result of extended exposure.

Another disadvantage of using solar arrays is that Jupiter is in excess of 750 million km away from the Sun. It is also typical of any extended mission that an expendable propellant for orbital manoeuvring is required. This will inevitably lead to a high 'wet' spacecraft mass at launch and/or limited lifetime in orbit. It is this reasoning, and because of the relatively strong Jovian magnetic field, that electrodynamic tether systems are being considered for use in the Jovian system. Preliminary results have indicated that a megawatt of power can be theoretically generated by a 10 km tether in near-Jupiter space. Specifically, an electrodynamic tether operating near the planet would experience induced voltages greater than 50,000 V, currents in excess of 20 A, power levels of approximately 1 MW and thrust levels of the order of 50 N **[51, 52]**.

3.3 Tethers For De-Orbit Manoeuvres

Present methods for de-orbiting spacecraft in LEO recommend that the vehicle is placed into a reduced lifetime orbit at the end of its operational mission. This can lead to a reduced mission lifetime, since the propellant required to place the spacecraft into this reduced lifetime orbit could be used to sustain the spacecraft's orbit and extend its mission.

An electrodynamic drag system, weighing just 1 to 2% of the host spacecraft, would permit the spacecraft to extend its operational mission lifetime by allowing the expenditure of all its propellant. When the mission is complete, the tether system can then be deployed, allowing the Earth's magnetic field to interact with the long conducting tether, and de-orbiting the host spacecraft. This would result in a reduced post-mission orbital lifetime, de-orbiting the spacecraft more rapidly than atmospheric drag alone. This could help free-up over-populated regions of space and minimise the collision threat the spacecraft poses to operational spacecraft. However, The NASA Safety Standard **[28]** recommends that:

> "If drag enhancement devices are to be used to reduce the orbit lifetime, it should be demonstrated that such devices will significantly reduce the area-time product of the system..."

Hence, for such an electrodynamic tether system to be viable for operation it needs to demonstrate its ability to significantly reduce the area-time product of a satellite

system. For example, a spacecraft in LEO could take hundreds or thousands of years to de-orbit due to atmospheric drag alone (i.e. a small area exposed for a long period of time). Whereas, an electrodynamic tether could de-orbit the spacecraft within weeks or months reducing its post-mission orbital lifetime (i.e. a large area exposed for a short period of time).

The following section considers the Terminator Tether^{TM}, developed by Tethers Unlimited Inc., which is specifically designed for de-orbiting spacecraft. The discussion places particular emphasis on its advantages, disadvantages and its de-orbiting capabilities.

3.3.1 The Terminator Tether^{TM}

The Terminator Tether^{TM} is a small lightweight tether system that will use passive electrodynamic tether drag to de-orbit a spacecraft from LEO (relatively) rapidly **[53]**. The advantages of such a system include:

- It is small and lightweight, so it can be attached to a satellite without greatly effecting the overall satellite mass budget.
- It represents mass savings compared to rocket based de-orbit systems (i.e. no propellant required for de-orbiting).
- Its ability to de-orbit, even if the host spacecraft has lost power and control. For example, a 5 to 10 km long tether weighing about 2% of the host spacecraft mass can de-orbit a typical LEO spacecraft within a few months.

Figure 3.8 shows the rate of perigee decay for the Terminator Tether^{TM} over a range of inclinations. Comparison of the curves clearly shows that the rate of descent decreases as inclination increases. This is because the interaction between the tether and the Earth's geomagnetic field at inclination's above 75° is much less. The descent rate for a polar orbit does not go to zero completely, because the Earth's magnetic dipole axis is tilted relative to the spin axis, and a spacecraft will therefore cross the magnetic field lines at some stage during its orbit **[54]**.

Figure 3.9 illustrates the de-orbit time of the Terminator Tether^{TM} as a function of inclination. Hence, using a tether with a mass of just 1% of the host spacecraft, an Iridium-type satellite could be de-orbited from an 850 km altitude, 50° inclined orbit

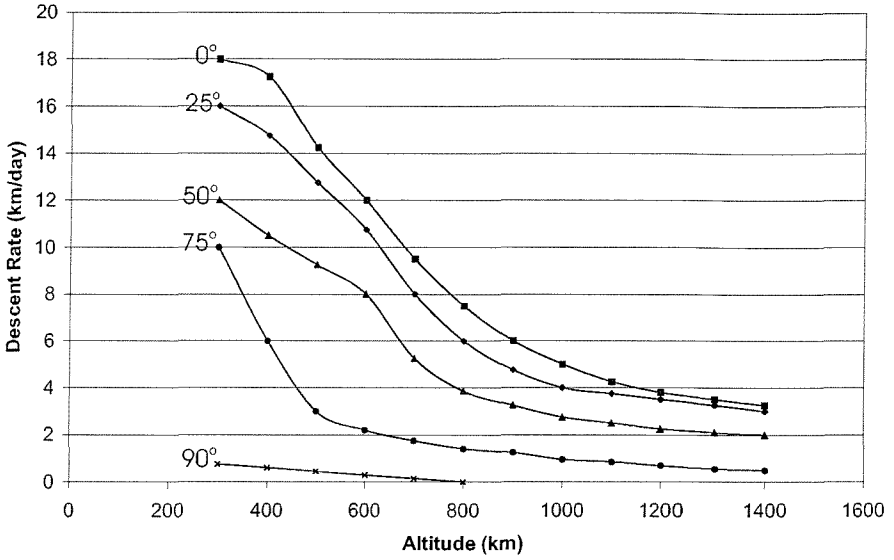

Figure 3.8: Descent rate for the Terminator Tether^{TM} at various inclinations [**54**]

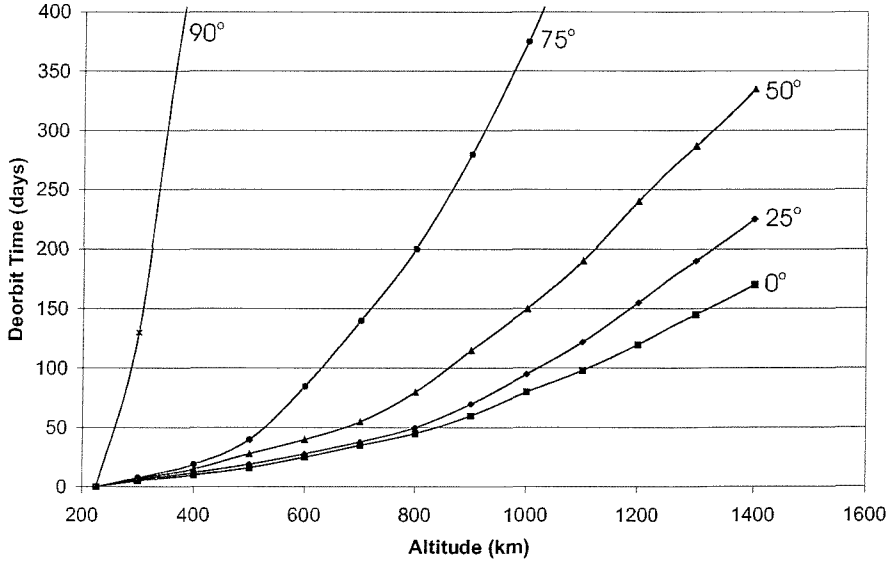

Figure 3.9: De-orbit time for the Terminator Tether^{TM} at various inclinations [**54**]

within about 3 months, and a SkyBridge-type satellite from a 1,475 km altitude, 55° inclined orbit in about 1.2 years [54]. These results suggest that a Terminator Tether™ could effectively de-orbit satellites in orbits with inclinations up to about 75°.

The primary purpose of the Terminator Tether™ is to de-orbit satellites and rocket bodies at the end of their operational lifetime, removing the collision threat they pose to other orbiting objects. However, when the Terminator Tether™ is deployed from a satellite, it greatly increases its cross-sectional area. This, in turn, greatly increases the probability that the system will suffer a random collision within a certain time period. However, the probability of collision not only depends on the cross-sectional area of the space system but also upon the time spent in orbit. A satellite left to de-orbit by atmospheric drag alone may have a relatively low cross-sectional area, but because the atmospheric drag effects are so small, the time spent in orbit may be hundreds or even thousands of years. So, even though the Terminator Tether™ increases the cross-sectional area of a satellite system, it may still reduce the chances of a random collision since the amount of time the satellite spends in orbit may be sufficiently reduced.

3.4 Survivability Issues

One of the most concerning aspects surrounding space tethers is their large cross-sectional area. The Tethered Satellite System, for example, if fully deployed would have had a length of 20 km and a width of 3 mm, giving a total cross-sectional area of 60 m^2. The combination of this with operational hazards and meteoroid risks results in a space tether system being vulnerable to impacts and subsequent mission failure. The ESA/Dutch 35 km tether deployment of the Young Engineers' Satellite (YES) [55, 56] from the Technology, science and education Experiments Added to MaqSAT (TEAM-SAT), for example, was abandoned in 1997. It was realised, due to the high perigee altitude of the Ariane 5 GTO (580 km), that a mission failure would cause the tether to remain in orbit for tens of years, thus endangering operational satellites in LEO [57].

Space tether systems are also more vulnerable to smaller debris impacts, unlike a typical spacecraft which can be shielded against such hazards. Estimates have suggested that particles half the diameter of the tether may cause a single strand tether to fail [58]. The lifetime for a single strand tether system has been estimated to be just a few days,

and this was demonstrated during the SEDS-2 mission, where the 20 km long tether was severed, apparently by a micro-meteoroid, 3.7 days after deployment (see Section 3.2.1).

The following sections consider three types of tether designs, paying particular attention to the risks associated with each design.

3.4.1 Single Strand Tether Systems

Single strand tether systems are the simplest of tether designs, consisting of a long, thin strand connecting two objects together. Such designs are very vulnerable when introduced into the space debris environment and are basically single point failure structures. Since the strands are thin, they are very susceptible to the small debris population. With our lack of detection capabilities for small debris populations, combined with large cross-sectional areas, the probability of failure of such tether systems may be unacceptably high.

3.4.2 Double Strand Tether Systems

A double strand tether system consists of two strands that are interconnected by a number of 'beads' (or 'knots') that ultimately join two objects together. Figure 3.10 illustrates a double strand tether system. The introduction of the second strand doubles the cross-sectional area compared to a simple single strand tether, increasing the collision probability. However, and more importantly, the sever probability of a double strand tether is greatly reduced since two strands in one segment both have to fail. Hence, increasing the number of 'beads' along the tether will reduce the sever probability even further because the cross-sectional area of each of the segments decreases, reducing the risk of both strands in one segment failing. However, there comes a point where too many 'beads' will result in an increase in the sever risk. This is because the 'beads' are effectively single point failure structures. Hence, to optimise the tether performance in terms of minimising sever risk, each tether system will have to be assessed individually, because of varying tether lengths.

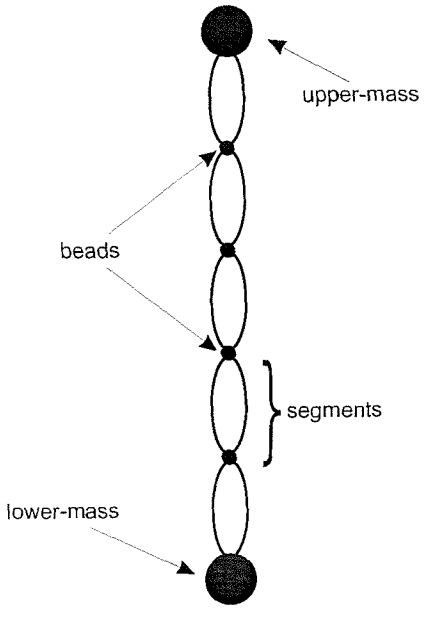

Figure 3.10: Double strand tether system

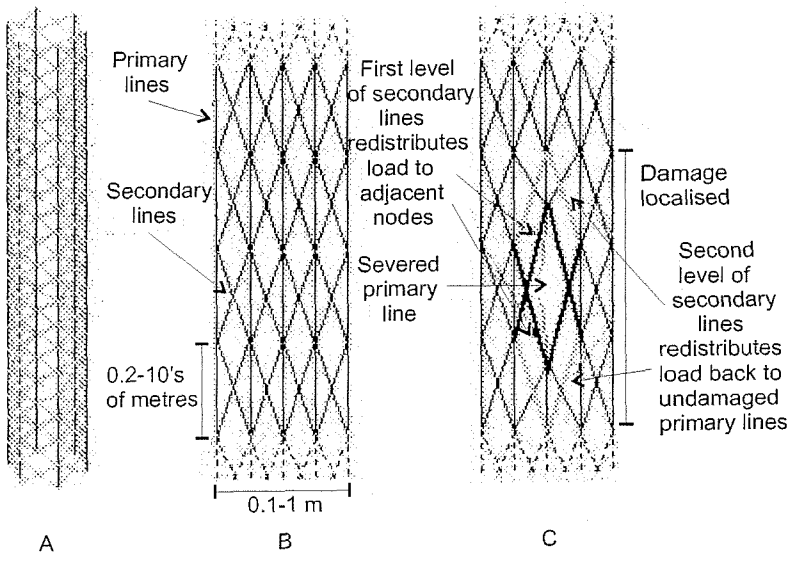

Figure 3.11: Hoytether^{TM} multi strand tether system **[60]**

3.4.3 Hoytether^{TM}

A Hoytether^{TM} [**59**], illustrated in Figure 3.11A, is a multi-strand tether system that has been developed by Tethers Unlimited Inc. It consists of a number of 'primary' strands that are interconnected by 'secondary' strands that are used to distribute the load, if a 'primary' strand is severed. A magnified section of an undamaged Hoytether^{TM} is shown in Figure 3.11B. If a 'primary' strand fails then the load of the tether system is redistributed using 'secondary' strands, effectively localising the damage - see Figure 3.11C. Ground analysis of a Hoytether^{TM} system has shown that the lifetime is greatly increased from just a few days, for a single strand tether system, to several tens of years.

3.5 Impact Assessment of Space Tether Systems

To deploy a space tether system successfully in orbit, a thorough understanding of the risks posed to them from the space debris environment is of vital importance. In an attempt to achieve this goal a number of hypervelocity impact tests were performed by McBride et al [**61**] to predict the expected failure rate of single strand tether systems in LEO. The model successfully predicted that the SEDS-2 tether system (20 km, 0.75 mm) would fail in less than two weeks. The model also suggested that thicker, shorter tether systems would be less susceptible to failure, and predicted that the TiPS tether system (4 km, 2 mm) would have a lifetime of around 1 year. However, the TiPS tether system survived unscathed for more than 4 years.

Further work to assess the lifetime of space tether systems have been carried out by Anselmo and Pardini [**58, 62**]. They performed a collision risk assessment for a single strand tether system for six circular orbits, spanning three altitude regions (600, 800 and 1,000 km) and two inclinations (30° and 50°) [**58**]. The results showed that for the orbital regions considered, and for particles larger than 1 mm in size, orbital debris was the dominant contributor to impact rates. For particles less than 1 mm, meteoroids gave comparable fluxes, but above 1 cm they contributed 10 to 30 times less to the impact rate [**58**].

Anselmo and Pardini [**62**] performed a second collision risk assessment to examine the survivability of a double strand tether system, in particular for de-orbiting satellites. The aim was to find a suitable design that would guarantee overall mission success.

It was predicted that a 5 km double strand tether system (0.7 mm diameter strands) would require a total of 501 'beads' ('knots') to guarantee a survival probability of at least 95%. For a survival probability of 99% a total of 2,001 'beads' would be required. However, the 'beads' are effectively single point failure structures and this seems to have been overlooked in the study. Including this probability into the analysis could significantly effect the overall survival probability of the tether system, reducing the chances of mission success.

A further study by Chobotov and Mains [**63**] was performed to determine the collision probability of the Tethered Satellite System (TSS) after it became separated from the Space Shuttle Orbiter. The results showed that the TSS would have expected to have been impacted by several particles larger than 0.1 mm in size. For objects 10 cm in size or larger the collision probability was on the order of 10^{-3} per month. It was concluded, however, that because the TSS re-entered within one month, after deployment, that the probability of collision with other objects, while in orbit, was small.

The following section considers the hypervelocity impact tests performed by McBride et al [**61**]. The case studies examined by Anselmo and Pardini [**58, 62**] are also considered, along with the TSS case study performed by Chobotov and Mains [**63**].

3.5.1 Hypervelocity Impact Tests

Seven experiments were performed by McBride et al [**61**] in total, five on a tether composed of Spectra 1000 with a diameter of 0.75 mm, and two on space-grade aluminium tethers with a diameter of 1 mm. A glass sphere projectile was fired at each of the tether strands with a speed of approximately 5 km/s. With the findings of these experiments and using a suitable penetration equation, an adequate prediction of tether survivability was developed. For example, a 0.3 mm diameter projectile fired at a 0.75 mm Spectra tether strand at 5 km/s would have a penetrating depth of approximately 0.82 mm, thus destroying the tether strand. However, a 0.2 mm diameter projectile would only penetrate about 0.53 mm, only damaging the tether strand. These results were confirmed by experimental data and are illustrated in Figure 3.12. Figure 3.12a shows that one of the tether strands has completely severed, with another damaged. Figure 3.12b shows no severed strands but that considerable damage has been done.

These initial results were then utilised to develop a model, which was used to predict the

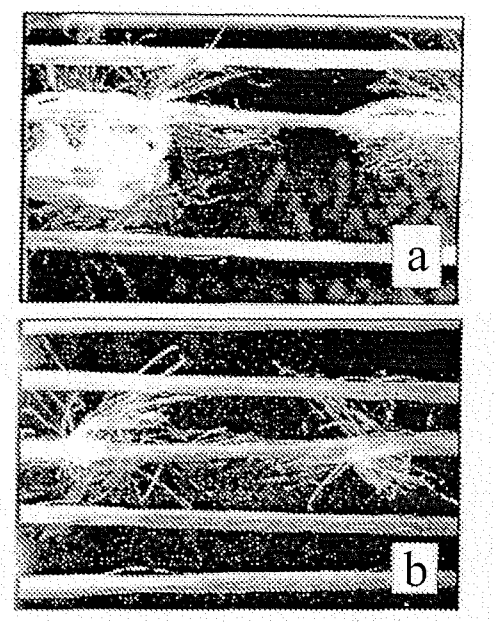

Figure 3.12: Impact tests on Spectra 1000 (0.75 mm) fired at 5 km/s. (a) 0.3 mm projectile damage. (b) 0.2 mm projectile damage [**61**]

tether system lifetime (and expected upper and lower prediction limits) of two tether missions, SEDS-2 and TiPS. SEDS-2 (20 km in length and 0.75 mm in diameter) was deduced to have a typical lifetime of 11^{+16}_{-8} days. The tether was actually severed about 3.7 days after deployment. The remaining 7.2 km tether left in orbit was then deduced to have a lifetime of around 31^{+45}_{-24} days. The actual tether was observed in orbit, with no apparent further breaks until re-entry around 50 days later. For the TiPS tether system (4 km in length and 2 mm in diameter) a prediction lifetime of 295^{+440}_{-230} days was deduced. The TiPS tether system has survived in orbit for over 4 years. Therefore, although good agreement was achieved for the SEDS-2 tether scenario, the TiPS tether system survived for more than twice its prediction lifetime.

3.5.2 Space Tether System Lifetimes

A number of case studies were performed by Anselmo and Pardini [**58, 62**]. These involved assessing the impact risk to single strand space tether systems for six circular orbits, spanning three altitude regions (600, 800 and 1,000 km) and two inclinations (30^{o} and 50^{o}) [**58**]. A second case study examined the survivability of a double strand

Debris diameter interval (cm)	Tether diameter					
	1 mm	2 mm	5 mm	7 mm	1 cm	2 cm
0.01–0.10	0.166E + 02	0.310E + 02	0.742E + 02	0.103E + 03	0.146E + 03	0.290E + 03
0.10–0.20	0.495E − 01	0.693E − 01	0.129E + 00	0.168E + 00	0.228E + 00	0.426E + 00
0.20–0.30	0.108E − 01	0.139E − 01	0.231E − 01	0.292E − 01	0.385E − 01	0.693E − 01
0.30–0.40	0.397E − 02	0.486E − 02	0.751E − 02	0.927E − 02	0.119E − 01	0.208E − 01
0.40–0.50	0.133E − 02	0.158E − 02	0.231E − 02	0.279E − 02	0.352E − 02	0.594E − 02
0.50–0.60	0.595E − 03	0.686E − 03	0.960E − 03	0.114E − 02	0.142E − 02	0.233E − 02
0.60–0.70	0.486E − 03	0.550E − 03	0.745E − 03	0.874E − 03	0.107E − 02	0.172E − 02
0.70–0.80	0.309E − 03	0.345E − 03	0.454E − 03	0.527E − 03	0.636E − 03	0.999E − 03
0.80–0.90	0.227E − 03	0.251E − 03	0.323E − 03	0.371E − 03	0.443E − 03	0.682E − 03
0.90–1.00	0.197E − 03	0.216E − 03	0.272E − 03	0.309E − 03	0.366E − 03	0.553E − 03
0.10–1.00	0.674E − 01	0.916E − 01	0.164E + 00	0.213E + 00	0.286E + 00	0.528E + 00
1.00–2.00	0.780E − 03	0.829E − 03	0.975E − 03	0.107E − 02	0.122E − 02	0.171E − 02
2.00–3.00	0.171E − 03	0.177E − 03	0.197E − 03	0.210E − 03	0.230E − 03	0.295E − 03
3.00–4.00	0.115E − 03	0.118E − 03	0.128E − 03	0.134E − 03	0.144E − 03	0.176E − 03
4.00–5.00	0.688E − 04	0.703E − 04	0.747E − 04	0.777E − 04	0.822E − 04	0.972E − 04
1.00–10.0	0.123E − 02	0.129E − 02	0.148E − 02	0.160E − 02	0.178E − 02	0.240E − 02
10.0–100	0.758E − 03	0.761E − 03	0.768E − 03	0.772E − 03	0.779E − 03	0.802E − 03

Table 3.2: Impact rate ($yr^{-1}km^{-1}$) as a function of orbital debris size and tether diameter (orbit altitude = 1,000 km; inclination = 50°) [**58**]

tether system while varying the distance between each of the 'beads' ('knots') along the tether system [**62**].

Single Strand Tether System Case Study

The six circular orbits chosen by Anselmo and Pardini [**58**] provide an overview of the expected impact rate for space tether systems in LEO. Table 3.2 summarises the results for a 1 km long tether system, operating at an altitude of 1,000 km and an inclination of 50°, as a function of orbital debris size and tether diameter. The impact rate for a particular tether system can be obtained by multiplying the length of the tether (km) by the entries in Table 3.2. Hence, applying the results of Table 3.2 to the TiPS tether system (4 km in length and 2 mm in diameter), and assuming that all the debris diameter intervals (in Table 3.2) are capable of severing the 2 mm tether strand, we find a severing impact should be expected once every 4 years. However, a 20 km long tether with similar characteristics as the TiPS tether system, and in the same orbit, would have an expected average survival lifetime of about 1 year [**58**].

The results confirmed the concern over the issue of survivability for single strand tether systems. However, it was noted that electrodynamic tether systems, used for satellite

Initial altitude	1,500 km
Orbital inclination	55°
Impedance	280 Ω
Payload mass	2,000 kg
Tether length	5 km
Electron collector diameter	10 m
Year of mission	2003

Table 3.3: Tether system reference case **[62]**

de-orbiting, could help in reducing the space debris problem, providing they could be made to survive the harsh debris environment. These conclusions resulted in a second study looking at double strand tether systems.

Double Strand Tether System Case Study

The purpose of this study **[62]** was to examine the impact risk of an electrodynamic tether system proposed for satellite de-orbiting. A reference case that defines the overall tether system and its performance is given in Table 3.3.

The average residence times were then calculated for a set of altitude bands depending on the amount of time the tether system spent in each of the altitude bands. Assuming that a particle with a diameter $\frac{1}{3}$ of the tether diameter causes it to be severed, a number of computations were performed to estimate the tether system's survival probability as a function of tether diameter **[62]**.

Firstly, a single strand tether with a diameter of 0.6 mm was considered. It was quickly realised, however, that such a system was not a viable option, with an average lifetime prediction of just 3 months. It was predicted that for a 95% mission success rate to be achieved, a single strand tether system would require a diameter of around 4 to 5 mm. However, such a solution would be impractical, being too heavy and bulky **[62]**. Hence, a new tether system consisting of two strands, each 0.7 mm in diameter, was considered. The aim now was to determine the number of 'beads' ('knots') required to guarantee the specified operational lifetime.

A distance of 100 m was considered between each of the 'beads' for the first study. However, the probability of tether failure, 35%, was still too high. To achieve an acceptable sever risk, the distance between each of the 'beads' had to be reduced to just 10 m. This

Altitude interval (km)	Residence time (yr)	Probability of tether severing
1,500 – 1,400	0.104	0.0016
1,400 – 1,300	0.112	0.0012
1,300 – 1,200	0.126	0.0015
1,200 – 1,100	0.110	0.0014
1,100 – 1,000	0.096	0.0017
1,000 – 900	0.107	0.0182
900 – 800	0.093	0.0058
800 – 700	0.090	0.0023
700 – 600	0.071	0.0010
600 – 500	0.055	0.0005
500 – 400	0.044	0.0002
400 – 300	0.036	0.0001
300 – 200	0.030	0.0001
1,500 – 200	**1.074**	**0.0356**

Table 3.4: Double strand tether system (0.7 mm) survivability analysis for a 'bead' distance of 10 m **[62]**

gave a sever probability of 3.6% and is detailed in Table 3.4. It was predicted that, for a 99% survival probability of operational mission, the 'bead' distance would have to be reduced to just 2.5 m **[62]**.

The results presented by Anselmo and Pardini **[62]** demonstrate the possibility of using tethers for long duration missions, provided that an adequate design is adopted to survive the harsh debris environment. However, the probability of a 'bead' failure seems to have been over-looked during the study. For a 99% chance of mission survival, a distance of 2.5 m between each of the 'beads' was predicted. This would result in a total of 2,001 'beads' along the 5 km tether system. However, the cross-sectional area for each 'bead' along the tether system is very small and will result in a low probability of failure.

3.5.3 Tethered Satellite System Collision Study

The TSS collision study performed by Chobotov and Mains **[63]** considered the collision probability of the tether component of the TSS-1R after it broke away from the Space Shuttle Orbiter in February 1996. In particular, the collision probability arising from the small debris population and the larger catalogued objects were considered.

Particle size (mm)	Flux (No/m^2/year)	$E = FA_tT$ (impacts/month)
> 0.1	0.4	1.88
> 1	4.0×10^{-4}	1.88×10^{-3}
> 10	1.0×10^{-6}	4.71×10^{-6}

Table 3.5: Estimated tether impacts with small particles for the TSS **[63]**

Firstly, the collision risk associated with the small debris population was considered. The NASA EVOLVE model **[32]** was utilised to estimate the cumulative cross-sectional area flux of the small debris population - see Table 3.5. The estimated number of encounters for the tether was then calculated using

$$E = FA_tT, \tag{3.16}$$

where F is the particle flux, A_t is the tether projected area (56.6 m^2 for the remaining TSS tether component), and T is the time. The estimated number of encounters are given in Table 3.5.

Secondly, an analytic collision risk associated with the large debris population was considered. A gravity-gradient stabilised tether, of length L, deployed in orbit as shown in Figure 3.13 was considered. Over time a number of objects would repeatedly pass through the area, A, swept out by the tether. Hence, the probability that an object, of diameter D, in a circular orbit would pass through the shaded region around the deployed tether in Figure 3.13 is given by

$$P_s = \frac{kL}{2\pi RL}, \tag{3.17}$$

where k is arbitrary and R is the radius of the circular orbit. The actual geometry is not considered in this formula because of the complexity of objects sizes and shapes.

The probability that a large object, of diameter D, impacting within a distance D of the tether is given by

$$P_i = \frac{2D}{k}. \tag{3.18}$$

Hence, the overall collision probability is given by

$$P_t\,(\text{col/pass}) = P_s \times P_i = \frac{D}{\pi R}. \tag{3.19}$$

For N_p penetrations over a given time interval, Δt, the probability of collision is given

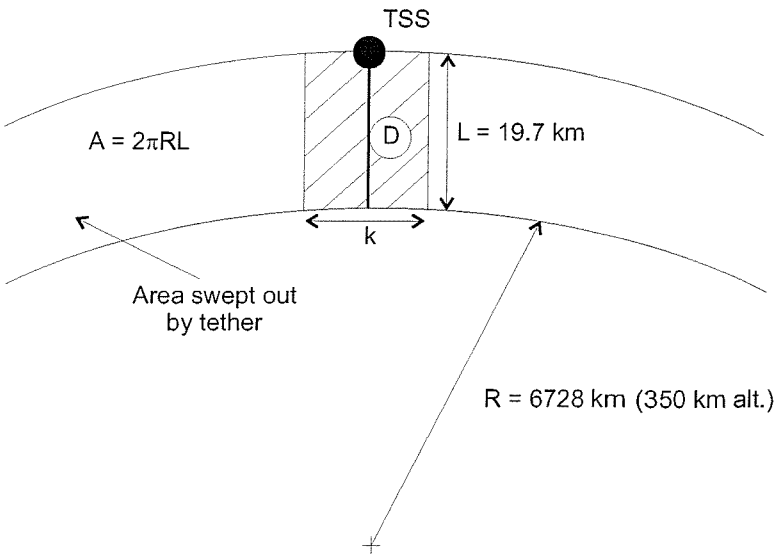

Figure 3.13: Tether geometry **[63]**

by

$$P_t(\text{col}/\Delta t) = \frac{N_p D}{\pi R}. \tag{3.20}$$

The simulation, which covered six months beginning from 1st March 1996, predicted 58,646 objects passing through the TSS's orbital path by 24 different satellites. Hence, assuming an average diameter of 5 m for each of the objects, the probability of collision in a six month period is given by

$$P_t(\text{col/6 months}) = \frac{58,646 \times 5}{\pi \times 6728 \times 10^3},$$

or 2.32×10^{-3} per month **[63]**. A statistical approach was also utilised in the study and approximated the probability of collision to be 1.527×10^{-3} per month.

The results presented by Chobotov and Mains **[63]** showed that the TSS was vulnerable to several impacts by small particles greater than 0.1 mm in size. The collision probability with large objects was in the order of 10^{-3} per month. Since the severed TSS re-entered within one month the collision hazard to other objects was generally small.

3.6 Discussion

There have been a number of proposals for the use of tethers in space, such as ISS re-boost, re-usable upper stage propulsion and for Jovian exploration. Space tether systems have also been proposed for a cheap and effective way of cleaning-up the space debris environment. It has been proposed that an electrodynamic tether system, weighing just 1 to 2% of the host spacecraft, could de-orbit an Iridium-type satellite, from an 850 km altitude, 50° inclined orbit, within about 3 months. However, these de-orbiting devices do not come without their own problems. Space tether systems are very susceptible to the space debris environment. It has been predicted and demonstrated (SEDS-2) that single strand tether systems have a survivability lifetime of just a few days. These survivability issues have been the focus of a lot of research and a number of tether designs have been proposed. The Hoytether^{TM} design, for example, has been predicted to have a lifetime of several tens of years. If tethers could be designed to withstand the space debris environment, then a cheap and effective means of de-orbiting satellites and spent upper stages would be available.

Chapter 4

Orbital Motion

In the early 17th century Johannes Kepler set about the task of understanding the orbital path of Mars. Finally, after struggling for almost a year to remove a discrepancy of just 8 minutes of arc, he came across the solution in the form of an ellipse. Thus, the Martian orbit was found, and in 1609 Kepler published his first two laws of planetary motion, with the third law following in 1619. Kepler's laws of planetary motion state:

1. The planets move in elliptic orbits, with the Sun occupying one focus.
2. The line joining the Sun to a planet sweeps out equal areas in equal time intervals.
3. The square of a planet's orbital period is proportional to the cube of its mean distance from the Sun.

However, Kepler's laws were only an empirical description of planetary motion. The underlying theoretical explanation of the planets motion fell to Sir Isaac Newton who presented his results in 1687 in the 'The Mathematical Principles of Natural Philosophy', or as its most commonly known, the 'Principia' **[64]**. It was here that Newton introduced his three laws of motion:

1. Every object in a state of rest or uniform motion in a straight line continues in this state unless it is acted upon by an external force.
2. The rate of change of an object's momentum is proportional to the force acting upon it and is in the same direction as that force.
3. To every action there is an equal and opposite reaction.

Newton's second law of motion can be expressed mathematically as

$$\mathbf{F} = m\ddot{\mathbf{r}} \tag{4.1}$$

where $\mathbf{F}$ is the force acting on a mass m and $\ddot{\mathbf{r}}$ is the acceleration of the mass measured relative to an inertial reference frame.

The purpose of the proceeding discussion is to introduce the orbital motion formulae implemented into the Tether Risk Assessment Program (TRAP) used to model the orbital debris population and an orbiting space tether system around the Earth. The TRAP model is capable of determining the collision and sever hazards, posed by the orbital space debris population, encountered by an orbiting space tether system. However, in order to produce meaningful assessments, the debris population and tether system have to be accurately modelled.

4.1 Orbital Debris Evolution

The TRAP model was developed to enable accurate collision and sever risk assessments for orbiting space tether systems, resulting from the orbital debris background population, and also from debris produced by a recent fragmentation event. Hence, accurate determination of the positions and velocities of the debris population at a given time is fundamental. The orbit propagator, implemented into TRAP, was not designed to produce the most accurate orbit propagator possible, but one which offers the optimum compromise between computational efficiency and accuracy. Orbital perturbations due to Earth's oblateness, J_2, and atmospheric drag are modelled because these are the dominant perturbation forces for the orbital regions being considered for future planned tether missions. The orbital perturbation effects of J_3 are also considered.

The following section considers the ideal orbital (Keplerian) motion of an object around the Earth. The discussion then focuses on the effects of orbital perturbations, which can significantly alter an object's orbital motion around the Earth. Attention is paid to Earth gravity perturbations, and in particular to the first order J_2 (second harmonic) secular variations, and the long-period oscillations of the third harmonic J_3. The effects of perturbations due to atmospheric drag are also discussed.

4.1.1 Ideal Orbital Motion

Along with his laws of motion, Newton also formulated the universal law of gravity, by stating that any two bodies attract one another with a force proportional to the product of their masses and inversely proportional to the square of the distance between them [**65**]. This can be expressed mathematically by

$$\mathbf{F} = -\frac{Gm_1m_2}{r^2}\left(\frac{\mathbf{r}}{r}\right), \tag{4.2}$$

where $\mathbf{F}$ is the force acting upon the mass m_2 due to mass m_1 and $\mathbf{r}$ is the position vector of m_2 with respect to m_1. The universal gravitational constant, G, has a numerical value of 6.670×10^{-11} N m^2/kg^2.

Kepler's three laws of planetary motion and Newton's universal law of gravitation form the basis of ideal orbital motion. The equations assume that the two attracting bodies are point masses, and that one of the bodies has negligible mass compared to the other (e.g. an Earth-orbiting satellite). This is a reasonable first approximation and can be applied for the majority of bodies in the solar system. The equations describing ideal orbital motion, as shown by Roy [**66**], are given by,

$$r = \frac{a\left(1-e^2\right)}{1+e\cos\theta}, \tag{4.3}$$

$$v = \sqrt{\mu\left(\frac{2}{r}-\frac{1}{a}\right)}, \tag{4.4}$$

$$\tau = 2\pi\sqrt{\frac{a^3}{\mu}}, \quad \left(n^2a^3=\mu\right), \tag{4.5}$$

$$E - e\sin E = M = n\left(t-t_p\right), \tag{4.6}$$

$$\tan\left(\frac{\theta}{2}\right) = \tan\left(\frac{E}{2}\right)\sqrt{\frac{1+e}{1-e}}. \tag{4.7}$$

Here $\mu = Gm_1$, where m_1 is the mass of the primary body, r is the satellite's distance from the centre of Earth, v is its orbital velocity, a is the semi-major axis of the orbital ellipse, τ is the orbital period, n is the orbital mean motion, e is the eccentricity, θ is the true anomaly, E is the eccentric anomaly, M is the mean anomaly, t is time and t_p is the periapsis (perigee) passage time. The equations outlined above, describe the state of an

orbiting body within the plane of the ellipse. However, to fully describe the state, the orientation of the orbital ellipse needs to be specified using a suitable reference frame.

Specifying The Orbit

The requirement, for the purpose of this discussion, is to accurately model the orbital debris population. Hence, the following discussion will focus on the motion of an object orbiting the Earth. Firstly, an inertial reference frame is introduced, XYZ, located at the centre of the Earth with the X-axis pointing to the First Point of Aries, the Z-axis pointing to the north celestial pole and the Y-axis completing the right hand set. The parameters most commonly used to specify the orbit orientation, for Earth orbiting objects, are as follows:

- **The orbital inclination**, i, is the angle measured between the orbit plane and the equatorial plane, measured at the ascending node (i.e. the point where the satellite crosses the equator, going from south to north).
- **The right ascension of the ascending node**, Ω, is the geocentric angle measured eastwards from the First Point of Aries, around the equator, to the ascending node.
- **The argument of perigee**, ω, is the geocentric angle measured in the direction of motion from the ascending node, around the orbit, to the perigee position.

Hence, i, Ω and ω, along with a, e and θ, make up the six orbital elements that describe the current location and trajectory of an orbiting satellite relative to the Earth. Figure 4.1 illustrates the orbital geometry.

Conversion of Orbital Elements to Cartesian Co-ordinates

In order to successfully propagate the orbital debris population, the six orbital elements have to be converted into Cartesian elements and vice versa. To achieve this, the orbital elements, a, e, i, Ω, ω and θ can be mapped uniquely onto $\mathbf{r}$ and $\mathbf{v}$ vectors. The Cartesian vectors, $\mathbf{r}$ and $\mathbf{v}$, are the position and velocity vectors, respectively, of the orbiting satellite with respect to an inertial reference frame, located at the centre of the

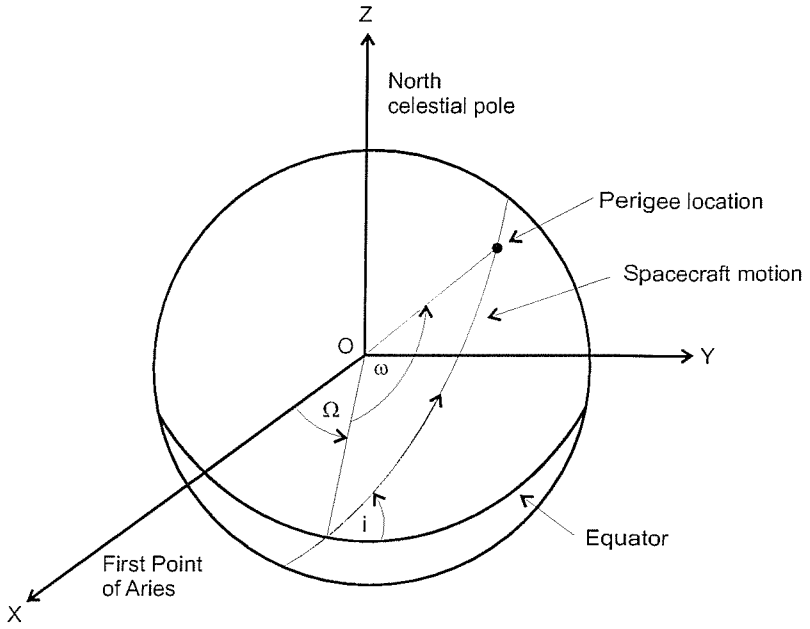

Figure 4.1: Geometry of an Earth orbit **[67]**

Earth. The position and velocity vectors are expressed respectively as

$$\begin{aligned} \mathbf{r} &= r\left(\cos\Omega\cos(\omega+\theta) - \sin\Omega\sin(\omega+\theta)\cos i\right)\mathbf{i_x} \\ &+ r\left(\sin\Omega\cos(\omega+\theta) + \cos\Omega\sin(\omega+\theta)\cos i\right)\mathbf{i_y} \\ &+ r\left(\sin(\omega+\theta)\sin i\right)\mathbf{i_z} \end{aligned} \tag{4.8}$$

and,

$$\begin{aligned} \mathbf{v} &= -\sqrt{\frac{\mu}{p}}\left(\cos\Omega(\sin(\omega+\theta)+e\sin\omega) + \sin\Omega(\cos(\omega+\theta)+e\cos\omega)\cos i\right)\mathbf{i_x} \\ &- \sqrt{\frac{\mu}{p}}\left(\sin\Omega(\sin(\omega+\theta)+e\sin\omega) - \cos\Omega(\cos(\omega+\theta)+e\cos\omega)\cos i\right)\mathbf{i_y} \\ &+ \sqrt{\frac{\mu}{p}}\left(\cos(\omega+\theta)+e\cos\omega\right)\sin i\,\mathbf{i_z}, \end{aligned} \tag{4.9}$$

where $p = a\left(1-e^2\right)$, and $\mathbf{i_x}$, $\mathbf{i_y}$ and $\mathbf{i_z}$ are Earth centred unit vectors with $\mathbf{i_x}$ pointing to the First Point of Aries, $\mathbf{i_z}$ pointing to the north celestial pole and $\mathbf{i_y}$ completing the right hand set. The conversion of the $\mathbf{r}$ and $\mathbf{v}$ vectors back to the orbital elements is

also required. This is achieved by the following set of equations,

$$a = \frac{1}{\left(\frac{2}{r} - \frac{v^2}{\mu}\right)}, \tag{4.10}$$

$$\mathbf{e} = \frac{1}{\mu}\left[\left(v^2 - \frac{\mu}{r}\right)\mathbf{r} - \mathbf{v}(\mathbf{r} \bullet \mathbf{v})\right], \tag{4.11}$$

$$i = \cos^{-1}\left(\frac{h_z}{|\mathbf{h}|}\right), \tag{4.12}$$

$$\Omega = \cos^{-1}\left(\frac{-h_y}{|-h_y\mathbf{i}_x + h_x\mathbf{i}_y|}\right), \tag{4.13}$$

$$\omega = \cos^{-1}\left(\frac{\hat{\mathbf{N}} \bullet \mathbf{e}}{|\mathbf{e}|}\right), \tag{4.14}$$

$$\theta = \cos^{-1}\left(\frac{\mathbf{r} \bullet \mathbf{e}}{re}\right), \tag{4.15}$$

where $\hat{\mathbf{N}}$ is the unit vector that points towards the ascending node from the centre of the Earth, $\mathbf{e}$ is the eccentricity vector that points from the Earth's centre to the perigee point and $\mathbf{h}$ is the orbital angular momentum vector (i.e. $\mathbf{h} = \mathbf{r} \times \mathbf{v}$), which is normal to the plane in a right-hand sense.

The set of equations outlined above describe an ideal Keplerian orbit of a satellite's motion around the Earth. However, when considering 'real orbits', there exist a number of additional forces that can significantly perturb a satellite's orbital path.

4.1.2 Perturbed Orbital Motion

The equations introduced thus far, although ideal for a first approximation, do not accurately predict a satellite's orbital motion about the Earth. Small deviations in a satellite's orbital motion are experienced due to external forces other than the central gravitational force of Equation (4.2). These perturbations to the ideal orbital motion occur because the two bodies have shape and density distributions, that can not be modelled as simple point masses. Also, the assumptions used in the two-body problem are violated when the Sun and Moon are introduced. These bodies exert additional perturbing forces upon the satellite. A satellite in low Earth orbit, typically below 1,000 km, will also experience a drag force resulting from Earth's upper atmosphere.

To predict a more realistic orbit the variations in a satellite's orbital elements, due to the major perturbation effects, are determined over a given time interval, Δt. The rate of change in these orbital elements, from each perturbation effect, are then accumulated, resulting in an overall change to the satellite's orbital elements. The orbital elements affected by the major perturbations include the semi-major axis, Δa, eccentricity, Δe, inclination, Δi, argument of perigee, $\Delta \omega$, and right ascension of the ascending node, $\Delta \Omega$. The satellite's orbital elements are then updated, by adding each change to its original value, at every time interval. Orbital perturbations due to Earth's oblateness, J_2, and atmospheric drag are modelled because these are the dominant perturbation forces for the orbital regions being considered for future planned tether missions. The orbital perturbation effects of J_3 are also included. These major perturbations are outlined below.

Geopotential Gravity

The geopotential gravity perturbation equations used in the TRAP model are summarised by Roy [66]. Table 4.1 shows the magnitude of some of the lower-order geopotential harmonic coefficients. It is apparent that the J_2 term is some three orders of

Harmonic	Magnitude
J_2	1082.6×10^{-6}
J_3	-2.53×10^{-6}
J_4	-1.62×10^{-6}
J_5	-0.23×10^{-6}
J_6	0.54×10^{-6}

Table 4.1: Magnitude of Earth's geopotential perturbations

magnitude larger than the others, and to a first approximation dominates the geopotential influences of the Earth. The first order J_2 (second harmonic) secular variation, due to the polar flattening of the Earth, causes the right ascension of the ascending node, Ω, and the argument of perigee, ω, to drift over time. The secular changes in Ω and ω can be modelled using the following equations,

$$\Delta\Omega = -\frac{3}{2}\left(\frac{J_2 R^2}{a^2\left(1-e^2\right)^2}\right) n\left(\cos i\right)\Delta t, \tag{4.16}$$

$$\Delta\omega = \frac{3}{2}\left(\frac{J_2 R^2}{a^2\left(1-e^2\right)^2}\right) n\left(2-\frac{5}{2}\sin^2 i\right)\Delta t, \tag{4.17}$$

where R is the Earth's mean equatorial radius.

The long-period oscillations due to the third harmonic J_3, are also accounted for, and cause the eccentricity and inclination to change according to the variations in the argument of perigee. The small variations in e and i can be modelled using **[66]**,

$$\Delta e = -\frac{3}{2}\left(\frac{nJ_3R^3}{a^3\left(1-e^2\right)^2}\right)\sin i\left(1-\frac{5}{4}\sin^2 i\right)\cos\omega\Delta t, \tag{4.18}$$

$$\Delta i = \frac{3}{2}\left(\frac{nJ_3R^3}{a^3}\right)\left(\frac{e}{\left(1-e^2\right)^3}\right)\cos i\left(1-\frac{5}{4}\sin^2 i\right)\cos\omega\Delta t. \tag{4.19}$$

Atmospheric Drag

Taking into account the effects of atmospheric drag on a satellite's orbital motion is considerably more difficult than determining the perturbation effects of geopotential gravity. Along with the required expressions describing how the orbital elements vary over time, the atmospheric drag model also requires some form of atmospheric model. Hence, the CIRA (Cospar International Reference Atmosphere) of 1972 is utilised, for its computational efficiency, providing values of atmospheric density and density scale height according to the perigee height of a satellite's orbit and the exospheric temperature, T_{ex} (K) **[68]**. CIRA was derived by studying the long-term atmospheric decay profiles of satellites with known cross-sectional areas, masses and drag coefficients.

The atmospheric density, ρ, at any given time, is dependent upon the chosen atmospheric model. The atmospheric model, which is completely independent of the element variation equations, can either be analytical or empirical in nature, and as simple or as complex as desired. The atmospheric model used in TRAP is a simplified version of the CIRA-72 model, with atmospheric density taken to be solely dependent on altitude. Figure 4.2 shows the density for an altitude range from 70 to 1,000 km, for a number of values of T_{ex}. If a satellite's altitude drops below 70 km it is assumed to have re-entered and is subsequently removed from the simulation. For altitudes above 1,000 km, the atmospheric density is assumed to be negligible, and therefore has no effect on the satellite. The atmospheric density value at a given altitude, generally, increases with exospheric temperature, T_{ex}, which in turn is strongly dependent upon solar activity. The atmospheric density profile observed in Figure 4.2 appears to be anomalous for $T_{ex} = 500$ K. However, this anomaly is due to the way atmospheric gases

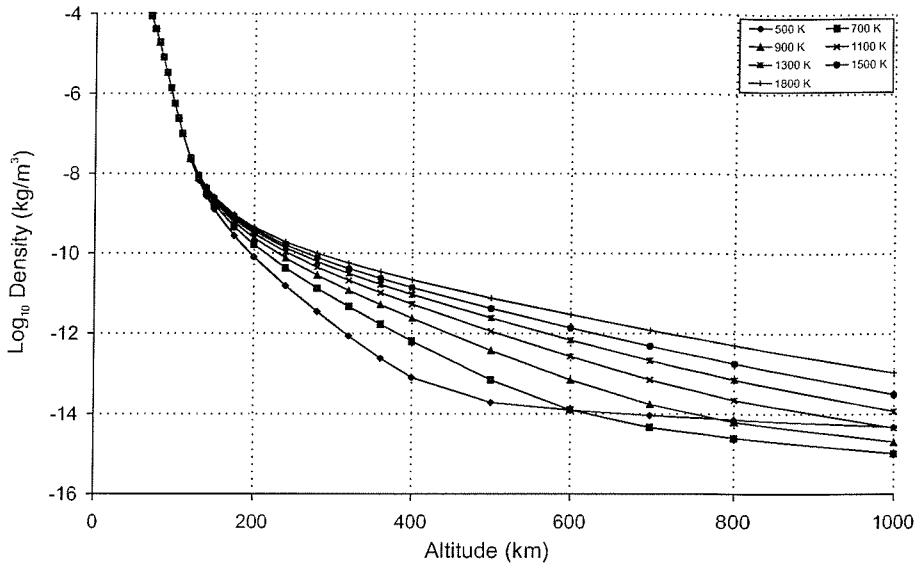

Figure 4.2: CIRA-72 density versus altitude profiles

mix at that temperature. In the CIRA-72 atmospheric model, hydrogen is not present below altitudes of about 500 km and at low exospheric temperatures is the dominant substance. This results in a levelling-out of the density versus altitude profile. However, with the increase in exospheric temperature, the number density of hydrogen falls below that of helium and atomic oxygen, and as a result its influence on ρ is diminished.

The exospheric temperature is determined using

$$T_{ex} = 1.15\,(379 + 3.24F_{10.7})\,. \tag{4.20}$$

Here the 30-day mean solar flux, at a wavelength of 10.7 cm, $F_{10.7}$, is used as an indicator of the level of solar activity in the model. The solar flux, and hence orbital decay rate, is therefore determined by the 11-year solar cycle, with maximum orbital decay rate occurring during the peak solar cycle. The $F_{10.7}$ value is user defined, in the TRAP model, and can vary from around 70 (10^4 Jy) at the solar minimum to about 200 (10^4 Jy) at solar maximum. The $F_{10.7}$ value can be determined from Figure 4.3 which was produced using average monthly solar flux values **[69]** and future predictions calculated from the NASA Goddard historical records **[70]**. Equation (4.20) is also dependent upon the diurnal factor, which varies daily due to solar heating. This periodic variation ranges between 1.0 (at nighttime minimum) and 1.3 (at daytime maximum) over the course of each orbit according to the local solar time. However, this has been set to a

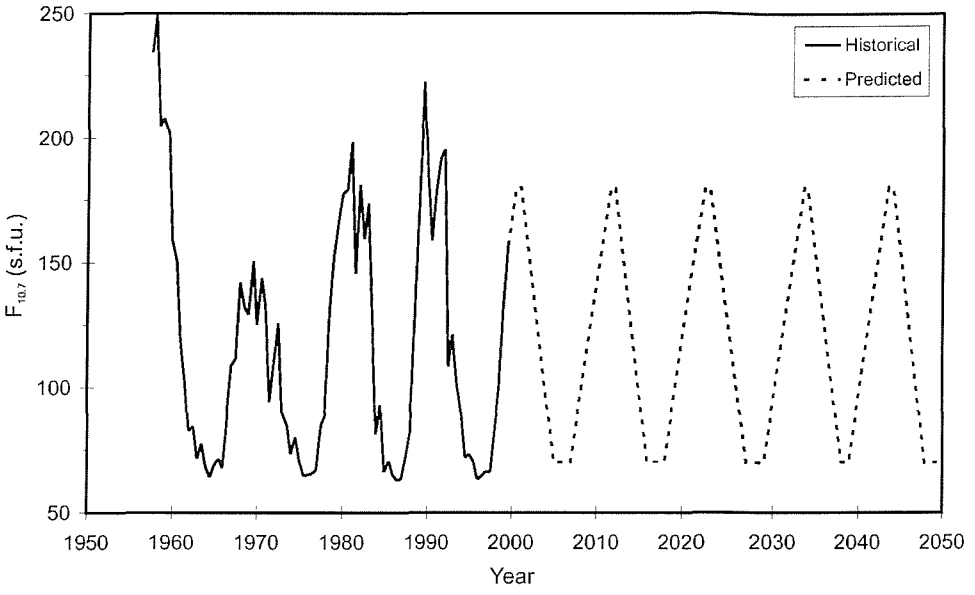

Figure 4.3: Historical solar flux, and future solar flux predictions

constant value of 1.15 in the TRAP model, allowing the diurnal density variations to be smoothed out.

Extensive research by King-Hele [**71**] has shown that for a spherically symmetric atmosphere, which is assumed in the adopted model, the changes to semi-major axis and eccentricity, with respect to the eccentric anomaly, are governed by,

$$\frac{da}{dE} = -2b\rho a^2 \sqrt{\frac{x^3}{y}} \left[1 - \frac{d\,(1-e)}{(1+e)}\right]^2, \text{ and} \tag{4.21}$$

$$\frac{de}{dE} = -2b\rho a \left(1-e^2\right) \sqrt{\frac{x}{y}} \left[1 - \frac{d\,(1-e)}{(1+e)}\right]^2 \cos E, \tag{4.22}$$

where

$$b = \frac{C_D A}{2m_s}, \tag{4.23}$$

$$d = \sqrt{1-e^2}\left(\frac{w_s \cos i}{n}\right), \tag{4.24}$$

$$x = 1 + e\cos E, \tag{4.25}$$

$$y = 1 - e\cos E. \tag{4.26}$$

Here, C_D is the drag coefficient, A is the cross-sectional area of the satellite, m_s is the satellite's mass, w_s is the Earth's sidereal rotation rate and E is the perturbed (by J_2 and J_3) eccentric anomaly.

The atmospheric drag model employed by TRAP can be computationally expensive if the changes to the semi-major axis and eccentricity are calculated at every time interval. However, this is resolved by using average changes over one orbit. This is achieved by numerically integrating the derivations around a nominal reference orbit (e.g. a Keplerian orbit perturbed by J_2 and J_3) and dividing the integrals by 2π. For example,

$$\overline{\Delta a} = \frac{1}{2\pi}\int_0^{2\pi}\left(\frac{da}{dE}\right)dE,$$

$$\overline{\Delta e} = \frac{1}{2\pi}\int_0^{2\pi}\left(\frac{de}{dE}\right)dE,$$

where $\overline{\Delta a}$ and $\overline{\Delta e}$ is the average change in semi-major axis and eccentricity over one orbit. With the continuing change in semi-major axis and eccentricity, due to atmospheric drag, the values for the satellite's mean motion, n, and its orbital period, τ, have to be re-calculated using the updated values of a. If the number of orbital revolutions considered is large, then $\overline{\Delta a}$ and $\overline{\Delta e}$ can be periodically re-calculated to ensure the desired degree of accuracy.

4.1.3 Validation of Orbital Perturbations Methodology

Validation is of crucial importance when implementing a new model of such complexity. It is the purpose of this section, therefore, to discuss the validation methods that were used in the development of the orbital motion equations applied to accurately model a satellite's (perturbed) orbital motion. A number of case studies were performed using the TRAP model and compared with results produced by Walker **[3]** and Barrows [4]. Here we will discuss one of these case scenarios.

An object, with known initial orbital elements from a 1993 epoch, was selected and modelled using the orbital perturbations model. In this case, the object chosen was an Ariane 4 third stage, with COSPAR ID 1991-050F, that was used to launch the ERS-1 spacecraft. The third stage was left in a high inclination, near-circular low Earth orbit. Although the mass of the Ariane 4 third stage is well known, there exists

an uncertainty in the knowledge of the cross-sectional area projected normal to the direction of motion. This uncertainty can cause discrepancies in the representation of the atmospheric drag perturbation. An area-to-mass ratio of 0.0196 m^2/kg was assumed during this simulation. The results produced by Walker [3] were validated by comparing the long-term orbital evolution predictions of the Ariane 4 third stage with the variations recorded in its two-line element (TLE) history, which was obtained from weekly USSPACECOM catalogues.

Figures 4.4 and 4.5 show the evolution of the semi-major axis for the TRAP and IDES predictions. Figure 4.5 also contains the TLE data. The TRAP model predicts a decay rate of semi-major axis similar to that of the IDES model with slight differences occurring because of the constant value of solar flux, $F_{10.7}$, assumed in TRAP, 125 (10^4 Jy) for this particular simulation. Walker [3] indicated that the rate of decay, which is approximately three times faster than the TLE data, was caused by an incorrect estimation of the area-to-mass ratio. However, the maximum difference in semi-major axis after six years of propagation is about 2 km, which is not unreasonable at an altitude of 770 km where the atmospheric density is low.

Figures 4.6 and 4.7 show the periodic fluctuations in eccentricity as predicted by the TRAP and IDES models, with good agreement. The TLE data, seen in Figure 4.7, shows a much smaller amplitude than both the TRAP and IDES predictions because the odd zonal harmonics in Earth's gravitational field (such as J_3) are known to be poorly represented by the TLE data. Hence, given the deficiencies in the TLE data, the TRAP perturbation orbit propagator produces an acceptable representation of the eccentricity fluctuations of this object.

Figures 4.8 and 4.9 show the long-term variations of inclination as predicted by the TRAP and IDES models. The decrease in inclination over the six years is around 0.2^o, with both models and the TLE data agreeing very well, in both trend and magnitude.

Figures 4.10 and 4.11 show the secular precession of the argument of perigee due to the J_2 second harmonic as predicted by the TRAP and IDES models, with good agreement. A secular variation, with a frequency of around three revolutions per year is visible, and typical of a near-circular low Earth orbit. The evolution of the right ascension of the ascending node is shown in Figure 4.12. An increase in a secular manner through a range of 360^o with a period of 1 year is visible, agreeing with that presented by Walker

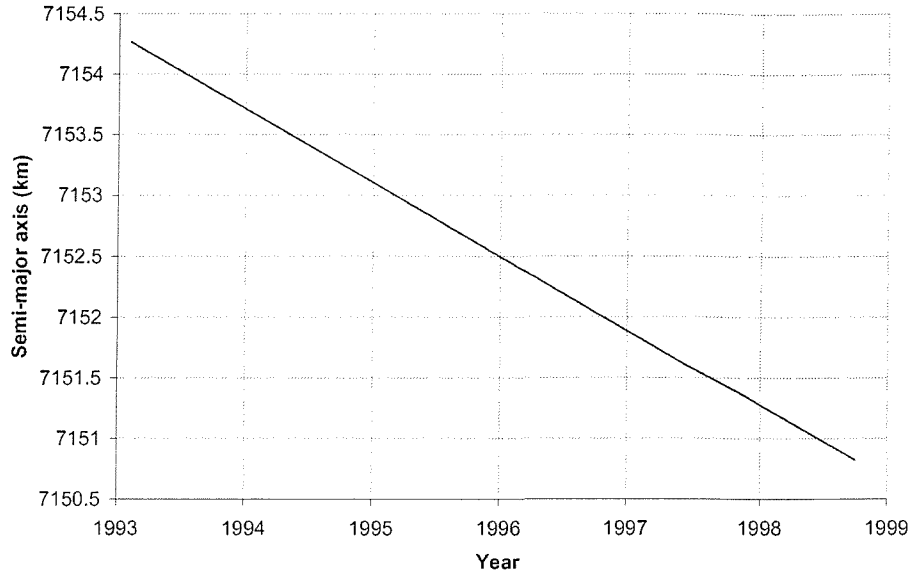

Figure 4.4: TRAP long-term predictions of semi-major axis

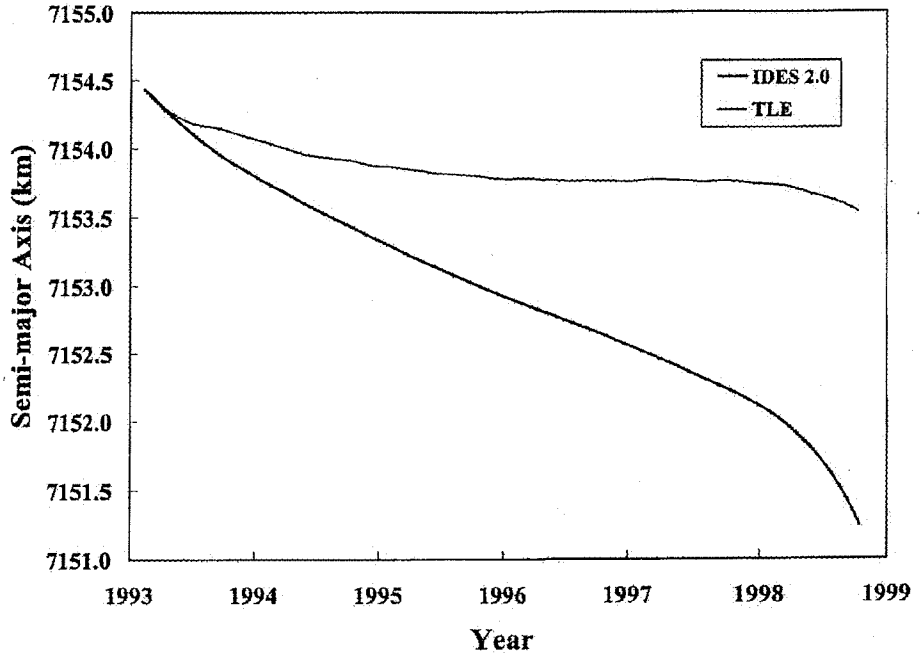

Figure 4.5: IDES long-term predictions of semi-major axis compared to TLE data [3]

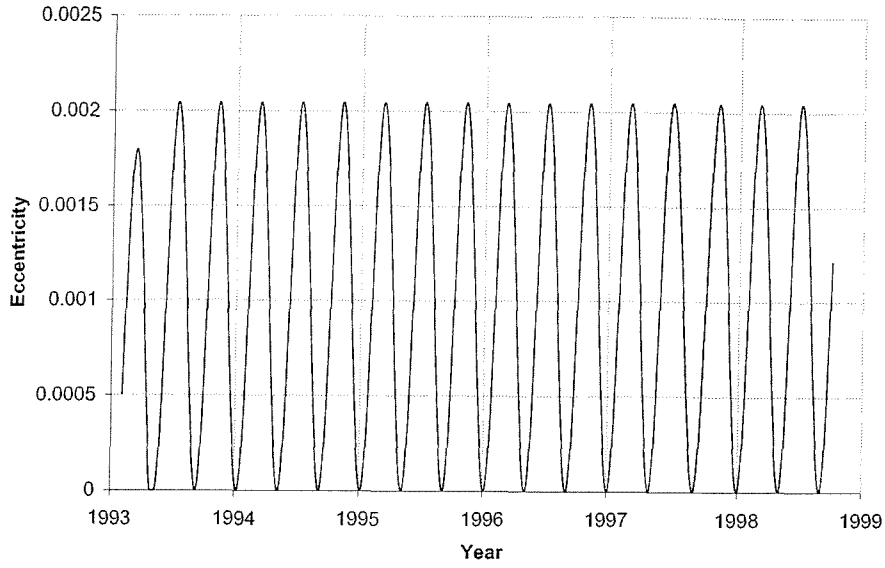

Figure 4.6: TRAP long-term predictions of eccentricity

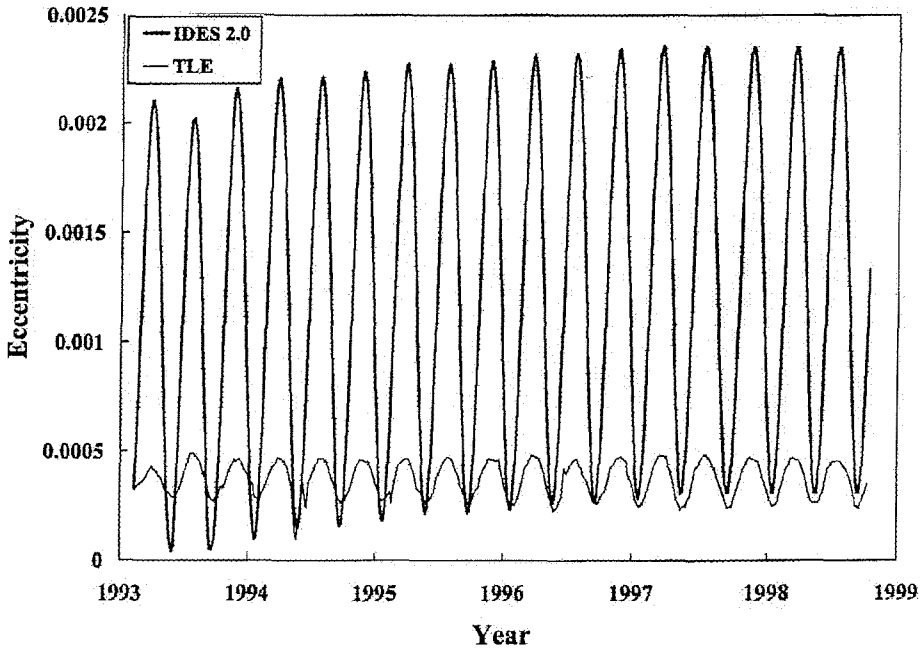

Figure 4.7: IDES long-term predictions of eccentricity compared to TLE data [3]

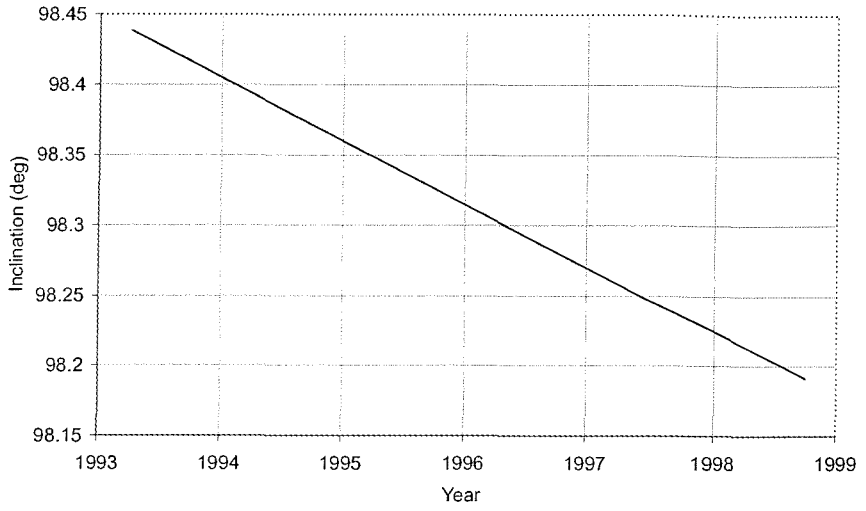

Figure 4.8: TRAP long-term predictions of inclination

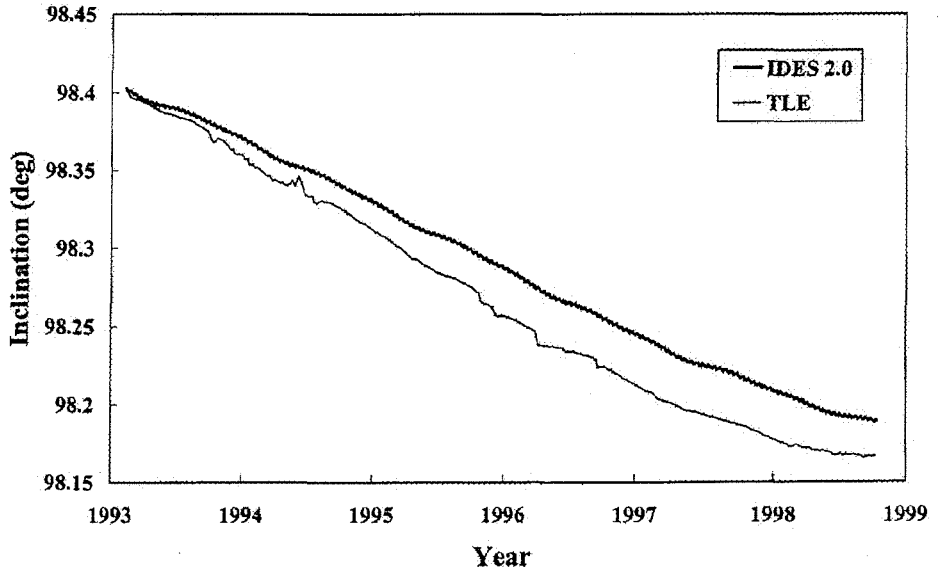

Figure 4.9: IDES long-term predictions of inclination compared to TLE data [3]

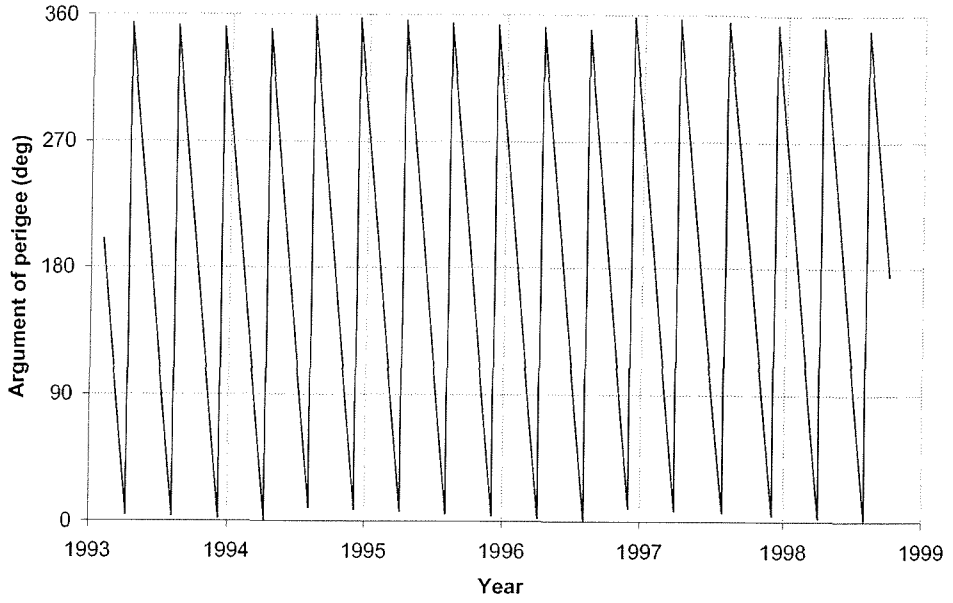

Figure 4.10: TRAP long-term prediction of argument of perigee

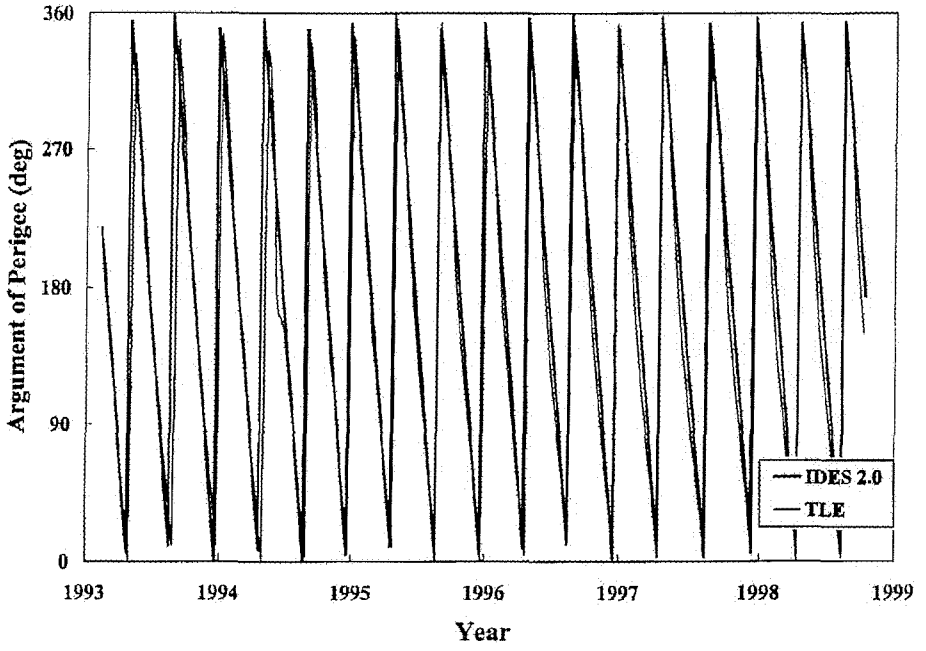

Figure 4.11: IDES long-term predictions of argument of perigee compared to TLE data [3]

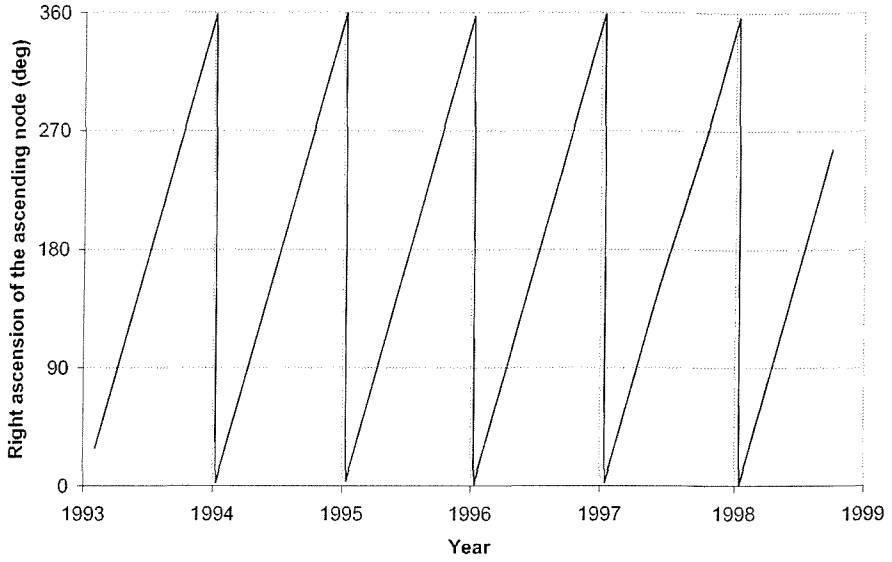

Figure 4.12: TRAP long-term predictions of right ascension of the ascending node

[3], and in keeping with a sun-synchronous orbit.

4.2 Tether System's Orbital Motion

The equations of motion for an orbiting satellite around the Earth have been introduced in the previous section. However, unlike a typical spacecraft, space tether systems are often extremely long and flexible and as such very complex to model. Typically, a space tether system will consist of two objects that are coupled together by a tether. In 1996 the Tether Physics and Survivability Experiment (TiPS) (see Chapter 3) was launched to provide a better understanding of tether dynamics [50].

The following sections will introduce the equations of motion for an orbiting space tether system consisting of two end-bodies connected by a flexible tether. A general model will be discussed first followed by a simplified model, which can be used to reduce the tether model's complexity. Finally, the massless tether model will be introduced providing the foundations for the 'bead' model, implemented into TRAP, which will be discussed further in Chapter 5.

4.2.1 General Model

There exist a number of sophisticated tether models that account for the tether bending stiffness, internal friction and the dimensions of the end-bodies. However, for the purpose of this discussion a tether system consisting of two point masses connected by a flexible thread will be considered. This is the model most commonly found in the literature [72].

In the general model, the length of the tether AB may vary due to tether deployment or retrieval from the end-bodies. Therefore, assuming the tether is completely deployed and unstrained, a parameter s is introduced that measures the arc length along the unstrained tether from A to B, such that $0 < s < l$, where l is the total length of the tether. Hence, at time t, three tether segments can be considered:

1. $0 \leq s \leq s_A(t)$, tether retracted into the body A.
2. $s_A(t) < s < s_B(t)$, tether deployed between the bodies A and B.
3. $s_B \leq s \leq l$, tether retracted into the body B.

Equations of Tether Motion

The position of a point s between A and B at a time t is specified by applying a geocentric reference frame, at the Earth's centre, where the X-axis points towards the First Point of Aries, the Z-axis points to the north celestial pole and the Y-axis completing the right-hand set. Thus, the position of a point s between A and B is given by the position vector $\mathbf{R}(s,\ t)$ - see Figure 4.13.

The tether tension force $\mathbf{T}(s,\ t)$ is introduced as an internal force acting upon the segment $\mathbf{R_A}$ to $\mathbf{R}(s,\ t)$ due to the segment $\mathbf{R}(s,\ t)$ to $\mathbf{R_B}$, and the distribution of mass per unit length, along the tether, is given by $\rho(s)$. Thus, we consider a small segment of tether from s to $s + ds$, where its mass is given by $\rho(s)ds$. Hence, the forces exerted at the ends of the segment are $\mathbf{T}(s + ds,\ t)$ and $-\mathbf{T}(s,\ t)$ - see Figure 4.14.

The effect of Earth's gravity is given by

$$\rho ds\mathbf{g} = -\rho(s)ds\frac{\mu\mathbf{R}}{R^3},$$

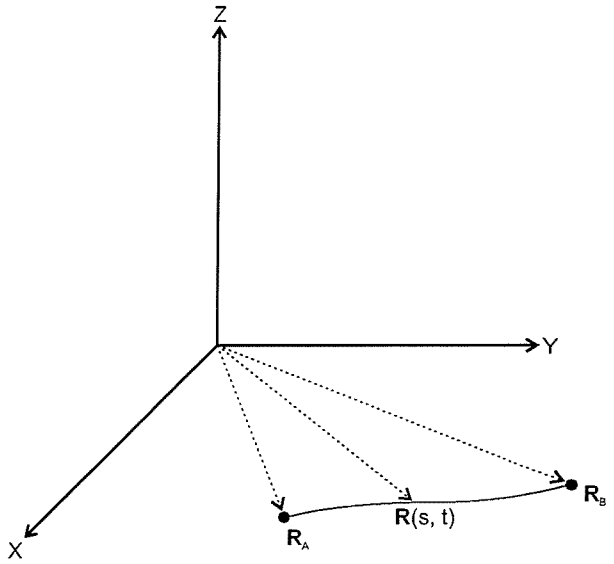

Figure 4.13: Tether position with respect to a geocentric reference frame [**72**]

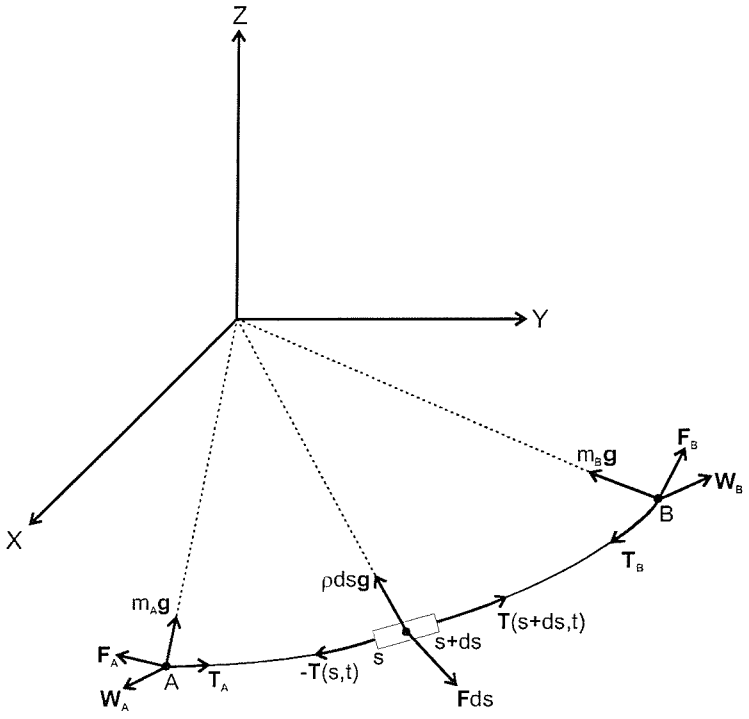

Figure 4.14: Forces exerted on the tether and end-bodies [**72**]

where $\mathbf{R} = \mathbf{R}(s,\ t)$ and $R = |\mathbf{R}|$. The influence of other gravitational perturbations from the Sun, Moon and other celestial bodies are represented by an overall perturbing force $\mathbf{F}$ per unit length. Thus, the small segment, ds, will experience a perturbation force $\mathbf{F}ds$. Hence, the equation of motion for the tether segment centre of mass is given by

$$\rho(s)ds\frac{\partial^2\mathbf{R}}{\partial t^2} = \mathbf{T}(s+ds,\ t) - \mathbf{T}(s,\ t) - \rho(s)ds\frac{\mu\mathbf{R}}{R^3} + \mathbf{F}ds,$$

which reduces to

$$\rho\frac{\partial^2\mathbf{R}}{\partial t^2} = \frac{\partial\mathbf{T}}{\partial s} - \rho\frac{\mu\mathbf{R}}{R^3} + \mathbf{F}. \tag{4.27}$$

By definition a flexible tether will not resist bending, and its tension force will always be tangential to the line of the tether,

$$\mathbf{T} = T\mathbf{n}, \tag{4.28}$$

where $\mathbf{n}$ is the unit tangent vector given by

$$\mathbf{n} = \frac{\partial\mathbf{R}}{\partial s}\left|\frac{\partial\mathbf{R}}{\partial s}\right|^{-1}.$$

The magnitude of the tension can be specified by adopting an appropriate law of elasticity, such as Hooke's law **[73]**,

$$T = E_x(\gamma - 1), \tag{4.29}$$

where $\gamma = |\partial\mathbf{R}/\partial s|$ and $E_x = E_x(s)$ is the tether extensional stiffness **[72]**.

Motion of The End-Bodies

The position of the end-bodies, A and B, at a time t are given by the geocentric radius vectors $\mathbf{R_A}(t) = \mathbf{R}(s_A,\ t)$ and $\mathbf{R_B}(t) = \mathbf{R}(s_B,\ t)$. The masses of the end-bodies along with the retracted tether at a time t are given by

$$\begin{aligned} m_A &= m_A^0 + \int_0^{s_A(t)} \rho(s)ds, \\ m_B &= m_B^0 + \int_0^{s_B(t)} \rho(s)ds, \end{aligned} \tag{4.30}$$

where m_A^0 and m_B^0 represent the end-body masses without the tether.

The rate of change of the masses, m_A and m_B, depend on the tether deployment or retrieval velocity. Thus,

$$\begin{aligned} \frac{dm_A}{dt} &= \rho(s_A)\frac{ds_A}{dt} + \frac{dm_A^0}{dt}, \\ \frac{dm_B}{dt} &= -\rho(s_B)\frac{ds_B}{dt} + \frac{dm_B^0}{dt}. \end{aligned} \tag{4.31}$$

Equation (4.31) also accounts for any mass reduction to m_A^0 and m_B^0 due to the expenditure of fuel as a result of any possible thrusting.

The velocity vectors of the end-bodies are given by

$$\begin{aligned} \mathbf{v_A} &= \frac{d\mathbf{R_A}}{dt}, \\ \mathbf{v_B} &= \frac{d\mathbf{R_B}}{dt}. \end{aligned}$$

Assuming the tether is deployed from the two end-bodies, we can assume that the value of $s_A(t)$ decreases, and for $s_B(t)$ to increase over time. Therefore, over a period dt, a segment $-ds_A$ of mass $-\rho(s_A)ds_A$ will be deployed from A, and a segment ds_B of mass $\rho(s_B)ds_B$ will be deployed from B. Hence, the tether velocities, relative to the end-bodies, at the points of deployment will be given by

$$\begin{aligned} \mathbf{u_A}(t) &= -\left(\frac{\partial \mathbf{R}}{\partial s}\right)_A \frac{ds_A}{dt}, \\ \mathbf{u_B}(t) &= -\left(\frac{\partial \mathbf{R}}{\partial s}\right)_B \frac{ds_B}{dt}. \end{aligned}$$

The calculation of the variation of momentum in the systems 'end-body A + segment $-ds_A$' and 'end-body B + segment ds_B' in a period dt, neglecting any possible thrusting and retaining terms linear in dt, gives

$$\begin{aligned} m_A(t+dt)\mathbf{v_A}(t+dt) - \rho(s_A)ds_A\left[\mathbf{v_A}(t) + \mathbf{u_A}(t)\right] - m_A(t)\mathbf{v_A}(t) \\ = \left[\mathbf{T_A} - m_A(t)\frac{\mu \mathbf{R_A}}{R_A^3} + \mathbf{F_A}\right] dt, \\ m_B(t+dt)\mathbf{v_B}(t+dt) + \rho(s_B)ds_B\left[\mathbf{v_B}(t) + \mathbf{u_B}(t)\right] - m_B(t)\mathbf{v_B}(t) \\ = \left[-\mathbf{T_B} - m_B(t)\frac{\mu \mathbf{R_B}}{R_B^3} + \mathbf{F_B}\right] dt, \end{aligned} \tag{4.32}$$

where $\mathbf{T_A} = \mathbf{T}(s_A,\, t)$ and $\mathbf{T_B} = \mathbf{T}(s_B,\, t)$ are the tether tension forces at the attachment points, and $\mathbf{F_A}$ and $\mathbf{F_B}$ are the overall perturbing forces on the end-bodies [72]. Thus, in the linear approximation of dt,

$$m_A(t+dt)\mathbf{v_A}(t+dt) - m_A(t)\mathbf{v_A}(t) = m_A(t)\frac{d\mathbf{v_A}}{dt}dt + \rho(s_A)ds_A\mathbf{v_A}(t),$$

$$m_B(t+dt)\mathbf{v_B}(t+dt) - m_B(t)\mathbf{v_B}(t) = m_B(t)\frac{d\mathbf{v_B}}{dt}dt - \rho(s_B)ds_B\mathbf{v_B}(t).$$

Finally, substituting into Equation (4.32), gives the equation of motion for each of the end-bodies,

$$\begin{aligned} m_A(t)\frac{d^2\mathbf{R_A}}{dt^2} &= \mathbf{n_A}\left[T_A - \rho(s_A)\gamma_A\left(\frac{ds_A}{dt}\right)^2\right] - m_A(t)\frac{\mu\mathbf{R_A}}{R_A^3} + \mathbf{F_A} + \mathbf{W_A}, \\ m_B(t)\frac{d^2\mathbf{R_B}}{dt^2} &= -\mathbf{n_B}\left[T_B - \rho(s_B)\gamma_B\left(\frac{ds_B}{dt}\right)^2\right] - m_B(t)\frac{\mu\mathbf{R_B}}{R_B^3} + \mathbf{F_B} + \mathbf{W_B}, \end{aligned} \tag{4.33}$$

where

$$T_A = E_x(s_A)(\gamma_A - 1),$$

$$\gamma_A = \left|\frac{\partial\mathbf{R}}{\partial s}\right|_A,$$

$$T_B = E_x(s_B)(\gamma_B - 1), \text{ and}$$

$$\gamma_B = \left|\frac{\partial\mathbf{R}}{\partial s}\right|_B.$$

Here $T_{A,B}$ represents the tension at the attachment points, and $\mathbf{W_{A,\,B}}$ the thrust forces, if any [72].

4.2.2 Simplified Model

The partial differential equations governing a tether system's motion, are complex, and their solution is far from straight forward. Here we will discuss how these equations can be simplified, producing the rigid tether model. An inextensible tether model ignores longitudinal strain in the tether, and instead of using the law of elasticity, the following constraint is assumed,

$$\left|\frac{\partial\mathbf{R}}{\partial s}\right| = 1. \tag{4.34}$$

This results in the tension, T, now playing the role of an indefinite Lagrange multiplier, depending both on time, t, and the arc length, s. This constraint leads to the 'dumb-bell' model of two point masses with a rigid rod between them. The model with a massless tether implies that $\rho = 0$ and $\mathbf{F} = \mathbf{0}$. Hence, Equation (4.27) is reduced to the condition of constant tension, $\partial \mathbf{T}/\partial s = \mathbf{0}$, while the unit tangent vector, in Equation (4.28), is expressed as

$$\mathbf{n} = \frac{\mathbf{R_B} - \mathbf{R_A}}{|\mathbf{R_B} - \mathbf{R_A}|}. \tag{4.35}$$

The law of elasticity, in Equation (4.29), is modified to allow for tether slackness, since the tether, on the whole, never withstands compression,

$$T = \begin{cases} E_x(\gamma - 1) & \text{if } \gamma > 1, \\ 0 & \text{if } \gamma \leq 1, \end{cases} \qquad \gamma = \frac{|\mathbf{R_B} - \mathbf{R_A}|}{s_B - s_A}. \tag{4.36}$$

The tension of an inextensible and massless tether is determined as an indefinite Lagrange multiplier associated with the constraint

$$|\mathbf{R_B} - \mathbf{R_A}| \leq s_B - s_A. \tag{4.37}$$

The motion of the end-bodies are governed by Equation (4.33) with

$$T_A = T_B = T,$$

$$\mathbf{n_A} = \mathbf{n_B} = \mathbf{n}.$$

The motion of a dumb-bell type tether system is described in more detail by Lee-Bapty **[39]**.

4.2.3 The Massless Tether Model

Historically, models with a massless tether were first applied to investigate a tether system's orbital motion. They have resulted in a number of qualitative and quantitative discoveries, regarding a tether system's orbital motion. Many more advanced models have since followed, but the massless tether model still retains its significance as a relatively simple method for calculating a tether system's orbital motion.

The general equations of a non-rigid orbiting tether system have already been introduced in Section 4.2.1 as a particular case of the general motion equations. Consider a tether system consisting of two end-bodies, A and B, where B is a massive satellite and A is a sub-satellite of relatively small mass, i.e. $m_B \gg m_A$, where m_A and m_B are the

end-body masses of A and B, respectively. Therefore, the tether system's centre of mass will coincide with the satellite, B.

The tether system's centre of mass is modelled by firstly introducing a geocentric inertial reference frame (xyz) with the y-axis pointing along the horizontal component of the velocity vector, the z-axis along the normal to the orbit plane and the x-axis completing the right hand set. The equations of the relative motion of the sub-satellite, A, tethered to the origin of the moving reference frame can then be derived from Equation (4.33),

$$m_A \left[\ddot{\mathbf{r}}_\mathbf{A} + \dot{n} \times \mathbf{r_A} + 2n \times \dot{\mathbf{r}}_\mathbf{A} + n \times (n \times \mathbf{r_A}) + \ddot{\mathbf{R}}_\mathbf{B} + \frac{\mu \mathbf{R_A}}{R_A^3} \right] = \mathbf{T_A} + \mathbf{F_A} \qquad (4.38)$$

where $\mathbf{r_A} = \mathbf{R_A} - \mathbf{R_B}$ is the radius vector of A with respect to the orbital frame, $\mathbf{R_A}$ and $\mathbf{R_B}$ are the geocentric radius vectors of A and B, n is the orbital angular rate, $\mathbf{T_A}$ is the tether tension force and $\mathbf{F_A}$ is the non-gravitational perturbations of the sub-satellite. Note that the time derivatives of $\mathbf{r_A}$ are calculated with respect to the orbital reference frame xyz, whereas the vector $\mathbf{R_B}$ is differentiated with respect to the geocentric reference frame XYZ.

The Keplerian motion of an Earth orbiting object is given by

$$\ddot{\mathbf{R}}_\mathbf{B} = -\mu \frac{\mathbf{R_B}}{R_B^3}.$$

Therefore, in the linear approximation of $\mathbf{r_A}$, the difference

$$\frac{\mathbf{R_A}}{R_A^3} - \frac{\mathbf{R_B}}{R_B^3} = \frac{\mathbf{r_A}}{R_B^3} - 3\left(\mathbf{r_A} \bullet \mathbf{R_B}\right) \frac{\mathbf{R_B}}{R_B^5}.$$

Ultimately, the equations of relative motion for the sub-satellite are given by

$$\begin{pmatrix} \ddot{x} - 2\dot{y}n - \dot{n}y - \left(1 + 2p^{-1}\right) n^2 x \\ \ddot{y} + 2\dot{x}n - \dot{n}x - \left(1 - p^{-1}\right) n^2 y \\ \ddot{z} + p^{-1} n^2 z \end{pmatrix} = \frac{1}{m_A} \begin{pmatrix} T_x + F_x \\ T_y + F_y \\ T_z + F_z \end{pmatrix} \qquad (4.39)$$

where $p = 1 + e\cos\theta$, and F_x, F_y and F_z are the components of the perturbing force $\mathbf{F_A}$ [72].

In accordance with Equation (4.27), a massless tether ($\rho = 0$) is not subject to gravitational forces. Therefore, once they are ignored, the next logical step would be to neglect non-gravitational forces also, i.e $\mathbf{F} = 0$. These assumptions, predict that a taut tether will always be stretched along the line AB, see Equation (4.35), and the tether tension

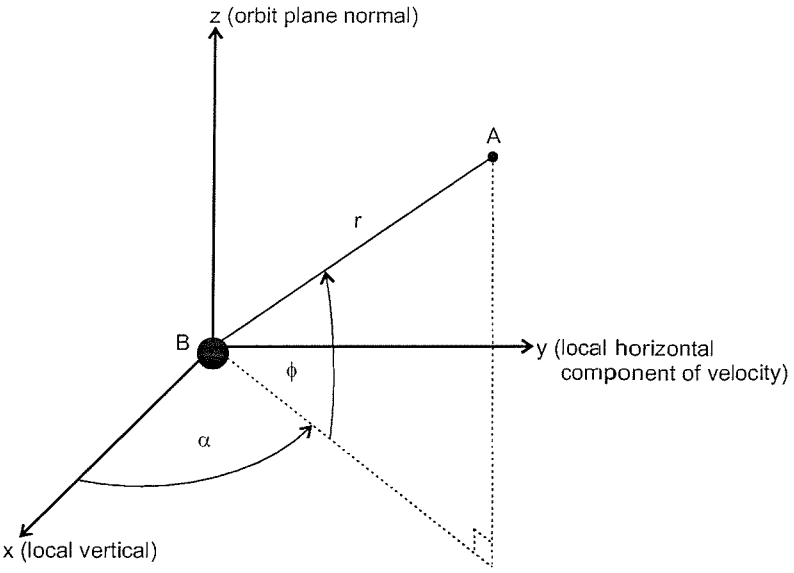

Figure 4.15: Relative position of a sub-satellite, A, tethered to a satellite, B, of greater mass

force will have the components

$$(T_x, T_y, T_z) = -\frac{T}{r}(x, y, z),$$

$$T = E_x\left(\frac{r}{l} - 1\right),$$

$$r = \sqrt{x^2 + y^2 + z^2},$$

where l is the unstrained tether length and E_x is the tether extensional stiffness.

The motion of an inextensible tether system, is conveniently specified by the spherical co-ordinates, r, α, ϕ, where r represents the distance from the object, α is the in-plane and ϕ is the out-of-plane rotation - see Figure 4.15. If we substitute

$$\begin{aligned} x &= -r\cos\alpha\cos\phi, \\ y &= -r\sin\alpha\cos\phi, \\ z &= -r\sin\phi, \end{aligned}$$

into Equation (4.39), we obtain

$$\ddot{\alpha}+\dot{n}+(\dot{\alpha}+n)\left(\frac{2\dot{r}}{r}-2\dot{\phi}\tan\phi\right)+\frac{3n^2}{p}\sin\alpha\cos\alpha=-\frac{F_\alpha}{m_A r\cos\phi},$$

$$\ddot{\phi}+\frac{2\dot{r}}{r}\dot{\phi}+\left[(\dot{\alpha}+n)^2+\frac{3n^2}{p}\cos^2\alpha\right]\sin\phi\cos\phi=-\frac{F_\phi}{m_A r}, \tag{4.40}$$

$$\ddot{r}-r\left[\dot{\phi}^2+(\dot{\alpha}+n)^2\cos^2\phi+\frac{n^2}{p}\left(3\cos^2\phi\cos^2\alpha-1\right)\right]+\frac{T}{m_A}=-\frac{F_r}{m_A},$$

where the disturbing force components, given by Beletsky and Levin [**72**], are

$$\begin{pmatrix}F_r\\F_\alpha\\F_\phi\end{pmatrix}=\begin{pmatrix}\cos\alpha\cos\phi & \sin\alpha\cos\phi & \sin\phi\\-\sin\alpha & \cos\alpha & 0\\-\cos\alpha\sin\phi & -\sin\alpha\sin\phi & \cos\phi\end{pmatrix}\begin{pmatrix}F_x\\F_y\\F_z\end{pmatrix}. \tag{4.41}$$

If we now take the true anomaly, θ, as an independent variable we get

$$\begin{aligned}\ddot{\alpha}+2(\dot{\alpha}+1)\left(\frac{\dot{r}}{r}-\frac{e\sin\theta}{p}-\dot{\phi}\tan\phi\right)+\frac{3}{p}\sin\alpha\cos\alpha &= Q_\alpha,\\ \ddot{\phi}+2\dot{\phi}\left(\frac{\dot{r}}{r}-\frac{e\sin\theta}{p}\right)+\sin\phi\cos\phi\left[(\dot{\alpha}+1)^2+\frac{3}{p}\cos^2\alpha\right] &= Q_\phi, \qquad (4.42)\\ \ddot{r}-2\dot{r}\frac{e\sin\theta}{p}+r(\lambda-u) &= Q_r,\end{aligned}$$

where

$$\begin{aligned}u &= \dot{\phi}^2+(\dot{\alpha}+1)^2\cos^2\phi+\frac{1}{p}\left(3\cos^2\phi\cos^2\alpha-1\right),\\ Q_\alpha &= -\frac{F_\alpha}{m_A n^2 r\cos\alpha},\\ Q_\phi &= -\frac{F_\phi}{m_A n^2 r},\\ Q_r &= -\frac{F_r}{m_A n^2},\\ \lambda &= \frac{T}{m_A n^2 r}\geq 0.\end{aligned}$$

Here dots indicate differentiation with respect to true anomaly [**72**]. Therefore, with true anomaly as an independent variable, and after the substitution of

$$\left(\tilde{x},\,\tilde{y},\,\tilde{z},\,\tilde{\lambda}\right)=p\,(x,\,y,\,z,\,\lambda)$$

Equation (4.39) takes the form

$$\begin{pmatrix} \ddot{\tilde{x}} - 2\dot{\tilde{y}} + \left(\tilde{\lambda} - 3\right) p^{-1}\tilde{x} \\ \ddot{\tilde{y}} + 2\dot{\tilde{x}} + \tilde{\lambda} p^{-1}\tilde{y} \\ \ddot{\tilde{z}} + \left(1 + \tilde{\lambda} p^{-1}\right)\tilde{z} \end{pmatrix} = \frac{p}{m_A n^2} \begin{pmatrix} F_x \\ F_y \\ F_z \end{pmatrix}. \tag{4.43}$$

The massless tether model has provided a number of qualitative and quantitative discoveries, regarding a tether system's orbital motion. Although many more advanced models exist, the massless tether model is still a very significant method for calculating a tether system's orbital motion. Hence, it is the massless tether model which is used to provide the foundations for the 'bead' model, implemented into TRAP. This is discussed further in the following chapter.

4.3 Summary

The equations introduced in Section 4.1 have been successfully implemented into the TRAP model and thoroughly validated using work by Walker **[3]** and Barrows **[4]**. They provide an accurate method for propagating the orbital space debris population, whilst taking into account the major orbital perturbation effects of an Earth type orbit.

The equations introduced in Section 4.2 gave an account of a tether system's orbital motion. Although a number of sophisticated tether models exist, the most commonly published model was adopted. Here the tether system is modelled as two point masses connected by a flexible tether. The first part of this discussion introduced the equations of tether motion and the motion of the end-bodies for a general tether model. A number of simplifications were then discussed which produces a rigid tether model. This removes a lot of the complexities in the model and is ideal for a first approximation. Finally, the massless tether model was introduced. In the past this model has resulted in a number of qualitative and quantitative discoveries, regarding a tether systems orbital motion. The massless tether model provides the foundations for the 'bead' model that is implemented into the TRAP model and is discussed further in the next chapter.

Chapter 5

Tether Risk Assessment Program

The first deployment of a tether in space was performed during the Gemini programme in the mid 1960's. A number of proposals for using tethers in space have since been put forward. Such proposals offer a wide range of applications, such as de-orbiting satellites, re-boosting the International Space Station and conducting atmospheric experiments. However, introducing a long thin structure, such as a space tether, into Earth orbit produces a number of problems. One major concern is the interaction of a space tether system with the orbital debris environment. A space tether is typically a few kilometres in length and just a few centimetres, or smaller, in diameter. This type of design produces very large cross-sectional areas which is very susceptible to debris impacts, with just one impact resulting in the possibility of mission failure. It is crucial, therefore, that a good understanding of the interaction between the orbital space debris environment and a space tether system is achieved.

The purpose of this chapter is to provide a comprehensive description of the Tether Risk Assessment Program (TRAP), which is capable of performing collision and sever risk assessments for an orbiting space tether system as a result of the orbital space debris environment. The TRAP model was implemented in Visual C++ with a Microsoft OpenGL graphical user interface, and consists of four main programs, namely:

- The **Breakup Program**, which determines the physical properties (e.g. mass, size, area) and Δv's for each breakup fragment generated. The Breakup Program can model either a low or high intensity explosion, or a catastrophic or non-catastrophic collision.

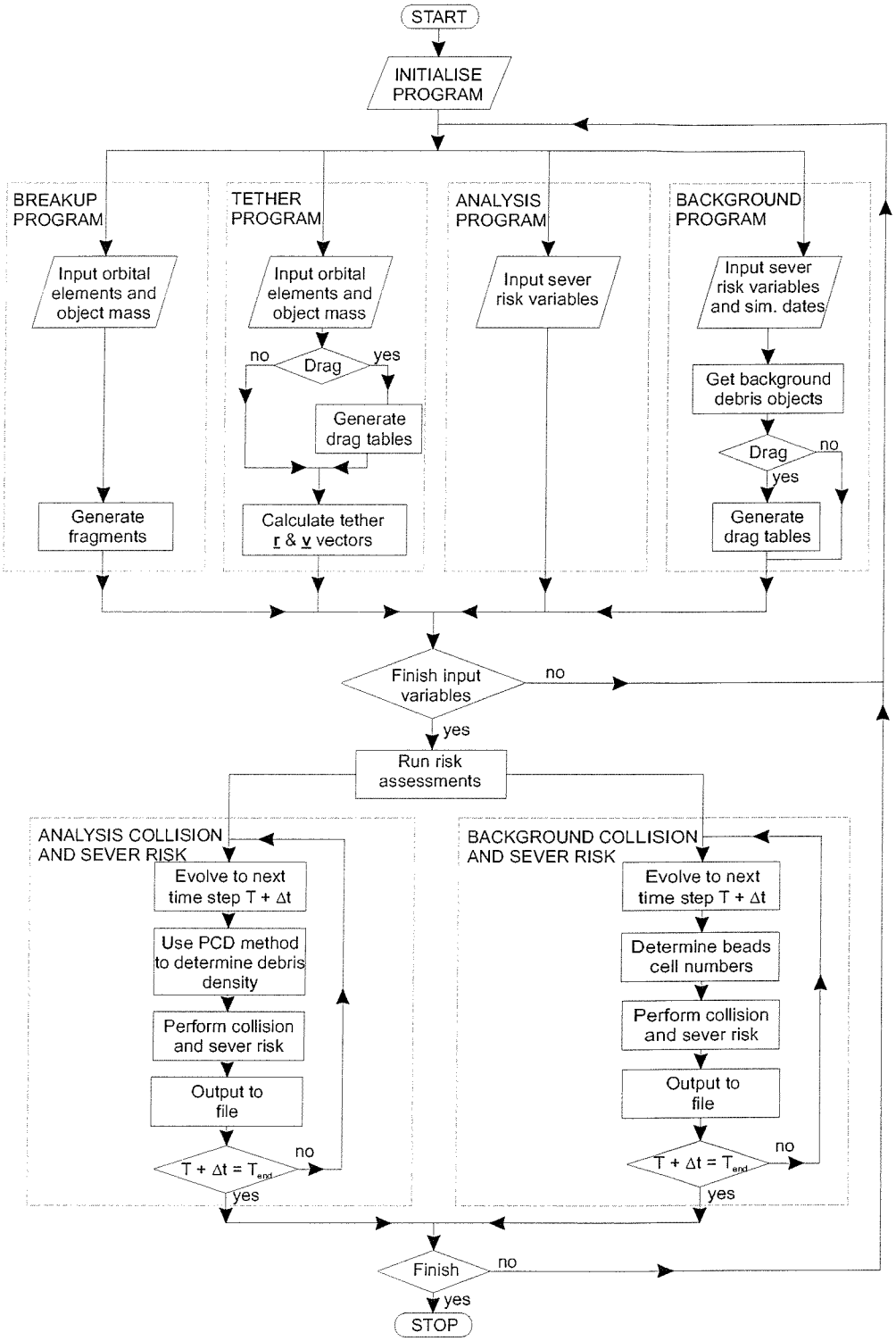

Figure 5.1: Tether Risk Assessment Program flowchart

- The **Tether Program**, which determines the position and velocity vectors for each of the 'beads' used to model the tether system.
- The **Analysis Program**, which models the collision and sever risks of an orbiting space tether system arising from a debris cloud produced by a fragmentation event (modelled by the Breakup Program).
- The **Background Program**, which models the collision and sever risks to an orbiting space tether system arising from the background orbital space debris environment. It is also used for predicting the future background debris population based on recent space activities.

The architecture, data and control flow of the TRAP model is illustrated in Figure 5.1.

5.1 The Breakup Program

The Breakup Program models a fragmentation event which can take the form of a low or high intensity explosion, or a catastrophic or non-catastrophic collision. However, a number of breakup models exist, and the choice of which one to implement may influence the outcome of the collision and sever probability assessments. An analysis of four leading breakup models was performed by Williams et al **[31]** to assess the sensitivity of the debris cloud properties to the different models used to generate the cloud.

Analysis of Breakup Models

Most space debris environment models use isotropic breakup models to generate a fragment population, which is subsequently propagated to define the future debris population. These breakup models rely heavily upon empirically derived equations that are used to determine the fragments initial conditions, such as mass, size, Δv and area-to-mass ratios. However, a number of ground-based experiments have resulted in a variety of data sets, such that a range of best-fit curves, and consequently, different defining equations and different initial parameters have been generated, depending on the experiment that was undertaken. This problem has been exacerbated because the experimental data is limited, in terms of mass, size, Δv and mass-to-area ratios, and

yet many models extrapolate the results beyond these limits, especially in terms of Δv [31].

Research conducted by Williams et al [31] analysed the sensitivity of the debris cloud properties to the breakup model used to generate them. Four breakup models, IDES [3], SDM [74, 75], MASTER [15, 16, 17] and EVOLVE 4.0 [32] were compared in terms of their distributions of the cumulative number of fragments, fragment Δv's, and mass-to-area ratios as a function of fragment mass. A number of breakup scenarios were considered, including low and high intensity explosions, and catastrophic and non-catastrophic collisions.

The results produced by Williams et al [31] showed, generally, that the IDES, SDM and MASTER models were in fairly good agreement, for most scenarios, whilst the results produced by EVOLVE 4.0 were significantly different. However, this is not too surprising since the breakup models that agree with each other do so because they have used the same equations or sets of equations, which have, in turn, been empirically derived from the same pool of limited data. Hence, the breakup models of IDES, SDM and MASTER are not truly independent. However, there remains a good deal of discrepancy between the models for certain distributions, especially when the EVOLVE 4.0 breakup model is compared to the other models. In the development of EVOLVE 4.0, NASA chose to base their equations on fragment diameter, and in the case of the Δv equations, on the area-to-mass ratio. Conversely, the other three models based their equations on fragment mass. This is the principal reason why the NASA EVOLVE 4.0 model produces significantly different results.

It is not possible to determine which of these breakup models most accurately predicts the actual outcome of a breakup event. Hence, it was concluded that a much larger number of ground-based experiments and on-orbit observations should be conducted, increasing the pool of data upon which the empirically derived equations are based.

As a consequence of the research conducted by Williams et al [31] it was decided that the IDES breakup model would be implemented into the TRAP model. The focus for the rest of this section will be to discuss the implementation of the IDES breakup model, highlighting the equations used to determine the cumulative number of fragments generated, mass, Δv's and mass-to-area ratios. In order to ensure the successful implementation of the IDES breakup model into the TRAP model, a method

of validation was adopted, which will also be discussed.

5.1.1 Implementation of The IDES Breakup Model

The IDES breakup model determines the physical properties for each fragment generated (e.g. mass, size, area). The model also calculates the Δv's imparted to each fragment as the original space system fragments. In order to determine these physical properties and Δv's, the IDES breakup model requires the original space system's orbital parameters and mass prior to the fragmentation event. If the fragmentation event is a collision, then the mass and velocity of the impacting projectile are also required. The following relationships, as discussed by Walker [3], have been derived for the IDES breakup model and are supported by deterministic data and comply with the laws of physics (i.e. mass and energy conservation).

Mass to Size/Area Relationships

The fragment mass, M (kg), is related to its size, d (m), using,

$$M = \begin{cases} 46.81 d^{2.26} & \text{if } d > 0.0062 \text{ m}, \\ 2094 d^{3} & \text{if } d \leq 0.0062 \text{ m}. \end{cases} \tag{5.1}$$

The fragment mass is also related to its area, A_{eff} (m^2), using,

$$M = \begin{cases} 61.5 A_{\text{eff}}^{1.13} & \text{if } A_{\text{eff}} > 3.0 \times 10^{-5} \text{ m}^2, \\ 3009 A_{\text{eff}}^{1.5} & \text{if } A_{\text{eff}} \leq 3.0 \times 10^{-5} \text{ m}^2. \end{cases} \tag{5.2}$$

Mass Distributions

The cumulative number of fragments, CN, greater than a mass, M (kg) , will depend on the type of fragmentation event. For low intensity explosions, we have,

$$CN = \begin{cases} 171 \exp\left(-0.6514\sqrt{M f_m}\right) & \text{for } M \geq 1.936 \text{ kg}/f_m, \\ 869 \exp\left(-1.8215\sqrt{M f_m}\right) & \text{for } M < 1.936 \text{ kg}/f_m, \end{cases} \tag{5.3}$$

where f_m is the ratio of 1,000 kg over the breakup object's mass, M_t (kg).

For high intensity explosions, we assume a 50:50 split of the breakup object's mass. That is 50% follows the low intensity exponential law, given by Equation (5.3), and

50% follows the power law given by

$$CN = \begin{cases} 171\exp\left(-0.6514\sqrt{Mf_m}\right) + P & \text{for } M \geq 1.936 \text{ kg}/f_m, \\ 869\exp\left(-1.8215\sqrt{Mf_m}\right) + P & \text{for } M < 1.936 \text{ kg}/f_m, \end{cases} \tag{5.4}$$

where

$$P = 0.331\left(\frac{M}{0.5M_t}\right)^{-0.78}.$$

For the low intensity portion, f_m is the ratio of 1,000 kg over 50% of the breakup object's mass, M_t. The power law coefficients were derived by McKnight et al **[76]** from a series of ground tests. However, the breakup object's mass split between the power law and the exponential law is not exactly known and the 50:50 split assumed here minimises the number of large size fragments produced by the exponential law and, more importantly, maximises the number of small and medium size fragments.

For catastrophic collisions, where the energy-to-target mass ratio, EMR, is assumed greater than 40 J/gram, we have,

$$CN = A\left(\frac{M}{M_t + M_p}\right)^{-B}, \tag{5.5}$$

where

$$B = 0.60 + 0.162\left[\frac{EMR - 40}{EMR}\right],$$

$$A = 1.6290 - 1.6636B.$$

Here M_p is the projectile mass (kg) and M_t is the target mass (kg) prior to the collision.

For non-catastrophic collisions, ($EMR < 40$ J/gram), we have,

$$CN = 0.4478\left(\frac{M}{M_e + M_p}\right)^{-0.7496}, \tag{5.6}$$

where

$$M_e = 10^{-6}M_p v^2,$$

is the total ejected mass (kg) and v is the relative impact velocity (km/s). To account for a loss of mass from the target object, the residual target mass is found by deducting the total ejected mass, M_e, from the original target mass, M_t.

Δv Distributions

The velocity, Δv, imparted to a fragment of given size, d, will depend upon the breakup scenario. For low and high intensity explosions we have,

$$\log_{10}(\Delta v_{\text{peak}}) = -0.0676(\log_{10} d)^2 - 0.804(\log_{10} d) - 1.514, \tag{5.7}$$

where Δv_{peak} is the characteristic velocity (km/s) and d is the debris size (m). The corresponding equation for collisions is given by,

$$\log_{10}(\Delta v_{\text{peak}}) = \begin{cases} 0.875 - 0.0676\left[\log_{10}\left(\frac{d}{d_m}\right)\right]^2 & \text{for } d > d_m, \\ 0.875 & \text{for } d \leq d_m, \end{cases} \tag{5.8}$$

where

$$d_m = \frac{\sqrt[3]{E_p}}{c}, \text{ and}$$

$$E_p = 0.5 M_p v_c^2.$$

Here, Δv_{peak} is the characteristic velocity (km/s), d_m is the cut-off diameter (m), c is a constant equal to 8×10^8 $\text{kg}^{1/3}\text{s}^{-2/3}\text{m}^{-2/3}$, v_c is the relative impact velocity (m/s), and E_p is the projectile kinetic energy (Joules).

To determine the Δv associated with each fragment, a spreading function is applied to the peak velocities, Δv_{peak}. This ensures that the Δv imparted to each of the fragments, of a given size and mass, is not the same. NASA's triangular spreading function has been implemented into the IDES breakup model, which bounds the imparted velocities between 0.1 and 1.3 of the peak velocities.

5.1.2 Validation of The Implemented IDES Breakup Model

To ensure that the IDES breakup model had been successfully implemented into the TRAP model a number of validation procedures were performed. This was achieved by simulating a number of historical fragmentation events and comparing the orbital distribution of the modelled debris clouds against actual debris clouds. Here we will discuss two examples.

The first example tested the model accuracy by simulating the fragmentation of the NOAA-3 Delta second stage rocket body, which exploded in 1973 at an altitude of

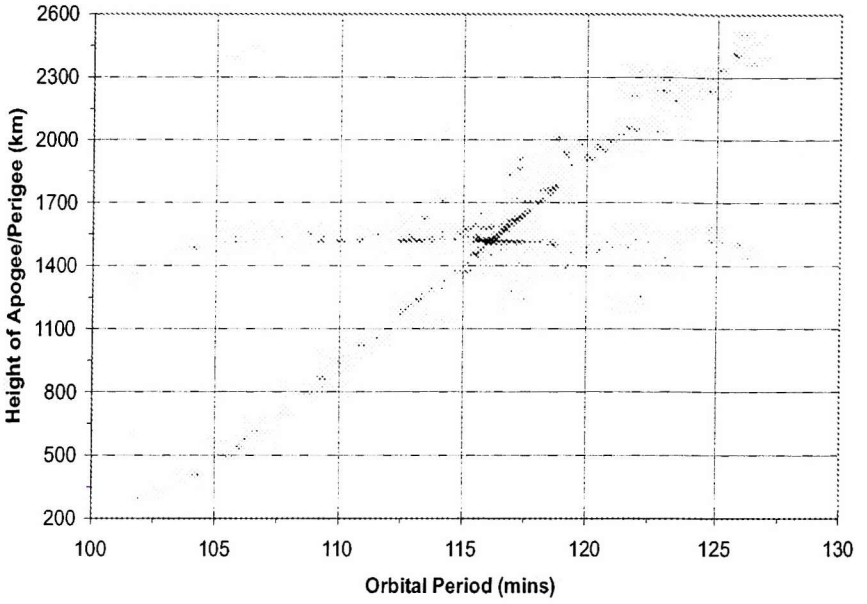

Figure 5.2: Gabbard diagram of tracked fragments from the NOAA-3 breakup

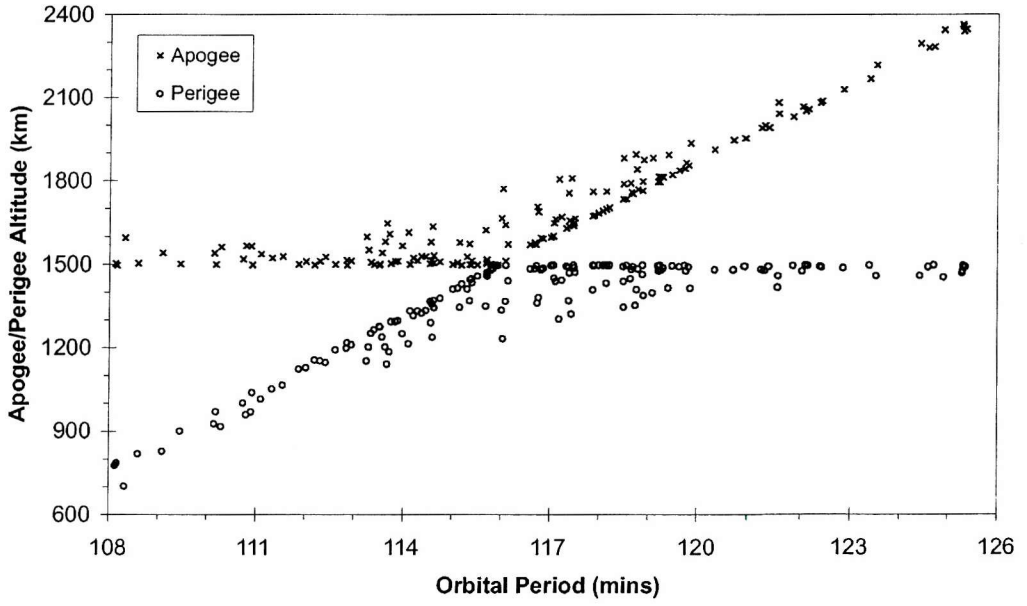

Figure 5.3: Gabbard diagram of the simulated fragments from the NOAA-3 fragmentation

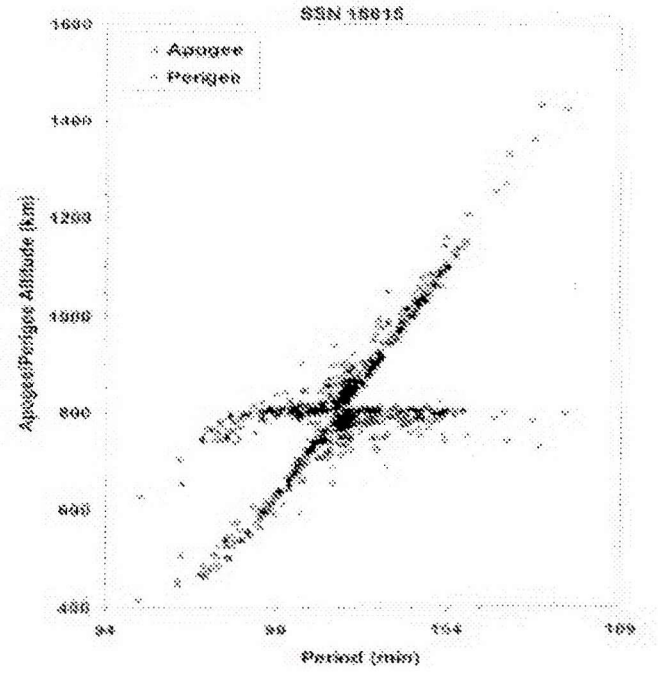

Figure 5.4: Gabbard diagram of tracked fragments from the SPOT-1 fragmentation

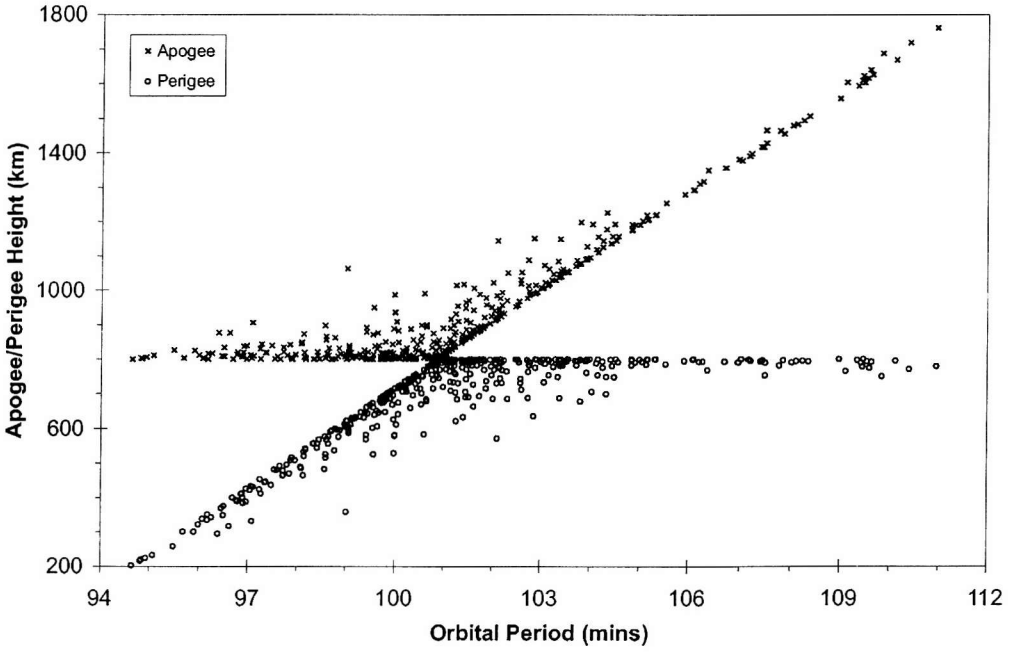

Figure 5.5: Gabbard diagram of the simulated fragments from the SPOT-1 fragmentation

around 1,500 km. This had a breakup mass of about 306 kg, and the simulated breakup generated 163 fragments greater than 10 cm in size (i.e. object's that can be tracked and catalogued at such altitudes from ground-stations). This compares reasonably well to the catalogued number of 182.

The Gabbard diagrams in Figures 5.2 and 5.3 show the apogee and perigee distributions of the actual and simulated cases, respectively. The simulated Gabbard diagram in Figure 5.3 is an instantaneous account of the fragmentation event after the breakup, whereas the actual Gabbard diagram was recorded some time after the fragmentation event occurred. This will account for the slight tailing off of the left-hand 'limb' in Figure 5.2 which is due to the effects of atmospheric drag on the fragments with low perigee altitudes.

The second example considers the fragmentation of the SPOT-1 rocket body, which exploded in November 1986 at an altitude of around 800 km. The rocket body had a mass of 1,634 kg and a total of 421 fragments, greater than 10 cm in size, were generated in the TRAP simulation. This compares reasonably well to the actual catalogued number of 489.

The Gabbard diagrams are illustrated in Figures 5.4 and 5.5, which show the tracked and simulated results, respectively. Figure 5.4 shows the tracked fragments some 3 months after the actual breakup event and the effects of atmospheric drag are once again quite noticeable on the left-hand 'limb'.

5.2 The Tether Program

The Tether Program models a tether system in Earth orbit. The issue of tether dynamics has been discussed in a variety of literature sources, from the 'dumbbell' type rigid tether system [**39**] to more complex models of non-rigid tether dynamics [**72**]. Other literature sources have also considered how the motion of one of the end-masses is perturbed by the presence of the other [**77**]. The dynamics of an orbital cable system (OCS) consisting of a vehicle with an engine have also been discussed [**78**].

The equations of tether motion for a general case were introduced in the previous chapter, where the tether system was modelled by two point masses connected by a flexible tether. The discussion then proceeded to introduce a number of simplifications

that led to the rigid tether model, before moving on to discuss the massless tether system model. This model provides the foundations for the 'bead' model which is implemented into the TRAP model.

The following sections will discuss the 'bead' model along with the OpenGL graphical user interface developed to enable the user to visualise the motion of an orbital tether system.

5.2.1 The Bead Model

The 'bead' model, implemented into the TRAP model, is an extension of the massless tether model, discussed in Section 4.2.3. The tether is not modelled as a continuous structure, but consists of n 'beads' (points) connected by straight, massless strands, referred to as tether segments. Increasing the number of 'beads' improves the model's accuracy, and as the number of 'beads' tend to infinity so the tether tends to a continuous flexible structure. Figure 5.6 illustrates the 'bead' model. The 'beads' at either end of the tether represent the tether system's end-bodies, the attributes of which subsequently determine the location of the tether system's centre of mass. The other 'beads' are positioned along the tether length using an automated 'bead' distribution method. This takes into account the length of the tether, the location of the centre of mass and the number of 'beads'. For example, if a tether system consisted of two end-bodies of equal mass, then the centre of mass 'bead' would be located at the centre of the tether, equidistant from the two end-bodies. If the tether model now required another two

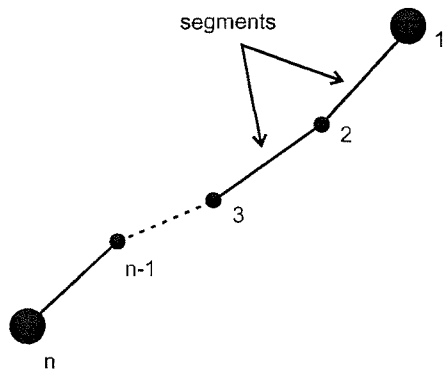

Figure 5.6: The bead model

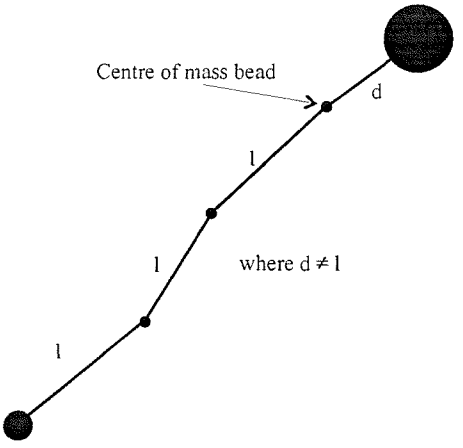

Figure 5.7: The bead distribution

'beads' to be positioned along the tether system, then the 'bead' distribution method would place each 'bead' either side of the centre of mass 'bead' at equal distances. However, if the tether system's centre of mass was in close proximity to one of the end-bodies, and another two 'beads' were required for the model, then placing each 'bead' either side of the centre of mass 'bead' would not be suitable. Therefore, the two 'beads' would be redistributed towards the opposite end-body, evenly spaced, providing a more accurate tether model - see Figure 5.7.

The equations of motion for a massless tether system were introduced in the previous chapter. Here we will discuss how these equations are used in determining the position vectors for each of the 'beads' along the tether system. The equations defining the 'bead' model are developed by assuming that the centre of mass 'bead' corresponds to the massive satellite, B. Thus, the position vector for the tether system's centre of mass is given by $\mathbf{R_{cm}}$. Before introducing the general equations used for determining the position vectors for each of the 'beads', however, a brief discussion will be presented that considers a tether system modelled using three 'beads'. That is the tether system's centre of mass 'bead' and the upper and lower masses.

With the position vector of the tether system's centre of mass known, $\mathbf{R_{cm}}$ $(= \mathbf{R_1})$, the position vector for each 'bead' either side of the tether system's centre of mass can be

determined using

$$\begin{aligned} \mathbf{R_2} &= \mathbf{R_1} + \mathbf{r_2}, \\ \mathbf{R_0} &= \mathbf{R_1} - \mathbf{r_0}, \end{aligned} \tag{5.9}$$

where $\mathbf{r_2}$ and $\mathbf{r_0}$ are the position vectors of the upper and lower masses, respectively, in the local vertical/local horizontal (LVLH) reference frame, given by

$$\mathbf{r_i} = (l_i \cos\alpha_i \cos\phi_i)\,\hat{\mathbf{x}} + (l_i \sin\alpha_i \cos\phi_i)\,\hat{\mathbf{y}} + (l_i \sin\phi_i)\,\hat{\mathbf{z}}. \tag{5.10}$$

Here l is the tether segment length, α is the in-plane libration angle, ϕ is the out-of-plane libration angle, i denotes the 'bead' number and ($\hat{\mathbf{x}}$, $\hat{\mathbf{y}}$, $\hat{\mathbf{z}}$) are the unit vectors in the directions of the x, y and z axes, respectively. The equations governing the in-plane and out-of-plane libration angles, given by Equations (4.40), are repeated here,

$$\ddot{\alpha} + \dot{n} + (\dot{\alpha} + n)\left(\frac{2\dot{r}}{r} - 2\dot{\phi}\tan\phi\right) + \frac{3n^2}{p}\sin\alpha\cos\alpha = -\frac{F_\alpha}{m_A r\cos\phi},$$

$$\ddot{\phi} + \frac{2\dot{r}}{r}\dot{\phi} + \left[(\dot{\alpha}+n)^2 + \frac{3n^2}{p}\cos^2\alpha\right]\sin\phi\cos\phi = -\frac{F_\phi}{m_A r}.$$

However, assuming the tether is always fully deployed and that there are no external forces are acting on the tether, this simplifies to

$$\begin{aligned} \ddot{\alpha} &= (\dot{\alpha}+n)\left(2\dot{\phi}\tan\phi\right) - \dot{n} - \frac{3n^2}{p}\sin\alpha\cos\alpha, \\ \ddot{\phi} &= -\sin\phi\cos\phi\left[(\dot{\alpha}+n)^2 + \frac{3n^2}{p}\cos^2\alpha\right]. \end{aligned} \tag{5.11}$$

The libration angles are found by numerical integration of Equations (5.11) at each time interval using a Runge-Kutta-Fehlberg 8th-order routine.

The solution discussed above is complete for a tether modelled using three 'beads'. However, for a tether system modelled using more than three 'beads' a more general method is required. This is achieved by generalising Equation (5.9)

$$\mathbf{R_i} = \begin{cases} \mathbf{R_{i-1}} + \mathbf{r_i} & \text{if } i > \text{cm}, \\ \mathbf{R_{i+1}} - \mathbf{r_i} & \text{if } i < \text{cm}, \end{cases} \tag{5.12}$$

where i denotes the 'bead' number, $0 \leq i \leq n$, where n is the total number of 'beads' used to model the tether.

Modelling Orbital Perturbations

The small deviations caused by orbital perturbations to a tether system's orbital motion have been implemented into the TRAP model, providing a more realistic orbit. This was achieved using the equations introduced in Section 4.1.2. The small changes in semi-major axis, eccentricity, inclination, argument of perigee and right ascension of the ascending node, of a tether system's (centre of mass) orbital elements, are then updated at each time interval. This is achieved by simply adding the changes caused by orbital perturbations to the tether system's initial orbital elements.

5.2.2 Validation of The Tether Bead Model

The tether model implemented into the TRAP model was validated using a Tether Simulator provided by JAQAR Space Engineering [**79**]. As with the TRAP model, the JAQAR Tether Simulator models a tether system as a number of 'beads' providing an ideal validation tool - see Figure 5.8. Given the tether system's orbital elements, for its centre of mass, along with its dimensions and the number of 'beads', the JAQAR Tether Simulator calculates the position and velocity vectors of each of the 'beads' at every

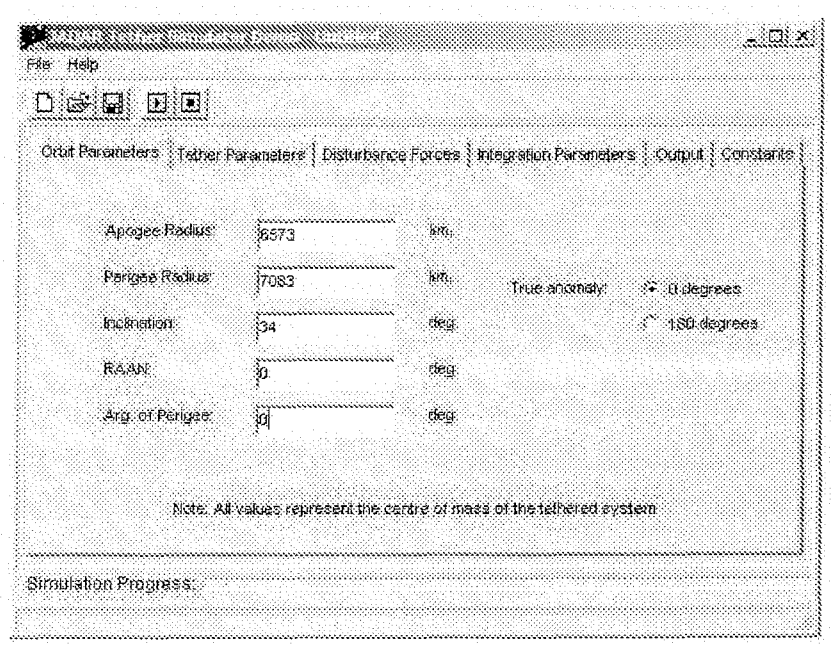

Figure 5.8: The JAQAR Tether Simulator

time-step. A number of simulations were performed using both the TRAP and JAQAR Tether Simulator models and a comparison of the results was carried out. Results indicated that a Runge-Kutta 4th-order routine, which was initially implemented into TRAP, was not sufficient for tether modelling, with discrepancies growing rapidly. These findings prompted the Runge-Kutta 4th-order routine to be replaced with a Runge-Kutta-Fehlberg 8th-order routine. This provided greater stability in the results, and a good comparison between the two models was achieved.

5.2.3 The OpenGL Graphical User Interface

The position and velocity vectors of each of the 'beads' used to represent the tether system in question can be used to visualise the tether system in orbit. This was achieved by the implementation of an OpenGL graphical user interface (GUI). The TRAP GUI is split into four views, which are explained in Table 5.1. Figures 5.9 and 5.10 illustrate the TRAP GUI for a 20 km long tether system. For this particular simulation it was assumed that the tether system was in a near-circular orbit at an altitude of 350 km, inclined at 32°. The end-bodies were assumed to be of equal mass, 25 kg, placing the tether system's centre of mass 10 km away from each end-body. The tether was also assumed to have an initial in-plane libration angle of 10° and an initial out-of-plane libration angle of 5°. Figure 5.9 shows the 20 km long tether system, represented by 7 'beads', at the beginning of the simulation, while Figure 5.10 shows the 20 km long tether system at the end of the 3-day simulation.

Name	**Explanation**	**Position**
In-plane view	Shows the in-plane libration of the tether system only (as viewed down the orbit plane normal to the local horizontal component of its velocity).	Bottom left
Out-of-plane view	Shows the out-of-plane libration of the tether system only (as viewed along the local horizontal to the orbit plane normal).	Bottom right
Tether view	Allows the user to rotate the viewing angle of the tether through the x, y, and z viewing axis	Top left
Orbit view	Shows the position of the tether system's centre of mass about the Earth. The user can also rotate the viewing angle and zoom in or out as necessary.	Top right

Table 5.1: TRAP GUI details

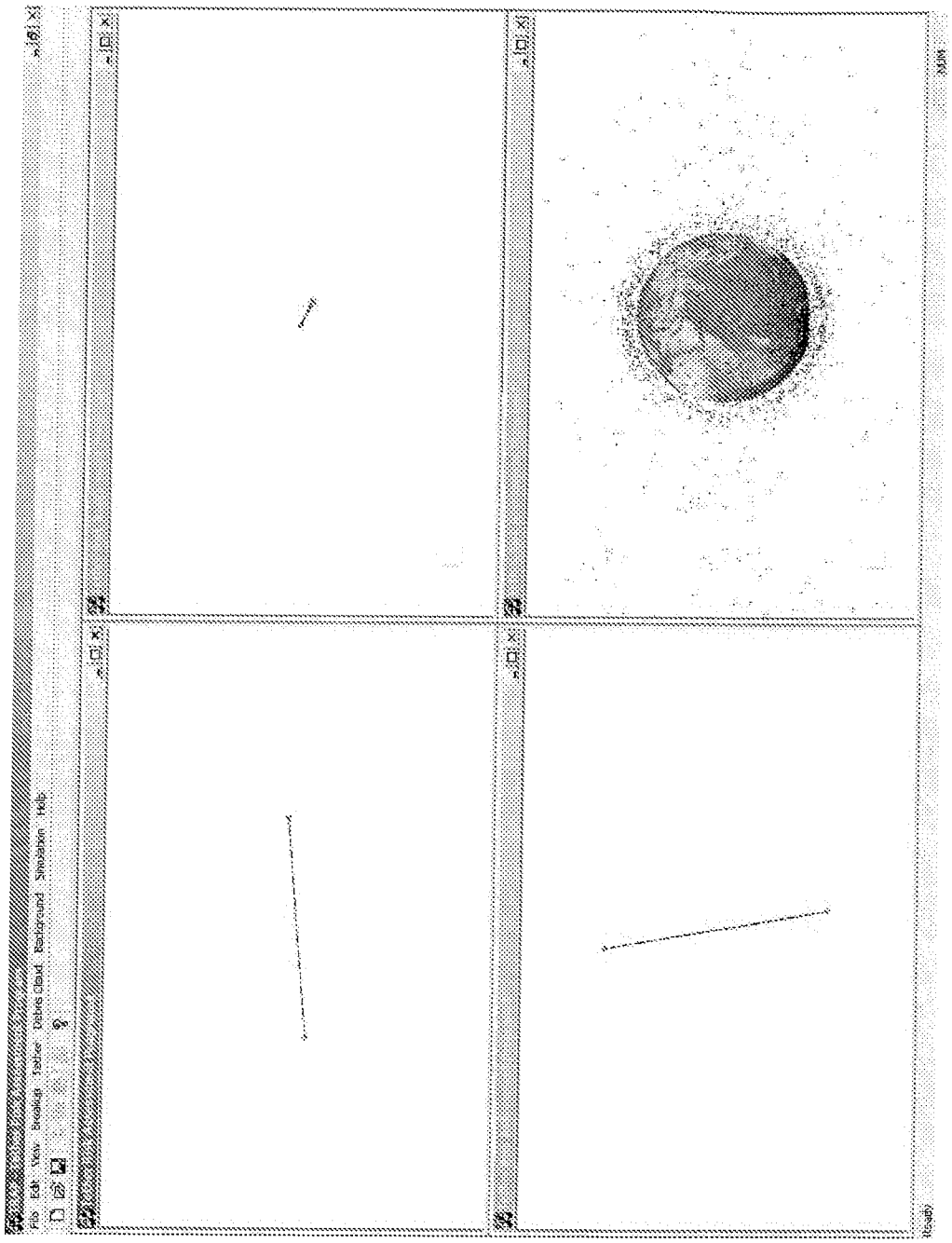

Figure 5.9: TRAP GUI illustrating a 20 km long tether system

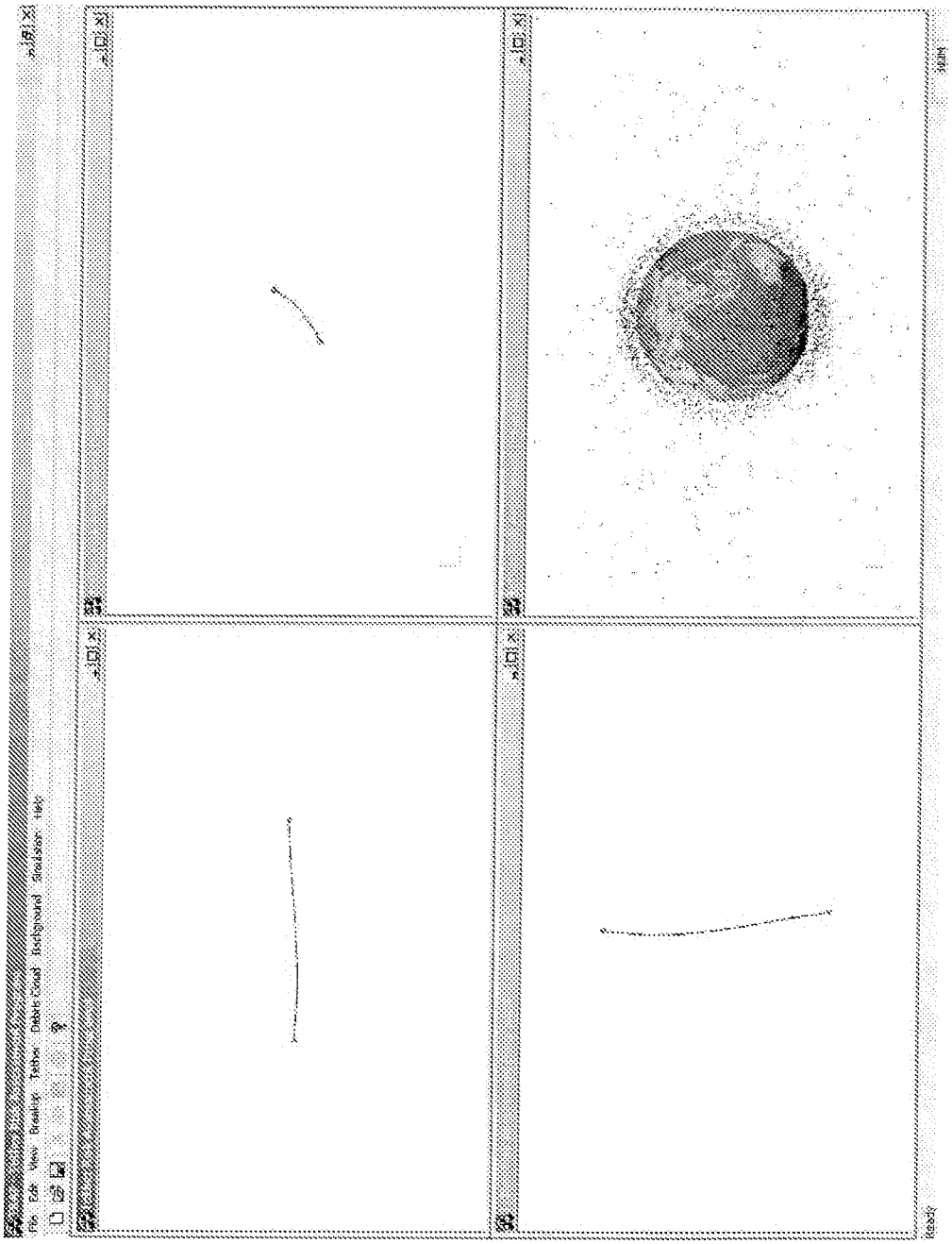

Figure 5.10: TRAP GUI illustrating the 20 km long tether system after 3 days

5.3 The Analysis Program

The Analysis Program is responsible for calculating the collision risk to an orbiting space tether system, within a given time interval, as a result of a fragmentation event, modelled by the Breakup Program. One method for estimating collision probabilities utilises the Poisson distribution and principles of the kinetic theory of gasses. The Poisson probability distribution function is given by:

$$P_k = \frac{R^k e^{-R}}{k!}$$

where P_k is the probability of k events, k is the number of events and R is the rate of occurrence parameter. The probability of no events occurring ($k = 0$) can then be found to be

$$P_0 = \frac{R^0 e^{-R}}{0!} = e^{-R}.$$

In general, a Poisson distribution can be used where the probability of two or more events occurring is very small. Assuming that the probability of more than one event is negligible, the probability of one collision can be represented by:

$$P_1 = 1 - P_0 = 1 - e^{-R}. \tag{5.13}$$

The rate of occurrence parameter, R, is then obtained from the kinetic theory of gasses. It is defined as the number of collisions during a given length of time between one molecule of gas with others in a confined volume, and is given by the molecule's size, density of gas, relative speed, and the length of time considered **[80]**. Therefore, by applying the same kinetic gas assumptions to a confined volume in space, the collision rate between a specified target object and all other objects in a given volume can be determined for a specified length of time. For an object in orbit, the rate of occurrence parameter, R, would be equal to the product of the target object's cross-sectional area, A_c, the average spatial density, ρ, the average relative velocity, v, and the time interval, t, under consideration. Substituting these values into Equation (5.13) gives:

$$P_1 = 1 - \exp(\rho A_c v t) \approx \rho A_c v t,$$

when dealing with small probabilities. Therefore, the equation for calculating collision risk, P, most commonly used in the literature, is given by

$$P = \rho A_c v t. \tag{5.14}$$

Here ρ is the debris cloud spatial density, A_c is the target collision cross-sectional area, v is the relative velocity and t is the time interval under consideration. Equation (5.14) is calculated for each tether segment, due to the variation of the debris density, collision cross-sectional area and relative velocity for each of the tether segments. The accumulation of each segment collision probability then provides the overall tether system collision risk resulting from a fragmentation event.

The Probabilistic Continuum Dynamics (PCD) method was applied to study the collision probability to an orbiting space tether system. The advantage of using this method over other methods, along with the 'bead' model implemented in the Tether Program, is that the debris density can vary over the length of the tether system. This method therefore provides an enhanced means of calculating collision risk assessments to orbiting space tether systems from orbital debris produced from a fragmentation event.

The method of modelling collision risk to an orbiting spacecraft using the PCD method has been used in the past. The Space Debris Simulation (SDS) suite [4] is one such example, which was developed at the University of Southampton under contract to the Defence Evaluation and Research Agency (DERA, now QinetiQ). The SDS model was designed to study impact hazards to satellites resulting from debris clouds produced by a fragmentation event. The software is ideal for short-term analysis and was initially designed to study impact hazards in LEO. However, in recent years the model has been updated and can now be used for longer-term studies and also for GEO studies. Debris clouds arising from both explosions and collisions can be considered, and the software may also be used to analyse the impact risk to a constellation of satellites. A number of such case studies have been performed by Swinerd [**26**] and Barrows [**81**]. At the 'heart' of the software is the method of PCD, which allows a 'target-centred' approach.

The following sections will discuss the PCD method that has been implemented into the TRAP model to assess the collision probability between an orbiting space tether system and a debris cloud produced from a fragmentation event. In order to determine the successful implementation of the PCD method into the TRAP model, the method of validation will also be discussed.

5.3.1 Probabilistic Continuum Dynamics

The Probabilistic Continuum Dynamics (PCD) method is principally based upon the solution of the Gauss-Lambert problem. This requires finding an orbital trajectory between two position vectors given a time of flight. This may be applied to the problem of estimating debris collision risk in the following way. Given the position vector of a fragmentation event, the current position of a 'target' object, and the time interval between them, the transfer orbit from the fragmentation event to the 'target' object can be determined. The transfer orbit solution can then be utilised to calculate the Δv at the fragmentation point, which is required to reach the 'target' object over the given time interval. If the Δv is greater than that defined by the fragmentation velocity distribution, then the 'target' object is outside the generated debris cloud. Conversely, if the fragmentation velocity distribution encompasses the Δv, the 'target' object is within the cloud. An estimate of the debris density at the 'target' object can then by determined by defining a transformation that maps the velocity distribution at the fragmentation event onto the spatial distribution at the 'target' object. This can then be translated into an estimate of collision probability **[26]**.

Consider a fragmentation event occurring at time $t = 0$, with position vector $\mathbf{r_0}$. The spatial density of the resulting debris cloud at a position $\mathbf{r}$ at time t can then be found as follows. Let $\dot{\mathbf{r}}_0$ represent an initial velocity vector that allows a fragment to travel from $\mathbf{r_0}$ to $\mathbf{r}$ in a time interval t. Hence, the number of fragments contained in a small volume element $d\mathbf{r}$ at time t will be equal to the number of fragments that had ejection velocities in a corresponding velocity element $d\dot{\mathbf{r}}_0$. Thus,

$$\rho\left(\mathbf{r}\right) d\mathbf{r} = f_v\left(\dot{\mathbf{r}}_0\right) d\dot{\mathbf{r}}_0, \tag{5.15}$$

where ρ is the spatial density of the debris and f_v, the distribution of initial velocities, is defined such that $f_v(\dot{\mathbf{r}}_0)d\dot{\mathbf{r}}_0$ is the number of fragments with initial velocities in the element $d\dot{\mathbf{r}}_0$. The elements $d\mathbf{r}$ and $d\dot{\mathbf{r}}_0$ are related by

$$d\mathbf{r} = |J|\, d\dot{\mathbf{r}}_0, \tag{5.16}$$

where J is the Jacobian of the transformation from $\dot{\mathbf{r}}_0$ to $\mathbf{r}$. The state transition matrix is given by

$$J = \begin{vmatrix} \frac{\partial x}{\partial \dot{x}_0} & \frac{\partial x}{\partial \dot{y}_0} & \frac{\partial x}{\partial \dot{z}_0} \\ \frac{\partial y}{\partial \dot{x}_0} & \frac{\partial y}{\partial \dot{y}_0} & \frac{\partial y}{\partial \dot{z}_0} \\ \frac{\partial z}{\partial \dot{x}_0} & \frac{\partial z}{\partial \dot{y}_0} & \frac{\partial z}{\partial \dot{z}_0} \end{vmatrix} \tag{5.17}$$

The debris density can then be calculated using

$$\rho(\mathbf{r}) = \frac{1}{|J|} f_v(\dot{\mathbf{r}}_0[\mathbf{r}]). \tag{5.18}$$

5.3.2 Implementation of The PCD Methodology

The method of PCD was implemented to determine the collision risk between an orbiting space tether system, and a debris cloud resulting from a fragmentation event. Given the orbital elements of the breakup object and the tether system, the determination of the collision probability requires three main steps. These correspond to the calculation of ρ, A_c and v in Equation (5.14). However, unlike a typical satellite, an orbiting space tether system can be many kilometres in length. Hence, the debris density along the length of the tether can vary significantly. The tether system is therefore divided into a number of segments. This is achieved by implementing the 'bead' model outlined in Section 5.2. Each corresponding 'bead' segment then requires the calculation of ρ, A_c and v separately. The collision probability for each segment can then be determined and summed to give the overall tether system collision probability. The calculation of ρ, A_c and v is outlined below for a specific tether segment, which is subsequently repeated for the remaining tether segments.

Firstly, the debris density from the fragmentation to the tether segment's position must be determined. This requires the solution of the transfer orbit (Gauss-Lambert) problem that links the breakup event to the tether segment's location in the time interval considered. Hence, the velocity vector of the transfer orbit at the breakup epoch and at time t can then be determined. Subtracting the breakup object's velocity vector, at the time of breakup, from the transfer orbit velocity vector solution, at the same epoch, determines the Δv of the transfer orbit relative to the breakup object's centre of mass. With knowledge of the Δv, and referencing back to the breakup model employed, the density of debris in spread velocity space can be obtained. The calculation of debris density at the tether segment's location requires the transformation from spread velocity space, at the breakup epoch, to position space, at the tether segment's position, taking into account the time between. This requires the evaluation of the state transition matrix $\Phi(\mathbf{r}, \dot{\mathbf{r}}_0)$ $(= \partial\mathbf{r}/\partial\dot{\mathbf{r}}_0)$ at the point in spread velocity space, obtained from the transfer orbit Δv, and for the orbital transfer time. The actual debris density is then calculated by dividing the spread velocity space value by the determinant of the state

transition matrix as shown in Equation (5.18) [4].

Secondly, the relative velocity between the debris and the tether segment must be evaluated along with the cross-sectional area of the tether segment, projected normal to this relative velocity. The relative velocity is determined by subtracting the solution of the transfer orbit at the tether segment's position from the tether segment's velocity vector. The knowledge of the relative velocity vector then enables the direction of debris flux to be determined with respect to the tether segment. Hence, the calculation of tether segment shape, dimensions and an orientation relative to its orbital motion, allows debris fluxes and thus collision probabilities to be calculated for individual surfaces of the tether segment.

The possibility of there existing more than one transfer orbit solution must be considered, especially as the debris cloud evolves and wraps repeatedly around the Earth. Hence, the procedure outlined above must be repeated for each transfer orbit solution obtained, with each of the contributions summed to determine the total collision probability for the tether segment in question. The above procedure is then repeated for the remaining tether segments.

The Transfer Orbit (Gauss-Lambert) Problem

The transfer orbit, or Gauss-Lambert, problem is well documented in the literature. A number of solutions exist to the problem such as those proposed by Gooding [**82**], Sun et al [**83**] and the original method proposed by Gauss [**84**]. However, it was the method of universal variables, proposed by Bate et al [**65**], that was utilised and implemented into the TRAP model.

The Gauss-Lambert problem is defined as follows. Given two position vectors, $\mathbf{r_1}$ and $\mathbf{r_2}$, the time of flight, t, from $\mathbf{r_1}$ to $\mathbf{r_2}$, and the direction of motion, d_m, find the velocity vectors at the two positions, $\mathbf{v_1}$ and $\mathbf{v_2}$. Obviously, there exist an infinite number of transfer solutions that pass through $\mathbf{r_1}$ and $\mathbf{r_2}$, but only two that have the specified time of flight (if multiple orbit solutions are ignored). These transfer solutions coincide with the type of transfer involved. A 'short-way' transfer occurs if the net range angle, ψ, between $\mathbf{r_1}$ and $\mathbf{r_2}$ is less than or equal to π radians. A 'long-way' transfer occurs when the net range angle is greater than π radians - see Figure 5.11. The type of transfer, and hence the direction of motion, d_m, which equals 1 or -1 for a 'short-way' or 'long-way'

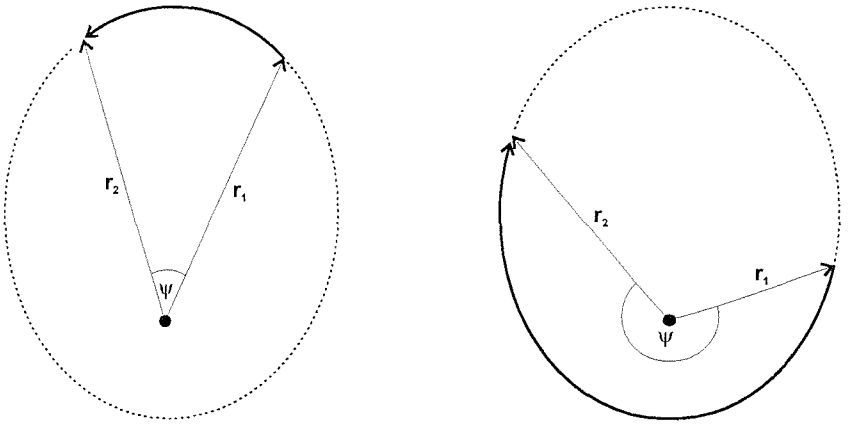

Figure 5.11: Short-way and long-way orbital transfers

transfer respectively, is determined from the orbital motion of the objects at $\mathbf{r_1}$ and $\mathbf{r_2}$. The value of ψ is calculated by taking the dot product of the two position vectors, $\mathbf{r_1}$ and $\mathbf{r_2}$.

The Δv required for a debris fragment to sustain an orbit in the opposite direction of the breakup object's centre of mass would be in the order of twice its orbital velocity. Hence, only transfer solutions orbiting in the same direction as the breakup object's centre of mass are considered in the TRAP model.

With the continuing evolution of the debris cloud, multi-revolution orbital transfers are possible. For such cases, a debris fragment may describe one or more orbits before arriving at the tether segment location. At any given time after a fragmentation event has occurred, the range of orbit revolutions to be considered is given by the minimum and maximum debris orbital periods. The minimum orbital period will correspond to the debris fragment that has the lowest orbital energy which has not already re-entered the atmosphere. For each orbital transfer considered, the determination of the transfer orbit is an iterative process, with the variable iterated upon, Z, being the square of the difference between the eccentric anomalies of the tether segment and breakup positions of the transfer orbit, $Z = (E_2 - E_1)^2$. The procedure for solving Z, and hence determining the transfer orbit, is given by Bate et al **[65]**, and is outlined below.

1. The orbital geometry parameter, A, is calculated using

$$A = d_m \sqrt{r_1 r_2 (1 + \cos\psi)}, \tag{5.19}$$

where d_m is the direction of the orbital transfer and is equal to 1 for a 'short-way' transfer and -1 for a 'long-way' transfer, r_1 is the geocentric distance of the breakup object's centre of mass, and r_2 is the geocentric distance of the tether segment.

2. An initial guess for Z is made from the orbital transfer geometry and the number of revolutions being considered.

3. The transfer time, Δt, given by the estimate of Z is calculated using

$$\Delta t = X^3 S + A\sqrt{Y}, \tag{5.20}$$

where

$$X = \sqrt{\frac{Y}{C}},$$

$$Y = r_1 + r_2 - A\frac{(1 - ZS)}{\sqrt{C}},$$

$$C = \begin{cases} \frac{1-\cos\sqrt{Z}}{Z} & , Z \neq 0 \\ \frac{1}{2} & , Z = 0 \end{cases}$$

and

$$S = \begin{cases} \frac{\sqrt{Z}-\sin\sqrt{Z}}{Z^{3/2}} & , Z \neq 0 \\ \frac{1}{6} & , Z = 0 \end{cases}$$

4. Repeat step 3, using a Newton iteration method for a new estimate of Z, if the difference between Δt and the actual orbital transfer time is greater than a given tolerance. If the difference is acceptable then the value of Z can be accepted.

5. Calculate the transfer orbit velocity vector at the breakup, $\mathbf{v_1}$, and the tether segment, $\mathbf{v_2}$, locations using

$$\mathbf{v_1} = \frac{\mathbf{r_2} - f\mathbf{r_1}}{g}, \tag{5.21}$$

and

$$\mathbf{v_2} = \frac{\dot{g}\mathbf{r_2} - \mathbf{r_1}}{g} \tag{5.22}$$

where

$$f = 1 - \frac{Y}{r_1},$$

$$g = A\sqrt{Y}$$

and

$$\dot{g} = 1 - \frac{Y}{r_2}$$

The above procedure assumes an ideal Keplerian orbital motion and does not take into account the effects of orbital perturbations. However, as discussed in the previous chapter, the effects of orbital perturbations can significantly effect an object's orbital path over time. Thus, a combination of the analytical procedure, outlined above, with a numerical minimisation routine has been developed to form a generalised hybrid transfer orbit solution algorithm. This is achieved by passing the ideal transfer orbit solution, returned by the universal variables method, into a positional difference minimisation routine. The technique implemented is a modified simplex method [**85**], iterating upon the positional difference between the actual tether segment position and that estimated by propagating the transfer orbit solution to the tether segment position epoch.

The orbital debris produced by the fragmentation event can be propagated using a combination of all or some of the orbital perturbation effects implemented into the TRAP model. If all the perturbations are switched off, then the debris cloud will have Keplerian motion, which provides an important check to the ideal transfer solution, returned by the universal variables algorithm. With the introduction of orbital perturbations, the use of an orbit propagator to check and perturb the initial transfer orbit solution also provides an opportunity to verify that the orbit calculated does not re-enter the atmosphere at any point. This is particularly important when the effects of atmospheric drag are considered. Any objects found to re-enter the Earth's atmosphere are subsequently removed from the simulation.

The combined analytical and numerical transfer orbit solution method is computationally expensive, particularly once the debris cloud has wrapped around the Earth several times. In order to speed-up and optimise the solution search procedure, a number of measures have been implemented. For example, a method that saves and records the solutions has been adopted to ensure that the best possible solution estimates are

passed into the minimisation algorithm, because this is where most of the calculation time is spent. The effects of orbital perturbations can also result in the transfer orbit solutions being considerably different from the ideal estimate. So, instead of using new (calculated) ideal estimates at every time interval, the perturbed solutions that were calculated and saved at the previous time interval are used. The saved solutions are continuously monitored, and if a saved solution is found to deviate and provide worse estimates for the transfer orbit than the ideal solution, then it is discarded. The solution obtained at each time interval are also recorded and checked against one another to ensure that there is no duplication.

An additional speed-up measure has also been implemented to save on computational requirements for the modelling of atmospheric drag. For example, every time a new solution to the transfer orbit problem is tested, the mean drag variations for the orbit need to be calculated. This process is computationally expensive and very time-consuming. Hence, to minimise the computational requirements, a look-up table is utilised to determine the small changes in semi-major axis and eccentricity with respect to eccentric anomaly. This look-up table consists of values for the small changes in semi-major axis and eccentricity calculated for a range of semi-major axis and orbital eccentricities.

The method outlined above has been rigourously tested for a number of orbital geometries and has shown to be very robust providing accurate solutions, while significantly reducing the computational effort.

State Transition Matrix Determination

The transformation of debris density in spread velocity space into spatial debris density at the tether segment location requires the calculation of the state transition matrix that links the two state spaces and epochs. Jenkin and Sorge **[86]** outline a number of methods that are available for the calculation of Φ. The method illustrated by Goodyear [**87**], which provides an efficient closed-loop solution to the problem of ideal orbital motion, was implemented into the TRAP model. A number of algorithms exist that attempt to incorporate orbital perturbations into the problem. However, there is no universally accepted method available. For complete generality a numerical approach is implemented into the TRAP model. The state transition matrix $\partial \mathbf{r}/\partial \dot{\mathbf{r}}_0$ is calculated

by using the following small $\Delta v\,(=\partial\dot{\mathbf{r}}_0)$ approximation,

$$\frac{\partial \mathbf{r}}{\partial \dot{\mathbf{r}}_0} \approx \frac{\Delta \mathbf{r}}{\Delta \dot{\mathbf{r}}_0}, \text{ as } \Delta\dot{\mathbf{r}}_0 \longrightarrow 0. \tag{5.23}$$

The perturbations in position space produced by the small perturbations in spread velocity space are calculated by determining the positional difference produced by the slight ejection velocity deviations from the transfer orbit solution debris breakup Δv [4]. This method is completely general in its application and, therefore, can be used for the orbital perturbations implemented in the TRAP model.

Orientation With Respect To Debris Flux

A cuboidal tether shape was applied in the TRAP model, dividing the tether into a number of surfaces. The collision probability for each of these surfaces can then be determined by resolving the debris encounter velocity into components expressed in the embedded tether segment body-axis frame. The overall tether segment collision probability can then be calculated by summing up each of the component contributions, which are processed separately. Also, each cumulative surface probability can be used to determine which tether surface encounters the most debris. This information can be particularly useful for double strand tether systems, which can be rotated to minimise its cross-sectional area exposed to the debris. The use of an orthogonal co-ordinate reference frame, with the body axes pointing out along the surface normals, results in each of the debris velocity components being normal to the tether segment surface [4]. The tether segment collision cross-sectional area is, therefore, the relevant face area of the cuboid taking into account the debris diameter. This will be discussed later, since the collision cross-sectional area will also depend on the type of tether being modelled. Figure 5.12 illustrates the body axis and surface numbering scheme employed in the TRAP model, where (X_b, Y_b, Z_b) denotes the body-axis co-ordinate reference frame.

To transform the relative debris-to-target encounter velocity to a vector in the body-axis co-ordinate frame, the orientation of the tether segment with respect to its orbital motion must be specified. The simplest approach is to assume the tether maintains one Earth-pointing surface, with the tether body-axis frame coincident with the orbiting axis frame. That is, the negative X_b-axis pointing out along the orbit radius and the Z_b-axis in the same sense as the orbital angular momentum vector [4]. This is the non-librating (default) condition in TRAP. Figure 5.13 illustrates the default tether

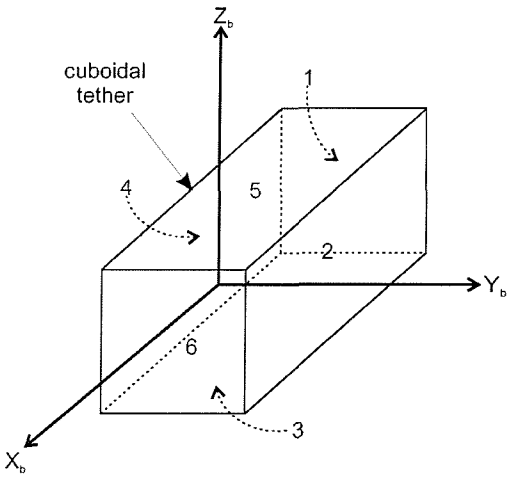

Figure 5.12: Tether surface numbering scheme with respect to the tether segment body-axis

Surface number	Flight orientation
1	Space facing surface
2	Trailing surface
3	Negative orbit normal
4	Ram surface
5	Orbit normal
6	Earth facing surface

Table 5.2: Tether in-flight orientation numbering scheme

flight orientation, where (X_o, Y_o, Z_o) denotes the orbiting axis frame, and Table 5.2 describing the surface number scheme.

A space tether system librates, however, and will not always maintain one Earth-pointing surface. Therefore, any librational motion in the tether segment is accounted for by rotating the tether segment body-axis frame with respect to its orbiting frame. In-plane (roll), out-of-plane (pitch) and yaw angles are used to rotate the tether segment about the orbiting X_o, Y_o and Z_o axes respectively. The yaw angles are only relevant for a double strand tether system.

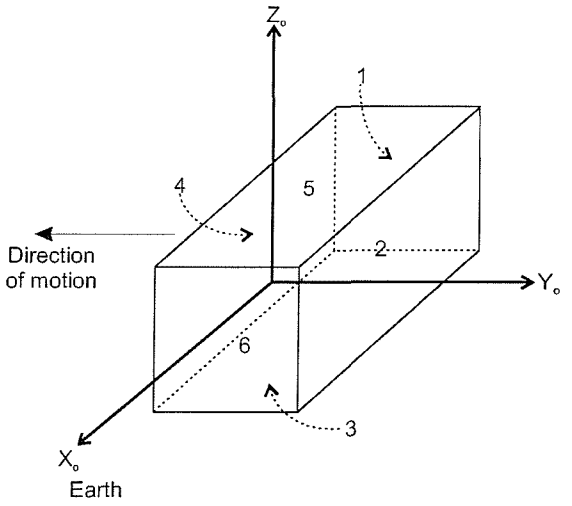

Figure 5.13: Default tether in-flight orientation

Collision Cross-Sectional Area Determination

The collision cross-sectional area, A_c, of a tether segment depends on the tether system under consideration (i.e. single or double strand). Chapter 3 introduced the two types of tethers that are considered in the TRAP model. Here we will discuss how the implementation of the 'bead' model is utilised in calculating the collision cross-sectional area for the two types of tether systems.

A single strand tether system consists of n 'beads' that are connected by straight inelastic strands, referred to as segments - see Figure 5.14. The 'beads' illustrated in Figure 5.14 do not form any physical part of the tether system and are there primarily for visual reference and mathematical convenience.

The collision cross-sectional area, A_c, of a segment of a single strand tether system is given by

$$A_c = L(D + d), \tag{5.24}$$

where L is the tether segment's length, D is the debris diameter and d is the tether diameter - see Figure 5.15. This is then substituted into Equation (5.14), along with the debris density ρ, and relative velocity v, giving the collision risk to a single strand tether segment during a specific time interval t.

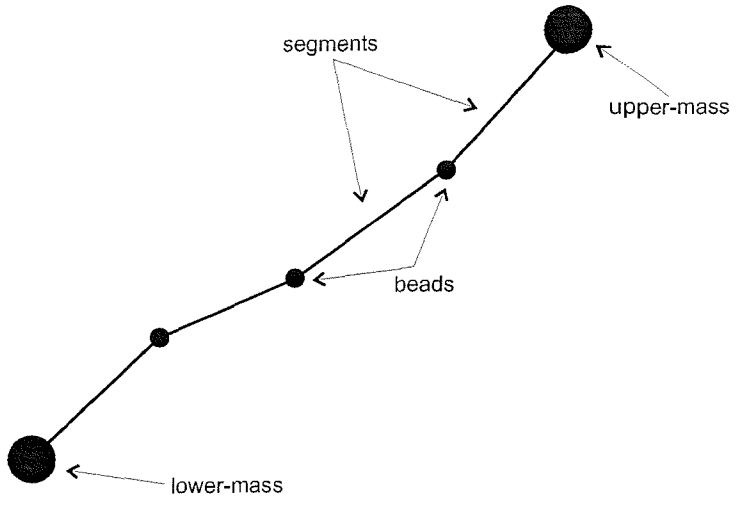

Figure 5.14: Single strand tether system

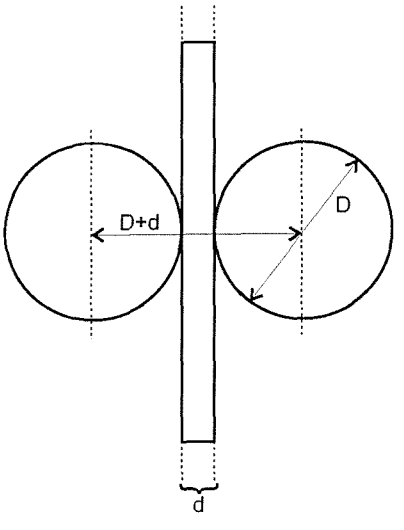

Figure 5.15: Cross-sectional area of a single strand tether system

A **double strand tether system**, like the single strand tether, consists of n 'beads', which are once again used for tether dynamics modelling. Unlike, the single strand tether system, however, the 'beads' actually form a physical component of the tether, linking two primary tether strands together - see Figure 5.16.

The collision cross-sectional area, A_c, for a double strand tether system depends on the diameter of the impacting debris object. If the debris diameter, D, is less than the gap between the two tether strands, i.e. $D < t_d - 2d$, where t_d is the sum of the gap between the two tether strands and their diameters, then the collision cross-sectional area corresponding to one strand is the same as given in Equation (5.24) - see Figure 5.17. However, since the tether system has two strands, either one of which the impacting debris object could impact, the collision cross-sectional area is doubled. That is

$$A_c = 2L(D + d). \tag{5.25}$$

However, if $D \geq t_d - 2d$, then the collision cross-sectional area is given by

$$A_c = L(D + t_d), \tag{5.26}$$

as is illustrated in Figure 5.17. Again, the substitution of this into Equation (5.14) will produce the collision risk associated with a double strand tether segment.

The 'beads' of a double strand tether system form a physical part of the tether and, therefore, their collision risk must also be considered. The TRAP model assumes that a 'bead' connecting the primary strands together is a sphere with a diameter equal to the total tether diameter, t_d. Hence, the collision cross-sectional area of one of the 'beads' is given by

$$A_c = 0.25\pi t_d^2. \tag{5.27}$$

As with the tether segments, the collision risk associated with each of the 'beads' is then calculated using Equation (5.14).

An averaging method involving the debris diameter has been implemented into the TRAP model to provide greater accuracy for the collision cross-sectional areas. Simply taking one average of the debris diameters was deemed to inaccurate. Therefore, four size ranges were considered, < 1 mm, 1 to 10 mm, 10 to 100 mm and > 100 mm. An average debris diameter was then produced in each of these size ranges. The collision probability is then calculated for each of these size ranges and accumulated to give the overall collision probability for the tether segment in question.

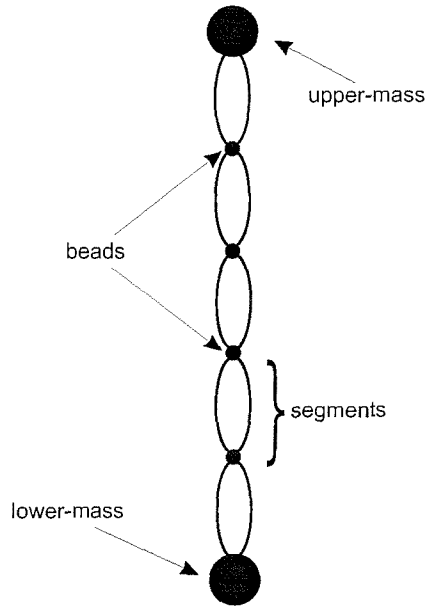

Figure 5.16: Double strand tether system

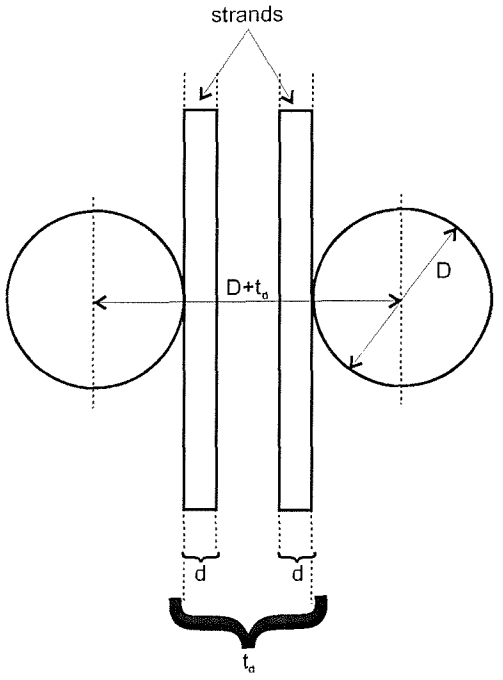

Figure 5.17: Cross-sectional area of a double strand tether system

5.3.3 Validation of The PCD Methodology

To ensure the PCD method had been successfully implemented into the TRAP model, a number of validation procedures were performed. This was achieved by running a number of simulations and comparing the results with those produced by the SDS model. Figures 5.18 and 5.19 compare the collision probability results as predicted by the TRAP and SDS models for one such example. The example illustrates the collision probability for an orbiting spacecraft resulting from a debris cloud produced by a low intensity explosion at an altitude of 350 km. The two objects were assumed to be in very close proximity to each other before the fragmentation occurred. Although the PCD method was developed independently of the SDS model, a good agreement between the two models was achieved, showing qualitative but not quantitative agreement. This is because the breakup model employed in the SDS model is different to the IDES breakup model employed in TRAP.

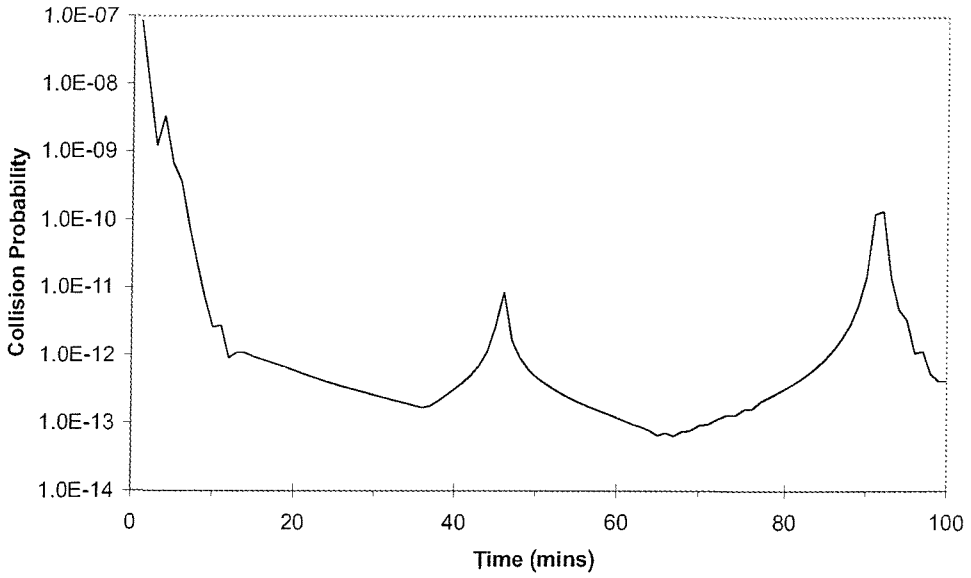

Figure 5.18: Collision probability as predicted by the TRAP model

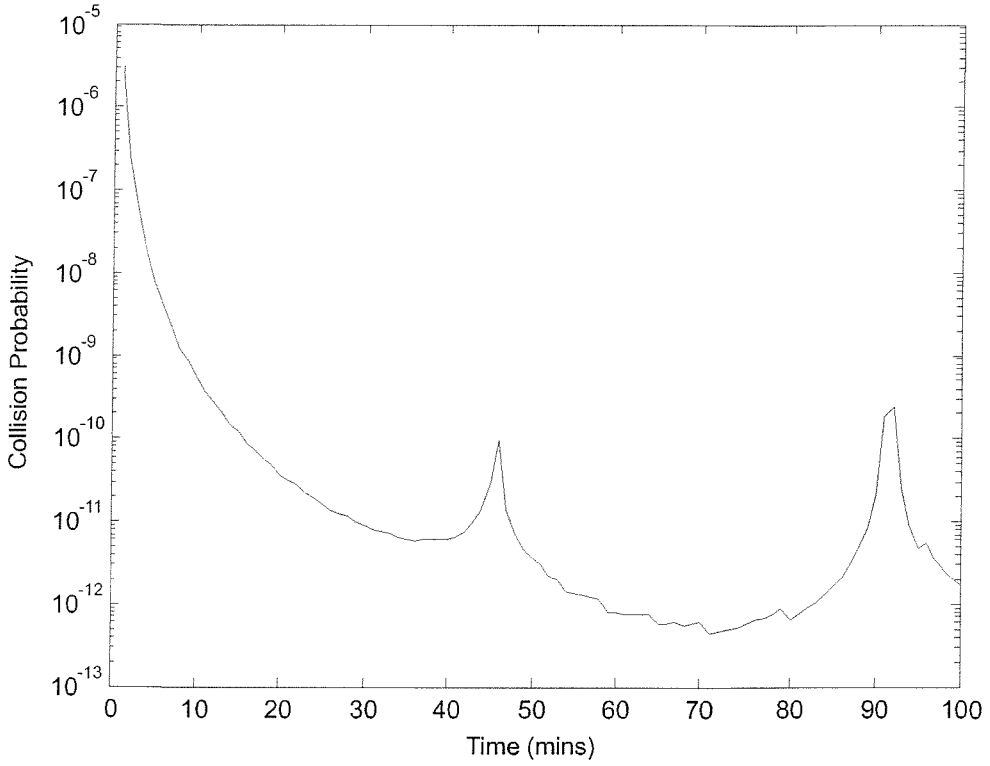

Figure 5.19: Collision probability as predicted by the SDS model

5.4 The Background Program

The Background Program implemented into the TRAP model is responsible for modelling the trackable background orbital space debris population. It is capable of modelling the historical background population, from the launch of Sputnik 1 in 1957 through to the 31st September 2000. Another important feature of the Background Program is its ability to predict future space activities, such as launches and fragmentation events, based on recent space activity trends. The Background Program is also responsible for calculating the collision risks to an orbiting space tether system associated with the background orbital debris population (historical and predicted). The collision risk is determined by solving Equation (5.14). As with the Analysis Program the collision probability is calculated for each tether segment, using the debris density, cross-sectional area and relative velocity. Each of these parameters is allowed to vary along the length of the tether. The accumulation of each segment collision probability then provides the overall tether system collision risk from the trackable background orbital debris population.

This section will discuss the orbital debris database with particular attention given to the development of the future launch traffic and future object fragmentation models. These models allow collision risk assessments to be predicted for future planned tether missions. This section will also discuss the method used to determine the debris flux values of the background debris population, at a given time interval using a suitable control volume.

5.4.1 Historical Orbital Debris Database

The historical orbital debris database used in the TRAP model contains data on over 24,000 objects associated with every launch and fragmentation event around the Earth. The database spans the period from the beginning of the space-age in 1957, with the launch of Sputnik 1, through to the 31st September 2000. The database was constructed using ESA's DISCOS (Database and Information System Characterising Objects in Space) [88] and contains the following information about each object:

- beginning-of-life (BOL) epoch,
- COSPAR ID,

- object classification code,
- orbital elements at BOL epoch,
- dry mass,
- mean cross-sectional area,
- end-of-life (EOL) epoch, and
- drag coefficient.

The drag coefficient is set to 0 for operational satellites, simulating orbit control to counteract drag, and 2.2 for debris objects, allowing uncontrolled objects to decay naturally due to the effects of atmospheric drag. The object classification code, consists of 9-digits, and is responsible for determining to which of the 410 different identified classes of objects it belongs. The code is constructed from sub-codes of nationality, orbit type, object type (which may include payloads, upper stages, payload mission related objects and launch vehicle related objects), and class name (or mission type and mass range as in the case of payloads) **[3]**.

The historical debris database allows the introduction of launch-related and (trackable) breakup objects into the evolving space object population with their correct initial conditions intact. The model can, therefore, be used to predict the orbital space debris environment at any date in the past. It also has the capability to simulate the build-up of other debris sources, including paint flakes released either by meteoroid or orbital debris impacts or natural surface degradation to payloads or rocket bodies (although these sources are not currently included in the model).

5.4.2 Future Orbital Debris Database

The future orbital debris database is based on predictions made from current and previous space activities. These predictions are implemented in the TRAP model, based on research carried out by Walker **[3]** who looked at an 8-year period of space activity. The database was examined from 31st March 1990 until 31st March 1998 where it was determined that a total of 2,522 objects were associated with launches carried out during this period. The database consisted of orbital data for 863 payloads, 798 rocket bodies,

and some 758 operational debris objects. A further 103 operational debris objects in the database have unknown orbital data.

Future Launch Traffic Model

The 9-digit classification code assigned to each object in the historical launch-related database allows for a high level of detail to be attained in the TRAP future launch traffic database. Work by Walker [3] involved studying 8 years (between 1990 and 1998) of launch-related objects in the historical event database to derive a high fidelity future launch traffic model. This comprised representative data on each of the object classes. This representative data includes the orbit parameters, mass and cross-sectional area. A relational database was also constructed to enable a link between the object classes. This 'object-oriented' approach enables the launch vehicle upper stage and operational debris objects, associated with a particular payload launch, to be added to the orbital debris population at the same time as the payload. Three data files were used for the future launch traffic database, and these are described in Table 5.3. These data files define the payload class launch rates, associations between the payload classes and other object classes, and the summary of the orbit/mass data on each of the 410 object classes [3]. Examples of these files are shown in Figure 5.20.

File Name	Description
Payload.dat	For each payload class code launching between 1990 and 1998: • mean launch rate (per year) • mean number of payloads per launch • mean operational lifetime (years)
Assoc.dat	For each payload class code launching between 1990 and 1998: • associated object class code • mean number of objects per launch for the associated object class • fraction/share of associated payload class launch (if associated object class is a launch vehicle upper stage)
Class.dat	For each object class code launching between 1990 and 1998: • representative (mean) semi-major axis (km) • representative (mean) eccentricity • representative (mean) inclination (deg) • representative mean mass (kg) • representative mean geometric cross-sectional area (m^2) • lethality ratio (J/g) of the object class (default 40 J/g)

Table 5.3: Description of future launch traffic files [3]

Example Payload.dat format:

Class no.	Class description	Launch rate (per/year)	obj./launch	op. life (years)
130552504	"FR VLP VLA VHI HM OBSSATS P"	0.125	1	4.98
240253104	"JP VLP VLA LI ESM SCISATS P"	0.250	1	2.50
440358304	"FSU VLP VLA MI SM MILSATS P"	0.375	1	0.00
440358504	"FSU VLP VLA MI HM MILSATS P"	3.000	1	2.90
451658004	"GB VLP HA VLI ISM MILSATS P"	0.125	2	1.00
466150304	"US HP HA VLI SM COMSATS P"	0.625	1	12.53
546150404	"EUTEL HP HA VLI MM COMSATS P"	0.250	1	12.96

Example Assoc.dat format:

Primary Class no.	Primary Class description	Assoc. Class no.		obj./ launch	assoc. r/body launch rate frac.
246152104	"JP HP HA VLI ESM OBSSATS P"	240252107	"JP VLP VLA LI ESM OBSSATS PMORO"	4	0.000
440358404	"FSU VLP VLA MI MM MILSATS P"	440303702	"FSU VLP VLA MI Molniya LVFS"	1	0.125
440358404	"FSU VLP VLA MI MM MILSATS P"	440306202	"FSU VLP VLA MI Tsyklon LVFS"	1	0.875
440353404	"FSU VLP VLA MI MM SCISATS P"	440306202	"FSU VLP VLA MI Tsyklon LVFS"	1	1.000
466150304	"FSU VLP VLA MI MM SCISATS P"	440306203	"FSU VLP VLA MI Tsyklon LMORO"	5	0.000
466150304	"US HP HA VLI SM COMSATS P"	461702002	"US VLP HA LI Delta II LVFS"	1	0.200
466150304	"US HP HA VLI SM COMSATS P"	462200702	"US VLP VHA LI Atlas II LVFS"	1	0.200
466150304	"US HP HA VLI SM COMSATS P"	440304503	"FSU VLP VLA MI Proton K LMORO"	1	0.000
466150304	"US HP HA VLI SM COMSATS P"	445204502	"FSU MP HA LI Proton K LVFS"	1	0.200
466150304	"US HP HA VLI SM COMSATS P"	511600203	"ESA VLP HA VLI Ariane 4 LMORO"	1	0.000
466150304	"US HP HA VLI SM COMSATS P"	511600202	"ESA VLP HA VLI Ariane 4 LVFS"	1	0.400
466150304	"US HP HA VLI SM COMSATS P"	510100203	"ESA VLP vHA VLI Ariane 4 LMORO"	1	0.000

Example Class.dat format:

Class no.	Class description						
070354404	"CN VLP VLA MI MM TECSATS P"	6632.660	0.00690000	56.95	2099.000	4.1937	40.0
440306602	"FSU VLP VLA MI Zenit LVFS P"	7164.160	0.00123000	70.39	8300.000	38.5691	40.0
440306603	"FSU VLP VLA MI Zenit LMORO P"	7310.863	0.01957791	70.59	233.083	2.8290	40.0
461358304	"US VLP MA MI SM MILSATS P"	16659.660	0.60570002	39.19	1075.000	2.4936	40.0
461600702	"US VLP HA VLI ATLAS II LVFS P"	24312.160	0.73049998	0.00	1802.000	29.1778	40.0
511600203	"ESA VLP HA VLI Ariane 4 LMORO P"	24354.357	0.72793883	6.02	384.736	7.9567	40.0
511600202	"ESA VLP HA VLI Ariane 4 LFVS P"	24631.053	0.73044270	6.31	1780.000	27.7412	40.0

Figure 5.20: Examples of the TRAP Future Launch Traffic Database Files [3]

The relational database allows for a realistic replication of launch-related object patterns into the long-term future. Another advantage of using this approach is that it allows the replication of the historical orbit and mass distribution of launch-related objects. Figure 5.21 shows the semi-major axis versus eccentricity distribution, while Figure 5.22 shows the eccentricity versus inclination distribution of all the object classes in the future launch traffic database. A very strong correlation between the historical traffic database and the future traffic database exists, with all key orbital regions being well represented, such as near-circular LEO, MEO and GEO. Also the high eccentricity GTO and Molniya type orbits are well represented [**3**].

The future launch traffic database was developed by Walker [**3**] for a simulated 8 year period, between 31st March 1990 and 31st March 1998, representing a 'business as usual' future launch traffic scenario from the 31st March 1998. On average, a total of about 330 launch-related objects will be added to the future launch traffic database every year, corresponding to a mean launch rate of 89 per year, resulting from 226 different payload classes. The relational database file, Assoc.dat, contains 475 different associations between the payload classes and other debris object classes. These include launch vehicle upper/final stages, launch vehicle operational debris and payload operational debris objects.

The three input files used in the future launch traffic database are used to predict specific launch events, along with their associated debris objects. These predictions are then stored in an output file containing the same characteristics as the historical database, namely the launch date, COSPAR ID, classification code, orbital elements, etc.

The Payload.dat input file is the main driving force behind the future launch traffic predictions. The future launch traffic process involves stepping through a given time interval from the 31st September 2000 (i.e. the end of the historical database) to a user-defined end date. For each time interval the launch rate of each payload class is taken into consideration. The Assoc.dat input file is then interrogated to determine any associations of that payload class with a launch vehicle upper stage class. For each association, the model calculates the launch rate by multiplying the overall payload class launch rate by the launch rate fraction of the association (i.e. the launch event prediction is based upon the launch rate of the payload-upper stage combination over a single time interval) [**3**]. The predicted number of events for a payload-upper stage

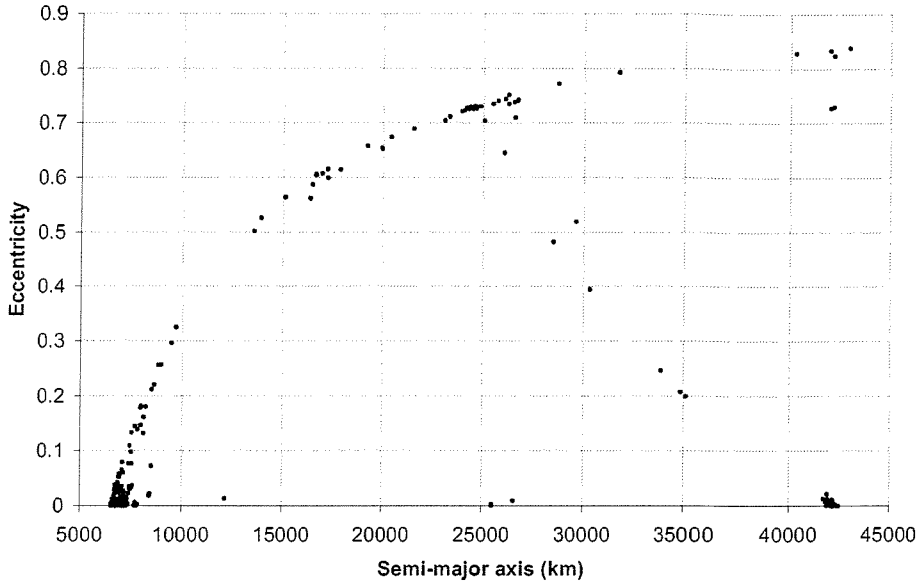

Figure 5.21: Orbital distributions of all object classes in the future launch traffic model

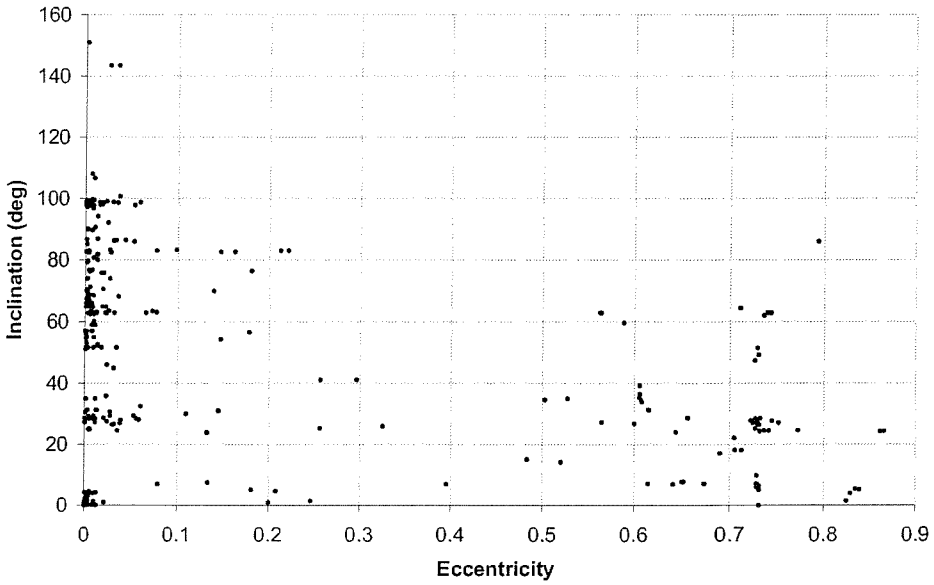

Figure 5.22: Orbital distributions of all object classes in the future launch traffic model

combination is then statistically determined using a Poisson distribution, from $n = 0$ to N events. This is achieved by calculating the event probability, P_n, using

$$P_n = \frac{\lambda^n}{n!} \exp^{-\lambda}, \tag{5.28}$$

where λ is the mean launch rate (per year) multiplied by the given time interval (years). The values of P_n are then accumulated, providing an overall probability, P_N. Each event probability is then normalised (in the range 0 to 1) by the value of P_N . The predicted number of events then corresponds to the maximum normalised event probability value that exceeds a random number, generated using a high precision uniform random generator [3].

If a launch is predicted for the payload-upper stage combination, then the average number of objects for the payload class, upper stage class and the associated operational debris classes are added to the future launch traffic database. Each of the objects will be assigned a semi-major axis, eccentricity, inclination, mass and area values based on their respective classification code contained in the Class.dat input file. The argument of perigee and right ascension of the ascending node are randomly determined for each object between the range 0^o to 360^o. It is assumed that all the objects associated with the launch event have the same beginning-of-life epoch which is randomly determined between the beginning of the simulation epoch (31st September 2000) and the end epoch (user-defined). Each of the payloads are also given an end-of-life epoch, determined from its beginning-of-life epoch and its mean operational lifetime given by the payload classification code in the Payload.dat input file.

Future Explosions model

The future explosion model adopts the same approach used in the future launch traffic model, where an average event rate is employed for the different object classes. These events are, once again, determined during a time interval spanning 8 years (31st March 1990 to 31st March 1998) of the historical data. The events are grouped into their classes by using the 9-digit classification code. In addition to this classification code, however, the classes still required further sorting into sub-classes. This is because objects of the same class may have several different groupings of common breakup semi-major axis, eccentricity, inclination and mass values [3]. Hence, sub-classes are developed, sorting the objects in a given class by the common (or similar) values of these parameters.

Once, the events are grouped into their classes and sub-classes, the semi-major axis, eccentricity, inclination and breakup mass fraction parameters are averaged to determine the representative values for each sub-class. These representative values are then taken from the explosion type and object mass parameter values, since they are the same in each sub-class. Finally, the explosion rate of the sub-class is determined by counting the number of events in the sub-class and dividing by the 8-year time interval. These representative parameters of each sub-class are then listed in a data file, along with the classification code and corresponding class description, taken from the object class database file Class.dat, thus producing the future explosion database **[3]**. Examples of these files are shown in Figure 5.23.

The method used to predict a future explosion event is similar to that used for the future launch prediction. The future explosion model considers each sub-class in the future explosion database and predicts the number of explosion events of the sub-class over the user-defined time interval. Once again, the Poisson distribution is utilised, where the predicted number of events for that sub-class, in the given time interval, is statistically determined using Equation (5.28) for $n = 0$ to N events. This will give the N event probabilities, P_n, which are accumulated to give the overall probability, P_N. Once again, the event probability is normalised in the range 0 to 1. The predicted number of events then corresponds to the maximum normalised event probability value that exceeds a random number, generated using a high precision uniform random generator. If an explosion is predicted for the sub-class, over the given time interval, then its event parameters are taken from the sub-class entry in the future explosion database. The breakup epoch is then randomly determined between the beginning of the simulation epoch (31st September 2000) to the (user-defined) end epoch. Also the right ascension of the ascending node, the argument of perigee and the true anomaly are randomly determined between 0° and 360°. The semi-major axis and inclination for the breakup event are randomised around the mean values given in the database **[3]**. Finally, the historical database is searched to try to match the predicted fragmentation event to a satellite with similar characteristics. This is achieved by checking the object classification code. If a match is observed, the orbital elements are searched to check for similarities to the predicted explosion event. If the two objects are seen to have similar orbits, the object in the historical database is removed and the predicted fragmentation event is associated with this object. Otherwise, if no match is observed, the predicted

Class No.	Class Description	Rate (/yr)	Explosion type	Semi-major axis (km)	Eccentricity	Inclination (deg)	Object mass (kg)	Breakup mass fraction
70501602	"CN VLP VLA VHI CZ-4 LVFS"	0.125	3	7265	0.0013	98.94	1000	0.1741
240202902	"JP VLP VLA LI H-II LVFS"	0.125	3	7440.5	0.1099	30	3000	0.1596
241702902	"JP VLP HA LI H-II LVFS"	0.125	3	18543	0.649	28.6	3000	0.1596
440301202	"FSU VLP VLA MI Cosmos LVFS"	0.125	3	7970.6	0.0159	74.03	1435	0.3727
440304503	"FSU VLP VLA MI Proton K LMORO"	0.125	3	7217.3	0.0011	66.54	55	0.5431
440306202	"FSU VLP VLA MI Tsyklon LVFS"	0.125	3	7328	0.0014	82.6	1360	0.7493
440306602	"FSU VLP VLA MI Zenit LVFS"	0.25	3	7224.9	0.0009	71.01	9000	0.0294
440352404	"FSU VLP VLA MI MM OBSSATS P"	0.125	3	6997	0.0021	82.5	1900	0.05
440358504	"FSU VLP VLA MI HM MILSATS P"	0.125	1	6645.5	0.0087	65	3000	0.0882
440358604	"FSU VLP VLA MI VHM MILSATS P"	0.625	1	6611.2	0.0068	66.38	6700	0
440358604	"FSU VLP VLA MI VHM MILSATS P"	0.25	1	6617.6	0.006	64.96	6500	0
440552404	"FSU VLP VLA VHI MM OBSSATS P"	0.125	3	6947.4	0.0027	98.01	1800	0.0241
440804503	"FSU VLP LA MI Proton K LMORO"	0.25	3	14134.3	0.5331	46.49	55	0.6233
440804802	"FSU VLP LA MI Proton K LMORO"	0.125	3	8418	0.019	64.8	1000	0.3827
441304503	"FSU VLP MA MI Proton K LMORO"	0.5	3	15952.4	0.5781	52.14	55	0.1614
441304503	"FSU VLP MA MI Proton K LMORO"	0.5	3	19410.4	0.6543	46.68	55	0.6233
441304503	"FSU VLP MA MI Proton K LMORO"	0.25	3	16129.9	0.5739	65.06	55	1
441804502	"FSU VLP HA MI Proton K LVFS"	0.25	3	24630.5	0.7307	50.05	3400	1
441804503	"FSU VLP HA MI Proton K LMORO"	0.125	3	24085.5	0.7262	46.77	55	0.6233
460304302	"US VLP VLA MI Pegasus LVFS"	0.125	3	7080.5	0.0166	82	97	1
460305902	"US VLP VLA MI Titan II LVFS"	0.125	1	6610.4	0.0033	67	2860	0.0214
460501903	"US VLP VLA VHI Delta 2000 LMORO"	0.125	3	7473.4	0.0015	99.96	900	0.9286
460558204	"US VLP VLA VHI VSM MILSATS P"	0.125	1	7167.4	0.0081	98.86	855	0
466106002	"US HP HA VLI Titan III LVFS"	0.25	3	40838.1	0.0043	11.8	1500	1
511600202	"ESA VLP HA VLI Ariane 4 LVFS"	0.25	3	22748	0.7089	5.36	1760	0.3831
511600202	"ESA VLP HA VLI Ariane 4 LVFS"	0.25	3	22730.3	0.7024	7.2	1250	0.3831

Figure 5.23: Examples of the TRAP Future Explosions Database Files [3]

explosion event is modelled.

5.4.3 Debris Flux Determination

With the knowledge of the background orbital debris population, a means of calculating debris flux values, at a given time interval, for an orbiting space tether system is required. This is achieved by representing the debris flux environment by a three-dimensional inertial control volume divided into volume cells by the spherical co-ordinate parameters of geocentric radius, declination and right ascension. The spherical control volume implemented into the Background Program is illustrated in Figure 5.24. This approach was first developed by Klinkrad [**89**]. The possibility of constructing spatial density profiles over altitude/declination is then achieved by transforming the orbital state of the debris population into spatial densities and intersection velocity vectors, for each of the volume cells in the control volume. Alternatively, different particle size ranges can be determined for collision risk assessment corresponding to the fluxes encountered by a single 'target' orbit.

Klinkrad's technique [**89**] is applicable because each object in the historical, and future, database is represented individually by its full orbital element set. For each object with orbital elements semi-major axis, a, eccentricity, e, inclination, i, right ascension of ascending node, Ω, and argument of perigee, ω, the method determines the true

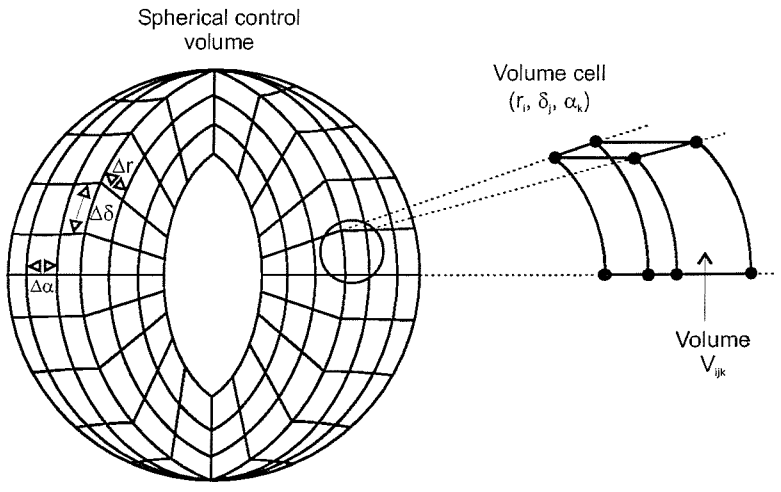

Figure 5.24: Debris flux environment representation

anomalies, θ, of the orbit which intersects the respective cell borders of the inertial control volume - see Figure 5.24. The cell borders are defined by the regularly spaced values of geocentric radius, r_i, declination, δ_j, and right ascension, α_k. The values chosen for the cell borders are crucial in determining accurate and meaningful collision risk assessments. One of the TRAP model's strengths lies in its ability to allow debris density to vary over the length of the tether system. Hence, the increments in geocentric radius vector is user defined so that a suitable value can be chosen, depending on the length of the tether and the number of 'beads' used to represent it. For example, a geocentric radius increment of 5 km would be suitable for a 10 km tether system represented by three 'beads'. The values chosen for the declination, δ_j, and the right ascension, α_k, increments, however, have been determined by performing actual case studies and by comparison with collision risk results.

It is assumed that as the increments in declination and right ascension are decreased, the collision risk prediction would become more acceptable since the large volumes of space, that the tether does not occupy, would be removed. However, as the increments in declination and right ascension decreases, the computational effort increases. Therefore, after performing a number of case studies an increment value of 45° was chosen for both declination and right ascension, providing a good balance between accuracy and computer efficiency.

Computer efficiency is a serious issue in the development of TRAP. One method used to improve computer efficiency was to consider those fragments that were in close proximity to the orbiting tether system. This was achieved by simply removing any fragments that had a semi-major axis ± 1,000 km away from the tether system. Although this would remove some of the objects in GTO's, the difference in the collision risk comparisons is very small. It was concluded, therefore, that with such improvements in computer efficiency, the removal of the GTO objects from the collision risk assessments is acceptable.

The debris density associated with a tether segment, at a specific time interval, can then be computed by obtaining the number of fragments occupying the same cell as the tether segment and dividing by the cell volume. This process is repeated for each tether segment, providing an efficient method of calculating the varying debris density over the whole tether system. The collision probability for each of the tether segments, at time t,

can then be determined by substituting the debris density values into Equation (5.14). However, before the collision risk can be calculated, the segment collision cross-sectional area, A_c, and relative velocity of the impact, v, are also required. These are calculated using the same procedure as previously discussed in the Analysis Program.

5.5 Tether Survivability Assessment

The issues discussed so far have been focused on the collision risk to an orbiting space tether system when introduced into the orbital space debris environment. However, this information alone is not sufficient in studying a tether system's survivability. Hence, predictions of debris encounters should be accompanied by information detailing if the tether system is able to survive such encounters. From this, the likelihood of a tether system failure following a debris encounter can be assessed.

The determination of a tether's survivability has been an issue for some time. A number of estimates have suggested that a single strand aluminium tether could be severed by a fragment $\frac{1}{3}$ of its diameter, while a woven aluminium single strand tether could be severed by a fragment $\frac{1}{2}$ of its diameter **[45, 62, 90]**. These type of estimates have led to the lethality coefficient method of determining the sever probability of a space tether system. This method assumes a constant lethal impact variable, k, typically in the range 0.2 to 0.5 **[60, 90]**. A debris object impacting a tether strand with

$$D \geq kd, \tag{5.29}$$

where D is the debris diameter and d is the tether diameter, is then assumed to sever the tether strand, regardless of the impact energy. To overcome the limitations of this method, a new methodology that takes into account the impact energy has been developed and implemented into the TRAP model. This impact energy method was developed by considering hypervelocity impact experiments, and using suitable penetration equations to enable accurate tether penetration depths to be estimated due to an impacting debris object.

Both the lethality coefficient and penetration (impact energy) methods are suitable for the determination of sever risks to a space tether system. However, for a double strand tether system, a means for determining if both strands fail is also required. For a double strand tether system to fail, both strands in one segment must be severed,

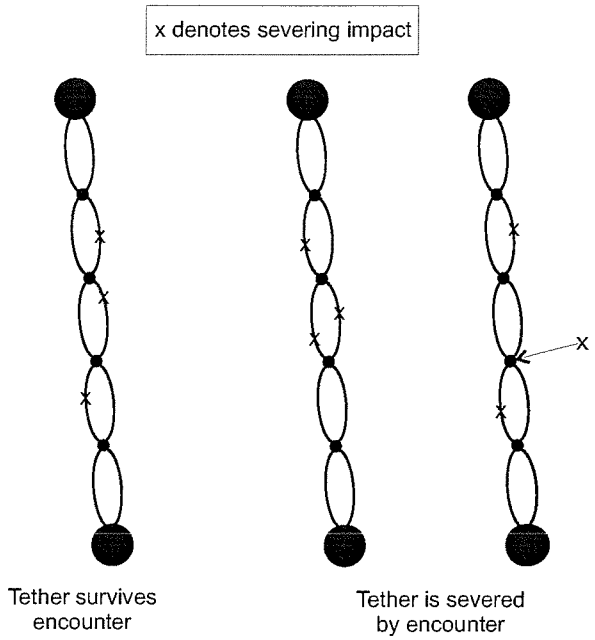

Figure 5.25: Double strand tether system failure scenarios

or one of the 'beads' connecting the tether strands together fails - see Figure 5.25. To look at this issue, two further methods have been developed, the so called LINEAR and TRAJECTORY methods. The LINEAR method is the simplest of these, and basically assumes that a debris object impacting the first strand will follow its original trajectory course with no deviations caused by the impact. The TRAJECTORY method, on the other hand, takes into account the debris object's impact angle and velocity to determine its new trajectory angle caused by the impact. If the debris object is determined to be on a collision course with the second strand then the lethality coefficient method or the penetration method are once again utilised to determine if the second strand is able to withstand the impact.

The following sections will discuss both the lethality coefficient and penetration methods that have been implemented into the TRAP model to determine if a tether system is able to withstand a debris encounter. The discussion will also focus on the LINEAR and TRAJECTORY methods that have been developed to determine the sever risk associated with a double strand tether system.

5.5.1 Lethality Coefficient Method

The lethality coefficient method implemented into the TRAP model assumes a value for the impacting debris size, typically between 0.2 and 0.5 the tether's diameter, capable of severing the tether, as given by Equation (5.29). This lethality coefficient, k, is then assumed for the entire simulation and does not take into account the impact energy of a possible collision. With the possibility of the orbital debris occupying a similar orbit to the tether system, low impact energies may be predicted, and as a result the value of k chosen may be unsuitable. The lethality coefficient method, however, can be used for producing maximum and minimum sever probabilities using the upper and lower limits for k, respectively. Figure 5.26 illustrates an example of the maximum and minimum sever probabilities to an orbiting tether system, of length 10 km and a diameter of 5 cm, as predicted by TRAP. For this particular example, a high intensity explosion was modelled with the original breakup object, of mass 1,000 kg, occupying a similar orbit to the tether system before the fragmentation occurred.

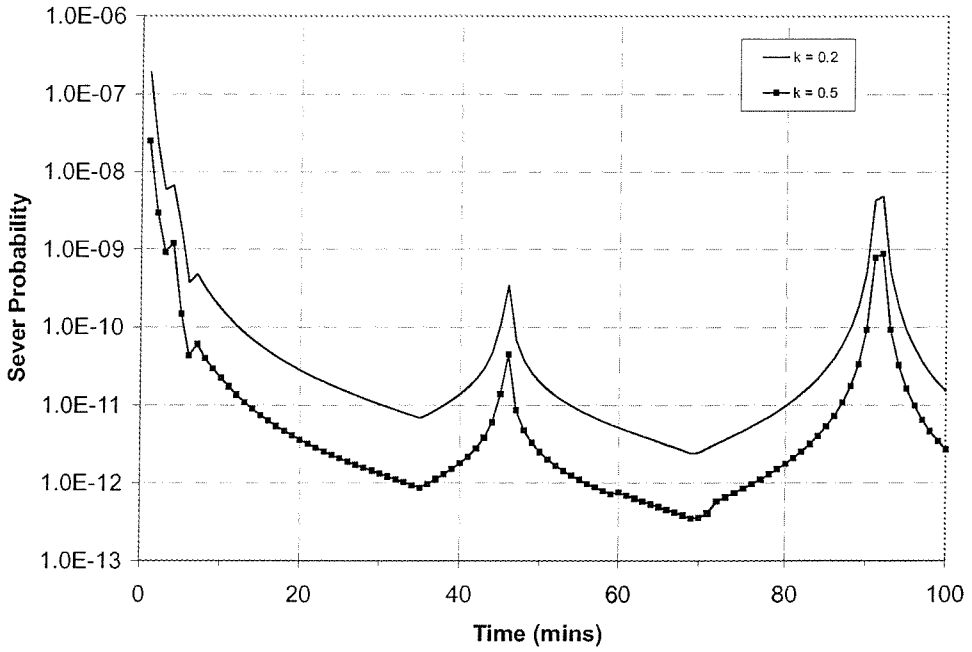

Figure 5.26: Maximum and minimum sever probability as predicted by the TRAP model using the lethality coefficient method

5.5.2 Penetration (Impact Energy) Method

The penetration (impact energy) method determines the penetration depth of a debris object impacting a tether strand, taking account of the impact energy. If the calculated penetration depth is given to be larger than the tether diameter, or a user-defined percentage, then the tether strand is severed. However, if the penetration depth is less than the tether diameter, or a given percentage, then the tether strand is assumed to have survived the encounter.

To determine the penetration depth to an orbiting tether system from a debris encounter, a suitable penetration equation is required. It was assumed that the Fish-Summers equation [**91**] would be suitable since it was recommended by Hayashida and Robinson [**92**] to establish threshold penetration depths for thin, ductile, metal plates. The Fish-Summers equation, as discussed by Drolshagen [**93**], is given by

$$P_d = k_1 m^{0.352} v^{0.667} \rho_p^{1.167}, \tag{5.30}$$

where P_d is the penetration depth (cm), k_1 is the target material constant (e.g. 0.42 for aluminium), m is the projectile mass (grams), ρ_p is the projectile material density (grams/cm^3) and v is the relative velocity (km/s). Table 5.4 gives the average densities for four different materials as given by Tomlin et al [**94**] and Hayashida et al [**95**].

Material	**Density (grams/cm^3)**
meteoroid debris	0.5
orbital debris	4.0
glass	2.0
aluminium	2.8

Table 5.4: Average mass densities

Spectra 1000$^{\text{TM}}$ is a very popular choice for tether material. Therefore, an estimate for the target material constant, k_1, was required for Spectra 1000$^{\text{TM}}$. Research conducted by McBride et al [**61**] studied a number of hypervelocity impact tests on tethers composed of Spectra 1000$^{\text{TM}}$. The projectiles were fired at a 2×2 cm target area holding 9 strands of tether (held under a few tens of Newtons tension). The experiment showed that a glass projectile, 0.3 mm in diameter and 5.6538×10^{-5} grams in mass, travelling at a relative velocity of 5 km/s would penetrate 0.82 mm into a Spectra 1000$^{\text{TM}}$ tether strand. Substituting these values into Equation (5.30) gave a value of $k_1 = 0.3906684$. A

second experiment showed that a 0.2 mm glass projectile, of mass 1.6752×10^{-5} grams, fired at 5 km/s would penetrate 0.53 mm into a Spectra 1000^{TM} tether strand. Again substituting into Equation (5.30) gave a value of $k_1 = 0.3874563$. Hence, taking an average of these two estimates, an approximate working value for the Spectra 1000^{TM} target material constant of $k_1 = 0.389$ was adopted in the TRAP model.

5.5.3 Double Strand Sever Risks

The two methods discussed so far are both suitable for determining sever probabilities to single strand tether systems. However, in order to determine sever probabilities to a double strand tether system, a method to calculate the probability of the second strand failing given the first has failed is required. Once again, the lethality coefficient and penetration methods are utilised. The lethality coefficient method again assumes that if $D \geq kd$ then the debris object is capable of severing both tether strands, providing its on a collision course with the second strand after it has severed the first. The penetration method, however, calculates the penetration depth of the first tether strand using the Fish-Summers equation. If the penetration depth calculated is larger than the tether diameter, and the debris object is on a collision course with the second strand, then the New Cour-Palais equation is utilised to calculate the penetration depth of the second strand. This is sometimes referred to as the 'Christiansen' equation, since it was first developed by Eric Christiansen [**96**] at Johnson Space Center (JSC). However, before calculating the penetration depth of the second tether strand, a method is required to determine the new trajectory course of the projectile, after it has severed the first tether strand, and its probability of impacting the second tether strand.

There is very little research literature that discusses what happens to a debris object that encounters a tether strand. For example, a small debris object of just a few millimetres may breakup during the impact, whereas a larger object, such as a defunct satellite, may sever the tether without being damaged itself. The TRAP model resolves this by assuming that debris objects less than 1 cm in size will fragment. Whereas, objects larger than 1 cm in size are assumed to survive the encounter.

Once an encounter between a debris object and the first tether strand occurs the (new) trajectory angle of the debris object must be determined. This (new) trajectory angle describes the path of the debris object after it has impacted (and severed) the first tether

strand. This enables TRAP to predict the debris object's probability of impacting the second tether strand. Two methods have been implemented into TRAP in order to calculate this new trajectory angle. The first of these is the so called LINEAR method which assumes that there is no deviation of the debris object's initial trajectory angle. The second method is called the TRAJECTORY method which calculates the debris object's new trajectory angle after the initial impact depending on its relative velocity and impact angle. With the new trajectory angle determined the probability of the second strand being hit is calculated using a linear (i.e. a linear probability model, not to be confused with the LINEAR method) or normal probability model. The probability models assume that a debris object on a (new) trajectory angle of 90° will impact the second tether strand with a probability of 0, whereas, a (new) trajectory angle of 0° will impact the second strand with a probability of 1, with a linear or normal distribution in between - see Figure 5.27.

For those objects that are assumed to breakup during the initial impact (i.e. objects < 1 cm), a suitable spray angle is also required along with its the new trajectory angle. This spray angle (or variance) determines the spread of the secondary debris cloud which forms after the initial impact. The trajectory, θ_1, and spray, ϕ_1, angles are illustrated in Figure 5.28.

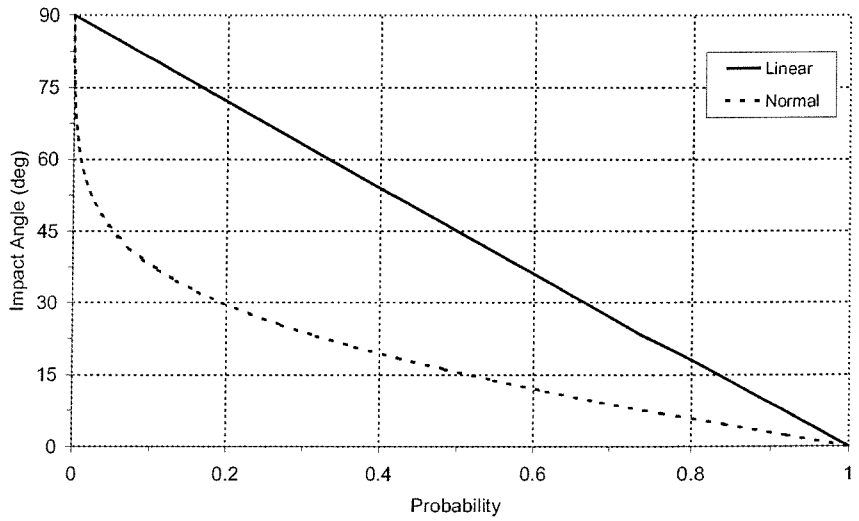

Figure 5.27: Linear and normal models used for determining probability of debris impacting with the second tether strand

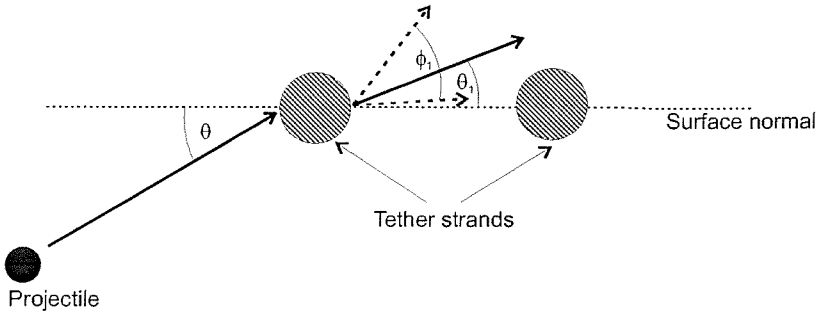

Figure 5.28: Tether cross-section illustrating the trajectory and spray angles of a secondary debris cloud

Sever Cross-Sectional Area

Although the collision cross-sectional area of a double strand tether system is double that of a single strand tether system, the sever cross-sectional area is considerably less. This is because, unlike a single strand tether system where one fatal impact will lead to mission failure, both tether strands, in one segment, have to fail. For debris objects smaller than the gap between the two tether strands, i.e. $D < t_d - 2d$, the sever probability will be the square of the probability of one strand failing, because strand one and strand two both have to fail and the probability of either strand failing is identical. However, if $D \geq t_d - 2d$ then the sever cross-sectional area, A_s is given by

$$A_s = L(D - t_d), \tag{5.31}$$

as illustrated in Figure 5.29.

A double strand tether system is also assumed to fail if an impact occurs causing a 'bead' connecting the two tether strands together to fail. However, the cross-sectional area of a 'bead' is very small, resulting in a small probability of failure. Another factor is the number of 'beads' along the tether length - as this tends to infinity, so the double strand tether tends to a single strand tether structure. Therefore, a critical number of 'beads' must exist where the probability of the tether system failing begins to be dominated by the impact-induced failure of a 'bead'. The probability of 'bead' failure has been neglected by some studies in the past and will be addressed in more detail in Chapter 6.

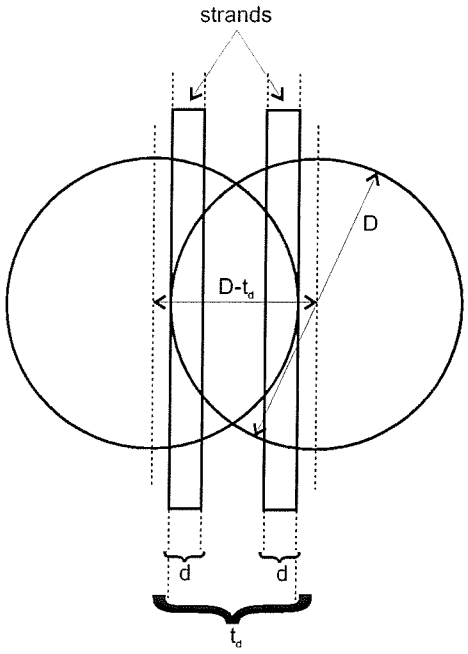

Figure 5.29: Sever cross-sectional area of a double strand tether system

The LINEAR and TRAJECTORY Methods

The trajectory angle calculation can be performed using either the LINEAR or the TRAJECTORY methods. The LINEAR method assumes the debris object suffers no deviation in its trajectory and continues to travel in the same direction prior to impact. The TRAJECTORY method, however, takes into account the impact angle and relative velocity, producing new trajectory and spray (if required) angles. The TRAJECTORY method used for calculating new trajectory and spray angles of secondary debris clouds, as discussed by Schonberg et al **[97]**, are determined from the following set of empirical equations outlined by Stokes **[98]**.

The trajectory angle, θ_1, is given by

$$\theta_1 = \theta \left[0.532 \left(\frac{v_p}{c_s} \right)^{-0.086} \left(\frac{t_s}{d_p} \right)^{-0.478} \cos^{0.586} \theta \right], \tag{5.32}$$

where v_p is the impact velocity (km/s), c_s is the speed of sound in the target material (km/s), t_s is the material thickness (cm), d_p is the debris object's diameter (cm) and θ is the impact angle (degrees) with respect to the tether surface normal, which is directed

outwards along the local horizontal component of its orbital velocity. However, in order to use this equation the following conditions (set 1) have to be satisfied,

$$\begin{aligned} 30^\circ < \quad & \theta & < 75^\circ \\ 2.0 \text{ km/s} < \quad & v_p & < 8.0 \text{ km/s} \\ 0.064 \text{ cm} < \quad & (t_s/d_p) & < 0.684 \text{ cm} \end{aligned}$$

If any of these conditions are not satisfied then the trajectory angle is given by

$$\theta_1 = \tan^{-1}\left[0.2536 \times 10^{-7}\left(\frac{v_p}{c_s}\right)^{-2.57}\left(\frac{t_s}{d_p}\right)^{-9.952}\cos^{1.088}\theta\right], \tag{5.33}$$

for the following conditions (set 2),

$$\begin{aligned} 0^\circ < \quad & \theta & < 65^\circ \\ 2.95 \text{ km/s} < \quad & v_p & < 6.9 \text{ km/s} \\ 0.152 \text{ cm} < \quad & (t_s/d_p) & < 0.315 \text{ cm} \end{aligned}$$

If these conditions are also not satisfied then the trajectory angle is assumed to follow is initial trajectory direction.

For debris that is assumed to fragment from impacting the first tether strand, a spray angle, ϕ_1, is also required. The spray angle, as discussed by Schonberg et al **[97]**, and outlined by Stokes **[98]**, is given by

$$\phi_1 = \tan^{-1}\left[1.556\left(\frac{v_p}{c_s}\right)^{1.096}\left(\frac{t_s}{d_p}\right)^{0.345}\cos^{0.738}\theta\right], \tag{5.34}$$

for the following set of conditions (set 3),

$$\begin{aligned} 0^\circ < \quad & \theta & < 75^\circ \\ 2.0 \text{ km/s} < \quad & v_p & < 8.0 \text{ km/s} \\ 0.064 \text{ cm} < \quad & (t_s/d_p) & < 0.684 \text{ cm} \end{aligned}$$

If any of these conditions are not satisfied then a spray angle of 10° is assumed. This ensures higher collision probabilities since the secondary debris cloud would not be too dispersed, since the distance between the two tether strands is generally very small (typically less than a few centimetres). Finally, with the new trajectory and spray angles determined, the probability of the debris object impacting the second tether strand can be determined using a linear or normal probability model. This is achieved

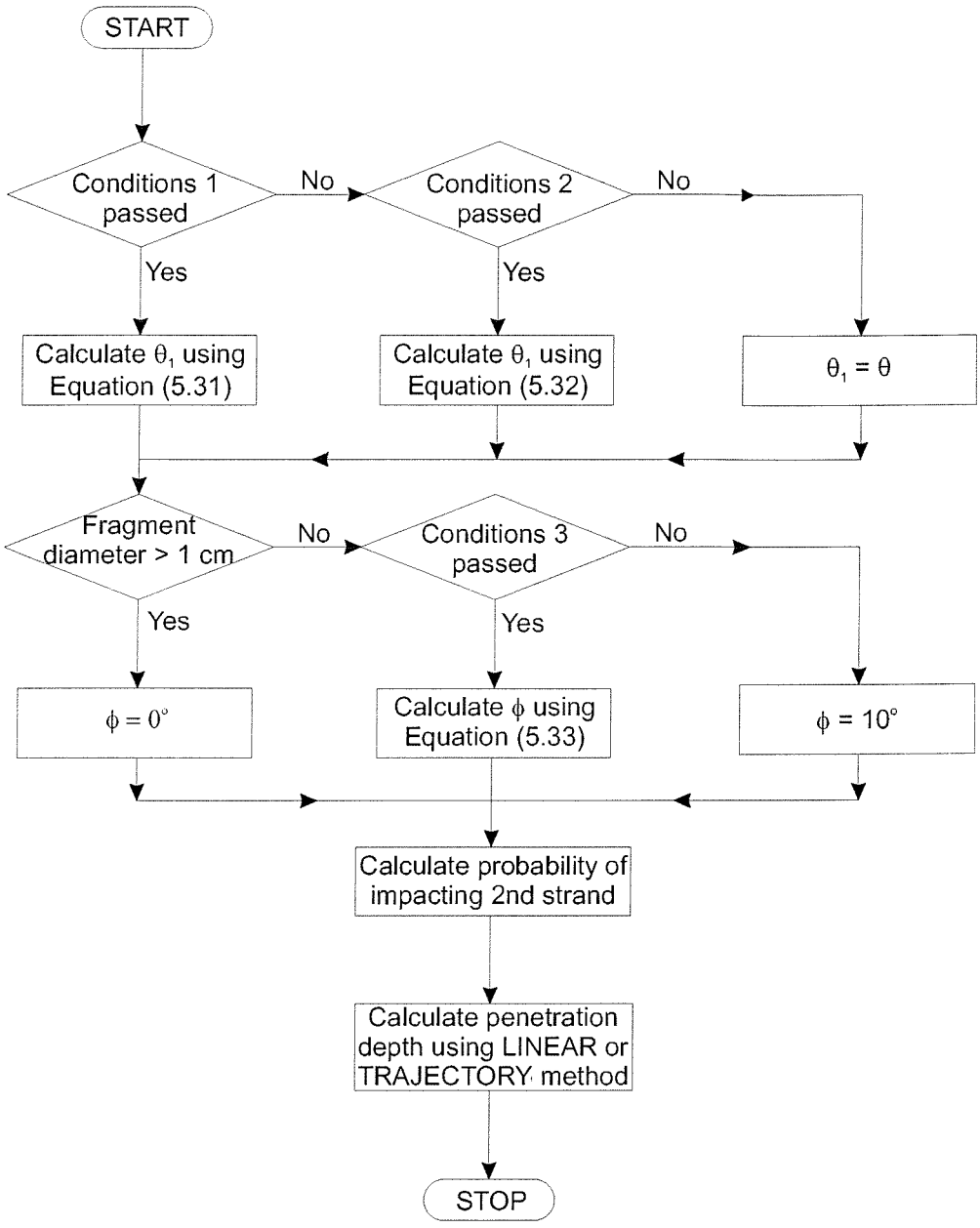

Figure 5.30: Flowchart illustrating the process followed for calculating new trajectory and spray angles

by assuming that a debris object on a new trajectory angle of 90° will impact the second tether strand with a probability of 0, whereas, a new trajectory angle of 0° will impact the second strand with a probability of 1, with a linear or normal distribution in between. With the collision probability determined the penetration depth needs to be calculated to determine if the collision results in the second tether strand failing. The above procedure is illustrated in Figure 5.30.

Lethality Coefficient Method

The lethality coefficient method implemented to determine sever risks to a double strand tether system is similar to that used for the single strand tether system case. If $D < kd$ the tether is assumed to survive the encounter and the sever probability is zero. However, if $D \geq kd$ then the first tether strand is assumed to have failed. With the knowledge that one of the tether strands has failed, the probability of the second tether strand being hit must be determined. This is achieved by using the LINEAR or TRAJECTORY methods discussed earlier. Once the probability of the debris object impacting the second tether strand is determined the lethality coefficient method is again used to determine if the object is capable of severing the second tether strand. If $D \geq kd$ then the second tether strand is assumed to fail. Otherwise the second tether strand is assumed to survive the impact and the sever probability is set to zero.

Penetration Method

The penetration method is a two-stage process. Firstly, the Fish-Summers equation, (5.30), is used to determine if the first strand is severed. If the penetration depth calculated is less than the tether diameter, or a user-defined percentage, then the strand is assumed to have survived the impact. If this is the case the sever probability is zero. However, if the penetration depth is larger than the tether diameter, or a given percentage, then the first strand is assumed to have been severed by the impact. With the knowledge that one of the tether strands has been severed, the probability of the second tether strand being hit must be determined. This is once again achieved by using the LINEAR or TRAJECTORY methods, discussed earlier. Once the probability of the debris object impacting the second strand has been determined the penetration depth of the second strand has to be calculated. This is achieved by implementing the

'Christiansen' equation, as discussed by Hayashida and Robinson [**99**], given by

$$d = \left[\left(t_w\left(\frac{\sigma}{40}\right)^{0.5} + t_b\right) / \left(0.6\left(\cos\theta\right)^{5/3}\rho_p^{0.5}v^{2/3}\right)\right]^{18/19}$$

valid for $v\cos\theta \leq 3$ km/s

$$d = \left\{\left[\left(t_w\left(\frac{\sigma}{40}\right)^{0.5} + t_b\right) / \left(1.248\rho_P^{0.5}\cos\theta\right)\right]^{18/19}\left(1.75 - \frac{v\cos\theta}{4}\right)\right\} + \left\{\left[1.071 t_w^{2/3}\rho_p^{-1/3}\rho_b^{-1/9}S^{1/3}\left(\frac{\sigma}{70}\right)^{1/3}\right]\left(\frac{v\cos\theta}{4} - 0.75\right)\right\} \quad (5.35)$$

valid for $3 < v\cos\theta < 7$ km/s

$$d = 3.918 t_w^{2/3}\rho_p^{-1/3}\rho_b^{-1/9}\left(v\cos\theta\right)^{-2/3}S^{1/3}\left(\frac{\sigma}{70}\right)^{1/3}$$

valid for $v\cos\theta \geq 7$ km/s

Here, d is the projectile diameter (cm), t_b is the material (first strand) thickness (cm), t_w is the material (second strand) thickness, ρ_p is the projectile density (grams/cm^3), ρ_b is the tether material density (grams/cm^3), θ is the impact angle measured from the surface normal (deg), v is the projectile velocity (km/s), S the space between the first and second tether strands, and σ is the material yield stress (ksi). The yield stress for Spectra 1000$^{\text{TM}}$ is 220 ksi (loaded to peak stress) as given by Oldson and Carroll [**100**] or 300 ksi (working stress) as given by Carroll and Oldson [**47**]. The 'Christiansen' equation determines the minimum fragment diameter capable of penetrating the second material layer. Therefore, if the actual debris fragment diameter is greater than the minimum diameter predicted, the tether is assumed to have been severed. Otherwise, the tether is assumed to have survived and the sever probability is zero.

5.6 Discussion

The TRAP model consists of a number of programs that have been independently implemented. The integration of these programs has resulted in an accurate collision and sever risk assessment model for orbiting space tether systems. Here we will outline some of the more important issues that have been uncovered in this chapter.

The implementation of the IDES breakup model, into the Breakup Program, is capable of modelling a fragmentation event resulting from an explosion or a collision. The model

requires the breakup object's orbital information and mass prior to the fragmentation, and as a result estimates the physical properties of each of the fragment's generated (e.g. mass, size, area) and the Δv's imparted to each fragment. If the fragmentation event is a collision, the mass and velocity of the projectile are also required. The model is supported by deterministic data and also complies with the laws of conservation of mass and energy.

The Tether Program, is capable of modelling an orbiting space tether system. The 'bead' model is implemented, which models the tether as a number of 'beads' connected by straight inelastic strands, referred to as 'segments'. As the number of 'beads' increases, so the tether tends to a more continuous structure. The ability to model an orbiting tether system in this way allows for accurate collision and sever risks to be achieved by looking at each segment separately.

The Analysis Program combines the output from the Breakup and Tether Programs to determine the collision risk for an orbiting tether system arising from a fragmentation event. The Probabilistic Continuum Dynamics (PCD) method is utilised in order to achieve accurate results. This method, although used in past models, such as the Space Debris Simulation (SDS) suite, to determine collision risks to satellites, is novel in its application to space tethers. One of the TRAP model's greatest strengths is its ability to allow debris density from the resulting debris cloud, to vary over the length of the tether system. The combination of this with the debris diameter averaging method, allows the calculation of the average debris diameters for four size ranges ($<$ 1 mm, 1 - 10 mm, 10 - 100 mm and $>$ 100 mm), which in turn enables accurate collision risk assessments to be made.

The Background Program is responsible for modelling the background orbital debris population. It is also capable of predicting future launch and fragmentation events based on recent space activities. The historical database contains information on over 24,000 objects associated with every launch and fragmentation event since the launch of Sputnik 1 in 1957 through to the 31st September 2000. The Background Program is also responsible for modelling the collision risk to an orbiting space tether system.

The TRAP model is also able to determine the sever probabilities associated with an orbiting space tether system. In the past, a lethality coefficient has been utilised in order to determine if a space tether would survive a debris impact. It was felt during

the development of TRAP, however, that this method was highly inaccurate and no consideration of impact energy is used in determining how big (or small) a fragment has to be to sever a tether strand. In order to enhance the accuracy of results, a penetration method was implemented into the TRAP model. This determined how far a debris object would penetrate a tether strand depending on its relative velocity, mass and impact angle. If the penetration depth was greater than the actual tether diameter, or a user-defined percentage of its diameter, then the tether is assumed to have failed. Otherwise it would survive the impact. In order to determine the penetration depth to a single strand tether system, it was assumed that the Fish-Summers penetration equation could be used.

The TRAP model is also capable of performing sever risk assessments for a double strand tether system. The sever risk to a double strand tether system involves the implementation of another penetration equation, the 'Christiansen' equation. The penetration depth of the first tether strand is then calculated using the Fish-Summers equation, and if it is found to be severed the 'Christiansen' equation is then applied to determine the penetration depth of the second strand. As with the single strand tether system, if the 'Christiansen' equation predicts a penetration depth greater than the tether strand's diameter, or a user-defined percentage, then the tether is assumed to fail, otherwise it will survive the encounter.

Chapter 6

Results

The previous chapters have discussed the orbital space debris environment and the concept of introducing a space tether into such an environment. Space tethers can be used for a number of new and interesting applications, such as artificial gravity and atmospheric research. Another application, which would be of considerable importance, is to use tethers for de-orbiting spacecraft at the end of their mission lifetime. It is agreed that eliminating debris pollution directly after use, is not only good practice, but also an important way of controlling the debris risk. However, as we have already discussed, tethers are particularly vulnerable to impacts from orbital debris, with just one impact resulting in the possibility of mission failure.

The purpose of this chapter is to use the Tether Risk Assessment Program (TRAP), discussed in the previous chapter, to predict the collision and sever probabilities of an orbiting space tether system. This will provide a good understanding of the risks posed to a space tether system from the orbital space debris environment, and what can be done to attempt to reduce such risks. However, before this can be achieved a number of sensitivity issues, identified during the development and testing phases of TRAP, must be addressed and clearly explained so that more accurate collision and sever risk assessments can be achieved. The TRAP model has also undergone a vigourous validation procedure and a number of comparisons between the TRAP model and those results found in the literature will be closely examined.

The IADC, the premiere forum in the area of space debris research, has established a number of action items (AI) to study the benefits and risks of using tethers in space,

and the TRAP model has been utilised to provide some helpful insights. Specifically, the issues raised by Pardini during the 21st IADC meeting held in Bangalore, India, on the 10-13th March, 2003, have been addressed concerning the debris impact risks to single and double strand tether systems.

6.1 Sensitivity Issues

The Space Debris Simulation (SDS) suite [4] has been used frequently in the past to investigate the collision probability for satellites arising from a debris cloud produced from a fragmentation event. A number of case studies, performed by Barrows [**4, 81**], can be found in the literature. A very important time-step sensitivity issue was discovered by Swinerd [**26**], who noted that smaller time-steps produced more 'collision probability structure'. Although the general trend of collision probability is similar to those cases with larger time-steps, a more accurate estimate of the threat posed to the satellite is achieved with smaller steps. This is because such methods of collision probability determination look at snapshots in time, and not what happens in between times. Hence, a satellite passing through the debris cloud's pinch point location, for example, would experience a very high debris density. However, if a time-step is chosen in such a way, that the satellite does not coincide with the pinch location, then this peak in debris density will be overlooked and result in a lower collision probability to the satellite in question.

A second sensitivity issue was discovered during the validation of the Analysis Program, when modelling collision and sever probabilities for a space tether system arising from a debris cloud produced by a fragmentation event. The issue, in this case, concerned the number of 'beads' used to model the tether system. The problem comes about due to the spherical control volume, discussed in the previous chapter, that is used to describe the debris environment. Unlike a typical satellite, a space tether system may be many kilometres in length. Therefore, at any one time-step, the tether system may occupy several different cells in the spherical control volume. The section of tether segment overlapping into another cell would then be modelled with an incorrect debris density value, since the cell the 'bead' occupies determines the debris density value for the whole of that segment. This 'overlapping error' can be reduced by increasing the number of 'beads' used to represent the tether.

The final sensitivity issue involves the radial size chosen for the cells in the spherical control volume used in the Background Program. The debris density should vary over the length of the tether system and, therefore, choosing a suitable cell radial size is vital in the process of modelling meaningful collision and sever probabilities. Ideally, the cell radial size would be equal to each of the tether segment lengths, with each of the cell borders passing through the 'beads'. However, this is only possible if the tether system's end-bodies are of equal mass, the tether is in a circular orbit with no orbital perturbation effects, and the tether is not librating. If the cell radial size is too large, then the whole tether system might be encompassed in just one cell, resulting in just one debris density value for the whole tether. Therefore, a suitable choice must be made depending on the tether length and its orbital parameters.

The following sections will consider the three sensitivity issues mentioned above. The discussion will also focus on how the influence of these sensitivity issues can be controlled and reduced during a particular simulation.

6.1.1 Time-Step Sensitivity

To investigate the time-step sensitivity issue in TRAP a number of simulations were performed. These simulations consisted of running a number of case studies where the time-step was varied, while keeping all other parameters constant. From the various simulations performed it was found that the general trends were similar, but that the 'absolute results' were dependent upon the chosen time-step, agreeing with Swinerd [**26**]. An example is discussed below.

To illustrate the time-step sensitivity issue, a high intensity explosion (HIX) scenario was considered. The parameters used throughout this simulation are provided in Table 6.1. The simulation was then performed over a 10-day time period, using three different time-steps (120, 60 and 30 minutes). Note that choosing a time-step that is greater than the orbital period of the 'target' object, such as the 120-minute time-step, would obviously result in lower collision probabilities since the debris cloud would spread around the Earth in just a few time-steps. For the three time-steps considered, it was decided to turn the perturbations off to prevent the debris cloud from dispersing too much around the Earth, ensuring the tether system remained within the debris cloud throughout the 10-day simulation. This allows for a thorough examination of the time-step sensitivity

Tether Details					
a	=	6,728 km	no. of beads	=	11
e	=	0.001	length	=	10 km
θ	=	0°	diameter	=	0.75 mm
			tether type	=	single strand
Breakup Details					
a	=	6,728 km	breakup type	=	HIX
e	=	0.001	on-orbit mass	=	1,000 kg
θ	=	355°	min. fragment size	=	1 mm

Table 6.1: Time-step sensitivity parameters

to be carried out because with perturbations switched on the tether may experience no threat from the cloud, resulting in no data to examine the time-step sensitivity issue. The results of these case studies are illustrated in Figures 6.1 to 6.3.

All three simulations show a general decrease in collision probability over the 10-day period, as the debris cloud expands and spreads around the Earth. It is clearly visible from a first glance that Figure 6.1 lacks some of the 'encounter structure' present in Figures 6.2 and 6.3. The reasons for this are three-fold. Firstly, the relative position vectors of the debris and tether are influenced. Secondly, there are a greater number of encounters with smaller time-steps. Finally, a time-step that positions the tether system in close proximity to the debris clouds pinch locations would have a profound effect on the debris density and, hence, collision probability.

From the above observations, it is obvious that a smaller time-step would result in more 'encounter structure' and, hence, more accurate collision probability assessments. Figure 6.4 shows the cumulative collision probability for the three different time-steps used. Although general trends are similar, the lack of 'encounter structure' for the 120-minute time-step, present in Figure 6.1, has resulted in a lower overall collision probability prediction than the 30-minute and 60-minute time-steps. However, smaller time-steps result in longer computational times. Hence, the time-step should be chosen at the user's discretion with perhaps shorter time-steps for shorter simulations and longer time-steps for longer simulations, bearing in mind the impact on the absolute collision probability. As a rule of thumb one might consider the following:

- Simulations with a run time of around 5 days or less should have small time-steps

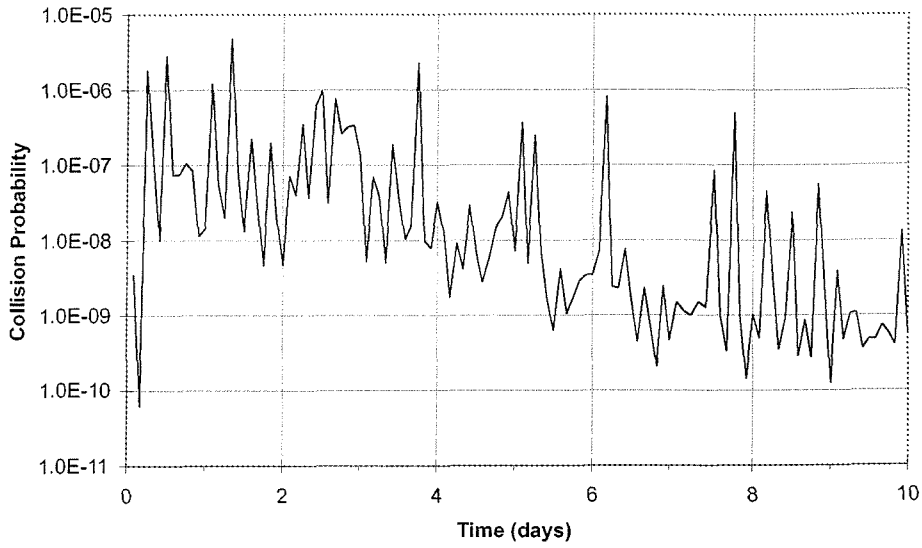

Figure 6.1: Collision probability with a time-step of 120-minutes over a 10-day period

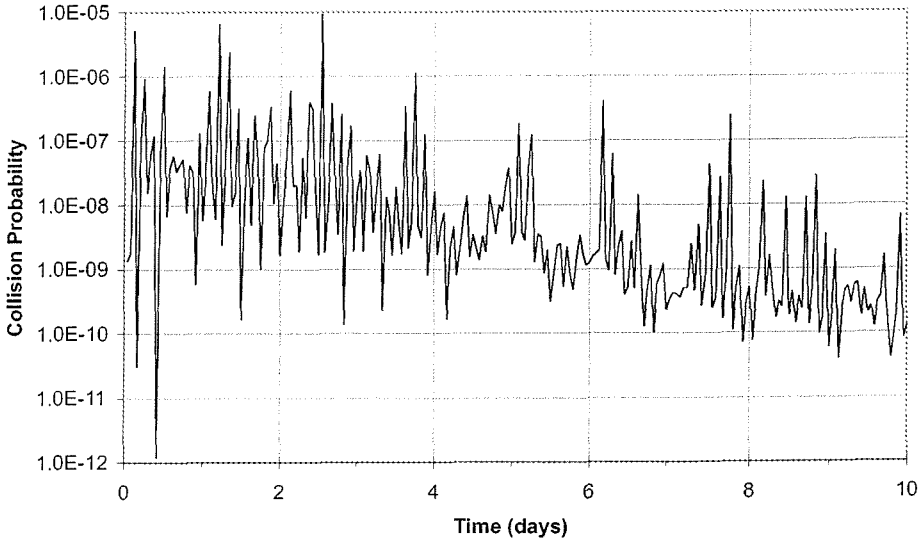

Figure 6.2: Collision probability with a time-step of 60-minutes over a 10-day period

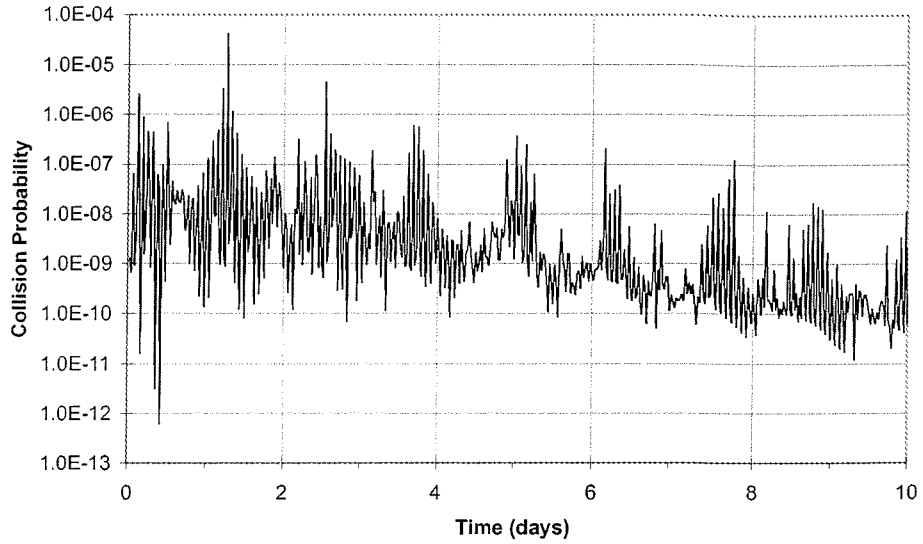

Figure 6.3: Collision probability with a time-step of 30-minutes over a 10-day period

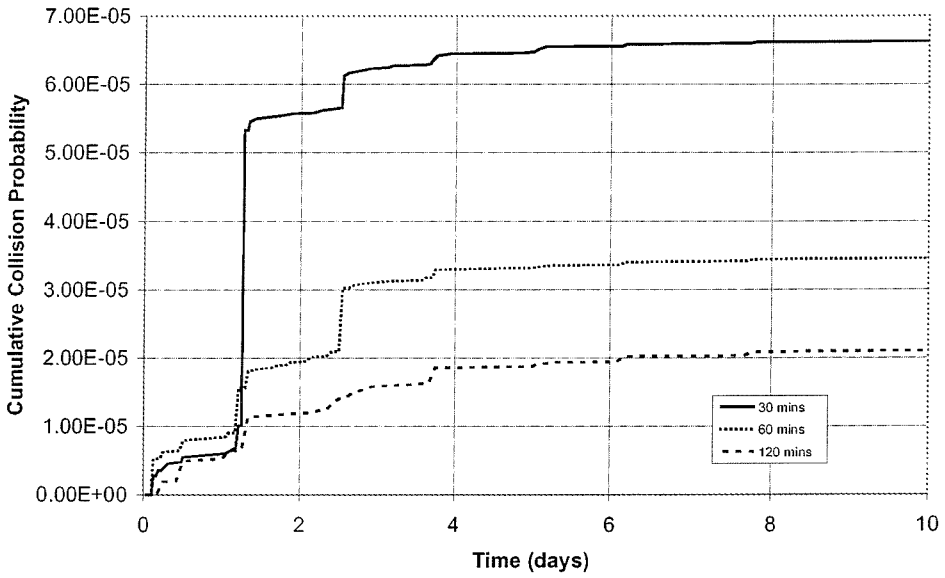

Figure 6.4: Cumulative collision probability predicted over a 10-day simulation using different time-steps

of about 1 to 5 minutes.

- Simulations with a run time of around 5 to 30 days should consider time-steps of about 5 to 30 minutes.
- Simulations longer than 30 days should consider time-steps of about 30 minutes or more.

6.1.2 Sensitivity to the Number of Beads

The sensitivity issue concerned with the number of 'beads', used to represent a tether system, was investigated by running a number of simulations. These simulations consisted of running a number of case studies where the number of 'beads' was varied, while keeping all other parameters constant. An example is discussed below.

Once again, a high intensity explosion (HIX) was modelled and the parameters used are outlined in Table 6.2. The corresponding debris cloud was then propagated, with no orbital perturbations, over a time period of 100 minutes using a time-step of 1-minute. The collision probability risks were then calculated for five tether systems, represented by 3, 7, 11, 15 and 19 'beads'. The results of which are illustrated in Figure 6.5.

Tether Details			
a = 6,728 km		length	= 10 km
e = 0.001		diameter	= 0.75 mm
θ = 0°		tether type	= single strand
Breakup Details			
a = 6,728 km		breakup type	= HIX
e = 0.001		on-orbit mass	= 1,000 kg
θ = 355°		min. fragment size	= 1 mm

Table 6.2: Bead sensitivity parameters

A good agreement can be seen for the tether systems modelled using 7 or more 'beads', while the tether modelled using just 3 'beads' has a much higher collision probability prediction. This is due to the 'overlapping error', discussed earlier, which is present when using a spherical control volume for space tether collision predictions. Unlike a typical spacecraft which will occupy just one cell of a spherical control volume, a tether system, which may be many kilometres in length, may occupy more than one cell. Since the

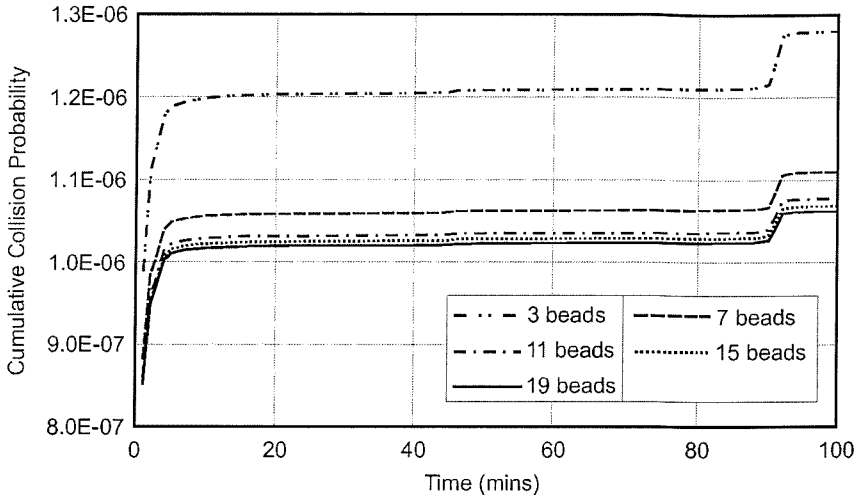

Figure 6.5: Cumulative collision probability comparisons for the bead tether model

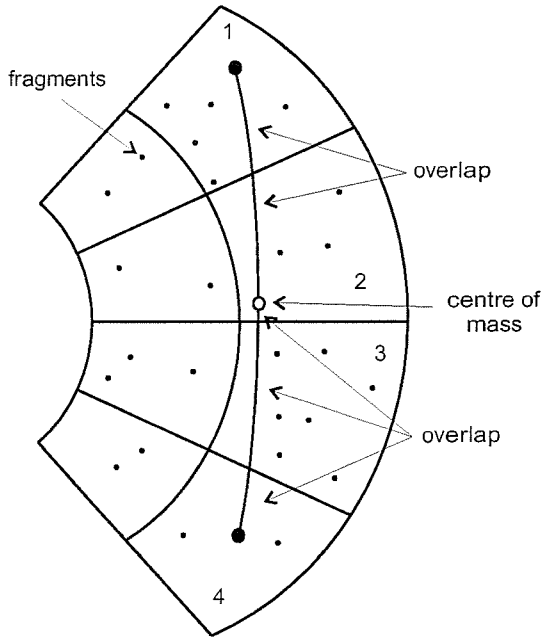

Figure 6.6: Overlapping issue of a tether system using a spherical control volume

'bead' dictates which cell the whole tether segment occupies, the debris density value may be inaccurate, resulting in less accurate collision probability predictions. This 'overlapping error' can be reduced, however, by increasing the number of 'beads' used to model the tether. Figure 6.6, for example, shows a 10 km long tether represented by 3 'beads'. The tether occupies four different cells, all of which have the same volume. The 'beads' along the tether system are then used to determine which cell each corresponding tether segment occupies. Since the tether will generally consist of n beads and $n-1$ segments the centre of mass 'bead' is not used during this process. Therefore, the upper 'bead' will correspond to the upper tether segment. Similarly, the lower 'bead' corresponds to the lower tether segment. Hence, the upper tether segment's collision probability is modelled using the debris density value obtained from cell 1, which is clearly higher than that of cell 2, which the tether segment also occupies - see Figure 6.6. Therefore, a higher collision probability will be measured. Similarly, the lower tether segment would have a lower collision probability prediction. Hence, introducing another two 'beads' would split the tether up into four segments, reducing the tether segment 'overlapping error' and producing a more accurate collision probability prediction.

The more 'beads' used to represent the tether the more accurate the collision assessment will be. However, increasing the number of 'beads' increases the computational effort required for the collision risk assessment. Hence, once again, the number of 'beads' used to represent a particular tether system is left to the user's discretion. One particular guideline to follow, however, is to increase the number of 'beads' for longer tethers, reducing the length of each of the tether segments. Table 6.3 gives a number of recommendations for the number of 'beads' to be used depending on the simulation time period and the tether length.

Length (km)	**Time Period (days)**	**Number of Beads**
≥ 20	< 5	> 15
≥ 20	5 - 30	7 - 15
≥ 20	> 30	3 - 9
< 20	< 5	> 5
< 20	5 - 30	3 - 15
< 20	> 30	3 - 9

Table 6.3: Bead sensitivity rules of thumb

6.1.3 Sensitivity to the Cell Radial Size

To predict the collision probability resulting from the background debris population, a suitable spherical control volume must be specified. The cell radial size plays a crucial part in this prediction because the size of each cell is critical in determining the variation in the debris density over the length of the tether system. A cell volume that encompasses the whole tether system, for example, is obviously insufficient. Hence, a suitable value must be chosen depending on the tether system's length, the number of 'beads' used to represent the tether and its orbit. A number of simulations have been performed to study this sensitivity issue and one of these examples is discussed below.

The collision probability resulting from the background population is examined over a 30-day time period, using a 1-hour time-step. The tether system is assumed to be in a circular orbit at an altitude of 350 km. The single strand tether system is 10 km long and 0.75 mm in diameter and is modelled using 5 'beads'. Three cell radial dimensions of 5 km, 2.5 km and 1 km were then subsequently studied. For this particular case study the effects of orbital perturbations were neglected. This is to ensure that the two end-bodies, of the tether system, would remain at the borders of the cells they occupied, throughout the simulation time period. This 'bead' structure is chosen deliberately so that the 5 'bead' tether model, which would split the tether into four 2.5 km segments, should then be modelled more accurately using a cell radial size of 2.5 km. Figure 6.7 shows the cumulative collision probability for the 10 km tether system arising from the background orbital debris environment, over a 30-day period, using three cell radial dimensions.

The results illustrated in Figure 6.7 show three distinct cumulative collision probability predictions. The cumulative collision probability produced by the 1 km cell radial size is referred to as a 'high collision' probability prediction, while the probability produced by the 5 km cell radial size is referred to as a 'low collision' probability prediction. These high and low collision probabilities exist because of the various parameters used in estimating collision probabilities. A large step in probability is a common feature produced by the 'high collision' probability prediction. This is generally due to a number of objects occupying a small cell volume, greatly increasing the debris density value for that particular cell, thus, increasing the collision probability. The 'low collision' probability prediction, on the other hand, is very smooth. This is because the objects

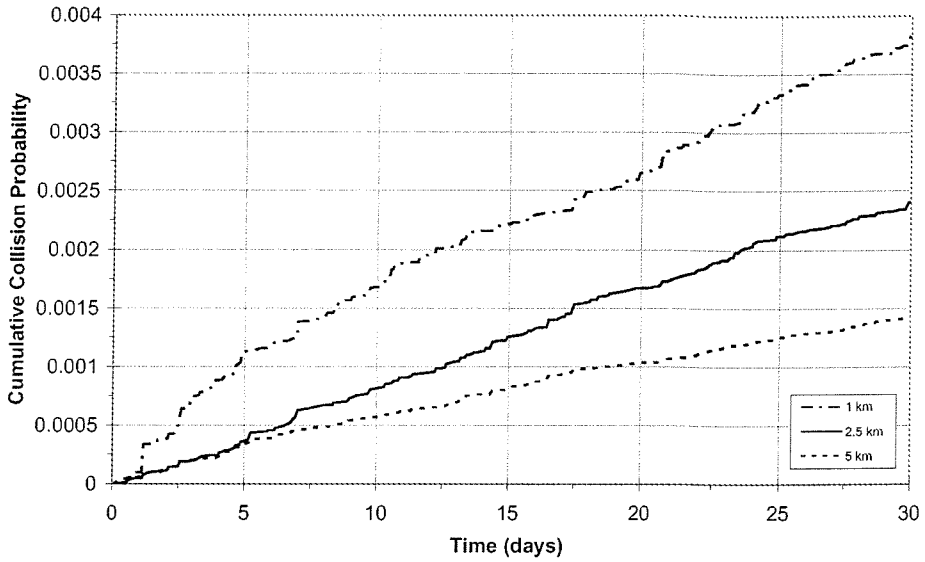

Figure 6.7: Cumulative collision probability from the background population using various cell radial dimensions

are now encompassed within a very large cell volume, reducing the debris density value, thus, decreasing and smoothing the overall collision probability. Therefore, choosing a cell radial size in between the 'high collision' and 'low collision' probability predictions will result in a best fit, producing more accurate collision probability predictions - see Figure 6.7. In order to determine the ideal cell radial size the user would have to choose a value that takes into account both the length of the tether and the number of 'beads' used to represent the tether system. As a rule of thumb the cell radial size should try to closely resemble the length of the tether divided by the number of 'beads'. If the tether system has equal end masses this distance would also match the tether segment lengths (i.e the distance between each of the 'beads').

6.2 Validation with Literature Sources

A number of collision risk assessments have been produced in the literature. In particular the risk assessments for an orbiting space tether system performed by Anselmo and Pardini **[58, 62]** and Chobotov and Mains **[63]**, which were discussed in Chapter 3, will be examined. A comparison between these literature results and those produced by TRAP will then be carried out to assess the TRAP model's accuracy. Anselmo

and Pardini [**58, 62**] carried out a number of simulations that look at both single and double strand tether systems. This research was conducted to evaluate the expected operational lifetime of a new space tether system, the Electrodynamic De-Orbiting And Re-entry Device (EDOARD), intended to fly in the near future to accomplish the end-of-life de-orbiting of spacecraft and spent upper stages. Chobotov and Mains [**63**] focused their research on the Tethered Satellite System Re-flight (TSS-1R) which broke away from the Shuttle during deployment in March 1996. The remaining 19.7 km long tether remained in orbit, attached to its end-body, for a further 3 weeks before re-entering the Earth's atmosphere.

The following section will compare the results predicted by the TRAP model with those produced by Chobotov and Mains [**63**]. The EDOARD case scenario will be discussed later in the chapter, focusing on issues raised by the IADC.

6.2.1 Tethered Satellite System Re-Flight

Chobotov and Mains [**63**] looked at the collision probability of the Tethered Satellite System Re-flight (TSS-1R), after it broke away from the Space Shuttle Orbiter. The tether, which had a cross-sectional area of 56.6 m^2, was exposed to the orbital debris environment for about 3 weeks before re-entering the Earth's atmosphere. The study examined the collision probability for the TSS-1R, arising from micrometeoroids and man-made orbiting objects. This was achieved by using analytical and statistical methods. The analytical approach involved calculating the number of objects penetrating an area in space swept out by the tether in one orbital revolution - see Figure 3.13 of Section 3.5.3. The statistical approach, on the other hand, was based on the frequency of close approaches by space objects to the tether over an extended period of time. This involved the determination of the closest approach distance by space objects that may result in a collision with the tether system. The analytical approach predicted a collision probability of about 2.23×10^{-3} per month for objects 10 cm in size or larger, which compared reasonably well with their statistical prediction of 1.527×10^{-3} per month.

In order to compare the results of the TRAP model with those produced by Chobotov and Mains, a simulation was performed using the same orbital and tether parameters as Chobotov and Mains [**63**]. Although the tether was ejected into a slightly eccentric orbit, after the tether broke away from the Shuttle, Chobotov and Mains assumed the

tether to be in a circular orbit at an altitude of 364 km inclined at 28.45°. They also assumed the tether to lie along the local vertical, as a result of stabilisation by the gravity gradient. The method used by Chobotov and Mains involved looking at the number of objects penetrating a particular area of space, swept out by the tether over one orbital revolution. Thus, the effects of atmospheric drag were turned off during the TRAP simulation to prevent the tether's orbit decaying. The sensitivity issues, discussed in the previous section, would have a profound effect on the outcome of the collision probability. Therefore, the simulation was performed a number of times with variations in the number of 'beads' used to represent the tether system, the cell radial dimension and the time-step. The results of these simulations are shown in Table 6.4 and compare exceptionally well with the analytical and statistical methods used by Chobotov and Mains [**63**].

The first run of the simulation (run 1) was used as a reference case. This provided a baseline case against which to compare other simulations when varying the three sensitive parameters. The first of these parameters was the number of 'beads' used to model the tether. The collision probability for the tether modelled using just 3 'beads' (run 2) is slightly higher than the other two (runs 1 and 3) which is due to the 'overlap error' discussed in Section 6.1.2. The next parameter varied was the time-step (runs 4 and 5). The collision probability is much more consistent in these cases. This was to be expected, however, since the issue of the time-step variation only effects the collision probability when a fragmentation event is modelled, and there exists a substantial change in debris density at the debris clouds pinch locations. The final two simulations (runs 6 and 7) focused on the variation of the cell radial dimension. Since the tether was nearly 20 km long and represented using 7 'beads' it was expected that

Run	No. of Beads	Cell Radial Size (km)	Time-step (mins)	Collision Probability
1	7	5	60	1.59×10^{-3}
2	3	5	60	4.69×10^{-3}
3	11	5	60	1.00×10^{-3}
4	7	5	30	1.52×10^{-3}
5	7	5	90	1.52×10^{-3}
6	7	3	60	2.33×10^{-3}
7	7	1	60	5.76×10^{-3}

Table 6.4: Collision risk to TSS-1R varying the sensitivity parameters

a cell radial size of 3 km would produce more accurate collision probability estimates, than the 1 km and 5 km cell radial sizes. This was because the length of tether between each 'bead' is about 2.81 km, close to the 3 km cell radial size.

6.3 Past Mission Assessments

A number of tether missions have been performed since 1966 where NASA first used a tether to link the Gemini XI manned spacecraft to their Agena upper stage. Tethers have since been used to perform a number of space experiments, enabling vast research to be carried out to study tether dynamic issues and conductive tether experiments. In particular the TSS, SEDS, PMG and TiPS experiments were crucial in laying down the foundations for future tether missions (see Chapter 3).

The following sections will consider two past tether missions, SEDS-2 and TiPS. A number of simulations will be performed, studying the collision and sever probabilities of such tether systems, arising from the background orbital debris environment. Further simulations will consider the risks posed to space tethers from a debris cloud, generated by a recent breakup event. The discussion will also compare the results with flight data acquired during the tether experiments.

6.3.1 Small Expendable Deployer System

The SEDS-2 mission was launched on the 9th March 1994 into a near-circular orbit at an altitude of 350 km, inclined at 32°. The actual tether consisted of a single strand that was 20 km long and just 0.75 mm in diameter. The experiment was able to demonstrate that by using a closed-loop control law, the libration angle in the tether could be kept to a minimum. After deployment, the tether was left attached to the Delta II second stage, to study the long-term tether survivability and micro-meteoroid impact risks. Unfortunately, the tether was severed, allegedly by a micro-meteoroid, 3.7 days after deployment which resulted in the payload re-entering within hours (due to increased area to mass ratio and momentum transfer). However, approximately 7.2 km of tether remained attached to the Delta II second stage for a further 56 days, before re-entering the Earth's atmosphere, with no apparent further breaks.

Here we will discuss two case scenarios that will attempt to estimate the collision and

sever probabilities for the SEDS-2 tether system, prior to failure. The first scenario examines the effects of the background population over a 1-month time period, providing a good understanding of the risks encountered by a long, thin tether system arising from the large, trackable, debris population. The second scenario will consist of modelling an explosion, using the Breakup Program, to study the effects of the smaller, un-trackable, debris population. The orbital and breakup parameters used during these case scenarios are outlined in Table 6.5. Note that the original breakup object occupies a similar orbit to that of the tether system before the fragmentation. This results in 'low-energy' interactions between the generated debris fragments and the tether system.

Tether Details					
a = 6,728 km	ω = 0°	no. of beads	=	7
e = 0.001	Ω = 0°	length	=	20 km
i = 32°	θ = 0°	diameter	=	0.75 mm
		in-plane libration	=	8°
		out-of-plane libration	=	3°
Breakup Details				
a = 6,728 km	ω = 0°	breakup type	=	HIX
e = 0.001	Ω = 0°	on-orbit mass	=	500 kg
i = 32°	θ = 355°	min. fragment size	=	1 mm

Table 6.5: SEDS-2 mission profile input into the TRAP model

Background Debris Simulation

The background simulation was performed over a 1-month time period, using a 60-minute time-step, and a cell radial size of 3 km. The cumulative sever probability, predicted using the penetration (impact energy) method, is illustrated in Figure 6.8, clearly showing a steady increase in sever probability over time. The cumulative collision probability was found to be identical to the cumulative sever probability. This is because the objects modelled in the background population are large, 10 cm in size or larger for such altitudes, while the tether system diameter, just 0.75 mm, is very small by comparison. It was determined that the SEDS-2 tether system would experience about 1.28×10^{-3} fatal impacts over a time scale of just one month from the background orbital debris population. However, with the inclusion of the small debris background population this sever probability will be much higher - see Table 6.10 which shows TRAP

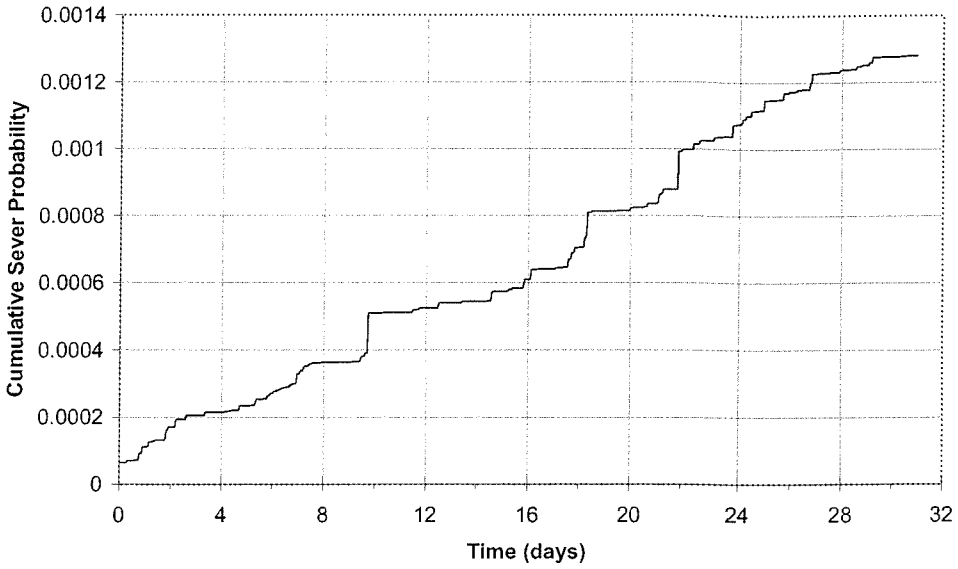

Figure 6.8: Cumulative sever probability to the SEDS-2 tether system, over a 1-month period, from the background orbital debris population

to predict a sever probability about 2 orders of magnitude lower than those predicted in the literature by Anselmo and Pardini **[58, 62]**. The implementation of the small debris background population is recommended, and discussed, in Chapter 7.

High Intensity Explosion Simulation

The debris density encountered by all six tether segments, from the resulting debris cloud, over the 10-day simulation, using a 10-minute time-step, is illustrated in Figure 6.9. For similar altitudes the background orbital debris density is around 10^{-7} for objects 1 mm, or larger, in size, as predicted by the DAMAGE model in Figure 2.4. Figure 6.9 shows an initial debris density a few orders of magnitude above this, at the beginning of the simulation, where the debris cloud is still compact. However, as the debris cloud evolves and is dispersed around the Earth, the debris density begins to drop off, slowly falling towards the background debris density by the end of the simulation. The sever probability, predicted by the penetration method, shown in Figure 6.10, is in accord with the debris density plot, showing a sharp increase at the beginning of the simulation, and then steadily levelling out as the debris cloud is dispersed. From studying the results in detail, it was noticed that not all the fragments colliding with

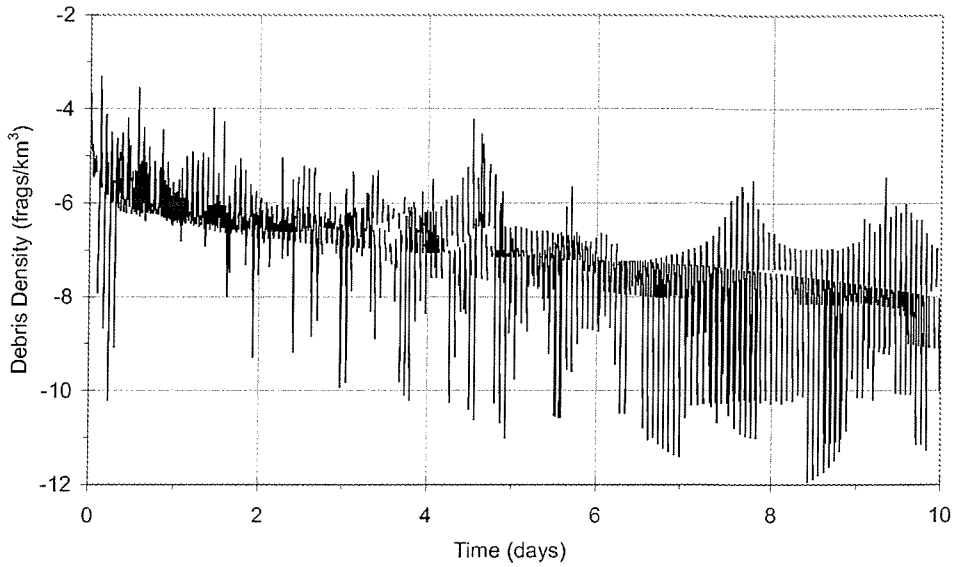

Figure 6.9: Debris density ($\log_{10}$) of the simulated debris cloud, over a 10-day period, encountered by all six tether segments representing the SEDS-2 tether system

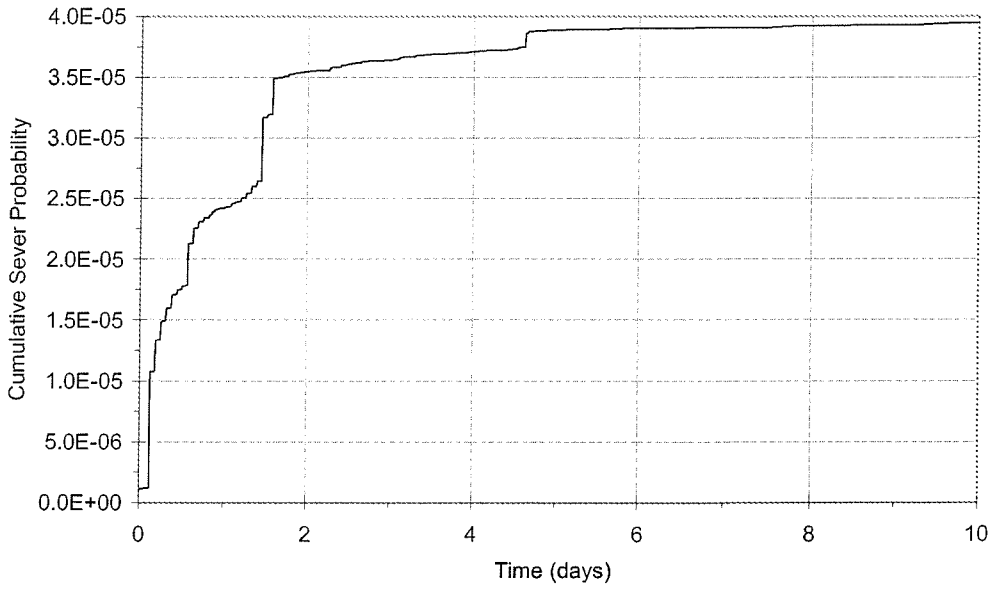

Figure 6.10: Cumulative sever probability to the SEDS-2 tether system, over a 10-day period, from the simulated debris cloud

the tether would actually cause the tether to fail. However, the difference was very small giving a total cumulative collision probability of 3.9459×10^{-5}, compared to the cumulative sever probability of 3.9455×10^{-5}.

The above observations indicate that thin tethers, less than a millimetre in diameter, are very susceptible to the small debris population, even with 'low-energy' interactions between the generated debris fragments and the tether system. To understand why the tether is so vulnerable to such impacts, the lethality coefficient method, discussed in the previous chapter, is utilised to estimate the minimum fragment diameter capable of severing a tether strand. This fragment diameter is given by

$$D = kd, \tag{6.1}$$

where D is the debris diameter capable of severing the tether strand, k is the lethality coefficient and d is the tether diameter. However, for sever predictions to be accurately made using this method a suitable value for k must be chosen, depending on the impact energy. The minimum fragment diameter capable of severing a tether strand for 'low-energy' interactions is obviously higher than for 'high-energy' interactions. Therefore, a high lethality coefficient is required for 'low-energy' interactions and a low lethality coefficient is required for 'high-energy' interactions. The impact energies in the SEDS-2 case study were relatively low, since the breakup occurred in a similar orbit to that of the tether. Therefore, a lethality coefficient of $k = 0.6$ was chosen. Substituting into Equation (6.1) along with the tether diameter, $d = 0.75$, gives a minimum fragment diameter, capable of severing the tether, of $D = 0.45$ mm. The minimum fragment diameter generated using the Breakup Program is more than twice this lethal minimum fragment diameter estimate. This demonstrates that thin, millimetre size, tether strands are particularly vulnerable to the small-sized space debris environment, with the possibility of the tether severing with 'low-energy' interactions.

6.3.2 Tether Physics and Survivability Experiment

The TiPS mission was launched on the 20th June 1996 into a near-circular orbit at an altitude of 1,022 km, inclined at 63.4°. The experiment was a free-flying satellite consisting of two end-bodies connected by a 4 km long, single strand tether, with a diameter of 2.5 mm. The purpose of this mission was to study long term orbit and attitude dynamics and tether survivability issues. The experiment was a complete

success providing a great deal of confidence in our ability to model tether dynamics, and showing that tethers could be made to survive the harsh space debris environment for long periods of time.

Here we will discuss three case scenarios to estimate the collision and sever probabilities for the TiPS tether system. The first scenario will investigate the effects of the background population over a 1-month time period, providing a good understanding of the risks posed to a short, thick tether system, from the large, trackable, debris population. The remaining two cases will consider fragmentation events. The first of these fragmentation cases will consist of a type of scenario similar to that considered in the SEDS-2 case study. That is, a fragmentation in a similar orbit to that of the tether, producing a risk assessment for 'low-energy' interactions. The second of these fragmentation events, however, will model a breakup in a different orbital geometry to that of the tether. This will produce 'high-energy' interactions where the two orbits intersect. This combination of cases provides a good insight into tether survivability issues for 'low-energy' and 'high-energy' interactions between the simulated debris and the tether. The parameters used for each of the three cases are outlined in Table 6.6.

Tether Details					
a = 7,400 km	ω = 0°	no. of beads	=	5
e = 0.001	Ω = 0°	length	=	4 km
i = 63.4°	θ = 0°	diameter	=	2.5 mm
		in-plane libration	=	0°
		out-of-plane libration	=	0°
Fragmentation Case Study 1 - 'Low-Energy' Interactions				
a = 7,400 km	ω = 0°	breakup type	=	Collision
e = 0	Ω = 0°	on-orbit mass	=	1,000 kg
i = 60°	θ = 350°	min. fragment size	=	1 mm
		projectile mass	=	5 kg
		rel. velocity vector	=	$[0.2\ 0.1\ 0.05]^{T}$ km/s
Fragmentation Case Study 2 - 'High-Energy' Interactions				
a = 7,400 km	ω = 320°	breakup type	=	Collision
e = 0	Ω = 90°	on-orbit mass	=	1,000 kg
i = 90°	θ = 10°	min. fragment size	=	1 mm
		projectile mass	=	5 kg
		rel. velocity vector	=	$[0.2\ 0.1\ 0.05]^{T}$ km/s

Table 6.6: TiPS mission profile input into the TRAP model

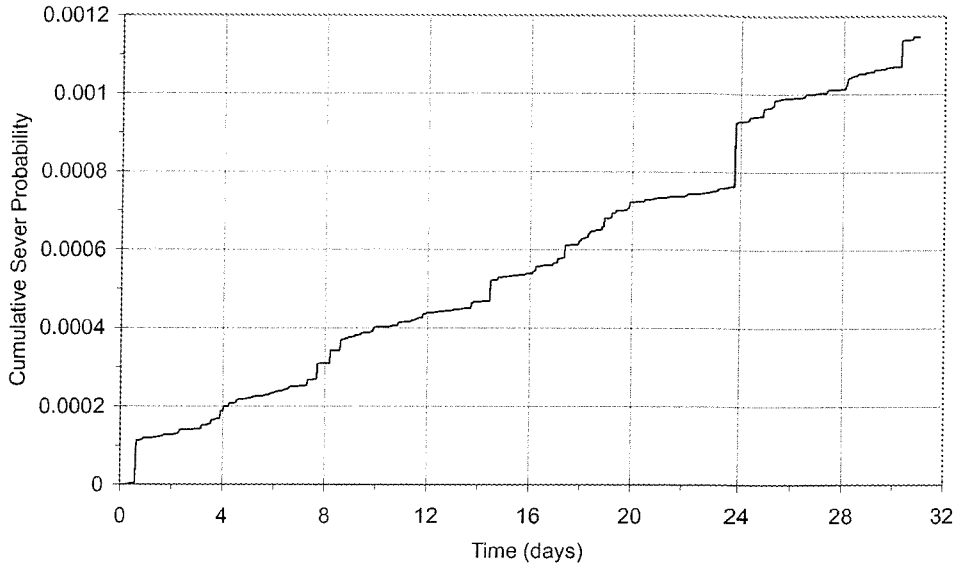

Figure 6.11: Cumulative sever probability to the TiPS tether system, over a 1-month period, due to the background orbital debris population

Background Debris Simulation

The background simulation was performed over a 1-month time period, using a 30-minute time-step and a cell radial size of 1 km. The cumulative sever probability, predicted using the penetration method, is illustrated in Figure 6.11, showing a steady increase over time. As with the SEDS-2 case study the cumulative collision probability was found to be identical to the cumulative sever probability, due to the nature of the background population size. It was determined that the 4 km long TiPS tether would experience about 1.148×10^{-3} fatal impacts over a 1-month time period from the orbital background population.

Fragmentation Case Study 1 - 'Low-Energy' Interactions

The debris density encountered by all four tether segments, from the debris cloud, over the 10-day simulation, using a 5-minute time-step, is illustrated in Figure 6.12. The background orbital debris density for similar altitudes is around 10^{-6} for objects 1 mm, or larger, in size, as predicted by the DAMAGE model. Figure 6.12 shows an initial debris density a few orders of magnitude above this, at the beginning of the simulation, where the debris cloud is still compact. However, as the debris cloud

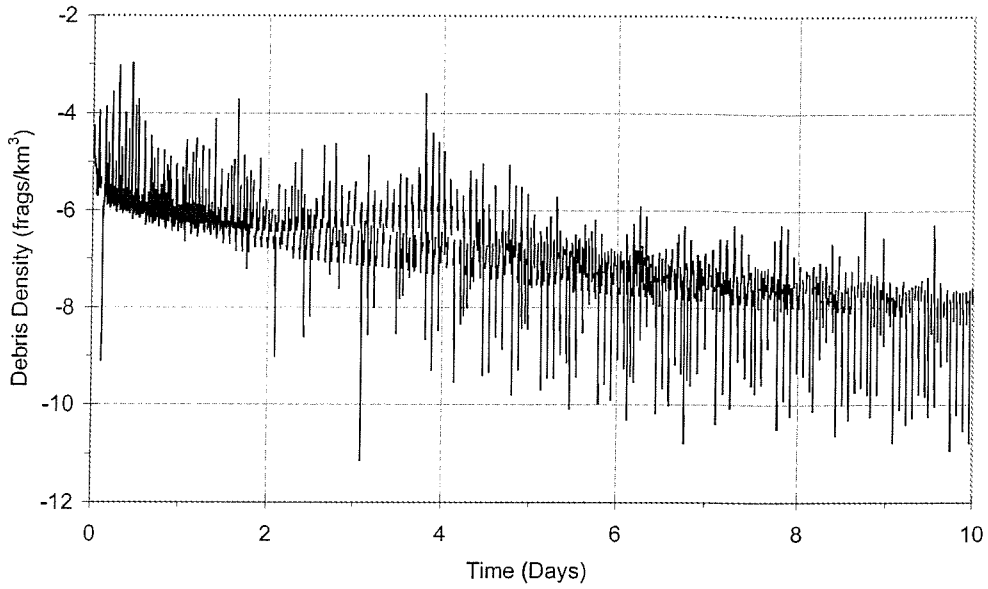

Figure 6.12: Debris density ($\log_{10}$) of the simulated debris cloud, over a 10-day period, encountered by all four tether segments representing the TiPS tether system

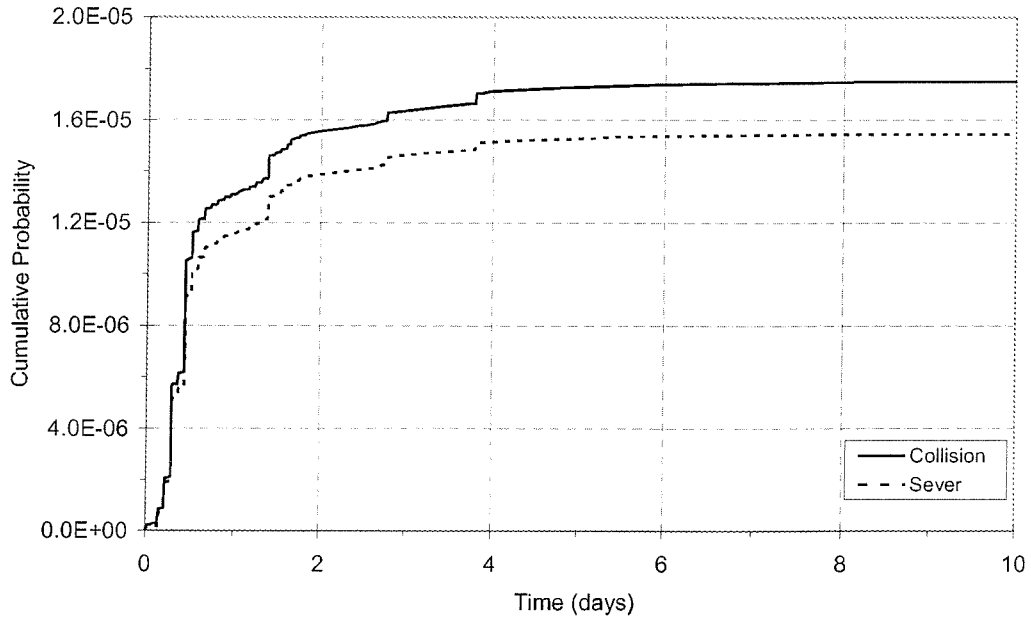

Figure 6.13: Cumulative collision and sever probability to the TiPS tether system, over a 10-day period, from the simulated debris cloud

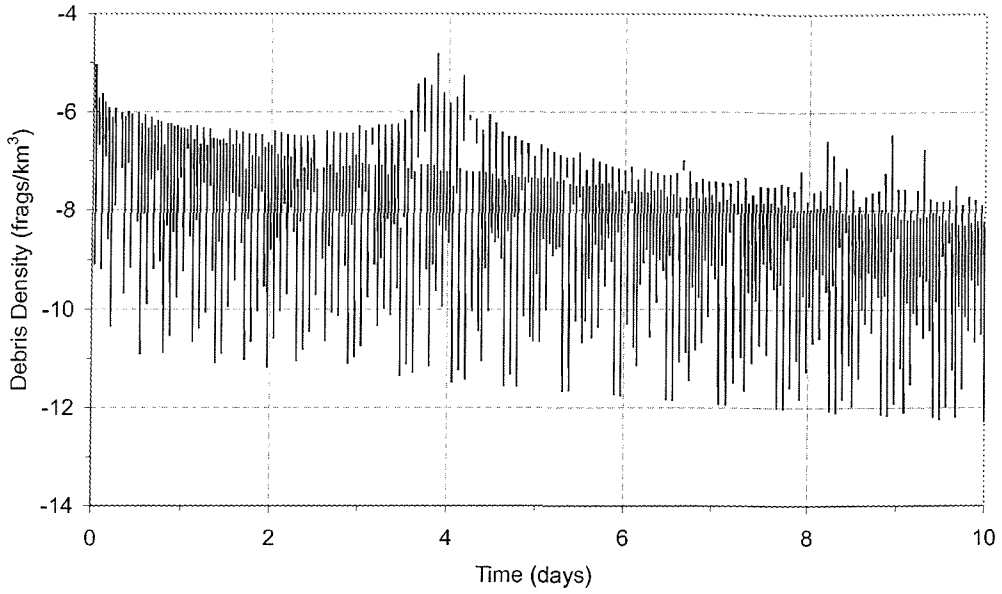

Figure 6.14: Debris density ($\log_{10}$) of the simulated debris cloud, over a 10-day period, encountered by all four tether segments representing the TiPS tether system

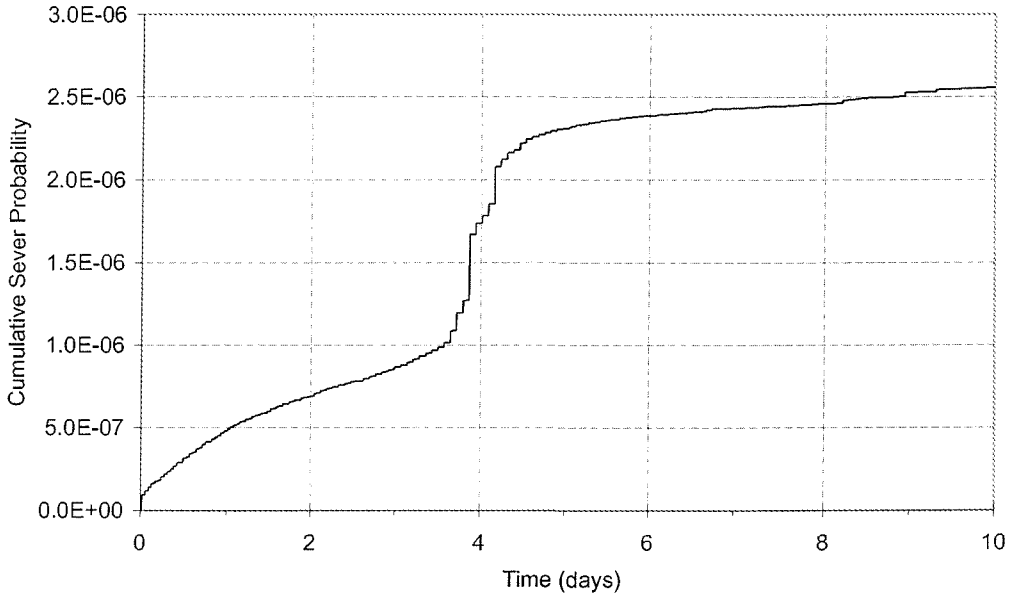

Figure 6.15: Cumulative sever probability to the TiPS tether system, over a 10-day period, from the simulated debris cloud

evolves and is dispersed around the Earth, the debris density begins to drop off slowly falling below the background debris density after around 6 days. The collision and sever probability, shown in Figure 6.13, is in accord with the trends presented in the density plot, showing a sharp increase in collision/sever probability at the beginning of the simulation, steadily levelling out as the cloud evolves. The sever probability, shown in Figure 6.13 as predicted using the penetration method, is less than the collision probability throughout the 10-day simulation, demonstrating that a tether system, with a significant tether diameter (2.5 mm), is capable of surviving 'low-energy' interactions with the small debris population.

Fragmentation Case Study 2 - 'High-Energy' Interactions

The debris density encountered by all four tether segments, over the 10-day simulation is considerably less than for the previous scenario, as shown in Figure 6.14. This is because the tether system spends less time within the debris cloud due to the orbital geometry of the breakup and tether orbits. However, the impact energies involved, where the two orbital paths intersect, is considerably higher than in the previous case. This results in a sever probability, predicted using the penetration method, that is identical to the collision probability, as illustrated in Figure 6.15. Although it has been shown that the TiPS tether system is capable of surviving 'low-energy' interactions, from a small debris fragment, the tether is far more vulnerable to 'high-energy' interactions. The cumulative sever probability also experiences a large increase in probability around day 4. This is because the interaction time between the debris cloud and the tether is very short, due to the different orbital geometries. During this interaction time the tether may experience a small or large debris density. Obviously, the debris density experienced around the fourth day of the simulation was higher than throughout the rest of the simulation, resulting in a large increase in sever probability. Since the simulation was only performed over a 10-day period it is not known if such an increase would occur again. However, the collision probability will generally reduce with the time as the cloud continues to evolve.

6.3.3 Findings From Past Tether Mission Experiments

The above case studies have examined the effects of the orbital space debris environment on two types of tether systems. The first considered the effects of the debris population on long, thin tether strands (20 km long and 0.75 mm in diameter). The second case study, on the other hand, considered a short, thick tether strand (4 km long and 2.5 mm in diameter), providing some evidence that such tethers may be able to survive the effects of the smaller debris population.

In reality, long thin tether strands are very susceptible to impacts arising from the debris environment, and this view was substantiated by the SEDS-2 tether system which was severed, apparently by a micro-meteoroid, 3.7 days after deployment. This was also confirmed from the breakup case scenario presented for the SEDS-2 tether system. The results showed that the tether was particularly vulnerable to the small debris population (1 to 10 mm) since even with 'low-energy' interactions, between the debris and tether, the tether system would still be severed. Single strand tethers, however, can be made to survive the harsh debris environment. This was demonstrated by the TiPS experiment which survived in orbit for over 4 years without any apparent breaks. This was confirmed from the first breakup case scenario, albeit over a shorter period of time, which showed that not all the small debris fragments colliding with the 2.5 mm diameter tether were capable of severing it. However, the debris to tether impact energies were relatively low, and further analysis of 'high-energy' interactions showed that the tether was just as vulnerable to the small debris population as the SEDS-2 tether system. Therefore, designing a more robust tether system, such as a double strand tether system, may be the solution if tethers are to be used successfully in the future. This will be discussed in the following section.

6.4 Future Mission Assessments

There are a number of future tether missions planned. Such missions include the Double Tethered Experimental Satellite (D-TES) developed at the Kyushu University in Japan. D-TES will be launched as a secondary payload aboard a Japanese H-IIA launch vehicle. Its primary objective is to deploy a 20 km tether so that data can be gathered regarding the dynamics of a double strand tether system.

In 1998, at the University Space Systems Symposium (USSS) - a joint Japanese/US student conference - the QUEST (Kyushu - US Experimental Satellite Tether) mission was proposed. The QUEST mission will also be launched as a secondary payload aboard a Japanese H-IIA launch vehicle. Its primary objective is the successful deployment of a 2 km tether, made of Kevlar, to study the control and dynamics associated with the deployment. After the operational mission, the tether will be cut to demonstrate and investigate orbit transfer.

In November 2001, another experiment, named QTEX, was proposed by Kyushu University. Launching as a secondary payload, the proposed tether will be 2 km in length. Its motion will be observed for at least four months to study the dynamics.

In the following section the Propulsive Small Expendable Deployer System (ProSEDS) will be discussed, which is a proposed space tether experiment due for launch in 2004. Launching as a secondary payload, the ProSEDS mission will deploy a 5 km bare wire tether, attached to a further 10 km of Spectra tether, from a Delta II second stage rocket **[101]**. This will provide approximately 0.4 N of electrodynamic drag, demonstrating the principle of de-orbiting by this means. It will also demonstrate its battery recharging capabilities using tether generated power. The aim of the mission is to de-orbit a Delta II second stage, which is estimated to take about 15 days.

6.4.1 The Propulsive Small Expendable Deployer System

The ProSEDS mission will be launched into a near-circular orbit at an altitude of about 350 km, inclined at 32°. The proposed tether will have a total length of 15 km and a diameter of about 3 mm. We have already shown that a single strand tether system, with a sufficient diameter (e.g. TiPS), can be made to survive 'low-energy' interactions with the small debris population. However, the probability of such a tether system surviving 'high-energy' interactions is less encouraging. Hence, the ProSEDS case study presented here will focus on the collision and sever probabilities arising from 'high-energy' interactions between a double strand type ProSEDS tether system and the debris population. The parameters used for this case study are outlined in Table 6.7.

Tether Details							
a	=	6,728 km	ω	=	180°	no. of beads	= 7
e	=	0.001	Ω	=	45°	length	= 15 km
i	=	32°	θ	=	20°	strand diameter's	= 1.0 mm
						system width	= 20 mm
Breakup Details							
a	=	22250 km	ω	=	340°	breakup type	= HIX
e	=	0.7	Ω	=	30°	on-orbit mass	= 3,000 kg
i	=	64°	θ	=	302°	min. fragment size	= 1 mm

Table 6.7: ProSEDS mission profile input into the TRAP model

Double Strand Case Scenario

The collision and sever probabilities for the double strand ProSEDS case scenario are illustrated in Figures 6.16 and 6.17, respectively. The two graphs show a large increase in probability between days five and six. This is due to the debris cloud evolving and wrapping itself around the Earth, presenting a higher probability of the tether encountering the cloud. The sever risk, however, is about two orders of magnitude lower than the collision probability, indicating that a double strand tether system is capable of surviving 'high-energy' interactions from the small debris population. Not only this, but the tether strand's are only 1 mm in diameter each, demonstrating that thin tether strands, when combined into a double strand configuration, can be made to survive the small debris population. With the level of vulnerability reduced, this clearly demonstrates that double strand tether systems would be more suitable to the debris environment than single strand tether systems.

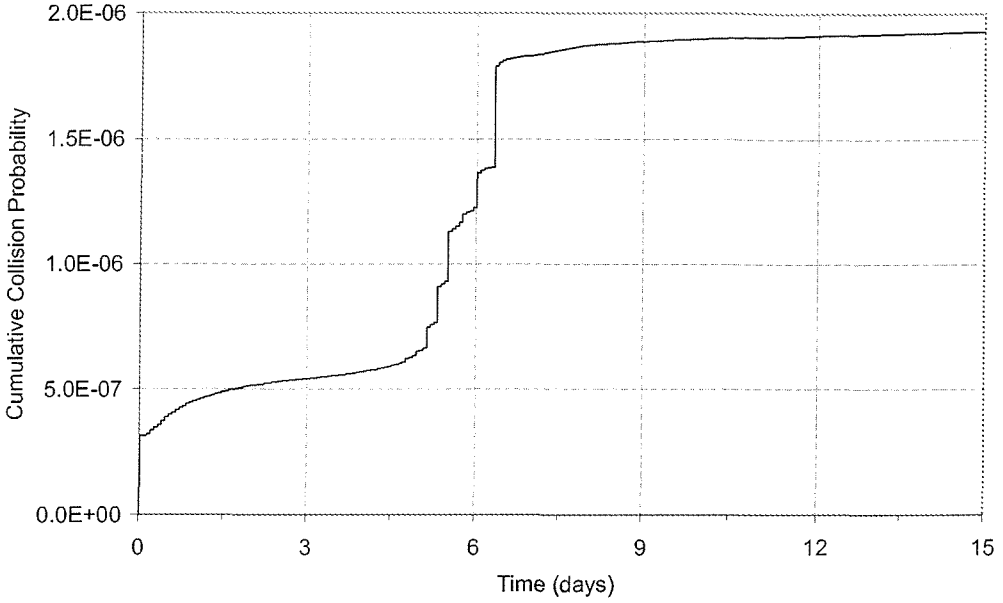

Figure 6.16: Cumulative collision probability to the ProSEDS double strand tether system, over a 15-day period, from the simulated debris cloud

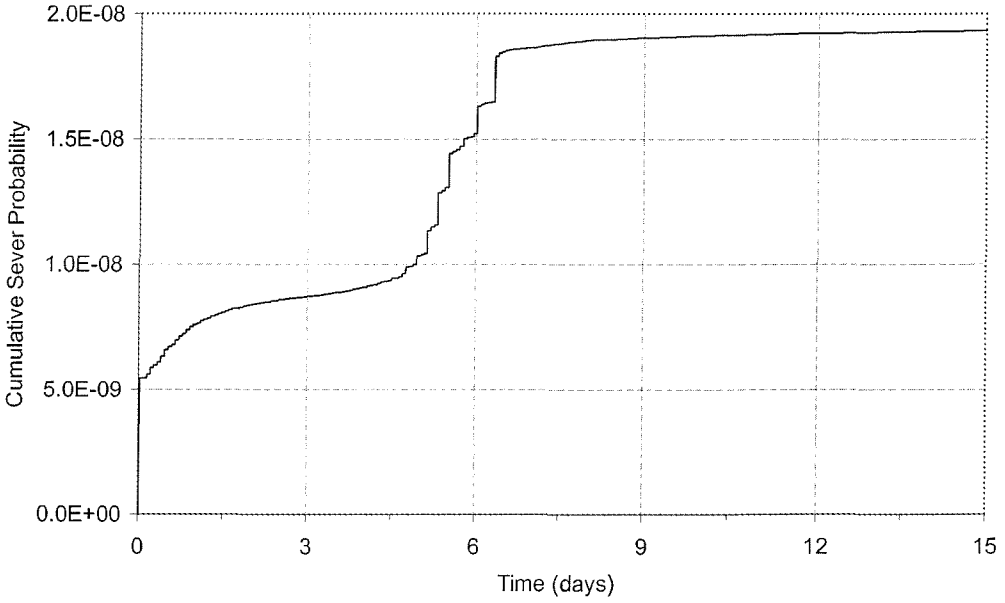

Figure 6.17: Cumulative sever probability to the ProSEDS double strand tether system, over a 15-day period, from the simulated debris cloud

6.5 Electrodynamic De-Orbiting And Re-entry Device

The Electrodynamic De-Orbiting And Re-entry Device (EDOARD) has been developed jointly in Italy by Alenia Spazio and the University of Rome, with a view to potential commercial exploitation. It is designed to de-orbit satellites and spent upper stages in the 600 to 4,000 kg mass range, and in the orbital region of 600 to 2,000 km altitude and up to an orbital inclination of 65° **[102]**. The benefits and risks of using tethers in space has been recognised by the IADC and an action item (AI 19.1) has been put into place to address this issue. A range of parameters, outlined in Table 6.8, were put forward by Pardini for the continuation of AI 19.1, during the 21st IADC meeting, held in Bangalore, India, 10-13th March, 2003.

Parameter	**AI 19.1 Range**
Tether length	5 to 10 km
Single-line diameters	0.5 mm to 5 cm
Double-line diameters	0.5 mm to 5 cm
Distance between knots	5, 10 and 100 m
Altitude	500 to 1,500 km
Inclination	0° to 75°

Table 6.8: A range of parameters issued for the continuation of AI 19.1 **[103]**

A number of case studies have been performed by Anselmo and Pardini **[58, 62]** to assess the collision risks posed to an orbiting space tether system (see Chapter 3). Here we will discuss a specific reference case that was chosen to have attributes similar to the EDOARD system. This reference case is presented in Table 6.9. A number of modifications were then proposed by Anselmo and Pardini to investigate, and to try to increase the lifetime of an orbiting space tether system. These included varying the thickness of a single strand tether and by increasing the number of 'beads' used when modelling a double strand tether system. They quickly realised, however, that a single strand tether system would not be a suitable choice, with the probability of mission success falling well below their target of 95%. Thus, a new configuration was proposed, two tethers, each 0.7 mm in diameter, connected by a number of 'beads'. It was concluded that by increasing the number of 'beads' along the double strand tether system the probability of failure was greatly reduced.

Parameter	EDOARD
Altitude	1,500 km
Inclination	55°
Tether length	5 km
Payload mass	2,000 kg
Electron collector diameter	10 m

Table 6.9: EDOARD reference case [62]

The following section will discuss the single and double strand tether modelling experiments performed by Anselmo and Pardini. Their predictions will also be compared with those produced by the TRAP model, providing further validation, but also providing an insight into how the tether system can be designed in order to maximise mission success.

6.5.1 Single Strand Tether Experiments

In order to compare the results produced by the TRAP model and those produced by Anselmo and Pardini [62] a number of simulations were performed, using the parameters listed in Table 6.9. The first case study involved modelling a single strand tether system with a diameter of 3 mm. The tether was modelled using 11 'beads' and a total of 13 simulations were performed, corresponding to the 13 altitude intervals studied by Anselmo and Pardini [62]. The results of this case study are presented in Table 6.10, along with those found by Anselmo and Pardini [62]. Note the residence time corresponds to the amount of time that the tether occupies a specific altitude interval. The sever probability prediction for the TRAP model is, on average, around two orders of magnitude lower than that predicted by Anselmo and Pardini [62]. This is because the TRAP model only considers catalogued objects, whereas Anselmo and Pardini also considered meteoroids along with the smaller debris population. Using the CNUCE reference population (CODRM-99R) [58, 104] and the Space Debris Impact Risk Analysis Tool (SDIRAT) [105], Anselmo and Pardini were able to determine the impact risk to tethers in circular orbits, as a function of altitude, inclination, debris size and tether diameter [62]. Figure 6.18 gives their prediction of the cut rate per year per kilometre of a single strand tether, at an altitude of 800 km, inclined at 50°, as a function of orbital debris size. A comparison of the results of Figure 6.18, with those objects 10

Altitude interval (km)	Residence time (yr)	Probability of tether failure	
		Anselmo and Pardini	TRAP
1,500 to 1,400	0.104	0.028	0.000377
1,400 to 1,300	0.112	0.019	0.000524
1,300 to 1,200	0.126	0.021	0.000345
1,200 to 1,100	0.110	0.021	0.000303
1,100 to 1,000	0.096	0.029	0.0004
1,000 to 900	0.107	0.136	0.00129
900 to 800	0.093	0.070	0.000533
800 to 700	0.090	0.035	0.000651
700 to 600	0.071	0.016	0.000337
600 to 500	0.055	0.009	0.000518
500 to 400	0.044	0.006	0.000242
400 to 300	0.036	0.004	0.0000565
300 to 200	0.030	0.002	0.0000790
1,500 to 200	**1.074**	**0.396**	**0.005693**

Table 6.10: Single strand tether failure predictions

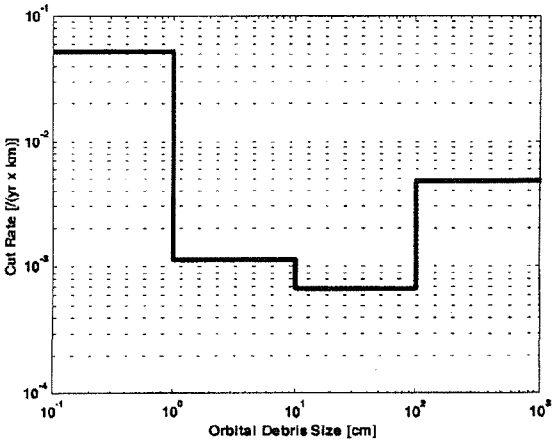

Figure 6.18: Differential cut rate as a function of orbital debris size (tether diameter = 3 mm; altitude = 800 km; inclination = 50°) **[62]**

cm in size or larger, and those predicted by TRAP for the 800 km altitude interval, in Table 6.10, shows good agreement.

6.5.2 Double Strand Tether System Experiments

Anselmo and Pardini [62] concluded that a single strand tether system fell short of their 95% tether survivability probability project requirement for the 13-months de-orbiting mission. As a next step, they then introduced a double strand tether system with a number of 'beads' connecting the two tether strands, each strand 0.7 mm in diameter. Once again, the TRAP model was utilised to compare the results with Anselmo and Pardini [62]. A double strand tether was modelled, represented by 11 'beads'. The results of the simulation are outlined in Table 6.11 along with the predictions calculated by Anselmo and Pardini [62]. As with the single strand case study, Anselmo and Pardini also included the sever risks associated with meteoroids and the smaller background debris population. In order to achieve a tether survival probability of 95%, for the 13-month de-orbiting mission, they estimated that the 'beads' would have to be separated by 10 m, resulting in a total of 501 'beads'. To achieve a tether survivability probability of 99% this 'bead' separation distance would have to be reduced to just 2.5 m, resulting in a total of 2,001 'beads'! However, the results produced by Anselmo and Pardini neglect

		Probability of tether failure		
Altitude	**Residence**	**Anselmo and Pardini**		**TRAP**
interval (km)	**time (yr)**	**51 beads**	**501 beads**	**11 beads**
1,500 to 1,400	0.104	0.0159	0.0016	0.000195
1,400 to 1,300	0.112	0.0116	0.0012	0.000276
1,300 to 1,200	0.126	0.0148	0.0015	0.0000953
1,200 to 1,100	0.110	0.0134	0.0014	0.000104
1,100 to 1,000	0.096	0.0166	0.0017	0.000172
1,000 to 900	0.107	0.1731	0.0182	0.000699
900 to 800	0.093	0.0564	0.0058	0.00033
800 to 700	0.090	0.0226	0.0023	0.000418
700 to 600	0.071	0.0101	0.0010	0.000138
600 to 500	0.055	0.0050	0.0005	0.00023
500 to 400	0.044	0.0024	0.0002	0.000121
400 to 300	0.036	0.0011	0.0001	0.0000291
300 to 200	0.030	0.0005	0.0001	0.0000493
1,500 to 200	**1.074**	**0.3435**	**0.0356**	**0.0028567**

Table 6.11: Double strand tether failure predictions

to take into account the failure rate of each of the 'beads', which could significantly effect the overall tether survivability. Hence, the TRAP model has been utilised to examine the effects of the smaller debris population on a double strand tether system taking into account the failure probability of each of the 'beads'. In order to examine the effects of the small debris population on the number of 'beads' used on a double strand tether system a catastrophic collision was modelled. Here we will discuss the two case scenarios that were studied. The parameters used for these modelling experiments are outlined in Table 6.12.

Tether Details					
a = 7,178 km	ω = 0°	no. of beads	=	11 and 51
e = 0.001	Ω = 0°	length	=	5 km
i = 55°	θ = 0°	diameter	=	0.7 mm
		system width	=	20 mm
Breakup Details				
a = 7,178 km	ω = 0°	breakup type	=	Collision
e = 0.001	Ω = 0°	on-orbit mass	=	1,500 kg
i = 55°	θ = 355°	min. fragment size	=	1 mm
		projectile mass	=	3 kg
		rel. velocity vector	=	$[2.0\ 1.0\ 0.7]^{\mathrm{T}}$ km/s

Table 6.12: EDOARD mission profile input into the TRAP model

Figure 6.19 illustrates the collision probability for the 'beads' along each of the two tether systems. The tether comprised of 51 'beads' has the highest collision probability, approximately an order of magnitude more than the tether system consisting of 11 'beads'. This result is not surprising, however, since the 51 'beads' comprise a higher total cross-sectional area exposed to the debris environment than the tether system consisting of 11 'beads'. Finally the sever probability associated with the two tether systems is modelled. This is illustrated in Figure 6.20, and is in agreement with Anselmo and Pardini **[62]** in as much as the 51 'bead' double strand tether system has a higher probability of mission success than the 11 'bead' double strand tether system. However, as previously mentioned, as the number of 'beads' tends to infinity the double strand tether system tends to a single strand tether structure. Therefore, there must exist a point where increasing the number of 'beads' actually causes the sever probability to increase.

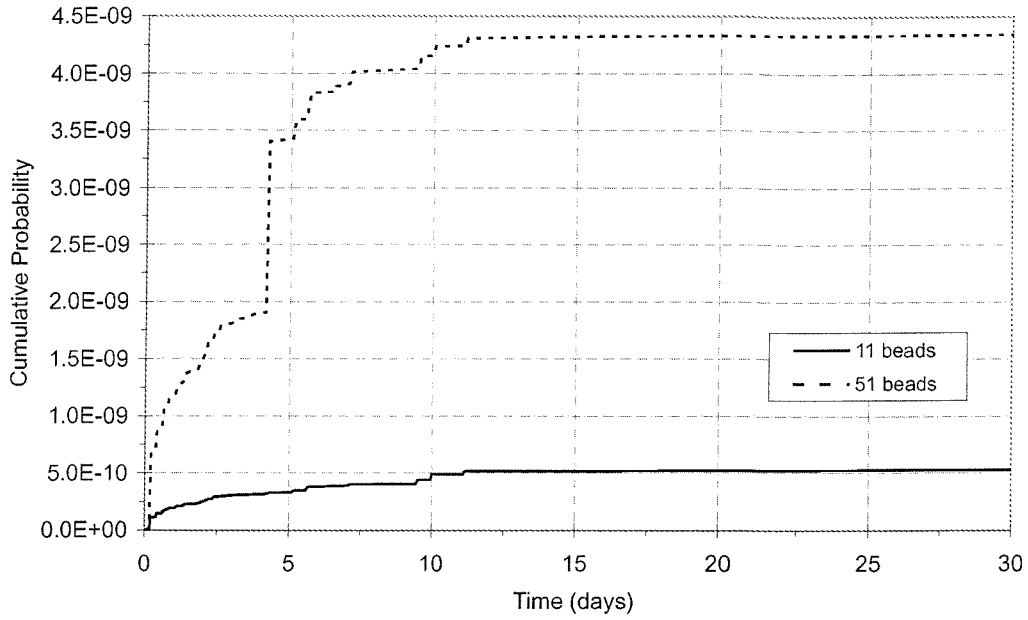

Figure 6.19: Cumulative collision probability for the 'beads' of a double strand tether system, over a 10-day period, from the simulated debris cloud

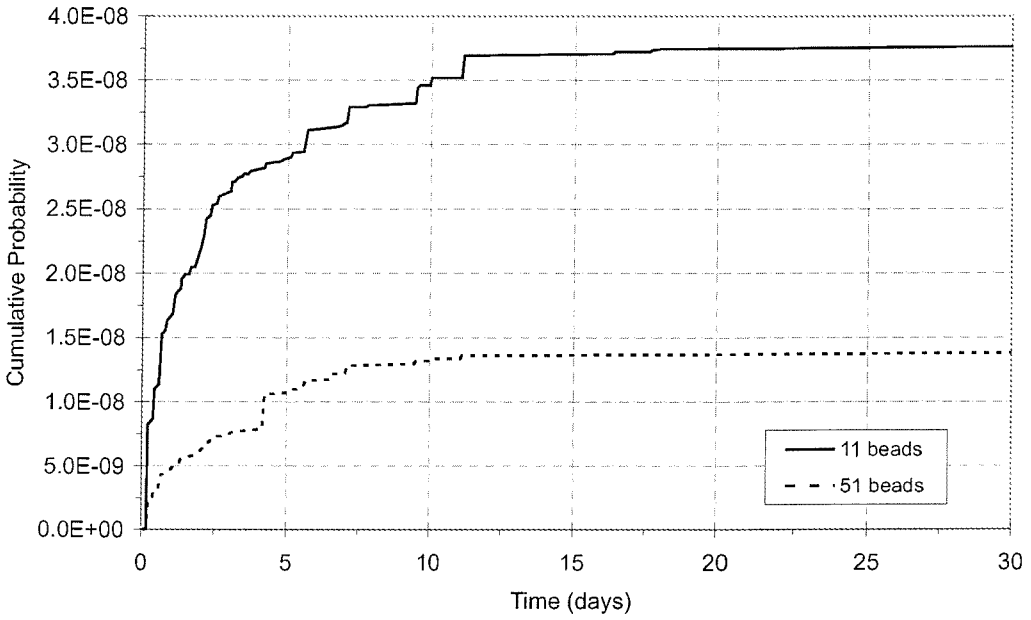

Figure 6.20: Cumulative sever risk for the two double strand EDOARD tether systems from a debris cloud produced by a catastrophic collision

How Many Beads?

Here we will discuss a case study which demonstrates that by introducing more 'beads', along a double strand tether system, the tether becomes more vulnerable. Since we are looking for the number of 'beads' that can cause the sever probability to increase, we can simply look at the probability over one time-step. In order to achieve this a low intensity explosion (LIX) was modelled to study the probability of failure of a 1 km long double strand tether system. The collision and sever risk associated with the tether system from the resulting debris cloud was then modelled over a period of 1-minute. In total, eight simulations were performed, coinciding with the eight different double strand tether systems. The results of these simulations are outlined in Table 6.13 and illustrated in Figure 6.21.

Number of Beads	Bead Spacing	Probability of Failure
51	20 m	7.47E-08
101	10 m	3.77E-08
201	5 m	1.90E-08
501	2 m	7.77E-09
1,001	1 m	4.15E-09
2,001	0.5 m	2.60E-09
4,001	0.25 m	2.36E-09
8,001	0.125 m	3.29E-09

Table 6.13: Double strand failure rate with increasing beads

The probability of failure continues to decrease as the number of 'beads' increases, until the double strand tether system is modelled with 8,001 'beads'. Here the probability of failure shows an increase. With closer examination of the results, one can actually understand why the probability has increased. A low intensity explosion (LIX) was modelled, producing fragments around the medium size range, i.e 1 cm in size or larger. The actual distance between each of the 'beads' is only 12.5 cm and, therefore, with fragments 1 cm in size or larger, the probability of a fragment impacting with a 'bead' increases. The results presented here show good evidence, for this specific case, that a 5 km long double strand tether system, modelled using 2,001 'beads', similar to the Anselmo and Pardini **[62]** modelling experiment, would reduce the probability of failure, as far as the medium size debris population is concerned.

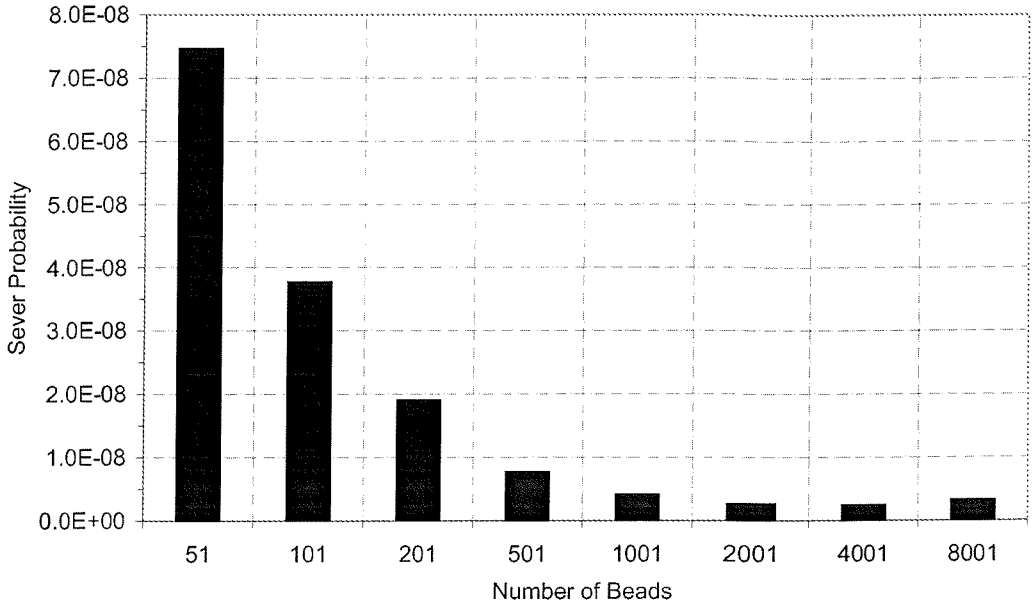

Figure 6.21: Sever probability for a double strand tether system as the number of 'beads' is varied, over a 1-minute time-step

6.6 Discussion

The TRAP model has been utilised throughout this chapter providing a number of collision and sever risk assessments to past and future planned tether experiments. However, for each of the assessments to be accurately calculated, a number of key sensitivity issues, which were found during validation, needed to be fully investigated and understood. These sensitivity issues included, the time-step, the number of 'beads' used to model the tether system, and the cell radial size used to determine the spherical control volume for the background population. Understanding these issues is important in order to provide the best results. For example, a small time-step would provide more accurate results, but more computational effort is required. Therefore, the 'best' time-step should be chosen depending on the orbital parameters used for each particular simulation. A short simulation, of just a few orbits, for example, may require a time-step of just a few minutes. A longer simulation, over a few months, however, will require a larger time-step.

A number of validation procedures, discussed in the previous chapter, were performed during the development of the TRAP model. However, one final validation check was

required to confirm that the TRAP model was producing valuable results. This was achieved by comparing the results produced by TRAP with those predicted in the literature. One example discussed, was the Tethered Satellite System (TSS) study performed by Chobotov and Mains **[63]**, who used both analytical and statistical approaches. The predictions from this study compared exceptionally well with the predictions produced by the TRAP model, providing an excellent method of validation.

Another set of validation procedures were performed by studying past tether missions. The TRAP model was utilised to study the collision and sever probability risks to a number of past missions. The results produced by the TRAP model agreed well with actual flight data. The predictions indicated that single strand tether systems are particularly vulnerable to the small debris population. Although, increasing the diameter provided some protection against the 'low-energy' interactions, it proved to be of little help when 'high-energy' interactions were considered. Since this increase in diameter also increases the cross-sectional area, one would have to seriously consider the potential use of such tether designs.

The TRAP model was also used to predict the collision and sever probability risks to future planned tether missions. The ProSEDS double strand case scenario demonstrated that such tether designs represent a more robust solution, with greatly reduced sever probabilities. This particular scenario also showed that thin tether strands (about 1 mm in diameter) can be used in the space debris environment when combined into such a configuration (i.e two thin tether strands connected by a number of 'beads').

Finally, an EDOARD-type case scenario, arising from the IADC AI 19.1 **[103]**, was discussed. The results once more confirmed that double strand tether systems are less vulnerable than single strand tethers. The results also demonstrated that by increasing the number of 'beads' along the tether the probability of mission failure can be reduced. However, the gap between each of the 'beads' should be kept to a minimum of about 1 m. Otherwise the failure of the 'beads' begin to dominate the risk of failure.

Chapter 7

Conclusions

The development of any complex model to enable collision and sever risk predictions to an orbiting space tether system is not a trivial matter. However, by taking an integrated, system level approach to the design and development, the Tether Risk Assessment Program (TRAP) has been implemented as an extremely flexible risk analysis tool with state-of-the-art capabilities.

This process initially comprised information gathering, in order to determine state-of-the-art techniques for calculating collision risk probabilities. The method of Probabilistic Continuum Dynamics (PCD) was chosen, and modified, providing an accurate technique for calculating collision risks associated with an orbiting space tether system arising from debris produced by a fragmentation event. However, the collision risk alone is insufficient and does not provide any indication of whether or not the tether system survives such encounters. Therefore, a method was developed that could determine the sever probability of the tether system, providing an excellent insight into tether survivability issues. Firstly, the lethality coefficient method was implemented. This method determines the minimum lethal fragment size which is capable of severing the tether strand, using a suitable lethality coefficient. This lethal fragment size is then 'set in stone' throughout the simulation, and any impact with a fragment equal to, or greater than, this minimum lethal fragment size would then cause the tether to fail regardless of the impact energy. It was quickly realised that, without knowledge of the impact energy, this method was not accurate enough and that new techniques would be required to determine tether sever probabilities. Thus, the penetration method was developed. This method was developed using a number of suitable penetration equations such as

the Fish-Summers equation [91], for single strand tethers, and the 'Christiansen' equation [96], for double strand tethers. These two equations allow the penetration depth of an impact to be determined, taking into account the impact energy. This method of sever analysis provides a more realistic and accurate means for calculating tether failure predictions over the more traditional lethality coefficient method.

The TRAP model has a number of applications and can be used for predicting collision and sever probability assessments for both single and double strand tether systems. This allows comparisons between both single and double strand tether systems to be made from the historical, current and future orbital debris population. Not only this but the TRAP model can also be used for predicting collision and sever risk assessments associated to tethers from debris produced by recent fragmentation events, such as on-orbit explosions or collisions.

The TRAP model was developed to the highest of standards and has undergone a rigorous validation procedure in order to assess the model's accuracy. The results of these validation procedures are outlined in Chapters 4 and 5. The TRAP model was then extensively applied to study the collision and sever risks associated with a tether system arising from the orbital debris environment in Chapter 6. It is the purpose of the current chapter, therefore, to provide a summary of the overall findings and their implications for evaluating the survivability of tether systems.

7.1 Model Accuracy

The completion of any newly developed model is secured only when it has successfully passed through a series of validation procedures. The TRAP model is no exception to this rule and it was put through a number of validation checks. The TRAP model consists of four main programs and each of these were validated individually, before the model as a whole was tested and validated.

The Breakup Program was validated against results produced by Walker [3], Barrows [4] and actual fragmentation events. The Tether Program was validated using an established tether model, the Tether Simulator, produced by JAQAR Space Engineering [79]. As with the TRAP model, the Tether Simulator models the tether as a number of 'beads', allowing precise validation checks to be performed.

The PCD method implemented into the Analysis Program was easily validated using the Space Debris Simulation (SDS) suite [4]. However, in order to do this, the TRAP model was temporarily set up to model a typical satellite. The two models were then compared and showed excellent agreement.

The Background Program was validated by performing a number of confidence-building simulations. This was achieved by modelling past tether experiments and comparing results produced in the literature by Chobotov and Mains [63], and Anselmo and Pardini [58, 62]. The comparisons showed that the predictions produced by the Background Program were on average about two orders of magnitude lower than the predictions produced by Anselmo and Pardini. However, this was because Anselmo and Pardini included the meteoroid and smaller debris populations within their model along with the larger, trackable, debris objects. By using the CNUCE reference population (CODRM-99R) [58, 104] and the Space Debris Impact Risk Analysis Tool (SDIRAT) [105], Anselmo and Pardini were able to determine the impact risk to tethers in circular orbits, as a function of altitude, inclination, debris size and tether diameter [62]. When the results of this were compared with the TRAP predictions, very good agreement was achieved. Finally, the Background Program was also validated by comparing the results produced by Chobotov and Mains [63]. One such experiment, in particular, looked at the Tethered Satellite System Re-flight (TSS-1R) where a collision probability of 2.23×10^{-3} per month was predicted for objects 10 cm in size or larger by Chobotov and Mains [63]. Over the same time period the TRAP model predicted a collision probability of 1.59×10^{-3}, with 7 beads, a cell radial size of 5 km and a 60-minute time-step, giving excellent agreement with the results of Chobotov and Mains.

The main purpose of the TRAP model is to predict collision and sever risks to an orbiting space tether system arising from the orbital space debris environment. With the validation procedures, discussed above, and with the achievement of results which are comparable with those in the literature, confidence in the model for such risk assessments was greatly improved.

7.2 Implications for Evaluating Survivability of Tethers

A wide range of tether simulations have been performed using the TRAP model, to study the effects of the orbital debris environment on a space tether system. From these comprehensive studies, it was concluded that single strand tether systems with a diameter less than 1 mm are particularly vulnerable to the debris environment and should not be recommended for any future missions that will expose the tether to the environment for extended periods of time. The case studies also showed that, by increasing the tether's diameter, they could be made to survive some 'low-energy' interactions but not 'high-energy' interactions. However, this increased diameter also increases their cross-sectional area, therefore resulting in a potentially larger number of fatal impacts.

The TRAP model did show some encouraging results for double strand tether systems, providing good evidence that such systems are less vulnerable to the space debris environment than single strand tether systems. It was found that the sever probability of a double strand tether system is also controlled by the number of 'beads' used along the tether system, generally decreasing with increasing number of 'beads'. This was due to the collision cross-sectional area of each tether segment being reduced. However, increasing the number of 'beads' indefinitely would result in the double strand tether system tending towards a single strand tether structure. Thus, it was concluded that the distance between each of the 'beads' should not be less than about 1 m.

7.3 Further Work

The development of any new model is a very complex task and one that can never truly come to an end. This section will, therefore, discuss how the model can be improved. It also discusses briefly those elements, such as tether model improvements, which could have been implemented but were not, due to time constraints. The discussion will also focus on the need to develop more precise tether penetration equations in order to achieve higher accuracy sever predictions. Finally, the discussion includes possible future tether studies.

Improvements to Background Model Accuracy

The development and improvement of modelling the small background debris population is a very important area. This is especially important for studying sever risks to space tethers since, as we have seen throughout this thesis, tethers are particularly vulnerable to small debris impacts, and unlike a typical spacecraft they can not be shielded against such threats. Therefore, space debris models, such as the DAMAGE model [**18, 19**], are able to predict the spatial densities for the smaller debris population. This allows collision predictions to be made, providing good insights into the threat posed by the smaller debris populations. However, in order to determine collision and sever probabilities for space tethers the debris object's diameter must also be specified. This can be resolved by using a method, similar to the debris diameter averaging method implemented into TRAP. For example, dividing the small debris populations into various size ranges and using an average debris diameter for each range (e.g. the mid-point).

Tether Model Improvements

Modelling tether dynamics is a very complex problem and it was decided very early on in the research that this would be simplified as much as possible. The main reason for this was, while tether modelling was a necessity for the TRAP model, it was unlikely that a novel contribution in this area could be achieved and, hence, making the model more complex would use up valuable time and resource.

The model implemented into the TRAP model is therefore a compromise. It has been assumed that the tether is non-conducting, attached to two point masses. The implementation of a conducting tether model would require the knowledge of the tether's interaction with the ionospheric plasma. This would be very beneficial in enhancing the TRAP model's capabilities, with a number of planned electrodynamic tether experiments, such as ProSEDS, scheduled for launch. More ambitious developments may include varying the length of the tether, taking into account the deployment phase of a particular mission, or even allowing one of the end objects to change mass, due to an engine being fired. Looking into the future, it is also apparent that tether systems may have complex geometries consisting of more than two end-bodies.

Multi Strand Tether Systems

Presently, the TRAP model is constrained to modelling collision and sever risk assessments for single and double strand tether systems. More ambitious tether designs have been developed, however, such as the Hoytether^{TM} by Tethers Unlimited Inc. Including such designs into the TRAP model along with other designs, such as triple strand tether systems, will be an important application for the future, and one that will provide some scope for new research.

Improvement of Penetration Equations

The development and improvement of tether penetration equations is an important area and one that requires urgent research. The TRAP model has made use of two such equations, the Fish-Summers [**91**] and the Christiansen equations [**96**]. Chosen for their suitability in determining tether sever assessments, they were able to provide more accurate results than those predicted by using a constant lethality coefficient. However, like all such equations they are only as good as the data used to develop them. Hence, more experiments, such as those performed by McBride and Taylor [**61**], are essential for more accurate and precise predictions of tether sever probabilities.

Further Tether Studies

Space tethers offer a promising new area of technology and a number of ambitious tether experiments have been proposed for the long term future, such as the Jovian exploration mission using electrodynamic tethers to provide orbit change capability and electrical power. In the near-future, the Japanese have proposed a number of experiments using both single and double strand type tether designs of various length. The Double Tethered Experimental Satellite (D-TES), for example, has been proposed. This will deploy a 20 km long double strand tether system in order to gather information regarding the tether dynamics of such a system. Such planned experiments provide an excellent opportunity to utilise the TRAP model.

7.4 Summary

The TRAP model has been developed as an extremely flexible tool, providing an accurate collision and sever risk assessment tool for orbiting space tether systems. Such risk assessments may be determined from recent fragmentation events, or from the historic, current or future orbital debris background population. A number of novel techniques have been developed to greatly improve the accuracy of the model, including:

- Its ability to allow debris density to vary over the length of the tether system.
- The improved penetration method offering a more realistic approach to sever analysis than the more traditional lethality coefficient method.
- Its ability to model single and double strand tether systems for collision and sever risk analysis.

The PCD method was implemented and modified to allow the debris density to vary over the length of the tether system, providing more accurate and realistic collision and sever probability predictions. Two suitable penetration equations (the Fish-Summers [**91**] and the 'Christiansen' [**96**] equations) were implemented into the model producing more accurate methods of determining tether sever predictions than the commonly used lethality coefficient method. Two newly developed methods (the LINEAR and TRAJECTORY methods) were also implemented, allowing collision and sever risks for double strand tether systems to be performed. This allows comparisons between both single and double strand tether systems to be made from the historical, current and future orbital debris population.

Comprehensive studies using the TRAP model have indicated that single strand tether systems would not be a suitable design, due to its vulnerability in the space debris environment. The research presented in this thesis has suggested that double strand tether systems may provide a more reliable tether design. It was also noted that while increasing the number of 'beads' along the double strand tether system can reduce the sever probability, a certain amount of care must be taken. This is because as the number of 'beads' tends to infinity so the double strand tether structure tends to a single tether structure, increasing the sever probability. Anselmo and Pardini [**58, 62**] demonstrated that for the EDOARD tether system to have a 99% chance for mission

success a total of 2,001 'beads' would be required, giving a distance of 2.5 m between each of the 'beads'. This prediction was also confirmed by TRAP which showed that by reducing the 'bead' distance to just 0.25 m, the sever probability would continue to decrease. However, reducing this distance any further would result in an increase in sever probability. Hence, a distance of around 1 m between each of the 'beads' was deemed a suitable distance for minimising the sever probability.

References

1. D.J. Kessler. *Collision cascading: The limits of population growth in low earth orbit.* Advances in Space Research, volume 12, issue 12, pp. 63-66, 1991.

2. C. Mazza, J. Fairclough, B. Melton, D. de Pablo, A. Scheffer and R. Stevens. *Software Engineering Standards.* Prentice Hall, Hemel Hempstead, England, 1994.

3. R. Walker. *The long-term interactions of satellite constellations with the orbital debris environment.* Thesis, The University of Southampton, Faculty of Engineering and Applied Sciences, School of Engineering Sciences, February, 2000.

4. S. Barrows. *Evolution of artificial space debris clouds.* Thesis, The University of Southampton, Faculty of Engineering and Applied Sciences, School of Engineering Sciences, March, 1996.

5. R. Walker, C. Martin, H. Stokes, J. Wilkinson, H. Sdunnus, S. Hauptmann, P. Beltrami and H. Klinkrad. *Update of the ESA space debris mitigation handbook.* Executive summary, ESA contract 14471/00/D/HK. July, 2002.

6. N.L. Johnson and D.S. McKnight. *Artificial space debris.* 2nd Edition, Orbit Book Company, 1991.

7. N. Johnson, P. Anz-Meador, E. Cizek and S. Portman. *History of on-orbit satellite fragmentations.* 12th Edition, NASA/JSC JSC29517. July, 2001.

8. J.P. Loftus Jr. *Orbital debris from upper stage breakups.* Progression in Astronautics and Aeronautics. Martin Summerfield Series Editor-in-Chief, volume 121, 1989.

9. *Technical report on space debris.* United Nations Publication, New York, ISBN 92-1-100813-1. 1999.

10. D. Leonard. *Space debris damages french military satellite.* Space News, August 26 - September 1, 1996.

11. C. Wiedemann, J. Bendisch, H. Krag, P. Wegener and D. Rex. *Modelling of copper needle clusters from the Westford dipole experiments.* Proceedings of the 3rd European Conference on Space Debris (ESA SP-473), pp. 315-320, ESOC, Darmstadt, Germany, 2001.

12. P.J. Newman, N. Mackay, S.P. Deshpande, S.F. Green and J.A.M. McDonnell. *Derivation of particulate directional information from analysis of elliptical impact craters on LDEF.* LDEF - 69 Months in Space: 2nd LDEF Post-Retrieval Symposium, NASA CP-3194, part 4, pp. 417-429, 1993.

13. R. Aceti, G. Drolshagen, L. Gerlach and G. Racca *Meteoroid and debris investigation on EURECA.* Proceedings of the 1st European Conference on Space Debris (ESA SD-01), pp. 215-222, Darmstadt, Germany, 1993.

14. G. Drolshagen, H. Svedhem and E. Grn. *Measurements of cosmic dust and microdebris with the GORID impact detector in GEO.* Proceedings of the 3rd European Conference on Space Debris (ESA SP-473), pp. 177-184, ESOC, Darmstadt, Germany, 2001.

15. H. Sdunnus, J. Bendisch and H. Klinkrad. *The ESA MASTER-99 space debris and meteoroid reference model.* Proceedings of the 3rd European Conference on Space Debris (ESA SP-473), pp. 299-307, ESOC, Darmstadt, Germany, 2001.

16. H. Klinkrad, J. Bendisch, K.D. Bunte, H. Krag, H. Sdunnus and P. Wegener. *The MASTER-99 space debris and meteoroid environment model.* 33rd COSPAR Scientific Assembly, Warsaw, Poland, 16-23 July, 2000.

17. K.D. Bunte. *Populations for a Divine based space debris model.* Proceedings of the 3rd European Conference on Space Debris (ESA SP-473), pp. 279-285, ESOC, Darmstadt, Germany, 2001.

18. H.G. Lewis, G. Swinerd, N. Williams and G. Gittins. *DAMAGE: a dedicated GEO debris model framework.* Proceedings of the 3rd European Conference on Space Debris (ESA SP-473), pp. 373-378, ESOC, Darmstadt, Germany, 2001.

19. H.G. Lewis, G. Swinerd, N. Williams and G. Gittins. *Investigating the long-term evolution of the debris environment in high earth orbit using the DAMAGE model.* Space Debris, AAS, Science and Technology Series, volume 105, 2001.

20. K.B. Hayashida, J.H. Robinson and S.A. Hill. *SEDS tether M/OD damage analysis.* Marshall Space Flight Center, Alabama, NASA/TM-97-206311, November, 1997.

21. The National Science and Technology Council Committee on Transportation Research and Development. *Interagency report on orbital debris.* Washington DC, 1995.

22. National Research Council. *Orbital debris: a technical assessment.* National Academy Press, Washington DC, 1995.

23. The Aerospace Corporation, Center for Orbital and Re-entry Debris Studies, http://www.aero.org/cords/debrisks.html.

24. C.A. Belk, J.H. Robinson, M.B. Alexander, W.J. Cooke and S.d. Pavelitz. *Meteoroids and orbital debris: effects on spacecraft.* NASA Reference Publication 1408. August, 1997.

25. K.R. Housen. *The short term evolution of orbital debris clouds.* The Journal of the Astronautical Sciences, volume 40, number 2, pp. 203-213, April-June, 1992.

26. G. Swinerd, H. Lewis, N. Williams and C. Martin. *Self-induced collision hazard in high and moderate inclination satellite constellations.* Space Debris 2000, AAS, Science and Technology Series, volume 103, pp. 231-243, 2001.

27. P. Eichler and D. Rex. *Debris chain reactions* AIAA-90-1365. AIAA/NASA/DOD Orbital Debris Conference: Technical Issues and Future Directions, Baltimore MD, USA, April, 1990.

28. *NASA Safety Standard: Guidelines and assessment procedures for limiting orbital debris.* NSS 1740.14, Washington DC, August, 1995.

29. *European space debris safety and mitigation standard (draft)*, issue 1, revision 3, November, 2001.

30. R. Walker, C.E. Martin, P.H. Stokes, J.E. Wilkinson and H. Klinkrad. *Analysis of the effectiveness of space debris mitigation measures using the DELTA model.* 33rd COSPAR Scientific Assembly, Warsaw, Poland, 16-23 July, 2000.

31. N. Williams, G.G. Swinerd, H.G. Lewis and G. Gittins. *A sensitivity analysis of breakup models.* Space Debris, AAS, Science and Technology Series, volume 105, 2001.

32. N.L. Johnson, P.H. Krisko, J.-C. Liou and P.D. Anz-Meador. *NASA's new breakup model of EVOLVE 4.0.* 33rd COSPAR Scientific Assembly, Warsaw, Poland, 16-23 July, 2000.

33. V.A. Chobotov. *Orbital Mechanics second edition.* AIAA Education Series, 1996.

34. D.J. Kessler. *Orbital debris environment in low Earth orbit: An update.* Advances in Space Research, volume 13, number 8, pp. 139-148, 1993.

35. D.J. Kessler. *The current and future environment: An overall assessment.* The Preservation of Near-Earth Space for Future Generations, Cambridge University Press, 1994.

36. K.E. Tsiolkovsky. *Grezy O. Zemie i Nebe(i) Na Veste.* Moscow, izd-vo AN SSSR p. 35. 1959. (Speculations between Earth and sky, and on Vesta; science fiction works.)

37. A.C. Clarke. *The fountains of paradise.* Warner Books Inc., ISBN - 0759505284, 2001.

38. NASA, http://liftoff.msfc.nasa.gov/academy/tether/SpaceTowers.html

39. I.P. Lee-Bapty. *The use of tethers for space transportation.* Defence Research Agency, Technical Report 91058, October, 1991.

40. R. Hoyt. *Tether systems for satellite deployment and disposal.* 51st International Astronautical Congress, Rio de Janeiro, Brazil, IAF-00-S.6.04. 2-6 October, 2000.

41. R. Hoyt. *Private e-mail communication.* Tethers Unlimited Inc., 26 August, 2003.

42. G. Colombo, E.M. Gaposchkin and M.D. Grossi, *Shuttle-borne 'Skyhook;' A New Tool for Low-Orbital-Altitude Research.* Smithsonian Institution Astrophysical Observatory, 1974.

43. N.L. Johnson, http::/sec353.jpl.nasa.gov/apc/Tethers/02.html. NASA MSFC.

44. N.H. Stone. *Tethered satellite system interaction with the ionospheric plasma.* Space Science Laboratory, NASA Marshall Space Flight Center, Huntsville, Al, USA.

45. M.L. Cosmo and E.C. Lorenzini (editors). *Tethers in space handbook third edition.* Smithsonian Astrophysical Observatory, Cambridge, Massachusetts, USA, December, 1997.

46. H.F. Smith. *The first and second flights of the small expendable deployer system (SEDS).* The 4th Small Satellite Conference, pp. 43-55, Logan, Utah, USA. 1995.

47. J.A. Carroll and J.C. Oldson. *Tethers for small satellite applications.* Small Satellite Conference, Logan, Utah, USA. 1995.

48. J.E. McCoy et al. *Plasma motor-generator (PMG) flight experiment results.* The 4th Small Satellite Conference, pp. 57-82, Logan, Utah, USA. 1995.

49. W. Barnds, S. Coffey, M. Davies, B. Kelm and W. Purdy. *TiPS: Results of a tethered satellite system experiment.* Advances in the Astronautical Sciences, 97-600, August, 1997.

50. K.T. Alfriend, W.J. Barnds, S.L. Coffey and L.M. Stuhrenberg. *Attitude and orbit determination of a tethered satellite system.* AAS/AIAA Astrodynamics Specialist Conference, Halifax, Nova Scotia, Canada, AAS 95-351. 14-17 August, 1995.

51. L. Johnson, R.D. Estes, E. Lorenzini, M. Martinez-Sanchez, J. Sanmartin and I. Vas. *Electrodynamic tethers for spacecraft propulsion.* 36th Aerospace Sciences Meeting and Exhibit. Reno, NV. 12-15 January, 1998.

52. D.L. Gallagher, F. Bagenal, J. Moore and L. Johnson. *An overview of electrodynamic tether performance in the jovian system.* Proceedings of the 1997 NASA Tether Technology Interchange Meeting, Huntsville, AL. September, 1997.

53. R.L. Forward and R.P. Hoyt. *Application of the Terminator Tether electrodynamic drag technology to the de-orbit of constellation spacecraft.* Tethers Unlimited Inc. AIAA-98-3491, 1998.

54. R.L. Forward and R.P Hoyt. *The Terminator Tether: autonomous de-orbit of LEO spacecraft for space debris mitigation.* Tethers Unlimited Inc. AIAA-00-0329, 1999.

55. M. Kruijff and E.J. van der Heide. *The YES satellite: a tethered momentum transfer in the GTO orbit.* Proceedings of Tether Technology Interchange Meeting, NASA/CP-1998-206900. January, 1998.

56. M. Kruijff *The Young Engineers' Satellite.* Flight results and critical analysis of a super-fast hands-on project, IAF Amsterdam, IAF-99-P.1.04. 1999.

57. E.J. van der Heide and M. Kruijff. *Tether and debris mitigation.* 51st International Astronautical Congress, Rio de Janeiro, Brazil, IAA-00-IAA.6.6.04. 2-6 October, 2000.

58. L. Anselmo and C. Pardini. *Assessing the impact risk of orbital debris on space tethers.* Space Debris, volume 1, number 2, pp. 87-98, 2000.

59. R.L. Forward. *Failsafe multistrand tether structures for space propulsion.* 28th Joint Propulsion Conference and Exhibit, Nashville, TN, AIAA 92-3214. 6-8 July, 1992.

60. R.L. Forward and R.P. Hoyt. *Failsafe multiline Hoytether lifetimes.* 31st Joint Propulsion Conference, San Diego, CA, 95-2890. July, 1995.

61. N. McBride and E.A. Taylor. *The risk to satellite tethers from meteoroid and debris impacts.* Proceedings of the second european conference on space debris (ESA SP-393), pp. 643-648, ESOC, Darmstadt, Germany, 1997.

62. L. Anselmo and C. Pardini. *The lifetime of space tether systems in orbit around the Earth.* 52nd International Astronautical Congress, Toulouse, France, IAA-01-IAA.6.5.05. 1-5 October, 2001.

63. V.A. Chobotov and D.L. Mains. *Tether satellite system collision study.* Space Debris, volume 1, number 2, pp. 99-112, 2000.

64. I. Newton. *Principia.* Motte's translation revised by Cajori, volume 1, Berkeley and Los Angeles, University of California Press, 1962.

65. R.R. Bate, D.D Mueller and J.E. White. *Fundamentals of astrodynamics.* Dover Publications, 1971.

66. A.E. Roy. *Orbital Motion.* Adam Hilger, Bristol, 1982.

67. P. Fortescue and J. Shark (Editors). *Spacecraft systems engineering.* Second edition, John Wiley and Sons, 1995.

68. CIRA-72. Cospar International Reference Atmosphere 1972. *Academic Verlag.* Berlin, 1972.

69. Solar flux information. www.drao.nrc.ca/icarus/www/sol_home.shtml

70. K. Schatten. NASA/GSFC, *Solar flux predictions.* Solar Geophysical Data Bulletin, published by the National Geophysical Data Center, June, 1998.

71. D.G. King-Hele. *Satellite orbits in an atmosphere.* Blackie, 1987.

72. V.V. Beletsky and E.V. Levin. *Dynamics of space tether systems.* Advances in the Astronautical Sciences, volume 3, 1993.

73. P.M. Fishbane, S. Gasiorowicz and S.T. Thornton. *Physics for scientists and engineers.* 2nd Edition, Prentice Hall Inc., 1996.

74. A. Cordelli, P. Farinella and A. Rossi. *The influence of the fragmentation threshold on the long-term evolution of the orbital debris environment.* CNUCE, 16 December, 1997.

75. A. Rossi, L. Anselmo, A. Cordelli and P. Farinella. *The 1997.0 CNUCE orbital debris reference model.* 8th AAS/AIAA Space Flight Mechanics Meeting, AAS 98-173.

76. D. McKnight, R. Maher and L. Nagl. *Refined algorithms for structural breakup due to hypervelocity impact.* Hypervelocity Impact Society Symposium, Sante Fe, NM, 16-20 October, 1994.

77. J.E. Cochran,, S. Cho, Y-M Cheng and D.A Cicci. *Dynamics and orbit determination of tethered satellite systems.* AAS 96-147, AAS/AIAA Space Flight Mechanics Meeting, Austin, Texas, 12-15 February, 1996.

78. V.V. Beletskii and E.M. Levin. *Dynamics of the orbital cable system.* Acta Astronautica, volume 12, number 5, pp. 285-291, 1985.

79. JAQAR Space Engineering, http://www.jaqar.com/

80. *On-orbit hazard analysis in low earth orbit using the poisson probability distribution.* Kaman Sciences Corporation, Engineering Sciences Division, August 26, 1992

81. S.P. Barrows, G.G. Swinerd and R. Crowther *Assessment of target survivability following a debris cloud encounter.* Space Forum, volume 1, pp. 329-353, 1996.

82. R.H. Gooding. *A procedure for the solution of Lambert's orbital boundary-value problem.* Celestial Mechanics, volume 48, number 2, pp. 189-192, April, 1995.

83. F.T. Sun, N.X. Vinh and T.J. Chern. *Analytic study of the solution families of the extended Godal's time equation for Lambert's problem.* The Journal of the Astronautical Sciences, volume 35, number 2, pp. 213-234, April-June, 1987.

84. P.R. Escobal. *Methods of orbit determination.* John Wiley and Sons Inc., 1965.

85. W.H. Press. *Numerical recipes: the art of scientific computing.* Cambridge University Press, 1986.

86. A.B. Jenkin and M.E. Sorge. *Debris clouds in eccentric orbits.* AIAA Space Programs and Technology Conference, Huntsville, AL, AIAA 90-3903, 25-28 September, 1990.

87. W.H. Goodyear. *Completely general closed-form solution for coordinates and partial derivatives of the two-body problem.* The Astronautical Journal, volume 70, number 3, pp. 189-192, April, 1995.

88. ESA's DISCOS (Database and Information System Characterising Objects in Space), http://mas15.esoc.esa.de:9000/

89. H. Klinkrad. *Collision risk analysis for low Earth orbits.* Advances in Space Research, volume 13, issue 8, pp. 177-186, 1993.

90. R.P. Hoyt and R.L. Forward. *The Hoytether: a failsafe multiline space tether structure.* Tether Technology Interchange Meeting, NASA/MSFC, Huntsville, AL, 9 - 11 September, 1997.

91. R.H. Fish and J.L. Summers. *The effect of material properties on threshold penetration.* Proceedings of the 7th Hypervelocity Impact Symposium, volume 6, February, 1965.

92. K.B. Hayashida and J.H. Robinson. *Single wall penetration equations.* Structures and Dynamics Laboratory Science and Engineering Directorate, NASA Technical Memorandum, TM-103565, December, 1991.

93. G. Drolshagen. *Hypervelocity impact effects on spacecraft.* ESA/ESTEC, NL-2200 AG Noordwijk, Netherlands.

94. D.D. Tomlin, G.C. Faile, K.B. Hayashida, C.L. Frost, C.Y. Wagner, M.L. Mitchell, J.A. Vaughn and M.J. Galuska. *Space tethers: design criteria.* NASA/TM-1997-108537, July, 1997.

95. K.B. Hayashida, J.H. Robinson and S.A. Hill. *SEDS tether M/OD damage analysis.* NASA/TP-97-206311, Marshall Space Flight Center, Alabama, November, 1997.

96. E.L. Christiansen. *Design and performance equations for advanced meteoroid and debris shield.* International Journal of impact Engng, volume 14, pp. 145-156, 1992.

97. W.P Schonberg, A.J. Bean and K. Darzi. *Hypervelocity impact Physics.* NASA CR-4343, 1991.

98. P.H. Stokes. *The implementation of cost effective debris protection in unmanned spacecraft.* Thesis, The University of Southampton, Faculty of Engineering and Applied Sciences, School of Engineering Sciences, February, 2002.

99. K.B. Hayashida and J.H. Robinson. *Double-plate penetration equations.* NASA, TM-2000-209907, Marshall Space Flight Center, Alabama, February, 2000.

100. J. Oldson and J.A. Carroll. *Potential launch cost savings of a tether transport facility.* AIAA-95-2895, 1995.

101. M. Matney, D. Kessler and N. Johnson *Calculation of collision probabilities for space tethers.* Space Debris, volume 103, pp. 131-136, 2000.

102. C. Pardini *De-orbiting spacecraft with electrodynamic tether devices.* IADC AI 19.1 on 'Benefits and Risks of Using Tethers in Space', 21st IADC Meeting, Bangalore, India, 10-13 March, 2003.

103. *Working Group 2: Environment & Database.* Meeting Minutes, 21st IADC Meeting, Bangalore, India, 10-13 March, 2003.

104. C. Pardini, L. Anselmo, A. Rossi, A. Cordelli, and P. Farinella. *A new orbital debris reference model.* The Journal of the Astronautical Sciences, volume 46, number 3, pp. 249-265, 1998.

105. C. Pardini and L. Anselmo. *Assessing the Risk of Orbital Debris Impact.* Space Debris, volume 1, number 1, pp. 59-80, 1999.